PB-228 229

BASIC STUDY OF AIR POLLUTION CONTROL WET SCRUBBERS

Seymour Calvert, et al

Pennsylvania State University
University Park, Pennsylvania

1 September 1966

DISTRIBUTED BY:

NTIS
National Technical Information Service
U. S. DEPARTMENT OF COMMERCE
5285 Port Royal Road, Springfield Va. 22151

THE CENTER FOR AIR ENVIRONMENT STUDIES

The Center for Air Environment Studies is an interdepartmental unit of the Pennsylvania State University established to build and coordinate a balanced research and educational effort on the interaction of man and his air environment. Air pollution is our major problem and it offers opportunities for the practice of many professional fields through a federation of departmental (usually individual professor's) programs with some research by the Center staff.

The Center's program is concerned with understanding the air environment problem and developing methods for its control. We need to know what are the effects and limits of tolerance for polluted air, how can we analyze and define the air environment, what are the engineering-science-economic factors in control, and what are the human factors in control. Some of the Center's projects are on:

Effects on trees and pre-disposition to disease because of pollution damage.
Studies of small particle behavior leading to the development of better air analysis and air pollution control equipment.
The development of high accuracy, low cost airborne analysis equipment for studying large air bodies.
Effects on animals including central nervous system responses.
Studies of the basic combustion processes involved in incinerators.
Survey of attitudes toward air pollution in Johnstown, Pa.
The description and analysis of the political, legal, and administrative systems for air pollution control through studies in Pennsylvania, New York, and the Delaware Valley.
The operation of an air pollution information center and the periodical publication of information retrieval tools such as "Air Pollution Titles" and "Index to Air Pollution Research." (See inside back cover.)
Deposition of small particles in the lungs.

The Center has also developed a unique set of Air Pollution Training Programs supported by grants from the U. S. Public Health Service. In one program graduate students do thesis work on an air pollution problem in their major field and take a minor course sequence in air pollution topics. The Center manages the program, organizes the course sequence, and bears the responsibility for the focal course in Air Pollution and for the total community air pollution program upon which the course is based.

Air pollution administrators are trained in another program which involves one term of full time work on campus and one term of field experience with the Pennsylvania State Air Pollution Control Division. The on-campus portion of this program is offered in the summer for students between their junior and senior years.

Instrument technicians are trained in still another curriculum initiated by the Center. The training and continuing education needs of in-service air pollution control agency personnel are being studied in preparation for the establishment of a program to meet them.

Robert Anderson

PB 228 229

Interim Progress Report on

BASIC STUDY OF AIR POLLUTION CONTROL
WET SCRUBBERS

U.S. Public Health Service Research Grant AP 00320-04

By

Professor Seymour Calvert
Principal Investigator

and

Richard Barton
R. Lee Byers
George A. Coulman
Fay Fun
Steve Jackson
Dale Lundgren
Dilip Mehta
Thomas L. Sweeney
Mansoor Taheri
Eugene Y. Weissman

Reproduced by
NATIONAL TECHNICAL
INFORMATION SERVICE
U S Department of Commerce
Springfield VA 22151

September 1, 1966

Center for Air Environment Studies
The Pennsylvania State University

Contents:

TABLE OF CONTENTS

Introduction

Research Plan

    Introduction and Specific Aims
    Method of Procedure
    Significance of this Research

Progress

    Detailed List of Reports

Appendix 1 "Design of Baffled Conduit Particle Collectors"

Appendix 2 "Entrained Particle Collection in Packed Beds"

Appendix 3 "Particle Collection in Packed Beds"

Appendix 4 "A Technique for Determining Particle Penetration - Diameter Relationships"

Appendix 5 "Removal of Small Particles from Air by Foam"

Appendix 6 "Gas Sorption by Suspensions of Activated Carbon in Water"

Appendix 7a "Absorption by Bubblers in Series

Appendix 7b "Sorption by Suspensions in a Sieve Plate Column"

Appendix 8 "Deposition of Particles from a Turbulent Stream by Thermal Force"

Appendix 9 "Deposition of Particles from a Turbulent Stream by means of Thermal Force"

Appendix 10 "Particle Collection in Secondary Flows"

Appendix 11 "Aerosol Sampling with a Side Port Probe"

Appendix 12 "Reprints of work reported before but published since 1964:

    Appendix 12a "Gas Absorption in a Ribbon-Grid Column"

    Appendix 12b "Mass Transfer in Horizontally Moving Stable Aqueous Foams"

    Appendix 12c "Gas Absorption in a Fin-Wall Conduit"

    Appendix 12d "Experimental and Analytical Study of Plate-Type Gas Absorber Dynamics"

Interim Progress Report on
BASIC STUDY OF AIR POLLUTION CONTROL
WET SCRUBBERS

Under the support of a research grant (AP00320-02 through -04) from the Air Pollution Division of the U.S.P.H.S., there has been a continuation of the research program last summarized in January, 1964. This interim progress report, as the previous ones, has been prepared to accompany a grant renewal application and is not intended for general circulation. Research results are intended to be published through technical journals and most of the research described here has been or will be so published.

Most of the work has been performed by graduate students as thesis research and is identified with the name of the student because of the personal responsibility for the sector of research. Another consequence of the strong integration with graduate research is that the various portions of the study are taken up when students interested in them elect to join the program. The use of undergraduates and technicians has contributed some continuity and added to the scope covered.

An overall view of the program is provided in the research proposal, portions of which are reproduced below:

"I. RESEARCH PLAN

A. Introduction and Specific Aims

The research proposed here is a continuation of the program carried out under Grant number AP 00320-01 and preceding numbers at Case Institute of Technology and, since September 1, 1963, at Penn State University. It will be an academic research program (i.e., including doctoral and masters thesis work) on certain fundamental aspects of gas scrubbing equipment; especially of particle and vapor removal equipment which is applicable to air pollution control. The specific subject matter of the program will be the investigation of several gas treating mechanisms which show evidence of being especially effective. These subjects are as follows:

1. Gas contact with suspensions of adsorbent or reactive particles.
2. Gas contact with wetted and dry surfaces in geometries which provide strong secondary flow patterns in the gas.
3. Gas contact with liquid in the form of froth or foam.
4. Gas contact with packed beds for the removal of particulates.
5. Hot gas interaction with cold surfaces for (a) the removal of particles under the influence of combined inertial, thermal, and possibly mass flux forces and (b) condensation on particles due to radiative and convective heat transfer.

The aims of this work are to define as completely as possible the basic mechanisms involved in gas absorption and particulate collection in the above systems. The attainment of these specific aims will bring us nearer to the ultimate goal of being able to completely define the performance of low pressure drop gas scrubbing equipment. This will require an understanding of the basic mechanisms involved and of the effects of all significant variables such as fluid properties, flow rates, system geometry, particle properties, etc.

B. Method of Procedure

The general method of procedure would be to define and carry out specific studies as doctoral and masters thesis programs. These thesis programs would be coordinated by the principal investigator and would be augmented by his work plus that of part-time student research assistants and other supporting personnel, where required. Part-time undergraduate students would be employed to perform routine tasks in the aerosol tunnel experiments.

The proposed research would continue, expand, and follow the leads of the work in progress. Because of the basic character of these studies, the development of a method of analysis of experimental results constitutes a major part of the problem and can not be set forth in advance of the work.

Approaches on each of the component investigations are as follows:

1. Contact with suspensions of adsorbent particles is being studied by D. S. Mehta as his Ph.D. thesis. Emphasis is on the complete definition of this type of contact in plate column equipment such as sieves. The major resistances to transfer are in the liquid and in the adsorbent pores for low-solubility gases. Thus the understanding of and ability to minimize these factors is vital for design. Gas-adsorbent systems will be chosen on the basis of solubility and experimental convenience.

   Contact with reactive particles suspensions is a closely related problem which will be studied in the same manner as adsorbents. This topic will be taken up in the future by one of the new graduate students.

2. Contact with wetted and dry surfaces in geometries which provide strong secondary flow patterns in the gas will be studied in the aerosol tunnel for exploratory purposes. Variations on baffled conduit design will be screened and the more promising ones studied in detail. A large number of possibilities have come to mind during the past several years but it has not been possible to evaluate them within the confines of a thesis approach. The availability of the aerosol tunnel now makes it possible to do this kind of work on a fairly routine basis with undergraduate student help.

3. Contact with foam for the purpose of particle collection will be studied by M. Taheri. Both unstable and stable foams will be used and the effects of inertial and diffusional mechanisms will be evaluated. Because of the importance of interfacial tension, several types of particle-liquid systems will be used.

4. Contact with packed beds will be studied in the aerosol tunnel and smaller scale apparatus on the same basis as the secondary flow systems. S.Jackson's M.S. work will give a definite indication of the next stage but at this time it appears that an intermediate goal of obtaining design information and exploring many variants will be proper. The leads developed will then be exploited in more detailed research.

5. Interactions between hot gases and cold surfaces for particle collection will be studied by S. Jackson and a new graduate student. The two classes of interactions are:

a. Particle collection under the combined influence of inertial, thermal, and possibly mass-flux forces. The simplest experimental systems would be cold dry cylinders or plates in contact with hot aerosol streams. Direct cooling by water spray would add the complexity of mass flux. Inertial mechanism would be investigated via gas impingement on cylinders, etc., and diffusional mechanism by gas flow inside straight conduits with cooled walls.

b. Condensation of vapors on particles under the influence of convective and radiative heat transfer. The radiative mechanism is especially interesting as a means of increasing particle size for collection without having to cool the bulk of the gas to the same temperature (wet bulb) as the particles. Heat sinks at very low temperatures could thus be used without the penalty of a high refrigeration load just to cool the gas. A basic experimental approach would be to pass the aerosol through a glass (radiation transparent) tube which is set inside a cold metal shell. The particles will radiate to the cold shell but the glass window(s) and perhaps additional devices would provide a convection shield between the gas and the cold shell. Mechanism and rate of condensation will be defined in terms of particle, carrier gas, and condensible vapor properties as well as flow rates, temperatures of gas, conduit, and heat sink, particle concentration, etc.

C. Significance of This Research

The proposed research would be significant to the field of public health and particularly to air pollution control engineering in that:

1. The gas contacting mechanisms being studied are significant in the realm of effective, low pressure drop gas scrubbing. Some of these mechanisms are involved inadvertently or by intent in presently employed scrubbers and others are not presently used. In all cases, however, we are in need of more complete understanding and quantitative definitions of the transport phenomena and mechanics which would enable us to:

   a. Decide upon the optimum mechanism(s) to include in new scrubber designs and to make closer (more accurate) design predictions of efficiency, pressure drop, and capacity.

   b. Evaluate the effects of these mechanisms as they exist in presently employed scrubber designs.

2. The research will be important to both our general educational program in air pollution control engineering and to the encouragement and support of advanced study and thesis research in this area.

In addition to the above points, which can be foreseen with a fair degree of confidence and which have been supported by the experience with our present program there are the unforeseen "by-products." Examples of such by-products are the three papers on analytical (or laboratory) gas absorbers which have resulted from the past program. It is clear that basic knowledge of gas contacting operations is not limited in application to specific types or sizes of hardware.

A further point, somewhat remote from the technological realm of equipment design but of true significance, is that the ability to make closer designs contributes to better air pollution control. On one hand the closer design (and thereby cheaper equipment) encourages more widespread use. On the other hand closer design enables lower legal limits on emissions because these limits are based to a large extent on the ability to conform at reasonable cost.

Some specific comments regarding the problems under study are as follows:

1. Baffled conduit collectors have been developed and studied for the first time on this (and preceding - S84) Research Grant. This type of apparatus has been shown to have good performance capabilities both for particle collection and gas absorption. The geometries now being studied are more suitable for cheap construction than the first models.

2. The use of suspensions of adsorbents for gas scrubbing offers intriguing possibilities for attaining unusual characteristics and is an orginal study of this Grant. The potential advantages are the means for making a solvent with high capacity and the ability to be regenerated which are characteristic of a solid adsorbent while having the ease of handling of a fluid and the ability to operate in counter-current fashion without attrition of the particles.

3. Froth contacting is relatively new and little or no work has been done in this country on certain aspects such as particulate collection. Extremely low pressure drop operation with very high surface area is possible with low density foams.

4. Packed beds have been used for particle collection but there is no published design information. There is great practical need for the ability to predict the efficiency of beds packed with materials commonly used in gas absorbers.

5. Thermal effects have received comparatively little research attention although they are inescapable in hot gas cleaning and may be well worth imposing in cold gas cleaning. Spray coolers are commonly used before high-efficiency collectors on cupolas, open hearths, etc., yet no credit for particle collection in the cooler can be taken because of ignorance of this factor. Further, the use of packing in the cooler is viewed with apprehension rather than being exploited as a means to increase heat transfer and particle collection. In general, thermal precipitation has not been exploited.

   Condensation on particles is a known means of increasing their size for collection or for counting purposes. Even air at or near the temperature of cooling water could be treated in this way be means of refrigerated heat sinks and conceivably at acceptable cost. Knowledge which would enable the prediction of the magnitude and rate of this effect and the design of systems for its implementation would be very useful."

II. PROGRESS

Reports and reprints based on the results of work carried out since the last progress report are given in appendix. Brief summaries of each study are given in the following:

Appendix 1 "Design of Baffled Conduit Particle Collectors", S. Calvert and M. Taheri, British Chemical Engineering II, #4, 254, 1966.

Collection efficiency and pressure drops were determined for a slotted plate type of multiple channel baffled conduit and were found to be substantially the same as for the single channel models studied previously. Water washing keeps the baffles clean of dust and does not change the collection efficiency appreciably from dry operation. The slotted plate construction provides a lower cost baffle than the previous wall baffle concept and it is capable of airly high efficiency at moderate pressure drop. It may be used to remove entrained liquid or solid particles from gases.

The relationship between number of particle transfer units and pressure drop (or power requirement) is derived from the efficiency and pressure drop relationships. It is clear that the number of transfer units for a given particle size and power input is a function of collector geometry and is not independent of it as has been previously suggested by some investigators.

Appendix 2 "Entrained Particle Collection in Packed Beds", Steven Jackson and Seymour Calvert presented at A.I.Ch.E. Meeting in Las Vegas, 1965, accepted for publication in A.I.Ch.E. J.

Small particle collection in packed beds is described by an inertial impaction theory which fits experimental observations. Rings, saddles, spheres, and spherical packings of 1/2-, 1-, and 1-1/2-in. size were used at air velocities up to 30 ft./sec. for the collection of an oil mist of known size. Particle collection efficiencies up to 50% for 1.0 micron particles were obtained.

Appendix 3 "Particle collection in Packed Beds", S. Calvert and S. Jackson, presented at A.I.H.A. Meeting, Houston, 1965 - being submitted for publication.

Particle collection efficiencies were determined for oil mist passing vertically through packed beds. Commonly used tower packings (Raschig Rings, Berl Saddles, marbles, Pall Rings, and 3" to 5" coke) in 1/2", 1", and 1-1/2" sizes were studied in a 18" diameter tower with bed depths of 14" and 24". A fairly good correlation in terms of an inertial mechanism were developed. Questions still remain as to the effects of particle bounce and re-entrainment.

Appendix 4 "A Technique for Determining Particle Penetration - Diameter Relationships". M. Taheri and R. Barton, to be offered for publication.

A technique has been developed for obtaining the relationship between particle penetration (or collection efficiency) and diameter from experimental data. A general mathematical treatment provides the means of utilizing size distributions into and out of the experimental system for computing exact point values of efficiency. Previously published methods employ a difference or averaging technique which gives collection efficiency over a range of particle diameters. A new experimental technique enables one to use the Goetz aerosol spectrometer with convenience and rapidity to provide the needed data.

Appendix 5 "Removal of Small Particles from Air by Foam", Mansoor Taheri's Ph.D. thesis report.

Particle collection by foams produced on sieve plate apparatus is being studied in a 3" x 3" square column and in a 2" diameter circular column. Experimental data have been obtained for several aerosols and most of them being for methylene blue particles and polystyrene spheres. The Goetz aerosol spectrometer provides most of the recent (and most extensive) data. A very low minimum efficiency point at about 1 micron diameter has been found and is in contradiction to the Russian data.

Still to be completed are experiments on the effects of surface properties, foam height and density, and fluid flow rates.

Appendix 6 "Gas Sorption by Suspensions of Activated Carbon in Water", by Dilip Mehta and S. Calvert. To be presented at A.I.Ch.E. Meeting, Detroit, 1966.

Gas scrubbing by suspensions of adsorbent particles in liquids offers the advantages of high capacity, fluid handling, and inexpensive solvent losses. Capacity and mass transfer efficiency are reported for carbon dioxide, methane, propane, n-hexane, ethylene, acetone, trichlorethylene, butyl alcohol, amyl alcohol, benzene and toluene sorption in activated carbon suspended in water. The data reported here were taken in small bubblers of 500 cc capacity. Solubility of the transferring component in water is the major factor affecting transfer rate.

Appendix 7 "Sorption by Suspensions" report on Ph.D. thesis work of D. S. Mehta.

Gas scrubbing by suspensions of adsorbent particles in liquids offers the advantages of high capacity, fluid handling, and inexpensive solvent losses. Mass transfer efficiency was studied for carbon dioxide, methane, propane, n-hexane, ethylene, acetone, trichloroethylene, butyl alcohol, amyl alcohol, benzene, and toluene sorption in activated carbon suspended in water. The data were taken in small bubblers of 500 cc capacity. It was concluded that the solubility of the transferring component in water is the major factor affecting transfer rate.

Side studies were made in bubblers, analytical and experimental, to contribute to the understanding of the above experimental work. Generalized equation was derived and charts prepared for unsteady absorption in n-bubblers in series. Validity of the equations were proved experimentally by absorption of carbon dioxide in one, two, and three bubblers in series respectively. Data was also taken from literature and was found to behave as predicted by equations. There was no effect of flow rate on the intrinsic efficiency of a bubbler. Desorption studies supported all the above conclusions. Studies were also made for absorption with chemical reaction. Inadequacy of the assumption of infinitely rapid second order reaction for absorption of carbon dioxide by sodium hydroxide solution was proved. Second order finite rate allows reasonably good predictions.

Sorption by suspension in a sieve plate is presently under study. Absorption measurements have already been completed for ethanol, methanol, acetone, benzene, and carbon dioxide. Results of sorption of acetone by suspension has indicated that the highest efficiency that can be achieved can not be greater than the intrinsic efficiency for absorption of the same component.

Appendix 8 "Deposition of Particles From A Turbulent Stream by Thermal Force" R. Lee Byers and S. Calvert, Presented at A.I.Ch.E. Meeting, Dallas, February, 1966.

A theoretical model for the deposition of particles from turbulent streams by means of thermophoresis, is presented. Predictions indicate that thermophoresis can be an effective mechanism for cleaning high temperature gases and that fouling rates of heat exchanger surfaces of simple geometry can be determined.

Appendix 9 "Deposition of Particles from Turbulent Streams by Thermal Force", Report on Ph.D. thesis work by R. Lee Byers.

Particle deposition by means of thermal force is being investigated for conditions of turbulent flow of hot gases. A hypothetical model has been developed to predict collection efficiencies for Reynolds numbers from 4,000 to 20,000. Values of collection efficiency fall from 80% at the onset of turbulence to less than 50% at a Reynolds number of 16,000.

The objectives of the laboratory investigation is to determine the affect of particle size, physical properties of particulate material (thermal conductivity and density), absolute temperature, diameter of gas duct, and gas velocity upon particle deposition.

Appendix 10 "Particle Collection in Secondary Flows". Report on Ph.D. thesis work by R. Barton.

The collection efficiency in helical conduits for low Reynold's numbers, where gravitational precipitation is dominated, is being determined both experimentally and analytically, and compared to the collection efficiency in a straight conduit. The collection efficiency at high Reynold's number, where the inertia parameter is high, are also determined both experimentally and analytically.

To date, data has been obtained for two conduit diameters, two particle diameters, and four aspect ratios. Several models have been proposed to calculate the collection efficiency and particle trajectories have been computed to verify various assumptions.

Future work includes the study of particle collection in the diffusional range and the determination of transfer coefficients. Particle collection in larger conduit diameter and higher aspect ratios will also be investigated.

Appendix 11 "Aerosol Sampling with a Side Port Probe," by Dale Lundgren and Seymour Calvert. Presented at Pittsburgh, A.I.H.A. Meeting, 1966.

This work was supported by a combination of research grant, training grant, and University funds. A side port probe is a straight section of tubing, positioned at right angles to the air flow direction, with which an aerosol sample is obtained by drawing in air through a side inlet or an end opening. Sampling biases for side port and straight inlet probes were determined and shown to be functions of two dimensionless parameters, the inertial impaction parameter and a velocity ratio. Experimental results show that the side port probe can be used to obtain essentially representative samples under conditions of low impaction parameter valves.

Appendix 12 Reprints of work reported before but published since 1964.

66.074.2

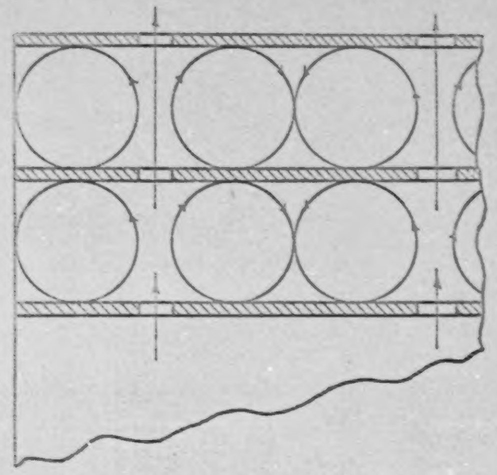

FLOW PATTERNS FOR FLOW PAST BAFFLES

Design of baffled conduit particle collectors

by S. Calvert and M. Taheri

The demand for clean atmosphere has stimulated the development of cheaper and more efficient particle collectors. In this article the authors explore the possibilities of using secondary flow patterns as an effective mechanism which operates in the baffled conduit collector. The aim of the work described below was to determine collection efficiency and pressure drop characteristics of this type of collector and to discover the effects of particle size, conduit geometry, and flow rate, upon its performance

THE separation of small particles from gases by means of inertial force is probably the most commonly used method. Knowledge of this mechanism has been developed for a number of simple geometries and flow patterns so that particle collection efficiency can be predicted for cyclone separators, single cylinders, impinging jets, fibre beds, and similar cases. An investigation of particle behaviour in the more complex cases, secondary or separated flows, has been undertaken to explore the possibilities for exploiting these flow patterns and also to be able to account for them when they occur in collection apparatus.

Eddies which occur behind baffles when the gas flows past them have been studied previously (1, 4) for both particle collection and mass transfer and are now known to offer worthwhile and unique characteristics. In order to extend the practicality of the first baffled conduit geometry which was studied the present authors have studied the multiple baffled conduit which is provided by a number of slotted plates set in series. This concept is illustrated in Fig. 1, which shows the experimental apparatus with its front cover plate removed and Fig. 2, which shows the layout of one slotted plate. Air flows vertically through the slots which are in line with one another and provide a straight flow path. The spacing is set so that two round eddies can form between each pair of slots and one round eddy can form between each of the end slots and the conduit walls.

The aims of this study were to determine the particle collection efficiency and pressure drop characteristics of the multiple channel baffled conduit and to develop methods for the prediction of these in engineering design. Experimental investigations of the effects of particle size, conduit geometry, and flow rate were conducted. The capability of cleaning the apparatus and maintaining collection efficiency was established by operating with continuous water addition to the inlet end of the collector.

Mechanisms

The nature of particle collection efficiency is described by the mechanism proposed by CALVERT and HODOUS (1) and as modified to fit the present situation. The collection efficiently of one eddy, E_o is represented mathematically by:

$$E_o = \frac{3\pi}{g}\,\frac{U_o\bar{U}}{b K^2} \qquad \ldots.(1)$$

where the terms have the meanings presented in the list of nomenclature and the baffle dimensions are as shown in Fig. 2. Particle terminal velocity is defined by Stokes law and the Cunningham correction for slip.

The overall collection efficiency E in the baffled conduit where n eddies are in series is given by the following equation:

$$\mathrm{E} = 1 - (1 - \mathrm{E}_o)^n \qquad \ldots.(2)$$

Equation 2 gives the separation efficiency to be expected for a unique particle size, whereas the test aerosol is composed of particles covering a range of sizes. Consequently the overall efficiency is a summation of the efficiency of each particle size multiplied by the fraction of the particle in that size range. Overall efficiency for particles covering a range of D_1 to D_2 can be expressed by Equation 3.

$$E_d = \int_{D_1}^{D_2} E F_m \, dD_p = \int_{D_1}^{D_2} E \left(\frac{dm}{dD_p}\right) dD_p \qquad \ldots.(3)$$

where F_m is defined to be the rate of change in sample mass with particle diameter and is the slope of the cumulative distribution curve based on mass fraction analysis.

By the nature of the flow through an orifice or slot, it is apparent that the flow lines actually reach a minimum cross sectional area at a point known as the vena contracta. Consequently, the pressure loss from form friction is likely to be considerable. This part is taken into account by fraction K_v of velocity head in Equation 4.

$$P_1 = K_v \frac{\bar{U}^2 \rho a}{2 g_c} \qquad \ldots.(4)$$

At the same time boundary layers are established on the baffle surfaces and momentum is transferred to them by the fluid. The pressure drop caused by this can be estimated by Equation 5.

$$P_2 = \frac{2.5\mu\bar{U}}{g_c K}\left(\frac{\bar{U}}{S\nu K}\right)^{1/2}\left(\frac{S}{b}\right) \qquad \ldots.(5)$$

The authors are with the Pennsylvania State University, Centre for Air Environment Studies.

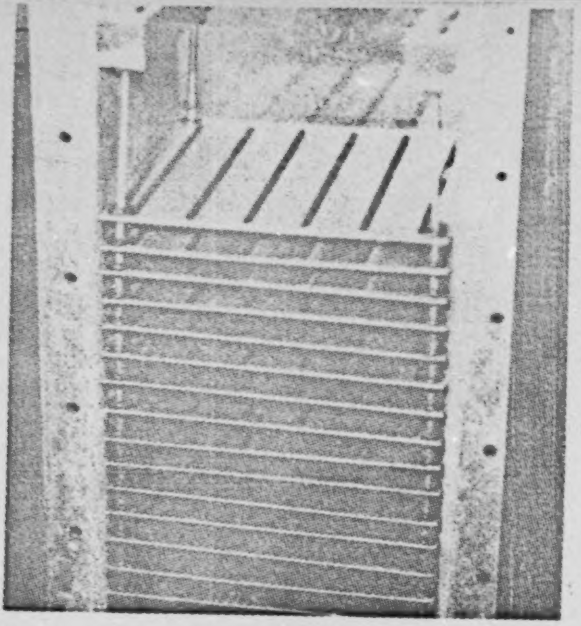

1 *A baffled conduit.*

Symbols Used

b = width of a slot, ft (see Fig. 2).
c = particle concentration, wt/unit volume;
d_p = average particle diameter, micron;
D_p = particle diameter, ft;
D_{eq} = equivalent diameter, four times the cross-sectional area divided by the wetted parimeter, ft;
E = overall particle collection efficiency for "n" baffles and for one particle diameter, dimensionless,
E_t = overall particle collection efficiency for the entire particle size distribution, dimensionless;
E_o = particle collection efficiency of a single vortex for one particle diameter, dimensionless;
f = friction factor — $\frac{D_{eq} g_c P}{2 \bar{U}^2 L}$, dimensionless;
g = acceleration in the gravity field, ft/s²;
g_c = dimensional constant, 32.174 lb ft/lb s²;
K = ratio of main stream velocity to tangential velocity of the eddy, dimensionless;
K_v = slot orifice coefficient, dimensionless;
L = length of the column, ft;
n = number of spaces between baffles in a baffled conduit, dimensionless;
N = number of slots in a single tray, dimensionless;
N_{Re} = Reynolds number, dimensionless, = $D_{eq} \bar{U}$;
N_{tt} = number of particle transfer units, dimensionless;
P = pressure, lb/ft²;
S = baffle spacing, ft;
$\bar{U}$ = average linear velocity, based on (NbW), ft/s;
U_s = terminal settling velocity of particle, ft/s = $\frac{D_p^2 g \rho_p}{18\mu}$
U_t = tangential velocity of eddy, ft/s;
W = length of the slot (see Fig. 2), ft, 0.31 ft for this work;
Δ = finite difference, final minus initial value;
μ = viscosity, lb/ft s;
ρ_a = density of air, lb/ft³;
ρ_p = density of particles, lb/ft³;
ν = kinematic viscosity, ft²/s;
π = 3.1415.

The detailed derivation of Equation 7 is given in reference (2). The pressure drop will be described in terms of a friction factor given by:

$$f = \frac{D_{eq} g_c \Delta P}{2 \rho_a \bar{U}^2 S} \qquad \ldots.(6)$$

where D_{eq} is the equivalent diameter and is defined by Equation 7.

$$D_{eq} = \frac{4Wb}{2(W+b)} = \frac{2Wb}{W+b} \qquad \ldots.(7)$$

The slot width b is very small when compared with W, the slot length, and therefore:

$$D_{eq} = 2b \qquad \ldots.(7)$$

Combining Equations 4, 5, 6 and 8, we have for overall friction factor:

$$f = \frac{K_v}{2}\left(\frac{b}{\bar{S}}\right) + \frac{2.5\sqrt{2}}{K\sqrt{\bar{K}}}\left(\frac{b}{\bar{S}}\right)^{1/2}(N_{Re})^{-1/2} \qquad \ldots.(9)$$

Experimental

The collection efficiency and pressure drop studies were made in a rectangular conduit formed by two galvanized walls and two Plexiglass walls. The baffles as a unit were held in the conduit by four brass rods. The rods were fastened to two rectangular section bars which were bolted to the conduit walls. The baffles were fixed to the rods by means of rubber grommets in each of the corners. This kind of connection allowed the baffles to be moved. A 4 in. × 5 in. tray with three or more slots provided a parallel baffle arrangement. The dimensions and types of arrangement are given in Table I.

TABLE I—Specifications of the Baffled Conduits

Column	S (in.)	b (in.)	n	N	K	K_v
1	[illegible]	[illegible]	32	3	3.4	0.432
2	[illegible]	[illegible]	32	3	3.55	0.396
3	[illegible]	[illegible]	16	3	3.35	0.396
4	[illegible]	[illegible]	45	6	4.0	0.408
5	[illegible]	[illegible]	65	6	4.0	0.408

The conduit was set on an air mixing box, which was approximately a one-foot cube. Air from a blower was introduced at the side of the box through a rotameter. Water, when used, was introduced at the top of the column through two ½ in. dia tubes and the air was also introduced at the top during these runs.

All of the dry collection experimental work was done using a modified Collison atomizer (3) which produced a narrow size distribution from a uranine dye solution. The aerosol was diluted and dried. As it passed through a heated tube, another rotameter measured the flow of this air. The aerosol passing through this heating tube was introduced into the main stream of the air at a point between the rotameter outlet and the mixing box inlet. The aerosols used ranged from 0.6 to 1.3 microns geometric mean diameter by weight, with geometric standard deviation of about 1.7, and density of 1.2 g/cc.

For the water washing runs a substantial dust loading (about 1 grain/ft³) was desired and a dry dust dispersal system was employed. AC Fine test dust was dispersed with an air jet ejector and the aerosol then classified with a cyclone separator designed to cut at about 3 microns dia. The resulting dust had a geometric mean diameter of 1.23 microns by weight, geometric standard deviation of 1.4, and a density of 2.42 g/cc.

Sampling System

After the aerosol was generated and dispersed into the air it was then necessary to determine its concentration at the inlet and the outline of the column. The inlet and the outlet were sampled by using glass sample tubes connected with milipore filters. Determination of the filter loading for uranine by colorimetry or dust by weight along with measurement of the air flow through the filter, then permitted the concentration of the tracer to be calculated.

Results

Dry Collection

The collection efficiency for different sized particles of the baffled conduit was measured and the results were used to evaluate the constant K in Equation 1. In order to find the appropriate value of K from the data, solutions for overall efficiency as generated by a Burroughs 220 digital computer were used. For a given size distribution, assuming different numerical values of K, a series of theoretical curves were generated. The most appropriate theoretical curve and corresponding K were chosen by comparing each theoretical curve with the experimental one. The value of K for each geometric arrangement is given in Table I.

Fig. 3 shows the variation of collection efficiency with particle size. The experimental values of efficiency can be compared

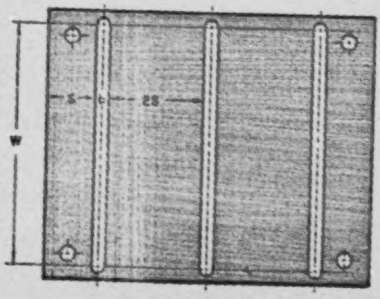

2
A single tray with three slots.

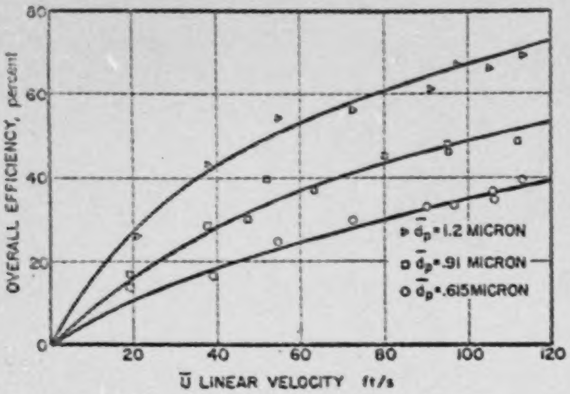

3 *Efficiency versus linear velocity for column No. 2.*

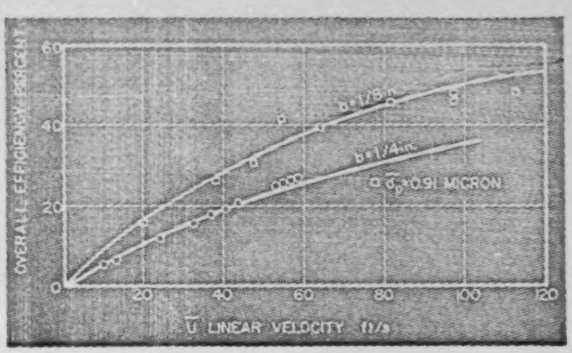

4 *Overall efficiency versus linear velocity with slot width D as parameter.*

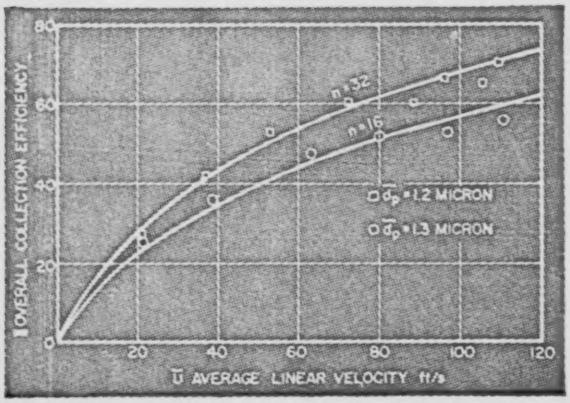

5 *Overall collection efficiency versus average linear velocity with number of baffles as parameter.*

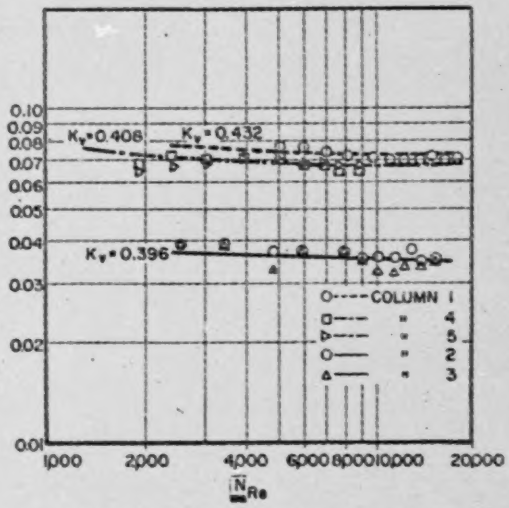

6 *Friction factor versus Reynolds number for various geometrics.*

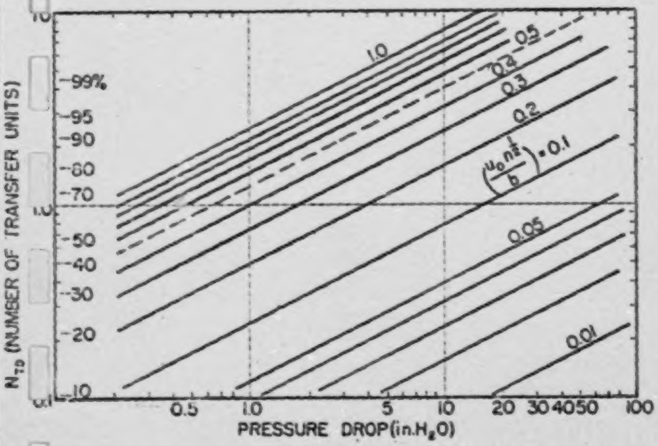

7 *Number of transfer units versus pressure drop for various baffle conduit geometrics.*

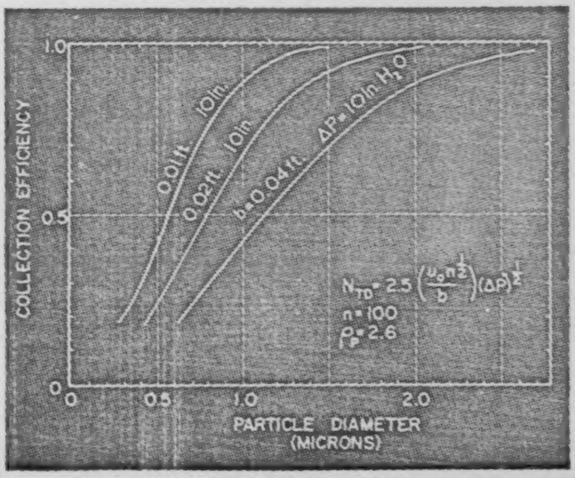

8 *Collection efficiency versus particle diameter.*

with the corresponding theoretical values from the curves. A comparison between these three curves indicates that the value of K is almost constant at about 3.5 to 3.6 Fig. 4 shows the effect of slot width and Fig. 5 shows the effect of the number of baffles. When the number of baffles was reduced to 16, a numerical value of 3.35 was obtained for K. This value indicates that there is no significant end effect in the baffled conduit.

The average value of $K = 4$ for columns 4 and 5 indicates the effect of decreasing the baffle space from ¾ in. to ⅜ in. Visual observation of the particle deposit on this type of baffle indicated that the baffle was collecting particles only on the bottom part of the slot edges. This indicated that the mechanism of the collection was impaction due to impingement of the flow stream, and that essentially the particle collection takes place in half a circle instead of three quarters of a circle.

Wet Collection

Wet collection efficiency was determined for 32 baffles with ¼ in. slot width at water flow rates of 1.7 and 2.8 litres per minute. The data can be represented by a value of 3.65 for K which compares fairly well with the values obtained for dry operation with uranine aerosol. Adequate washing of the baffles was obtained during runs of several hours' duration.

Pressure Drop

The pressure drop data were corrected by deducting the pressure drop because of the contraction at the entrance of the first baffle and expansion at the exit of the last baffle. The corrected pressure drop data were used to compute a friction factor.

The pressure drop characteristics in the form of the friction factor and Reynolds number for dry baffles are plotted in Fig. 6 which illustrates the following conclusions.

(1) the value of K_r is almost constant between 0.4 to 0.43

(2) The pressure drop caused by establishing the boundary layer on the surface of the baffles at $N_{Re} < 3000$ is not more than 10 per cent of the total pressure drop, and at $N_{Re} > 3000$ this value is practically negligible. Consequently, from a practical viewpoint the friction factor can be assumed a function of only (b/S); the ratio of the slot width to the baffle spacing.

The friction factors for wet operation of column No. 1 ($n = 32$, $b = \frac{1}{4}$ in.) were approximately 1.3 and 1.4 times the dry friction factor for water rates of 1.7 and 2.8 l/min. respectively. The air velocity ranges up to 43.5 ft/s based on slot area.

Design Equation

For the design and optimization of baffled conduit collectors it is desirable to derive one relationship between all of the pertinent variables. Overall collection efficiency is conveniently expressed in terms of particle transfer units, defined as follows:

$$-\frac{dc}{dn} = E_0 c \text{ (for } n \text{ large)} \qquad \ldots.(10)$$

$$\ln\frac{c_1}{c_2} = N_{td} = E_0 n = \ln\left(\frac{1}{1-E}\right) \qquad \ldots.(11)$$

By neglecting the boundary layer term in Equation 9 and evaluating K_r as 0.4 we can combine Equations 1, 9 and 11 to yield:

$$N_{td} = \left(\frac{3\pi U_0}{gbK^2}\right)\left(\frac{\triangle p g_c n}{0.2\ \rho_a l}\right)^{1/n} \qquad \ldots.(12)$$

If we take the representative value of $K = 3.5$, evaluate ρ_a as 0.075 lb/ft³ for standard air, and let $\Delta P'' =$ pressure drop in inches of water we find:

$$N_{td} = 2.5\left(\frac{U_0 n^{1/n}}{b}\right)(\triangle P'')^{1/n} \qquad \ldots.(13)$$

Fig. 7 is based on Equation 13 and shows the relationship between number of transfer units and pressure drop for several values of the parameter. Fig. 8 was drawn from Equation 13 for the case of $n = 100$ baffles and $\rho_p = 2.6$ g/cc for the purpose of illustration in more familiar terms.

Summary and Conclusions

Collection efficiency and pressure drop characteristics of the multiple channel model are substantially the same as for the single channel models studied previously. Water washing keeps the baffles clean of dust and does not change the collection efficiency appreciably from dry operation. The slotted plate construction provides a lower cost baffle than the previous wall baffle concept and it is capable of fairly high efficiency at moderate pressure drop. It may be used to remove entrained liquid or solid particles from gases.

The relationship between number of particle transfer units and pressure drop (or power requirement) is derived from the efficiency and pressure drop relationships. It is clear that the number of transfer units for a given particle size and power input is a function of collector geometry and is not independent of it as has been previously suggested by some investigators.

ACKNOWLEDGEMENT

The financial support provided by the United States Public Health Service which made this work possible is gratefully acknowledged.

REFERENCES

1. Calvert, S. and Hodous, R., "Collection of Small Particles in Baffled Conduits", *APCA Journal*, Vol. 12, No. 7 (July, 1962), 326-331.
2. Taheri, Mansoor, "Particle Collection in a Multiple Baffle Conduit", Master's Thesis, Engineering Division, Case Institute of Technology, June 1964, 13-19.
3. Green, H. L., and Lane, W. R., "Particulate Clouds: Dusts Smokes and Mists." Toronto, London, New York and Princeton, N.J.: D. Van Nostrand Co. Inc., 1957, 39-41.
4. Sweeney, T. L., "Gas Absorption in a Finwell Conduit", Ph.D. Thesis, Engineering Division, Case Institute of Technology, June, 1962, 43-47.

Two methods for foam insulation of storage vessels

POLYURETHANE foam is in many ways an ideal material for insulating large storage tanks, being a highly efficient insulator, relatively inexpensive, and, unlike conventional slab or batt type insulation material, giving a continuous covering with no troublesome joints. However, the application of the foam presents difficulties, depending on the size and shape of the vessel, the site conditions, etc., and two recent examples, one relating to a spherical vessel and the other to cylindrical tanks, show that there are several ways of meeting these problems.

The first example occurs at the storage field of Imperial Oil Co. at Sarnia, Ontario, where the problem was the insulation of a refrigerated hortonsphere used for storing hydrocarbons. The sphere, 55 ft in diameter, has a surface area of 10,000 ft² and, as the spraying was carried out during the severe Canadian winter, the sphere was temporarily enclosed in a tent of 6-mil polythene, spread over an erected scaffolding to ensure production of a foam layer of satisfactory quality. During the spraying operation steam was injected into the sphere to keep it at 38°C. The air space inside the polythene tent was also heated. Layers of foam, applied to a total thickness of 1½ in., were subsequently coated with aluminium mastic. The insulation will maintain the inside temperature of the sphere at 4½°C.

The foam insulation was applied by Commercial & Industrial Insulation Ltd., of Sarnia. They used Daltolac and Suprasec foam-making chemicals manufactured by the Dyestuffs Division of I.C.I. and sold by Canadian Industries Ltd. (an I.C.I. subsidiary).

At the Rotterdam complex of Shell Nederland Chemie N.V. there is no shortage of storage tanks, and no difficulty in obtaining rigid urethane foam, since this is also a Shell product. But the usual methods of insulation were found laborious: spraying of foam by hand seems attractive but necessitates the erection of scaffolding round each tank. Special equipment was developed, therefore, making use of two small pneumatic motors for moving the spray gun along the tank wall, either horizontally or vertically. Dispensing pumps and other machinery, which are mounted on a small car beside the tank wall, are connected with the spray gun by long hoses. All movements of the spray gun are controlled from the ground, and in this way two men can apply a 2-in.-thick foam layer on a surface of 3000 ft² in 8 hours. Some tanks which have been insulated in this way have withstood 2 years' weathering without any foam degradation.

Entrained Particle Collection in Packed Beds

STEPHEN JACKSON and SEYMOUR CALVERT

Pennsylvania State University, University Park, Pennsylvania

Small particle collection in packed beds is described by an inertial impaction theory which fits experimental observations. Rings, saddles, spheres, and spherical packings of ½-, 1-, and 1½-in. size were used at air velocities up to 30 ft./sec. for the collection of an oil mist of known size. Particle collection efficiencies up to 50% for 1.0-micron particles were obtained.

Vapor from evaporators, boilers, and stills carries with it small drops of liquid. These drops can be formed by the bursting of bubbles during a boiling process, by the breakup of liquid sheets and ligaments, or by the condensation of saturated vapor. Mist entrained by the vapors causes problems such as corrosion of equipment, decrease in equipment performances, or a loss of the processed material. This same mist may also constitute a public nuisance, a health hazard, or a general air pollution problem.

Many types of mist separators or dust collectors may be used as entrainment separators. Generally, these are especially effective on the larger (10-micron diameter) particles, but have very little effect on particles below a few microns in diameter. A successful entrainment separator must have several essential characteristics: high collection efficiency, very low liquid reentrainment, and low pressure drop.

Towers packed with Raschig rings or coke have been used for many years to collect mists such as phosphorus pentoxide (*1* to *3*). The Tennessee Valley Authority obtained data for mist collection by burning phosphorus in air and passing the resulting gases through a tower irrigated with water or dilute acid. Efficiencies of 90% were obtained only with high velocity–high pressure drop operation. They obtained similar results with a tower packed with small size (1-plus ½ in.) coke. Additional results indicated that in certain cases, a twofold increase in depth produced practically no increase in mist recovery.

Baskerville (*1*), using a pilot scale tower packed with either 1-in. Raschig rings or with coke, studied the effects of gas velocity and bed depth on the recovery (collection) phosphorus pentoxide. He arrived at a set of semiempirical equations in which many factors such as particle size were omitted. Baskerville claimed, however, that the equations for recovery and pressure drop hold within the limits of accuracy of the data.

Silverman (*4*) has reported on the use of coke boxes for the collection of 0.5- to 3-micron mists in the sulfuric acid industry. Carefully sized and washed coke, ¼ to ⅜ in. in size, were placed between layers of coarser grades of coke and tested at superficial velocities of up to 10 ft./min. with corresponding pressure drops of 1 to 10 in. of water. By using finer coke sizes and lower gas velocities, efficiencies as high as 99% were obtained; increased bed depth caused higher collection efficiencies and higher pressure drops.

Strauss and Thring (*5, 6*) reported on the use of high-temperature insulating brick (5/16 in. to 7 B.S. mesh), crushed high-temperature fireclay refractories (14 to 24 B.S. mesh), and two types of ceramic filters to clean the fume from hot open-hearth furnace stack gas. From pilot plant studies they report efficiencies of 80 to 90% for the granular refractory, 50% for the fireclay, and 60% for ceramic filters when aerosols containing particles of 0.8 to 6 microns in diameter were used. The granular refractory had the lowest pressure drop. A regression analysis was made to correlate collection efficiency with mass flow rate, temperature, and inlet fume concentration.

THEORETICAL CONSIDERATIONS

Collection efficiency of fibrous filters has been studied by several investigators and is fairly well defined. Collection of particles by larger elements, such as the rings, saddles, spheres, etc., employed in gas absorption and distillation columns, is not as well investigated or as clearly understood.

In general there are five ways of removing particles from a gas stream: settling, inertial impaction, deposition diffusional, agglomeration, and electrostatic deposition. In packed beds, the collection of droplets—larger than a half-micron diameter or so—can be mainly attributed to the mechanism of inertial impaction.

Inertial collection occurs in the following manner. (1) Particles in a gas stream are impacted against the packing surface because of the particle's inertia or inability to follow the gas stream around the packing. (2) After a number of particles have been caught by a packing element surface, they coagulate and tend to flow along the packing surface and out of the collector. Although this draining flow may be partially reentrained and reduce overall efficiency, the effect may be identified separately and is not included in this study.

A particle tends to move in a straight line because of its inertia; therefore, when the suspending fluid flows around an obstacle, the particle tends to keep going toward the obstacle. Collection of a particle by an obstacle, or target, is determined by whether a particle reaches an obstacle or whether the particle is deflected sufficiently by the fluid to by pass or flow around the obstacle. If a particle bounces off from rather than sticks to a surface on impaction, the efficiency will be lower. In this paper the bounce off is assumed zero, although it may be significant for some circumstances.

A mathematical analysis of particle collection may be based on Newton's law of motion and on the assumption that the deceleration force on a particle is given by Stokes' resistance law for laminar flow through a continuous fluid. The probability or efficiency E with which a mist particle in an inertial field is removed from a fluid stream can be expressed as a function of at least three dimensionless parameters. The first of these K is a dimensionless ratio between the inertial force acting on a particle and the force of resistance to its motion relative to the fluid. The parameter K is called the inertial impaction parameter. When Stokes' law does not hold, that is, when the Reynolds number of a particle is more than unity, this Reynolds number must be taken into account. The third parameter is the Reynolds number for flow around the obstacle or collector.

Packed-bed collection efficiencies may be predicted by means of a simplified mathematical model of the collection system. It is first necessary to describe the flow passage and the flow pattern for the fluid. It is then possible to obtain the particle trajectories.

Assume that a packed bed can be represented by a series of bends of equal size and that the gas flows through a number of these passages. In a series of alternating bends the particles are thrown first toward one wall and then the other because of centrifugal forces. Ranz (7) has given an expression for the collection of particles in a sweeping bend: A uniform flow system in which there is no mixing of the particles was assumed. Some of the particles, subject to a collection force, are thrown out in the first half wave. The remainder travel through the system unaffected, as the remaining alternating waves will only cause the particles to move from side to side but will not remove them.

A more realistic way to characterize the collection of particles in a packed bed is to include the effect of turbulent mixing. Assume that mixing occurs either after flow through each bend or that it occurs continuously throughout the flow path. The latter approach will be used here. This effectively means that the particle concentration is constant across any cross section of a bend and that centrifugal sedimentation takes place in a laminar layer adjacent to the packing.

The expression for the collection efficiency E in a sweeping bend which was previously referred to is

$$E = \pi n K \qquad (1)$$

The definition for K includes a characteristic linear dimension for the impaction system. For a sweeping bend this dimension was chosen to be the thickness of the gas stream between the walls. The same definition will be used in applying this relationship to packed beds. For a packed bed this width will be called the channel width B, which is a function of the packing diameter. The term n is the number of 360-deg. turns during which the particles may be thrown out of the gas stream.

We may derive a similar expression for the case of turbulent mixing. If Stokes' law applies, then a force balance on the particle leads to

$$U_t = \frac{D_p^2 \rho_p a}{18 \mu_g} \qquad (2)$$

The flux of particles of size D_p against the outside wall at $R\theta$ is equal to CU_t. The consideration of the number of particles entering and leaving an element of flow $Rd\theta$ long, B thick, and of unit width gives the differential equation

$$-(V_o B)\, dC = CU_t\, Rd\theta \qquad (3)$$

where the gas velocity in the circumferential direction is assumed to be V_o everywhere.

By using the boundary condition that $C = C_o$, when $\theta = 0$, the following relationship for C as a function of $R\theta$ is developed:

$$\frac{C}{C_o} = \exp - \left[\left(\frac{U_t}{V_o} \right) \left(\frac{R\theta}{B} \right) \right] \qquad (4)$$

The fractional efficiency of impaction for this situation can be defined as the ratio of the number of drops of a certain size removed to the number of drops originally in the stream. That is, $E = (1 - C/C_o)$. The normal acceleration of a stream moving at a velocity V_o on a radius R is (V_o^2/R). If Stokes' law holds, the terminal velocity may now be expressed as

$$U_t = \left(\frac{D_p^2 \rho_p V_o^2}{18 \mu_g R} \right) \qquad (5)$$

By substitution

$$\frac{C}{C_o} = \exp - \left[\left(\frac{D_p^2 \rho_p V_o^2}{18 \mu_g R} \right) \left(\frac{R\theta}{B} \right) \right]$$

$$= \exp - \left[\frac{D_p^2 \rho_p V_o \theta}{18 \mu_g B} \right] \qquad (6)$$

Since K was previously defined to include the channel width B, the terms inside the inner brackets can be replaced by K giving

$$E = 1 - \exp(-\pi n\ K) \qquad (7)$$

Therefore, there are two distinct assumptions which lead to either of two relationships expressing the collection efficiency as a function of n and K:

For uniform flow $E_o = \pi n\ K$ (1)

For turbulent flow $E_o = 1 - \exp(-\pi n\ K)$ (7)

Figure 1 is a plot of collection efficiency vs. the expression $\pi n K$ as predicted by Equations (1) and (7). Figure 2 is a plot of predicted collection efficiency against particle diameter with the gas velocity, packing diameter, and the bed depth as parameters. The channel width B is a function of the packing diameter D and was estimated to be related to the free volume of cubic packed spheres. The ratio of channel width to the packing diameter is estimated to be a constant:

$$\frac{B}{D} = 0.1 \qquad (8)$$

The curves in Figure 2 were developed by using this particular constant ratio.

EXPERIMENTAL

The experiments were carried out on test apparatus whose main features are shown in Figure 3. The sampling system, a cascade impactor, was used to determine the mass concentration of aerosol mist in each of several particle size fractions. This allowed determination of impaction efficiencies for different ranges of particle sizes.

Operation of the test equipment is as follows. Air is drawn in from outside through a blower and is exhausted into a ducting system. An oil mist is introduced into this air stream and is carried by it to a test section. The air stream is sampled before and after passing through the test section. It then passes through a final air cleaner and is exhausted to the atmosphere.

A test aerosol generator provides a fuel oil mist having a mass median diameter of approximately 6 microns and with a standard deviation of 2.0 at an output flow rate of about 3.6 lb./hr. Fuel oil was chosen because it is relatively nonvolatile, nontoxic, and nonexplosive at the mist concentrations obtained in the test equipment. Important properties of the test oil are: specific gravity 60/60 = 0.83, viscosity at 100°F. = 2.3×10^{-2} poise, surface tension at 70°F. = 24 dynes/cm.

The test aerosol is sampled at positions approximately 6 in. before and after the test section. Samples are drawn from the duct center through a sampling tube connected to a four-stage cascade impactor fitted with a rapid opening plug valve. Following the impactor is a filter unit in which high efficiency filter paper is used to remove all remaining mist particles. Specific details on the systems mentioned are available from the authors.

EXPERIMENTAL PROCEDURE

Tests were carried out at the following approximate superficial velocities: 6, 8, 10, 20, and 25 ft./sec. In a few isolated cases it was also possible to reach 30 ft./sec. For each test condition, test runs were made in triplicate to insure representative efficiencies. Each packing was tested at the above flow rates before changed to another packing.

The test section was constructed from a 6-in.-long section of 14-in. diameter ducting with an inlet and outlet retainer screen of ⅜-in. hardware cloth. After a test bed was packed and the retainer screen fixed in place, the bed was fitted into a horizontal section of the test duct.

Although the mist concentration varied somewhat (minimum and maximum concentrations were 2.7 and 4.2 lb./hr., respectively), it was usually within 5% of 3.6 lb./hr. The aerosol distribution was computed from cascade impactor data and is shown in Figure 4 as a straight line on logarithmic-probability coordinates. A slight error was introduced because of collection on the bend of the sampling tube. By using sample bias provided from previous testing, the raw data can be corrected.

Overall efficiencies were calculated from samples taken before and after the collector being tested. The difference in the total amount collected in the impaction train before and after the collector represents that part of the stream which was removed. When the data were evaluated the weight of material on the first impaction stage was not included. This was done on the assumption that this should be reentrained mist, rather than droplets which have bounced off as the collection for that size range is essentially 100%. In general, this reentrained mist was in the range of 10 to 30 microns, depending upon the superficial velocity of the main stream and is large enough to be easily collected.

The results of these efficiency tests are shown in Figure 5 and 6. The packing size was ½ in. and the packing types were: glass spheres, Berl saddles, Raschig rings, and Intalox saddles. The experimental curves in Figure 5 apply to the spheres, the Berl saddles, and the Raschig rings; those in Figure 6 show the results obtained when Intalox saddles were used. Theoretical (predicted) curves for two velocities are also shown on the plots. All the curves, theoretical and experimental, are plots of efficiency vs. particle diameter with velocity as a parameter. In all cases the mass median diameter of the test aerosol was 6 microns (with geometric standard deviation of 2). In the figures the theoretical curves are obtained by applying the turbulent mixing expression, by using n (the number of 360-deg. turns) = 6 as a first approximation.

Overall efficiencies for the entire mist size distribution fed to the horizontal flow bed collector are shown in Figure 7. The curve for the Intalox saddles falls below that for the other types of packings at a lower velocity, but improves at high velocities. The overall efficiencies hide the effect of particle size, but are presented here to give an approximate basis for comparison with other entrainment separators as commonly reported.

On the basis of only the collection efficiency characteristics of the packings used, it would seem that any of the three types previously mentioned—spheres, Berl saddles, Raschig rings—would be superior to the Intalox saddles at the low velocities. Any of the four would be suitable at the higher velocities.

Pressure Drop

The pressure drops which were obtained with this installation ranged from low to moderate. The drop in pressure for the various velocities is shown in Figure 8, which shows that the Intalox saddles have the best operational characteristics. The experimental values for this particular set of tests are 0.5 to 1.0 times those calculated from published correlations (*8, 9*).

SUMMARY AND CONCLUSIONS

Beds of Raschig rings, Berl saddles, Intalox saddles, and glass spheres are very effective in removing entrained liquid droplets down to 2- to 3-micron diameter. Efficiencies up to 50% were obtained for 1.0-micron particles. A turbulent mixing model represents collector performance reasonably well and may be used to predict particle collection by impaction. Subsequent testing on a vertical-flow bed (*11*) has provided additional results which substantiate the model and the use of $n = Z/2D$ as an approximation. In the 6-in. bed used for these, Berl saddles and Raschig rings give the best performance at low velocities. When high velocities were attained, then the lower pressure drop developed in a bed packed with Intalox saddles made it superior. The roles of reentrainment and particle bounce remain to be defined.

ACKNOWLEDGMENT

The financial support for this project was provided by a U. S. Public Health Service Division of Air Pollution research grant and is gratefully acknowledged.

NOTATION

a = particle acceleration, cm./sec.^{2}
B = width of flow channel, cm.
C = number of particles of size D_p/unit volume of gas at a distance $R\theta$ from start of turn, No./cc.
C_o = number concentration of particles at R, $\theta = 0$, No./cc.
C_D = drag coefficient $= 24\mu_g/(U_t\rho_g D_p)$ for Stokes' law
D = diameter of packing, cm.
D_c = characteristic dimension of inertial impactor, cm.
D_p = diameter of mist particle, cm.
E_o = impaction or collection efficiency
K = inertial parameter $= \rho_p V_o D_p^2/9\mu_g B$
m = mass, g.
n = number of 360-deg. turns swept by gas stream
R = outside radius of bend, cm.
U_t = terminal velocity of a particle relative to the gas stream, cm./sec.
V_o = velocity, cm./sec.
Z = bed depth, cm.

Greek Letters

ρ_g = density of gas stream, g./cc.
ρ_p = density of liquid mist particles, g./cc.
μ_g = absolute viscosity of gas stream, poise
θ = angle, rad.

LITERATURE CITED

1. Baskerville, W. H., *Trans. Am. Inst. Chem. Engrs.*, **37**, 79 (1941).
2. ———, U. S. Patent 2,303,318 (1942).
3. Striplin, M. M., *Tennessee Valley Authority Chel. Eng. Rept. No. 2*, 1 ed., U. S. Government Printing Office, Washington, D. C. (1948).
4. Silverman, L., in "Proceedings of the United States Technical Conference on Air Pollution," ed., L. McCabe, McGraw-Hill, New York (1952).
5. Strauss, W., and M. W. Thring, *Iron Steel Inst. J.*, **196**, 62 (1960).
6. *Ibid.*, **193**, 216-21 (1959).
7. Ranz, W. E., *Eng. Res. Bull. B-66*, Pennsylvania State Univ., University Park (1956).
8. Perry, J. H., "Chemical Engineers' Handbook," 4 ed., McGraw-Hill, New York (1963).
9. Leva, M., "Tower Packing and Packed Tower Design," 2 ed., U. S. Stoneware Co., Akron, Ohio (1953).
10. Weissman, E. Y., and Seymour Calvert, *A.I.Ch.E. J.*, **2**, No. 2, 356-63 (March, 1965).
11. Calvert, Seymour and Stephen Jackson, paper presented at AIHA meeting, Houston (1965).

Manuscript received September 22, 1964; revision received April 20, 1966; paper accepted April 22, 1966. Paper presented at A.I.Ch.E. Las Vegas meeting.

Fig. 1. Collection efficiency vs. intertial parameter.

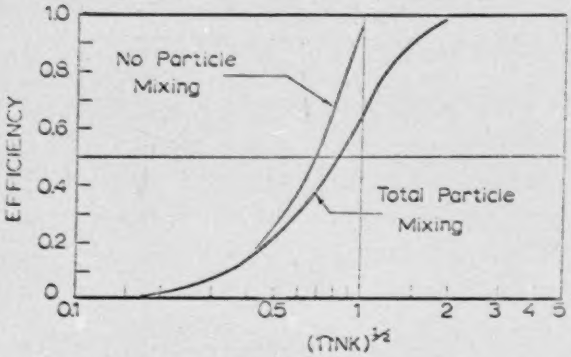

Fig. 2. Predicted efficiency vs. particle size.

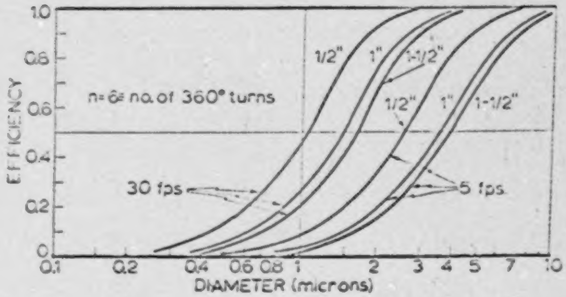

Fig. 3. Schematic diagram of aerosol tunnel.

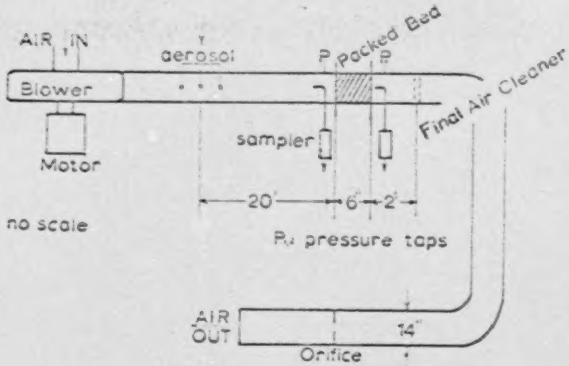
AIR IN
Blower
Motor
aerosol
P
Packed Bed
P
Final Air Cleaner
sampler
20'
6"
2'
no scale
P, pressure taps
AIR OUT
Orifice
14"

Fig. 4. Size distribution curve; $Dm = 6.0$ microns; $\sigma = 2.0$

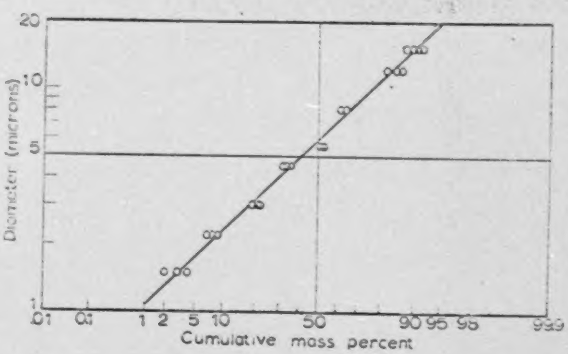

Fig. 5. Experimental collection efficiency. One-half-inch spheres, Berl saddles, and Raschig rings.

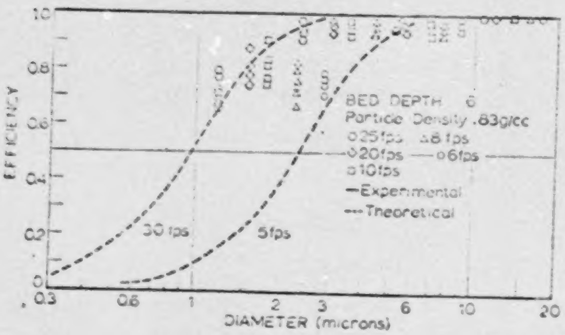

Fig. 6. Experimental collection efficiency. One-half-inch Intalox saddles.

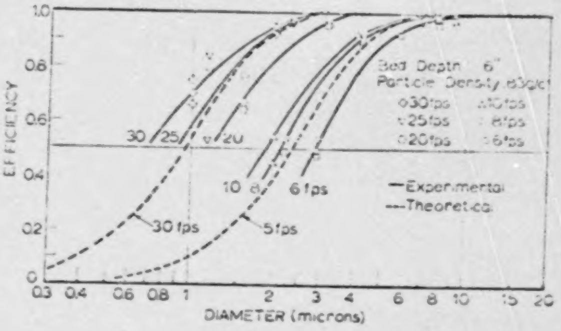

Fig. 7. Overall efficiency vs. superficial velocity.

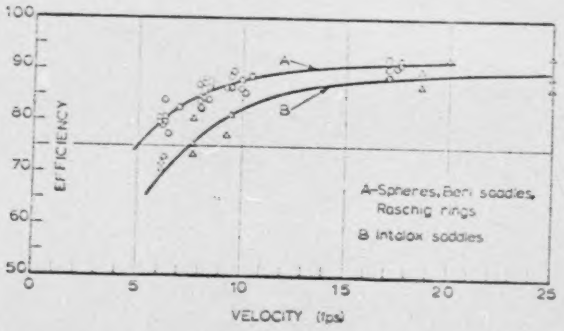

Fig. 8. Pressure drop for 1/2-in. packings.

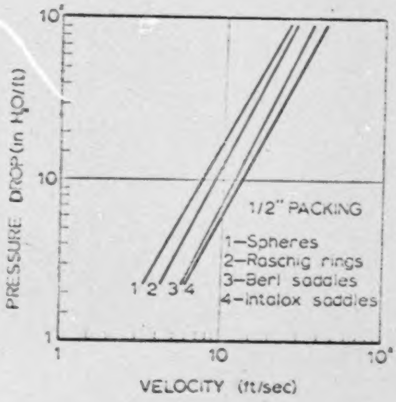

APPENDIX 3

Particle Collection in Packed Beds

By: Seymour Calvert and Steven Jackson

A paper under the above heading was presented at the A.I.H.A. Meeting, (May, 1965, Houston, Tex.) and is being submitted for publication. The following is an extract from that paper and presents all of the results. This work is the first basic study of particle collection in dense packed beds and its objective was to provide design information relating collection efficiency with particle, gas, and packing characteristics. Results on horizontal flow through 14" diameter by 6" thick beds of several 1/2" packings were presented in the Jackson and Calvert A.I.Ch.E. paper(1).

The present paper is based on experiments carried out in an 18" diameter vertical flow bed with packed depths of 14" and 24". Commercial packings of 1/2", 1" and 1-1/2" size and crushed coke of 3"-5" size were evaluated and the experimental results are consistent with an inertial impaction mechanism.

The main components of the experimental apparatus are an aerosol flow system capable of providing 400 - 4,000 CFM of metered air carrying a fuel oil mist, a four stage cascade impactor for sampling inlet and outlet aerosol, and a test section shown in figure 1. Details on the flow system and cascade impactor are given in references 1 and 2. Particle size distribution of the 0.83 density oil is log normal with a mass mean diameter of approximately 6.0 microns and a geometric standard deviation of 2.0.

Air velocities of up to 10.5 ft/sec. based on total (superficial) bed cross section and an oil rate of 3.6 lbs/hr. were used. Collection efficiency was determined for each impactor stage and was attributed to the mean diameter between the 50% cut point for that stage and the one above it. This proceedure may introduce errors of a few percent but acceptably small in view of the overall experimental error.

Hypothesis

A mathematical expression of an inertial impaction mechanism may be obtained along the lines given by Jackson (1). If we assume that the air negotiates a series of semi-circular bends of width "B" and is completely mixed by turbulence at all levels in the bed, we obtain for penetration:

$$P_t = e^{-\left[\frac{2\pi n \quad D_p^2 \quad \rho_p \quad v_b}{18\mu \quad B}\right]} = e^{-A_1} \qquad (1)$$

and we can write the exponent as:

$$A_1 = \pi n \left(\frac{D_c}{B}\right)\left(\frac{v_b}{v_s}\right) K \qquad (2)$$

We may now estimate that the gas turns 1/2 of a circle for each packing diameter of bed depth $\left(n = \frac{Z}{2\ D_c}\right)$, that $B = \frac{D_c}{7}$, and that $v_s = 0.7\ v_b$. Substitution into equation 1 yields:

$$P_t = e^{-\left[C_1 \left(\frac{Z}{D_c}\right) K\right]} \qquad (3)$$

with the constant C_1 having a value of about .15.

Experimental results are given in figures 2, 3, 4, and 5. The lines shown on these figures are solutions of equation (3) with the values of C_1 shown as the parameter on the curve. The data can be represented as follows:

Packing	C_2
1/2" Berl saddles, Marbles, Raschig rings, and Intalox saddles	10.7
1" Berl saddles, Raschig rings and Pall rings	10.0
1-1/2" Berl saddles, Raschig rings, and Pall rings	12.0
3-5" Coke	100.0

There is a slight unexplained effect of gas velocity for the 1" and 1-1/2" packings. Even so, the spread of data is about ± 10% about the correlated efficiency. The high value of C_1 for coke is probably due to the small size of the flow passages in comparison to the coke.

Conclusions

The proposed mechanism appears to be correct and provides a good basis for design calculations. Collection efficiencies can be predicted with confidence for the sizes below about 10 micron diameter. There is some remaining uncertainty about the collection efficiency for the larger sizes, which may be especially subject to bouncing off the packing.

References

1. S. Jackson and S. Calvert, "Entrained Particle Collection in Packed Beds", A.I.Ch.E. J. (1966).
2. W. E. Ranz and E. J. Katz, APCA J, 8, 328,(1959).

Table of Nomenclature

A_1 = Emperical constant

B = Width of flow channel (cm)

C_1 = Emperical constant

D_c = collector diameter or width (cm)

D_p = particle diameter (cm)

e = base of natural logarithms

$K = \frac{v_s \ \rho_p \ D_p^2}{9 \ \mu \ D_c}$ = inertial collection parameter

n = number of 360° turns taken by gas

P_t = penetration of collector by particles = $\frac{c_o}{c_i}$ (fraction)

v_b = velocity (cm/sec)

v_s = $0.7 \ v_b$

Z = height or length of scrubber (cm)

ρ_p = particle density (g/cm^3)

μ = viscosity (poise)

Figure 1

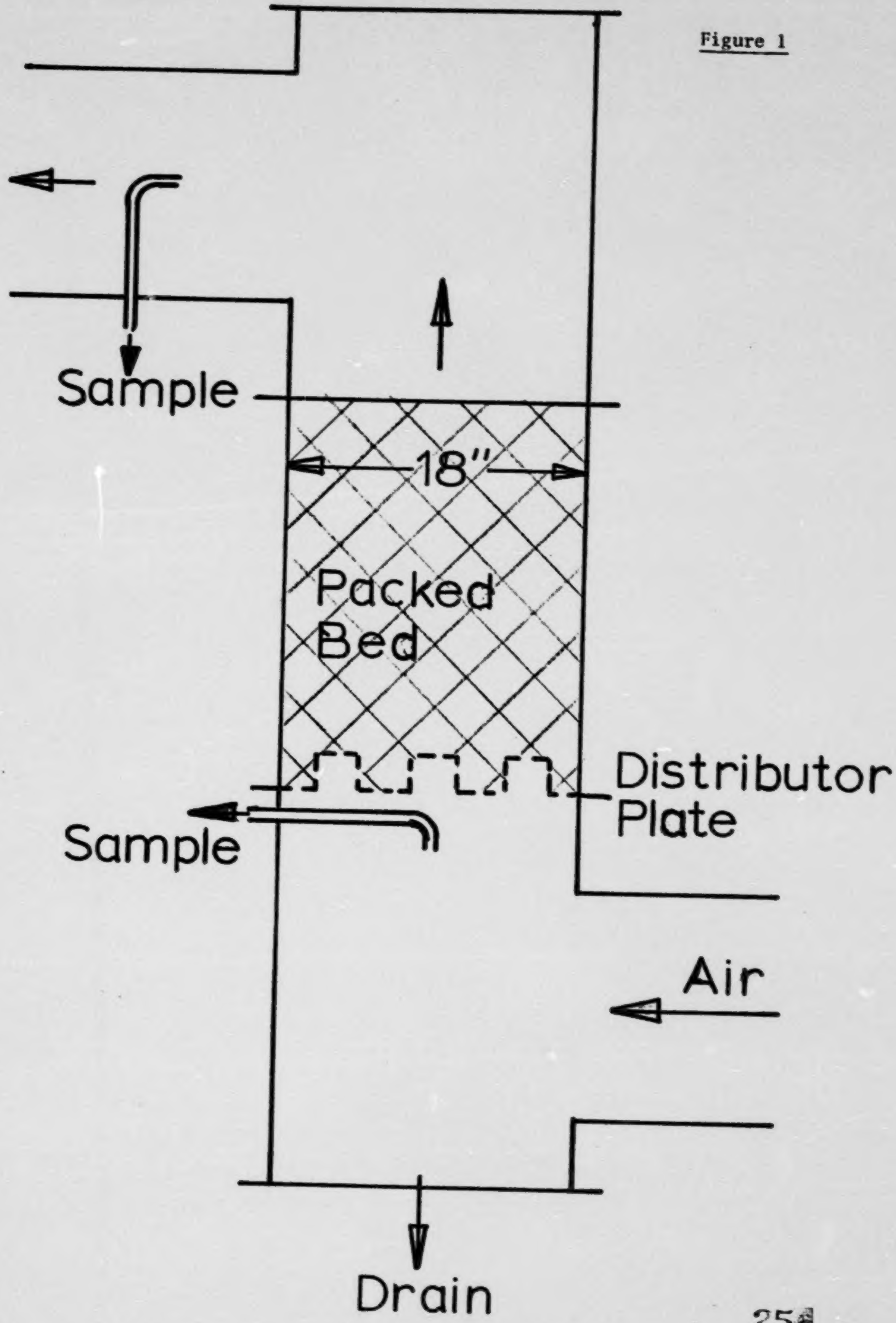
Sample
18"
Packed Bed
Distributor Plate
Sample
Air
Drain

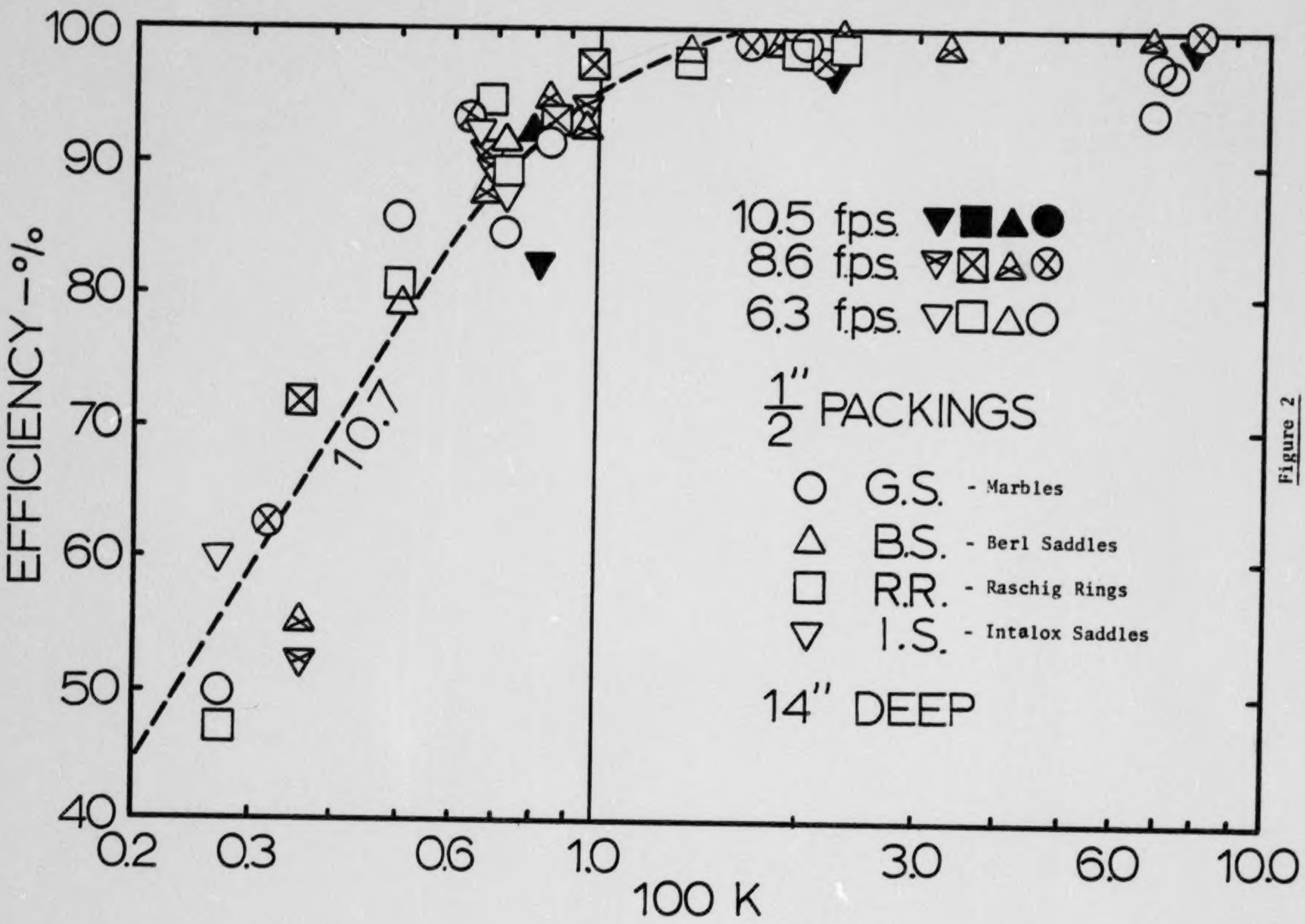
EFFICIENCY – %
100
90
80
70
60
50
40
0.2
0.3
0.6
1.0
3.0
6.0
10.0
100 K
10.7
10.5 f.p.s. ▼■▲●
8.6 f.p.s. ⊽⊠⧋⊗
6.3 f.p.s. ▽□△○
$\frac{1}{2}$" PACKINGS
○ G.S. - Marbles
△ B.S. - Berl Saddles
□ R.R. - Raschig Rings
▽ I.S. - Intalox Saddles
14" DEEP

Figure 2

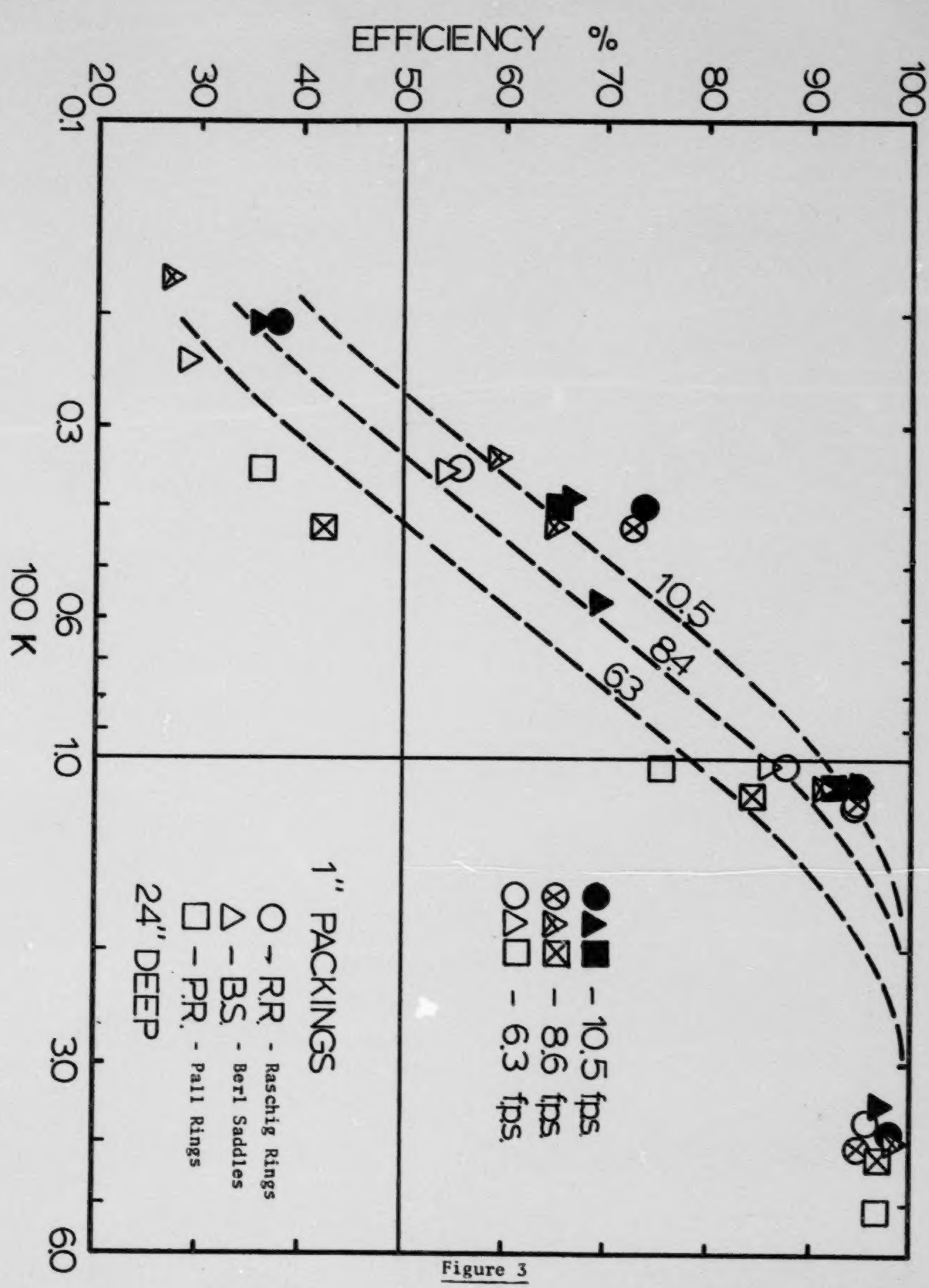

EFFICIENCY %
100
90
80
70
60
50
40
30
20
0.1
0.3
0.6
1.0
3.0
6.0
100 K
10.5
8.4
6.3
●▲■ - 10.5 fps.
⊗⊠ - 8.6 fps.
○△□ - 6.3 fps.
1" PACKINGS
○ - R.R. - Raschig Rings
△ - B.S. - Berl Saddles
□ - P.R. - Pall Rings
24" DEEP

Figure 3

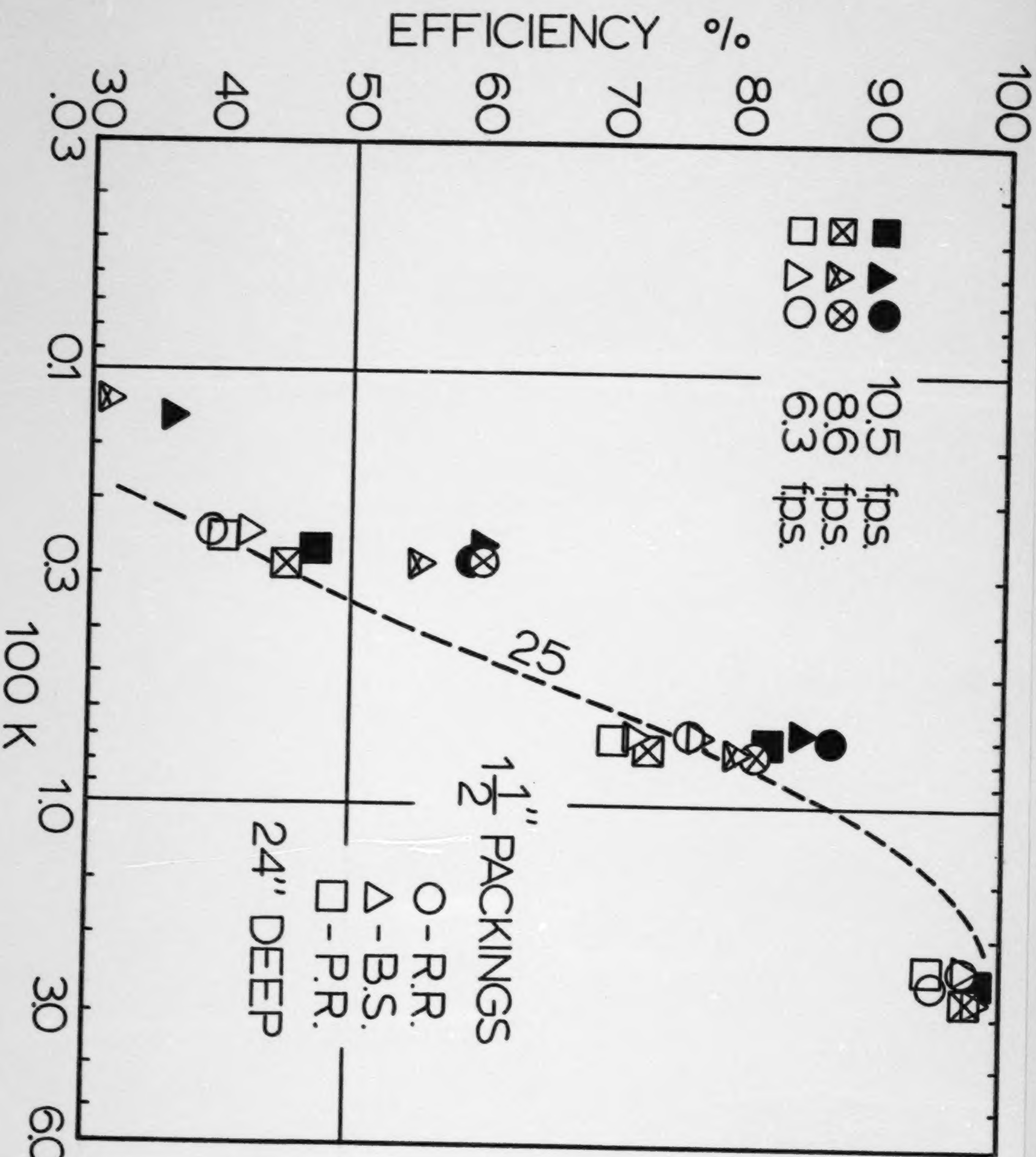
EFFICIENCY %
100
90
80
70
60
50
40
30
.03
0.1
0.3
1.0
3.0
6.0
100 K
■ ▲ ● 10.5 fps.
⊠ ⚠ ⊗ 8.6 fps.
□ △ ○ 6.3 fps.
25
1 1/2" PACKINGS
○ - R.R.
△ - B.S.
□ - P.R.
24" DEEP

Figure 4

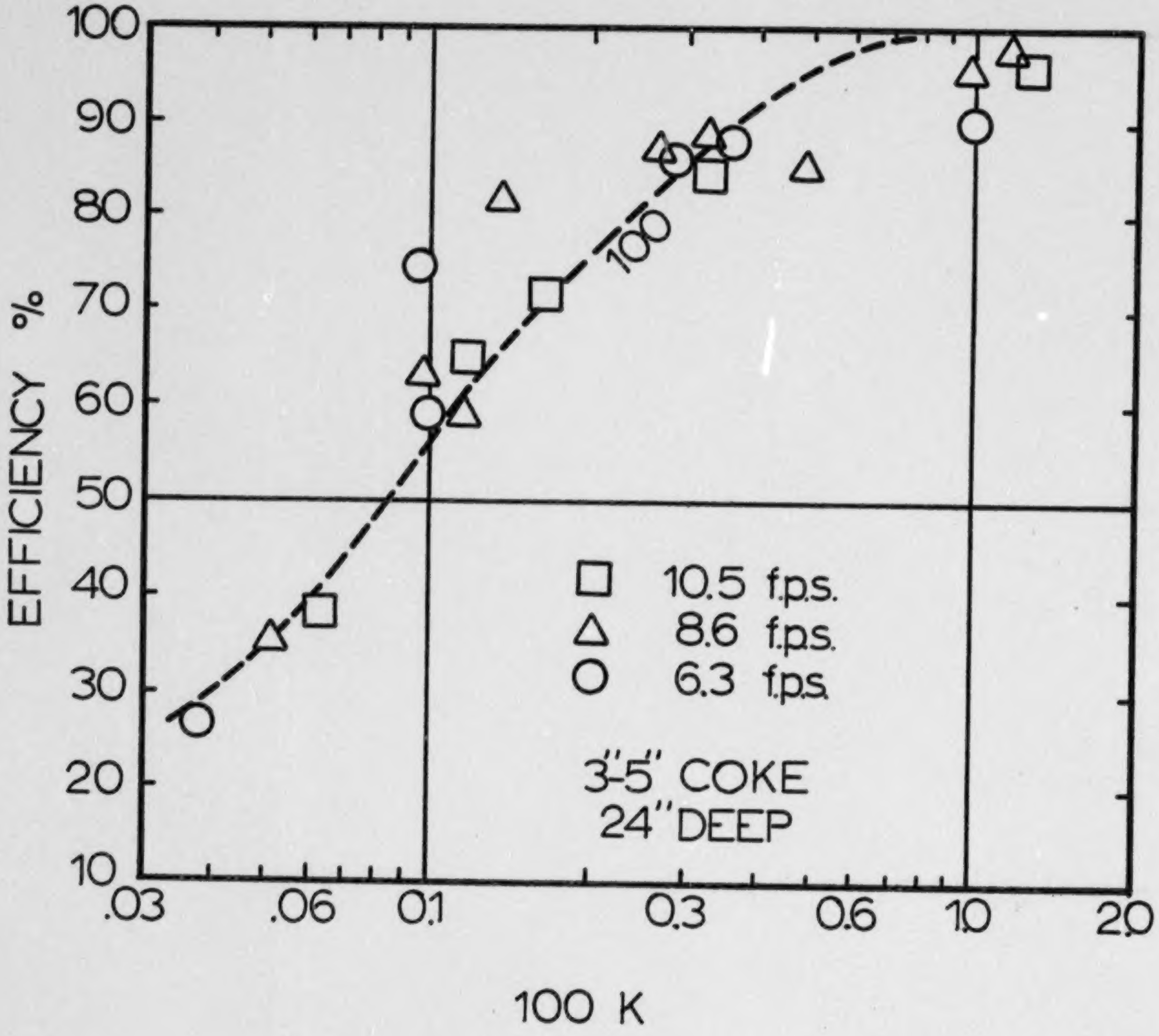
EFFICIENCY %
100
90
80
70
60
50
40
30
20
10
.03
.06
0.1
0.3
0.6
1.0
2.0
100 K
100
□ 10.5 f.p.s.
△ 8.6 f.p.s.
○ 6.3 f.p.s.
3"-5" COKE
24" DEEP

Figure 5

APPENDIX 4

A Technique for Determining Penetration as a Function of Particle Diameter

By: Mansoor Taheri, Seymour Calvert and Richard Barton

Research in behavior of aerosols requires changes in concentration of particles of uniform size, produced by a device or lapse of time, to be measured. Quite often these changes in particle concentration are difficult to determine using an absolute measure of the particle concentration. If monodisperse aerosols are used the absolute changes in particle concentration can be determined by known techniques. However, if a heterogeneous aerosol is used the entire particle mass distribution must be determined to measure the absolute change in particle concentration. Detailed knowledge of the particle size distribution over the entire range of diameters is very difficult to obtain with present techniques.

Aerosol research often does not require the measurement of the absolute change in particle concentration. In many instances the ratio of final concentration to the initial concentration (known as penetration) is sufficient to provide valuable data on hehavior of particles of different sizes. With a monodisperse test aerosol one can determine the penetration for a specific diameter. A heterogeneous aerosol provides a continuous distribution of particle size and the penetration can be determined over a particle size range from the observed particle mass distribution. The method described here has been developed to determine penetration as a function of diameter from the initial and final mass distributions.

A Goetz Aerosol Spectrometer (G.A.S.) was used to obtain the necessary data for determining the penetration as a function of particle diameter. This technique, which does not require the determination of the actual mass distribution, was verified by comparing the heterogeneous aerosol results with the results obtained using a monodisperse aerosol.

I. DERIVATION OF PENETRATION

General Principle

Hetrogeneous aerosol can be described by a frequency distribution $f_m(D)$ of the particle mass in the aerosol. The mass distribution can be determined by the functional relationship

$$\Delta F_m(D) = F_m(D_2) - F_m(D_1) = \int_{D_1}^{D_2} f_m(D)\, dD \qquad (1)$$

where $F_m(D)$ is the mass of particles smaller than D, $f_m(D)$ is the frequency distribution of the particle mass and D is the particle diameter.

Equation I in differential form is $d_m(D) = f_m(D)\, dD$. Penetration is defined as the ratio of final mass to the initial mass for a homogeneous aerosol and for a heterogeneous aerosol it is defined functionally as:

$$\left[F_m(D_2) - F_m(D_1)\right]_f = \int_{D_1}^{D_2} P(D)\, f_m(D)_i\, dD \qquad (2)$$

Equation 2 in differential form is

$$d F_m(D)_f = P(D)\, f_m(D)_i\, dD \qquad (3)$$

since $(fm(D)_i\, dD = dF_m(D)_i$

the penetration can be defined as

$$P(D) = \frac{[dF_m(D)]_f}{[dF_m(D)]_i} \tag{4}$$

Penetration in terms of derivative can be found by dividing numerator and denominator by dD

$$P(D) = \left[\frac{dF(D)}{dD}\right]_f \Big/ \left[\frac{dF(D)}{d(D)}\right]_i \tag{5}$$

or equation 5 describes the penetration, as the ratio of the final cumulative mass distribution curve slope to the initial mass distribution slope.

Application to the G.A.S.

The determination of initial and final size distribution is often inaccurate or involves a long and tedious analysis. The method developed by us using the G.A.S. to determine the ratio of slopes of cumulative curves eliminates many of the difficulties. This method will be discussed in more detail following a brief description of the G.A.S.

II. DESCRIPTION OF GOETZ AEROSOL SPECTROMETER

The Goetz Aerosol Spectrometer is described in References 1-4. It is an instrument which applies a high centrifugal force to a continuous laminar flow of aerosol and the particles of the aerosol are forced to settle out onto a foil or filter paper at positions depending on the centrifugal force and aerodynamic drag.

The high centrifugal forces and the laminar flow are created by rotating a conical rotor which has helical channels on the outside. The helical channels are rectangular in cross-section and the outer wall is formed by the inner surface of a tightly fitting detachable cup. The cup is lined with a removable filter paper or foil onto which the particles are deposited.

The deposition of particles on the outer wall is continuous. All particles are deposited along the wall until a distance is reached along the channel, referred to as the cut-off length, where the last particles of a given size have deposited. The larger particles are precipitated close to the channel entrance while successively smaller particles are precipitated at successively greater lengths from the channel entrance. The deposit yields a continuous band-shaped deposit(Fig. 1) which can be analyzed to determine the size distribution of the aerosol.

A unique feature of the process is that particles of a given diameter are uniformly deposited along the deposit length until the cut-off length is reached. This characteristic has been verified experimentally using polystyrene beads of a given diameter. Ref (3).

A more complete description of the instrument and the methods of analyzing the deposit can be obtained by referring to the references cited.

Mathematical Derivation

The G.A.S. precipitates particles of a given diameter from a heterogeneous aerosol continuously and uniformly until the cut-off length is reached. This unique feature means that any change in the total mass density, M_t, (mass or number per unit area) along the deposit area must be equal to the mass density of particles of diameter corresponding to the deposit area or in functional notation.

$$\Delta G_M(D) = G_M(D_2) - G_M(D_1) = \int_{M_{t1}}^{M_{t2}} A \, dM_t \qquad (6)$$

where $G_M(D)$ represents the total mass of particles smaller than D deposited on the foil, M_{t1} and M_{t2} are the corresponding mass density at D_1 and D_2 and A is the total deposit area. Due to leakage around the bearing and losses on the wall, $\Delta G_M(D)$ represents only a fraction E, of actual mass which is represented by $\Delta F_m(D)$

$$\text{or} \quad \Delta G_M(D) = \int_{M_{t1}}^{M_{t2}} A \, dM_t = \int_{D_1}^{D_2} E \quad f_m(D) \;\; dD \tag{7}$$

where E as reported by (4) is a function of diameter and operating conditions Equation 7 in differential form is

$$dG_M(D) = AdM_t = E \; (f_m \; (D) \; dD) = E \; (dF_M \; (D)) \tag{8}$$

upon substitution in equation 4 for dF_M (D), one obtains

$$P(D) = \frac{[AdM_t/E]_f}{[AdM_t/E]_i} \tag{9}$$

If the G.A.S. is operated under the same conditions for final and initial sampling, A and E would be the same and they cancel each other, or

$$P(D) \overset{=}{=} \frac{(d \; M_t)_f}{(d \; M_t)_i} \tag{10}$$

Penetration in terms of derivative can be found by dividing numerator and denominator by dD or

$$P(D) = \frac{\left(\frac{d \; Mt}{dD}\right)_f}{\left(\frac{d \; Mt}{dD}\right)_i} \tag{11}$$

or penetration is the ratio of final cumulative mass density slope to the initial cumulative mass density slope.

Possible Errors

The primary sources of errors which have a first order effect are listed below:

1) Air leakage and particle loss on the walls from the sample aerosol which does not pass through the helix and thus only a fraction of the total aerosol is deposited on the foil. This fraction, which is a function of operating condition and diameter, was taken into account by introducing a factor E in equation 7, and it was indicated that it does not affect the final results.

2) The entrance length of the G.A.S. causes a loss in concentration and a non-uniform deposit on the first 5 cms of the deposit length. Also secondary flow developed by the channel curvature cause a non-uniform deposit over the last 5 to 10 cms of the deposit length. In order to avoid these errors, the analysis of the deposit area was restricted to the interval of length between 5 and 35 cms.

Experimental Procedure

The practicality of the outlined method depends on the accurate control and measurement of the following parts:

1. Constant sampling rate at the initial and final period.

The sampling rate to the G.A.S. could change due to change of static pressure, which in turn changes the deposit length and calibration curves. In order to avoid this problem the flow rate to the G.A.S. was measured by determining its pressure drop through a 3/16" dia. straight tube and then controlled by adjusting the static pressure.

2. Reproducibility of the cutting area and determination of the mass per unit area.

This is accomplished by cutting 15 to 20 circles of approximately 1/4" diameter by an ordinary paper punch along the center of deposit length (Figure 1). Since all of these circles have the same size, the absolute area of the circle in the final calculation cancels out; therefore, the area of the circle could be considered as a unit area.

The subsequent determination of the mass on each circle by colorimetric, chemical, or any other tracer technique represents total mass per unit area M_t, at that particular cut off diameter. Figure 2 represents cumulative mass density curves for initial and final sampling period. Necessary corrections must be made in special cases when the total sampling time at the initial and final period are not the same or the concentration through out the test is not constant.

Evaluation of the Slopes from Experimental Data

The slope, $\frac{dMt}{dD}$, can be determined using graphical or numerical procudures. The authors found that graphically determining the slopes provided adequate values for the collection efficiency if the slopes were not close to the same value. A numerical procedure, using the Gregory Newton forward and backward differences and Gauss forward interpolation formulas, were used to determine the slopes. The graphical and numerical methods agreed with each other. The numerical procedure gives a better resolution of the collection efficiency when the inlet and outlet slopes are near the same value.

A description of the numerical procedures can be found in Reference (5).

Experimental equipment

In order to evaluate the above technique, the collection efficiency of a foam column was examined for particles of below 3.0 microns and the results were verified using a light-scattering technique and polystyrene beads. Foam was produced on a sieve plate column by bubbling air through demineralized water on the sieve plate. The aerosol generator consisted of a round flask 1000 ml. capacity which contained a solution of methylene blue and an atomizer. The rate of aerosol generation was controlled within 5% by controlling the air flow rate, pressure, solution concentration and level. The droplets of methylene blue which were formed by atomization were dried to solid particles of methylene blue and after mixing with the main stream of air introduced at the bottom of the column. Samples were taken for the same amount of time from the inlet and outlet of the column.

Analytical method

Methylene blue was extracted from each circle by methanol. After a few minutes when the methylene blue was extracted completely, the solution was analyzed by a Bausch and Lamb spectronic 20 colorimeter. This instrument at a wave length of 660 mμ required a sample in order of 10^{-5} to 10^{-6} gms which was collected on the circle area within 30 to 60 mins.

Results and Conclusions

Experimental verification of the methods described were obtained using foam as a particle collector. The collection efficiency of the foam was determined using the G.A.S. and dye aerosol. Verification was obtained using polystyrene beads and a lighting scattering system.

The collection efficiency using both methods is shown in Figure (3), plotted against particle diameter. Agreement between the two methods was obtained between particle diameters of 0.09μ and 3.0 microns.

The experimental data obtained indicated limitations in analysis of the deposit. The deposit length gives accurate concentration results only for deposit lengths between 5.0 and 35.0 cm. The extremes of the deposit length give inaccurate deposit concentrations because of entrance affects and secondary flows. Collection efficiency at small diameters (0.1μ) are difficult to obtain because the concentration of heterogeneous aerosols in this range are small. This requires either a size distribution with a small mean or a sampling time that is very long for both at the initial and final sampling of the aerosol.

The advantages of using the G.A.S. in obtaining penetration are evident. The method reduces the number of experiments to determine the monodisperse collection efficiency. The instrument allows one to investigate both the diffusion controlling and impaction controlling regions of the gas cleaning simultaneously. The diameter corresponding to minimum collection efficiency can be determined accurately from one experiment.

The financial support of this research work by a U. S. Public Health Service Air Pollution Division grant is gratefully acknowledged.

References:

1. Goetz, A. Journal of Air Pollution Control Association, 12, 479-486, 1962.
2. Goetz, A. IBID, 14, 213-219, 1964.
3. Goetz, A. and Preining, O. The Aerosol Spectrometer and its Application to Nuclear Condensation Studies, "American Geophysical Union" "Physics of Precipitation" Geophysical Monograph No. 5, NAS-NRC-NO. 746, 164-182, 1960.
4. Muller, D., et.al. Some Performance characteristics of the Goetz Aerosol Spectrometer "Model D" Proceedings of the 52nd annual meeting, APCA, Los Angeles, Calif., June 1959.
5. Kunz, K. S. Numerical Analysis, McGraw-Hill Book Company, Inc., New York, New York, 1957.

Nomenclature

A	Total area of deposit
D	Particle diameter
E	Collection Efficiency = (1 - P(D)
$F_m(D)$	Total Mass of Particles smaller than diameter D
$f_m(D)$	Frequency distribution of the particle mass
$G_M(D)$	Total mass of particle smaller than diameter, D deposited on the foil.
M_t	total mass per unit area
P(D)	Penetration, ratio of the outlet concentration to the inlet concentration

Subscripts:

i, refers to initial

f, refers to final

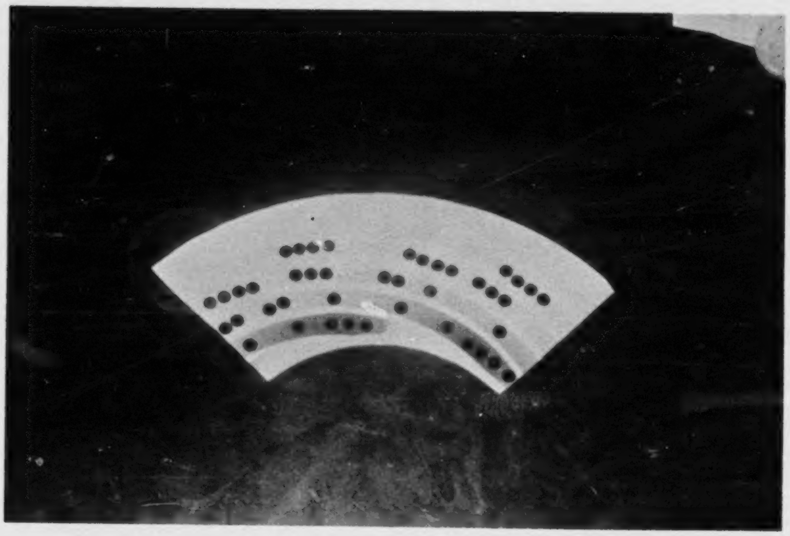

AEROSOL SPECTROMETER FILTER WITH SIZE CLASSIFIED DEPOSIT OF METHYLENE BLUE

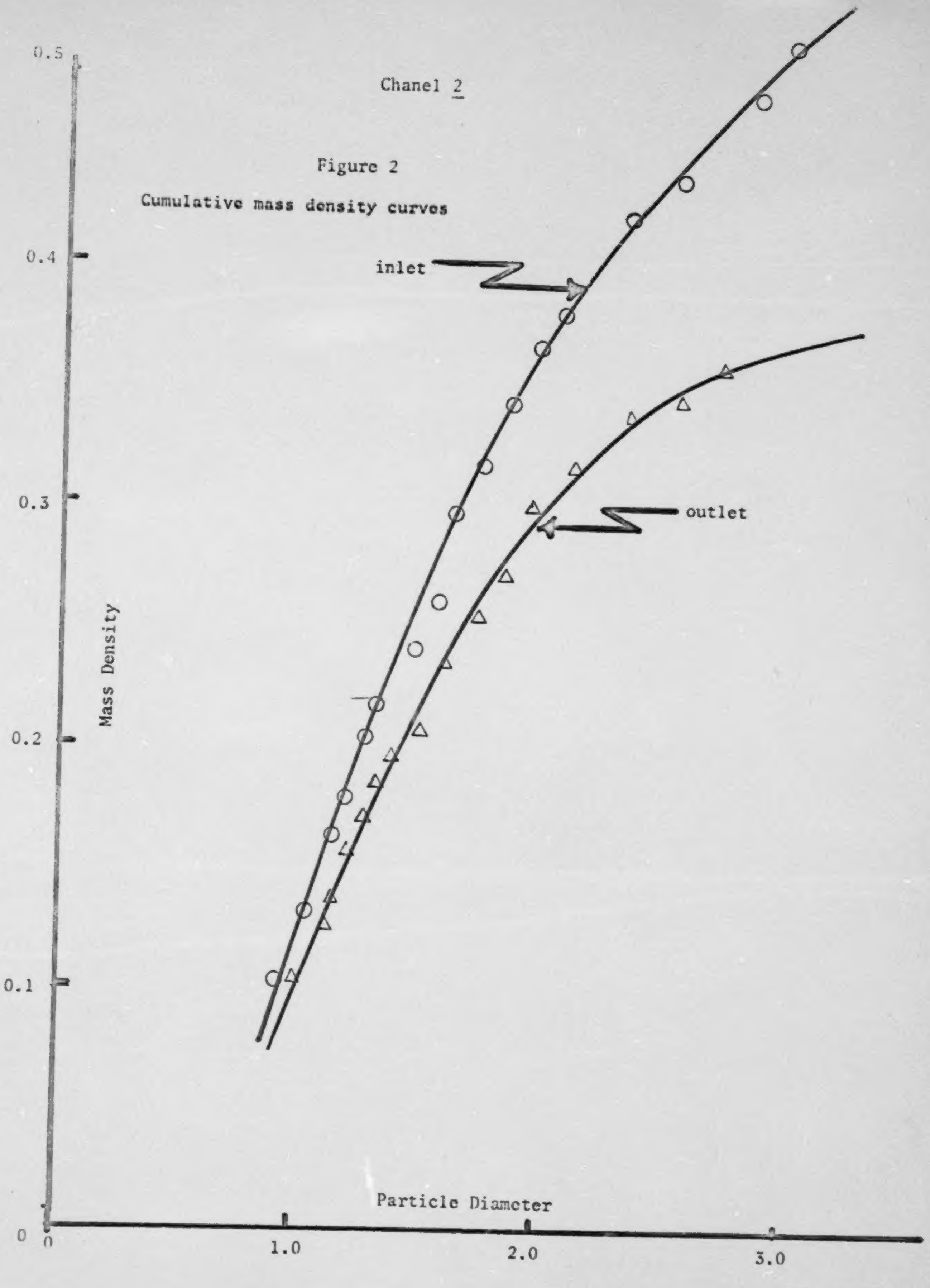

Figure 2

Cumulative mass density curves

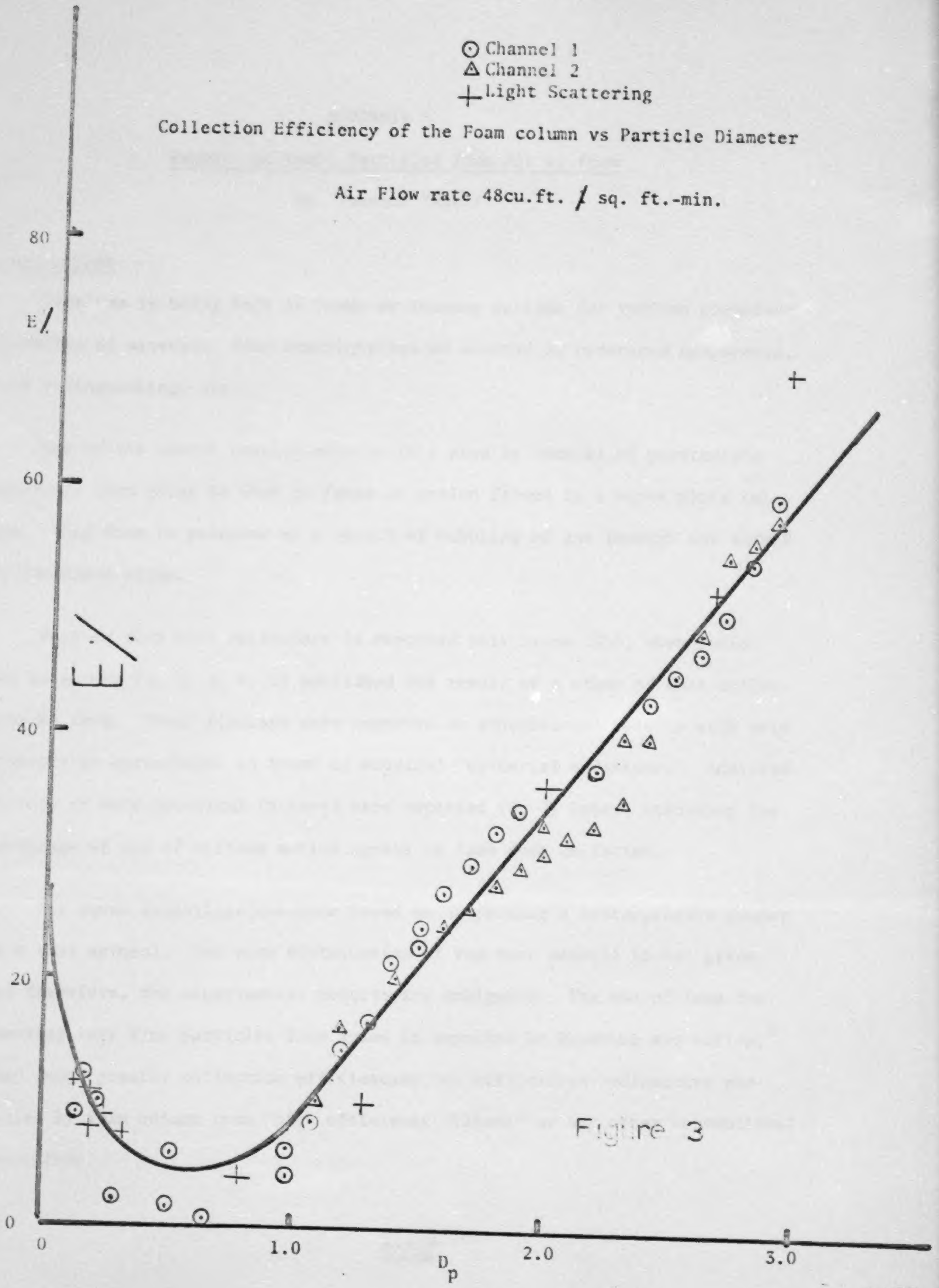

Collection Efficiency of the Foam column vs Particle Diameter

Air Flow rate 48cu.ft. / sq. ft.-min.

Figure 3

APPENDIX 5

Removal of Small Particles from Air by Foam

by Mansoor Taheri

Introduction

Wide use is being made of foams or foaming systems for various purposes: flotation of minerals, foam fractionation of desired or undesired components, fire extinguishing, etc.

One of the recent developments in this area is removal of particulate materials from gases by foam or froth in motion formed in a sieve plate column. This foam is produced as a result of bubbling of gas through the liquid on the sieve plate.

Work on foam dust collectors is reported only since 1955, when Pozin and Co-author (1, 2, 3, 4, 5) published the result of a study of dust collection by foam. Their findings were reported as experimental results with only attempts at correlation in terms of emprical "criterial equations." Additional data of only practical interest were reported (6, 7) later, stressing the advantage of use of surface active agents in foam dust collector.

All these investigations were based on dispersing a heterogeneous powder as a test aerosol. The size distribution of the test aerosol is not given and therefore, the experimental results are ambiguous. The use of foam for removing very fine particles from gases is reported by Browning and Ackley.[8] They found greater collection efficiencies for millimicron radioactive particles by foam column than "high efficiency filters" or any other conventional collectors.

Objective and Scope of the Present Work.

The collection efficiency of the foam and froth layer for particles with a well defined size distribution has not been reported in the literature. This is particularly true in the case of particulate materials below 3.0 microns. This size range is of most practical interest because of the difficulty of removal by ordinary mechanical collectors. This size range is interesting from a study point of view, too, because the particle diameter does not overshadow the effect of other variables, it is possible to study the influence of various physical parameters on collection efficiency more thoroughly than in the case of larger particles.

The objective is therefore, to study and analyze the mechanisms of removal of small particles (below 3.0 microns) from air by foam. The experimental work is directed toward collection of necessary data required to evaluate the mechanisms and solutions suggested to this problem. These mechanisms which are considered to be important for removal of this size range particles are as follows:

1. Inertia, mainly for particles larger than 1.0 microns.
2. Diffusion, mainly for particles smaller than 0.3 microns.

The variables considered to be important in the study of above mechanisms are as follows:

1. Particle diameter - density (Stokes' diameter).
2. Air flow rate - water flow rate.
3. Sieve plate geometry (preforation diameter and percentage of free area).
4. Foam height.

When a particle reaches to the liquid surface, the interaction of particle surface with water play an important role on the collection

Reproduced from best available copy.

efficiency. If the interfacial is low, the particle will tend to be wetted and collected by the liquid. If a high interfacial tension exists, the particle might not penetrate enough into the liquid and bounce back to the air. The surface property will be taken into account by studying the effect of liquid surface tension on collection efficiency.

By studying these variables it should be possible to determine the collection efficiency of the foam column as a funtion of its operating condition.

Accomplishment.

Proposed Mathematical Model

In order to estimate the effect of different variables discussed in the preceding section, it is possible to set up a model of the collection mechanism and to represent it in mathematical term. This will be discussed first, then the prediction will be compared with the experimental data to evaluate the proposed models.

The foam apparatus may be regarded as a two stage dust remover which includes:

a. Collection on the liquid during the formation of the bubbles.

b. Collection on the bubble walls after formation of the bubbles.

In the first stage during formation of the bubbles, the initial situation is similar to the impaction from a jet against a flat plate. However, this plate or in our case the bubble wall continuously changes its shape until the bubble is formed. The major collection mechanism is that due to the centrifuge effect of the air flowing within the circular path during formation of the bubbles. In this stage the particles will move radially outward under the centrifugal force equal to the opposing fluid drag force. Those particles which move far enough will strike the bubble walls and if they penetrate into the liquid, they presumably will be collected.

In setting up this mathematical model, the following assumptions are made:

1. The particles obey Stokes' law.
2. The air flow from the jet is divided into eddies confronting to the inner face of the bubble.
3. The thickness of these eddies along the inner face of the bubble remains constant.
4. The tangential velocity of the air flowing within the circular path remains constant and equal to the V_o, the jet velocity.

Based on the above assumptions, one obtains the collection efficiency as a function of size parameter.[9]

$$E = F \ (2\pi n)^{1/2} \ (\rho_p \ V_o/18\mu_g \ D_c)^{1/2} \ D_p \qquad (1)$$

where n represents the number of revolutions in contact with the bubble wall.

ρ_p = particle density

V_o = gas velocity in impaction process

D_c = the thickness of streams confronting bubble wall = K do

d_o = perforation diameter

D_p = particle diameter

Among the above variables D_p, ρ_p, V_o, d_o, and μ_g are physically measurable. However, in order to predict the collection efficiency and evaluate the above model, the ratio of $\frac{n}{D_c}$ or $\frac{n}{K}$ must be known. This ratio can be estimated by determining the collection efficiency experimentally where the other variables are known. When this ratio, at a particular run for a known particle diameter is determined, the collection efficiency due to inertia mechanism can be predicted and compared with the experiemtnal values for the entire size range of particles.

Collection After Formation of the Bubble

When the bubble is formed, because of the diffusional mechanism, particles move radially to the surface of the bubble. Those particles which strike the bubble wall will be absorbed and become part of the wall. Therefore, we can assume the concentration at the wall remains constant and equal to zero.

In setting up this model one can approach the problem based on one of the following assumptions:

1. Air inside the bubble is stagnant.
2. Circulation of air inside the bubble continues after the bubble is formed.

We shall consider these two models separately.

Bubble with Stagnant Air

If we consider the bubble as a sphere and we restrict ourselves to the case in which the diffusion is radial, we can write:

$$\frac{\partial c}{\partial t} = D \left(\frac{\partial^2 c}{\partial r^2} + \frac{2}{r} \frac{\partial c}{\partial r}\right) \qquad (2)$$

c is concentaation at the point r from the center of the bubble at time t.

D is the diffusivity coefficient for the particles and is given by the following equation:

$$D = \frac{RT}{N} \frac{1}{3\pi\mu D_p} \tag{3}$$

The solution of the above differential equation is given by:[10]

$$\text{Efficiency} = E_1 = \frac{M_T}{M_\infty} = 6 \left(\frac{Dt}{R^2}\right)^{1/2} \{\pi^{-1/2} + 2\sum_{n=1}^{\infty} \text{ierfc} \frac{nR}{Dt}\} - \frac{3DT}{R^2} \tag{4}$$

Error function for the value of above, 5 is in order of 10^{-5} and it is not listed in the ordinary mathematical table. Since this value compare to $\pi^{-1/2}$ is negligible, we can write:

$$E = 6 \left(\frac{Dt}{\pi R^2}\right)^{1/2} - \frac{3Dt}{R^2} = 6 \left(\frac{Dt}{\pi R^2}\right)^{1/2} \tag{5}$$

Second term in the above equation was omitted because D is in order of 10^{-5} - 10^{-6} cm^2/sec. Some prediction with various residence time and bubble diameter are listed in table 1. As it is shown the contribution of diffusion according to this model in most cases is negligible.

Bubble with Circulating Air

For this model it is assumed that the inside mass transfer coefficient of the bubbles (the gas phase coefficient) can be described in terms of the Highie Penetration Theory.

$$\frac{dc}{dt} = -Kg \frac{A_b}{V_b} C_b \tag{6}$$

TABLE 1: Diffusional Collection as a Function of Bubble Diameter, Particle Size, and Residence Time.

Bubble Diameter = 1.25 cm.   Diameter = 0.8 cm.   Diameter = 14 cm.

Time Sec.	D_P 0.05	0.1	0.2	0.05	0.1	0.2	0.05	0.1	0.2
0.1	0.625	0.441	0.312	0.995	0.704	0.497	3.98	2.8	1.97
0.2	0.885	0.625	0.443	1.41	0.995	0.704	5.65	3.99	2.81
0.5	1.40	0.99	0.70	2.23	1.58	1.12	8.9	6.27	4.32
1.0	1.98	1.40	0.99	3.16	2.23	1.58	12.6	8.86	6.25
5.0	4.42	3.12	2.21	7.05	4.97	3.52	28.5	20.2	14.2
10.0	6.25	4.41	3.12	9.95	7.04	4.96	39.8	28.0	19.8

Diffusivities of particles of various diameters are as follows:

Particle Diameter D_p microns	D sq. cm./sec.
0.05	1.4×10^{-5}
0.1	7×10^{-6}
0.2	3.5×10^{-6}

$$Kg = 2\sqrt{\frac{D}{\pi\theta}} \tag{7}$$

If θ, the surface renewal time is taken as the time required for the air to circulate half a turn, then:

$$Kg = 2\sqrt{\frac{D}{\pi}\frac{}{(\frac{\pi R}{\gamma})}} = \frac{2}{\pi}\sqrt{\frac{D\gamma}{R}} \tag{8}$$

Upon substitution into equation 5:

$$\frac{dc_b}{dt} = \frac{-2}{\pi}\sqrt{\frac{D\gamma}{R}}\;\frac{4\pi R^2}{4/3\pi R^3}\;c_b = \frac{-6}{\pi R}\sqrt{\frac{D\gamma}{R}}\;c_b \tag{9}$$

or

$$\text{in}\;\frac{c\ \text{final}}{c\ \text{initial}} = \frac{-6}{\pi R}\sqrt{\frac{D\gamma}{R}}\;t \tag{10}$$

$$\frac{c\ \text{final}}{c\ \text{initial}} = \exp\frac{-6}{\pi R}\sqrt{\frac{D\gamma}{R}}\;t \tag{11}$$

$$E_1 = 1 - \exp\left(-\frac{6}{\pi R}\sqrt{\frac{\Gamma\gamma}{R}}\;t\right) \tag{12}$$

Where E_1 represents the fraction of removal due to diffusion.

R = bubble diameter

t = residence time of the bubble

γ = circulating velocity of air inside the bubble

Both diffusional models predict higher collection efficiency for smaller bubble, finer particles (larger diffusion coefficient) and longer residence time. Results obtained by the second model depends upon the circulation velocity of air is up to 10 times higher than the results obtained by the stagnant model.

It is worth noting that the major contributor to the collection efficiency during formation of the bubble was considered to be inertial mechanisms and after formation of the bubble was considered to be diffusional mechanism. However, the models are sufficiently generalized that they are not restricted to the situation during formation of the bubble or after formation of the bubble.

The overall collection efficiency of the foam is determined by the sum of fractional removal due to inertial mechanism and fractional removal due to diffusional mechanism. For larger particles, contribution due to diffusion is negligible while for very fine particles contribution due to inertia is negligible. This suggests the existance of a minimum in efficiency versus particle diameter curve. This minimum appears because for the inertial mechanism, efficiency is a function of $D^2{}_pV$, while in the diffusional mechanism efficiency is a function of tD or $\frac{1}{VD_p}$.

Surface and Interfacial Effect

The theoretical solutions of collection efficiency discussed in the preceding section all assumed that every particle that hits the liquid surface will stick to it. However, in the presence of high interfacial tension this may not be true. The effect of surface property on collection efficiency will be considered when its influence has been determined.

Equipment

The study of collection efficiency by foams presents the following requirements:

1. A means of producing dynamic foam.
2. A means of accurately controlling and measuring the important physical parameters which affect the formation of foam.
3. A means of producing an aerosol with uniform size distribution and concentration throughout the tests.

Figure 1 is a diagram of the experimental set-up, which is composed of the following parts:

a. Foam apparatus

Foam is generated on a sieve plate 3" x 3" in a vertical plexiglass column, 4 feet long. The output of the aerosol generator is mixed with a stream of filtered air and introduced to the bottom of the column. This air is bubbled through demineralized water on the sieve plate which is continuously supplied from a constant head tank. Two overflow tubes located 3" above the sieve plate continuously remove the overflow water. In the present column the overflow tubes are located at a fixed point above the sieve plate.

The design and construction of a new foam column has been completed with the variable weir height. The main feature of this 2" glass column is a nipple stock inside a 6" x 2" reducer. This straight section is sealed with an 0" ring inside the larger flange of the reducer and can be easily changed with the nipples of various sizes.

b. Aerosol generator

At the beginning of this study a dust feeder was developed and used to disperse different types of powders. The results obtained by this system are listed in tables 2, 3, and 4. These exploratory trials indicated that the effect of air flow rate and water flow rate on collection efficiency was very little. This suggested that the quality of the test dust should be controlled very accurately in order to study the effect of other variables. Because this was not possible in the case of dry dust, the use of a different technique was considered to produce aerosol. This technique utilizes a modified "Collision Atomizer" which produces a relatively narrow size distribution of methylene blue aerosol from a methylene blue solution. This aerosol generator consists of a round flask 1000 ml. capacity, which contains the solution and atomizer. The atomizer is a unit of three ejectors with the following critical dimensions:

Jet diameter 0.0135 in.(drill number 80)
Solution feed pipe diameter 1/16 in.

The air flow to the atomizer is measured by a rotameter and the air pressure to the atomizer is controlled by a pressure regulator. The concentration and the level of the solution is adjusted after each run by adding a proper amount of the diluted solution.

The droplet of the methylene blue solution which is formed by atomization, are dried to solid particles of methylene blue by passing through a heated 2" diameter long tube and mixing with a stream of relatively dry air.

This aerosol is then mixed with the main stream of air and introduced to the bottom of the column.

c. Sampling system

After the aerosol is generated and dispersed into the air, it is then necessary to determine its concentration at the inlet and outlet of the column. The inlet and outlets are sampled by using glass sample tubes connected with milipore filters. Analysis of the filter for the test aerosol along with the air flow through the filter makes it possible for the concentration of the aerosol to be calculated. Sampling unit consists of a vacuum pump. two rotameters with critical orifice, and 1" diameter filter holders. Two magnehelic differential pressure gauges measure the pressure drop across each filter. Filters with a crack, which indicate very low pressure drop are discarded. In the case of methylene blue as a test aerosol, the concentration in the water is determined by analyzing a sample from the overflow tubes. When these concentrations are determined, the collection efficiency of the foam apparatus is obtained by using the following relationships.

$$\text{Collection efficiency} = \frac{\text{amount collected in the water}}{\text{total amount of tracer in the input feed}} =$$

$$\frac{\text{Inlet concentration - outlet concentration}}{\text{inlet concentration}}$$

d. Analytical method

1. The overall collection efficiency for heterogeneous aerosol.

   a. Dry dust

The collection efficiency for the dry dust as a test aerosol was obtained by weighing the filters at the inlet and outlet of the foam apparatus. In order to collect enough powder on each filter, the inlet and outlet were sampled between 1/2 - 1 hour with a rate of 5 L.P.M.

b. Methylene blue aerosol

Methanol was found to be a very good solvent for extracting methylene blue from the filter papers. After one or two minutes when the methylene blue is extracted completely, the solution is analyzed by a Baush and Lomb spectronic 20 colorimeter. This instrument at a wave length of 660 mμ requires a sample in order of 10^{-5} tp 10^{-6} gms. This total amount is collected on the filters within one to three minutes with a sampling rate of 1.0 L.P.M. The collection efficiency of the foam apparatus is determined by analyzing the concentration of methylene blue in the overflow water. Finally, the inlet-outlet and water concentrations are utilized to check the material balance.

2. Size distribution of the aerosol.

As previously mentioned, the particle size distribution of the aerosol in this study is of fundamental importance. Among the equipemtn available in the Center for Air Environment Studies, the following were tried:

a. Light microscope for dry dust and methylene blue

b. Coulter counter for dry dust

c. Cascade impactor for dry dust

d. Anderson Pipete (sedimentation method) for dry dust

e. Goetz Aerosol Spectrometer for methylene blue

Goetz was found to be the most successful instrument for determining the size distribution of methylene blue particles. In this instrument (Figure 4) particles are forced to settle out by applying a high centrifugal acceleration to a continuous laminar flow of aerosol. The air flows out along a pair of symmetrical channels represented by helical grooves on the outer surface of a rapidly turning conical rotor. The outer wall of these channels is formed by the inner surface of a tightly fitting detachable cup. This cup is lined inside with a removable filter paper or foil. According to the Stokes' law, the large particles are deposited close to the channel entrance and the cut-off for successively smaller particles lie further and further along the channel. This yields a continuous band shaped deposit which may be analyzed by the colorimetric technique. Different jets giving different flow rates, can be used in the two channels in order to resolve the end of the distribution better. In order to analyze a sample for size distribution, the density of the deposit (concentration per unit area) is determined along each channel. Since the particles of a given size are uniformly deposited along the deposit length, until they reach their cut-off point - as was shown by tests with strictly monodisperse aerosol - the mass fraction presented by the particles of a particular size class can be indicated by a rectangular field in a horizontal row (Figure 5). Details of the instrument and the analysis of a sample have been reported by Goetz[12, 13].

Procedures for Determining the Collection Efficiency for a Unique Particle Size.

The test aerosol is comprised of particles covering a range of sizes. For the purpose of analyzing and understanding the mechanism of collection efficiency, it is very important to obtain the collection efficiency for a unique particle size. Theoretically it should be possible to obtain the collection efficiency for a very narrow size range by utilizing the overall collection efficiency data, size distribution data at the inlet of the foam column and size distribution at the outlet of the column. However, in practice it was found that this method does not produce accurate results. Therefore, the technique was modified and refined as follows:

1. Instead of cutting the deposit area in 7 or 8 sections as Goetz[13] recommends 12 to 15 circles of approximately 1/4" diameter are cut with an ordinary paper puncher along the deposit area.
2. The concentration per unit area is obtained by colorimetric analysis of each sample.
3. The concentration per unit area versus diameter is plotted by using the above data for inlet and outlet.
4. As it was proved in the previous section (by M. Taheri, et al) the penetration for a particular diameter of D_p is given by the ratio of slope of outlet cumulative concentration curve to the slope of inlet cumulative concentration curve at D_p. This simple relationship proved to produce much more accurate results than the results obtained by using size distribution data.

$$E_{(D_p)} = 1 - \frac{(dc/dA)\ \text{out}}{(dc/dA)\ \text{in}} = \frac{(dc/dD_p)\ \text{out}}{(dc/dD_p)\ \text{in}} \qquad (15)$$

or $(1 - E_{(D_p)})$, penetration is given by the ratio of slope of outlet concentration curve to the slope of inlet concentration curve at A corresponding to D_p. This simple relationship proved to produce much more accurate results than the results obtained by using size distribution data.

Experimental Results

Thus far the major effort has been directed toward designing and assembling the experimental apparatus and insuring that all the components are functioning satisfactorily. All the instruments have been calibrated and the results to date are very promising.

This work was begun by obtaining some experimental data using dry dust as a test aerosol. The results are partially controversial to what has been reported in the literature. This controversy and the reason for the disagreement will be discussed first and then the results obtained by methylene blue as a test aerosol will be discussed.

Results of Collection Efficiency for Dry Dust

Several types of dry dust have been tried as follows:

1) Standardized fine air cleaner test dust. This powder after removing the fraction of the larger particles by a small cyclone separator resulted in a dust with standard deviation of approximately 1.39 and mass median diameter of 1.23 microns. Collection efficiency for this dust are shown in Table 2.

Table 2

Total Flow Rate	Jet Velocity	Inlet Sample WT mg	Outlet Sample Wt	Efficiency	Foam HT
5.8 C.F.M.	23 ft/sec	69.8	48.3	30.8	5.5"
5.8	23 ft/sec	70.1	48.0	31.4	5.5"
7.8	30.5	59.0	39.6	32.9	6.0"
7.8	30.5	53.9	37.1	31.2	6.0"

It is interesting to know that Pozin[1.2] and co-author have reported a collection efficiency of 74.1 for silica dust of in size range "below 2.5 microns." This size range can be interpreted as a test aerosol with the same characteristic that we have used. The variation in size distribution within the general class of "below 2.5 microns" probably has caused this controversy.

2- silica powder with a higher degree of purification than the standardized fine dust was ground for 5 days. A final test aerosol after removing the fraction of the larger particles was obtained with the following characteristics:

Std. dev. = 1.56

Mass median diameter = 0.6 microns

The collection efficiency of the foam apparatus using this dust as a test aerosol is reported in Table 3.

Table 3

Flow rate C.F.M.	Jet Velocity ft/sec	Inlet sample weight m.g.	Outlet sample weight m.g.	Efficiency
6.8	27.0	57.4	48.0	16.4
5.8	23.0	77.0	61.8	19.8
9.8	38.8	57.4	46.0	19.9

It is noticeable that the flow rate has not changed the collection efficiency significantly.

3) Pozin[1] reports collection efficiency of above 86˚/. for particles of larger than 5 microns. Because of the controversial results in collection efficiency for finer particles, collection efficiency of the foam apparatus was obtained for particles above 5 microns. For this purpose a sample of glass beads with the following characteristic was used as a test aerosol:

Mass median diameter 10 microns

Std. dev. 1.45

Table 4

Flow Rate C.F.M.	Jet Velocity	Inlet Wt. m.g.	Outlet Wt. m.g.	Efficiency %.
5	20	24.2	0.9	95.8
5	20	17.2	0.4	97.6
2	8	24.0	0.6	97.5
2	8	36.8	0.5	99 %

As Table 4 indicates the collection efficiency for large particles agrees with that reported by Pozin.

All the above data indicated that the effect of air flow rate and water flow rate on collection efficiency is insignificant. The second conclusion from the above study was that these effects cannot be studied unless the size distribution of the test aerosol is known accurately. Based on the above conclusions, since the size distribution of dry dust could not be controlled and measured with a desired degree of accuracy, the experiments using dry dust as a test aerosol were discontinued.

b) Results of Size Analysis and Collection Efficiency for Methylene Blue Aerosol

1) Size distribution analysis

The size distribution of methylene blue aerosol generated by atomizing a solution of methylene blue is plotted on logarithmic probability paper Figure 6. This figure which shows the size distribution of particles down to 0.1 microns was obtained by operating the aerosol spectrometer under the following condition:

Jet No.	Sampling Flow Rate L.P.M.	R.P.M.	Particle Size Range (Microns)
No esternal jet	3.7	6000	4.0 - 0.9
6	2.4	6000	3.2 - 0.68
6	5.0	12000	1.5 - 0.46
4	3.6	12000	1.0 - 0.26
3	2.9	18000	0.87- 0.17

The experimental points, especially within the overlapping region agrees with each other very good. This indicates that the results obtained by this instrument are accurate and reproducible. The mass median diameter lies between 0.85 and 0.88 microns and the geometric standard deviation lies between 2.33 and 2.27. The corresponding values obtained by a light microscope were 1.1 to 1.5 microns for mass median diameter and 1.6 to 1.9 for standard deviation. Since the limit of resolution of ordinary optical microscopy is of the order of 0.2 microns, a large number of particles which are below 0.2 microns cannot be seen under the microscope. Therefore, the results obtained by light microscope lead to a higher mass median diameter and lower standard deviation than that obtained by the Aerosol Spectrometer. This aerosol, which from the degree of finess view point can be classified within the same catagory as that of silica test dust with a mass median diameter of 0.6 microns, was used to determine the effect of air and water flow rate on collection efficiency.

2) Results of Collection Efficiency

A. Overall Collection Efficiency

The overall collection efficiency characteristics for methylene blue aerosol in the form of efficiency versus air flow rate with water flow rate as parameter are plotted in Figure 7. This figure illustrates the following conclusions:

a) The results confirm the collection efficiency data for silica test dust (Table 3). This is expected since they are both approximately within the same size range.

b) The effect of air flow rate on collection efficiency and appearance of a minimum indicates a combination of inertial mechanism and diffusional mechanism. This is further confirmed by the effect of air flow rate on collection efficiency for particles of uniform size.

c) The effect of water flow rate on collection efficiency as indicated in the case of dry dust, remains insignificant.

B. Collection Efficiency for Particles of Uniform Size

Analysis of the samples obtained by aerosol spectrometer at the inlet and outlet of the foam column produced curves of concentration per unit area versus area. The collection efficiency for each unique particle size was obtained from the ratio of slopes of these two curves. The result of such analysis for a particular run is plotted in Figure 8. The results obtained by the above technique were checked by using the light scattering method to measure the collection efficiency for polystyrene beads of 0.088, 0.126, 0.264, 0.365, 0.796, 1.3, 1.75, 2.0, 2.68, and 2.96 microns. Results are plotted in the same figure. As it is indicated, very good agreement has been obtained for particles of various sizes. The shape of this curve and existence of a minimum, confirms a combination of inertial mechanism and diffusional mechanism as it was the basis for setting up the mathematical model. Figure 9 indicates the effect of air flow rate on collection efficiency for particles of uniform size. Collection efficiency for particles of above one micron increases with increasing air flow rate. However, the change in collection efficiency due to change of air flow rate does not correspond to a change in collection efficiency in case of impaction on a solid surface. This is indicated in Figure 10, where the collection efficiency is plotted versus inertial parameter.

Figure 11 indicates the effect of perforation diameter on the collection efficiency in the case of using smaller perforation diameter for the same jet velocity the collection efficiency has decreased. This could have been caused by a corresponding decrease in the foam density.

Figure 12 indicates the effect of water flow rate on the collection efficiency for particles of uniform size. As it was indicated in the case of overall collection efficiency the effect of water flow rate on the collection efficiency is insignificant.

Figure 13 indicates the effect of surface active agent on the collection efficiency. As it is shown in this figure the collection efficiency decreases by adding surface active agent. Again in this case it could have been caused by a corresponding decrease in the foam density.

Figure 14 indicates for a proposed model of circulation inside the bubble. This figure indicates that the proposed model agrees very well with the experimental data.

Figure 15 indicates the theoretical collection efficiency for both diffusional model on log paper. As it was expected most of the data points falls somewhere in between the highest collection efficiency point corresponds to absorption of ethanol which is highly soluble by the same system.

Conclusions:

1) Particle collection by foam was shown to differ from the Russian description in the small diameter region, while being comparable at larger diameters.

2) It was shown that foam column provides a feasiable particle collector device in range of above 2 microns (with $\rho_p = 1$).

3) The particle collection in foam can be defined in terms of combination of two basic models.
    a) Inertial model
    b) Diffusional model

4) The particle collection in the foam can be predicted based on the above model with some modification for taking into account the effect of hydrodynamics (foam density, bubble size, etc.).

5) Perforation diameter - water flow rate does not have any significant effect on collection efficiency. The only effect is on the change of foam density which results to a slight change in the collection efficiency.

6) The effect of particle diameter on the collection efficiency is very significant.

7) After a certain foam height, during which the foam films are continually losing their liquid content by drainage, the foam becomes nonactive with resulting no significant change in collection efficiency with the change of foam height.

List of Symbols

A_b = Surface area of the bubble, cm^2

C = Number of particles of size D_p/unit volume of gas at a distance r from the center of the bubble, n_o/cc

D = Particle diffusivity, cm^2 $sec.^{-1}$

D_c = Characteristic dimention of inertial impactor

D_p = Particle diameter, cm

do = Perforation diameter, cm

E = Collection efficiency

K_1 = Constant, $\frac{D_c}{do}$

K_g = Mass transfer coefficient, cm/sec.

M = Mass - grams

N = Avogadro's number, 6.23 x 10^{-23} molecules - g - $mole^{-1}$

R = Bubble's radius, cm

r = Distance from the center of the bubble, cm

t = Time, sec.

V_o = Air velocity through perforation, cm/sec.

w = Mass, gm.

μ = Viscosity, poise

ρ_p = Density, gm./cm.

Bibliography

1. Pozin, M.E., etal, J. Applied Chemistry (U.S.S.R.) 28, 805-811 (1955).

2. Pozin, M.E., etal, ibid, 28, 1071-1074 (1955).

3. Pozin, M.E., etal, ibid, 1187-1189 (1955).

4. Mukhlenov, I.P., etal, ibid, 28, 877-880 (1955).

5. Pozin, M.E., etal ibid, 30, 297-302 (1957).

6. Zemshov, etal, ibid, 35, No. 11, (1962).

7. Phillips, R. A., M.S. Thesis, Northwestern University (1965), Evanston, Illinois.

8. Browning, W. E., etal, Nuclear Reactor Chemistry Report, TID-7641, U.S. A.E.C., 130-147 (1962).

9. Ranz, W. E., Engineering Research Bulletin, B-66 "Principles of Inertial Impaction, (1956), The Pennsylvania State University, University Park, Pa.

10. Crank, J. Mathematics of Diffusion, Oxford University Press, London, England (1956).

11. Green, H. L. and Lane, W. R., Particulate Clouds, Dust, Smoke and Mist, Toronto, London, New Yorkm and Princeton, N.J., D. VanNostrand Co., Inc. (1957).

12. Goetz, A., Journal of the Air Pollution Control Association, 14, 213, 219, (1964).

13. Goetz, A., ibid, 12, 479-486 (1962).

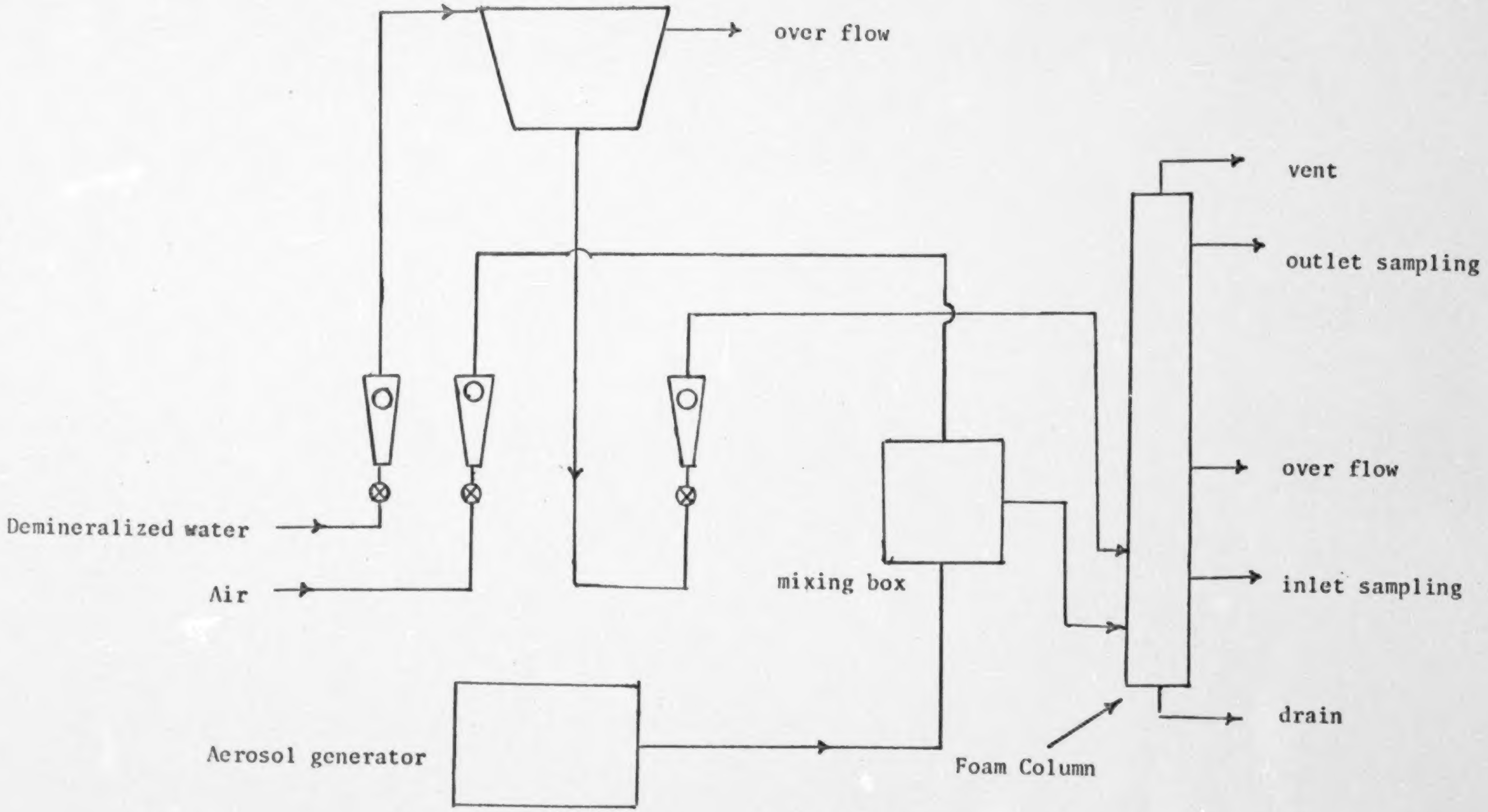
over flow
vent
outlet sampling
over flow
inlet sampling
drain
Demineralized water
Air
mixing box
Aerosol generator
Foam Column

Figure 1

Experimental Set-up

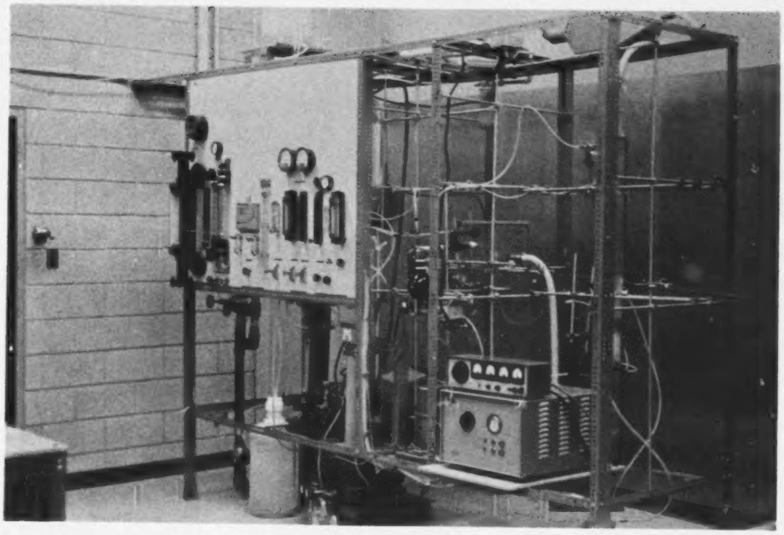

PHOTOGRAPH OF EXPERIMENTAL SET UP

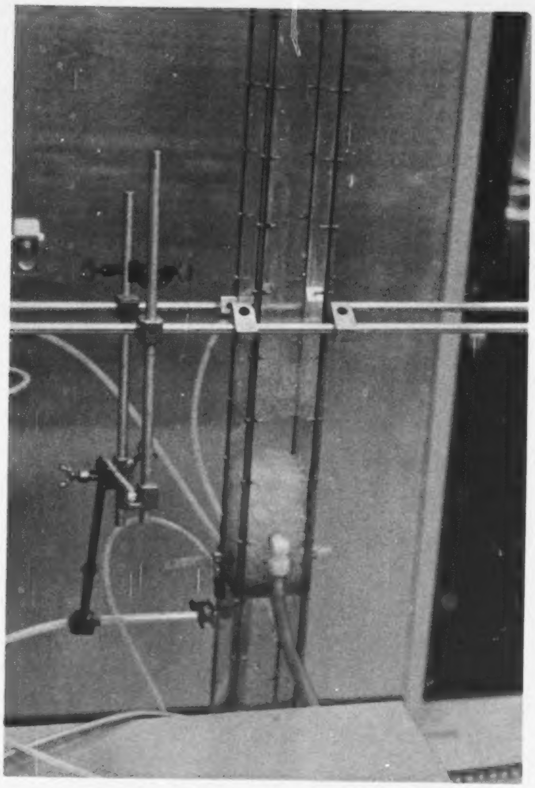

FOAM COLUMN IN OPERATION

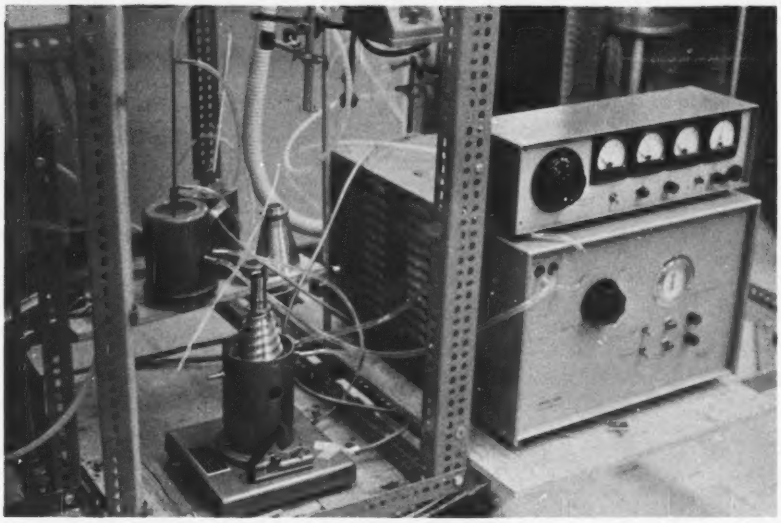

GOETZ AEROSOL SPECTROMETER
Partially Disassembled, showing
Refrigerator Unit, Conical Rotor with Channels

Figure 5

Particle Mass Distribution on the Deposit Area of the Aerosol Spectrometer

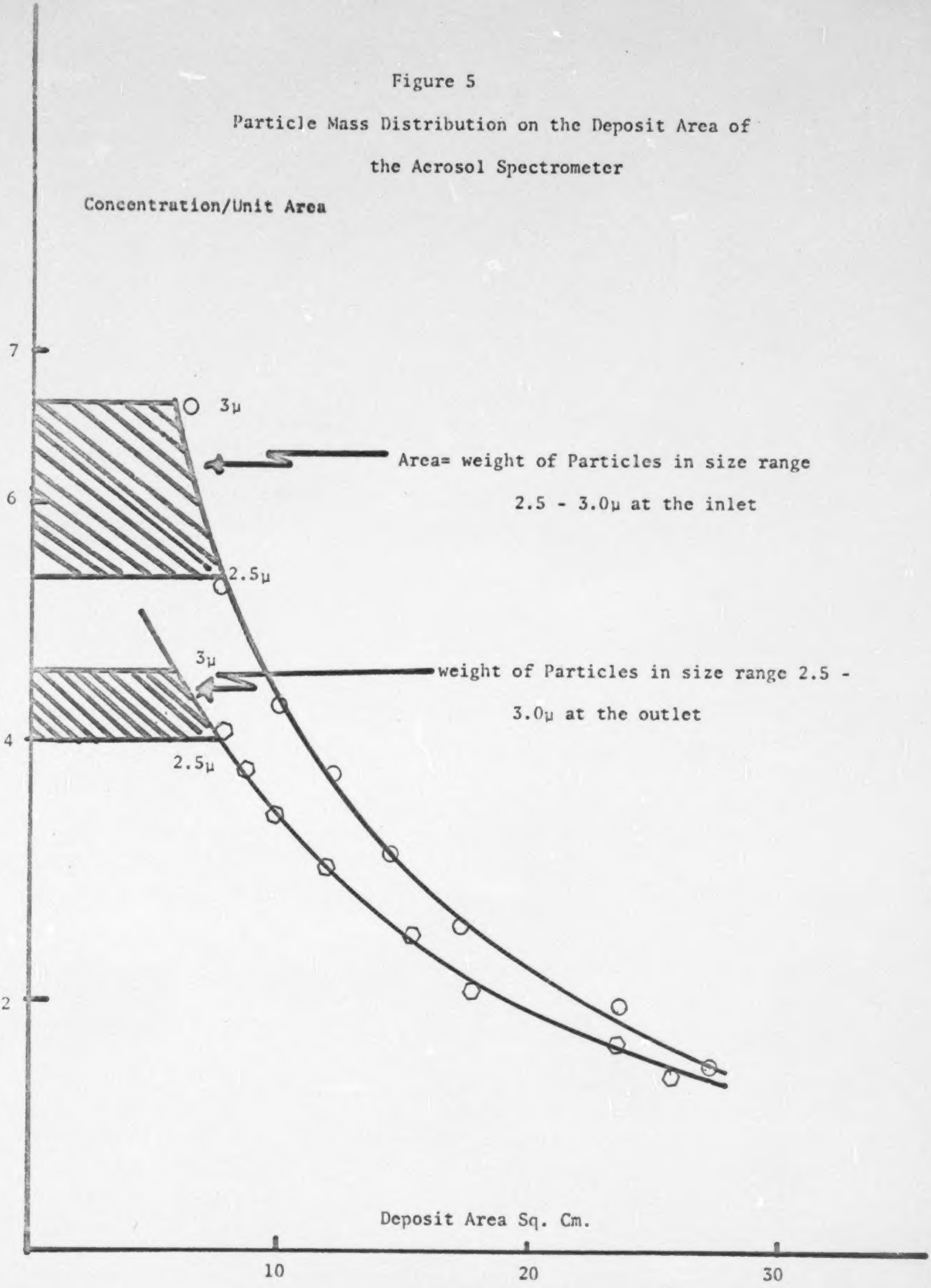

Figure 6

The Weight Distribution of
Methylene Blue Aerosol Determined By
Goetz Aerosol Spectrometer

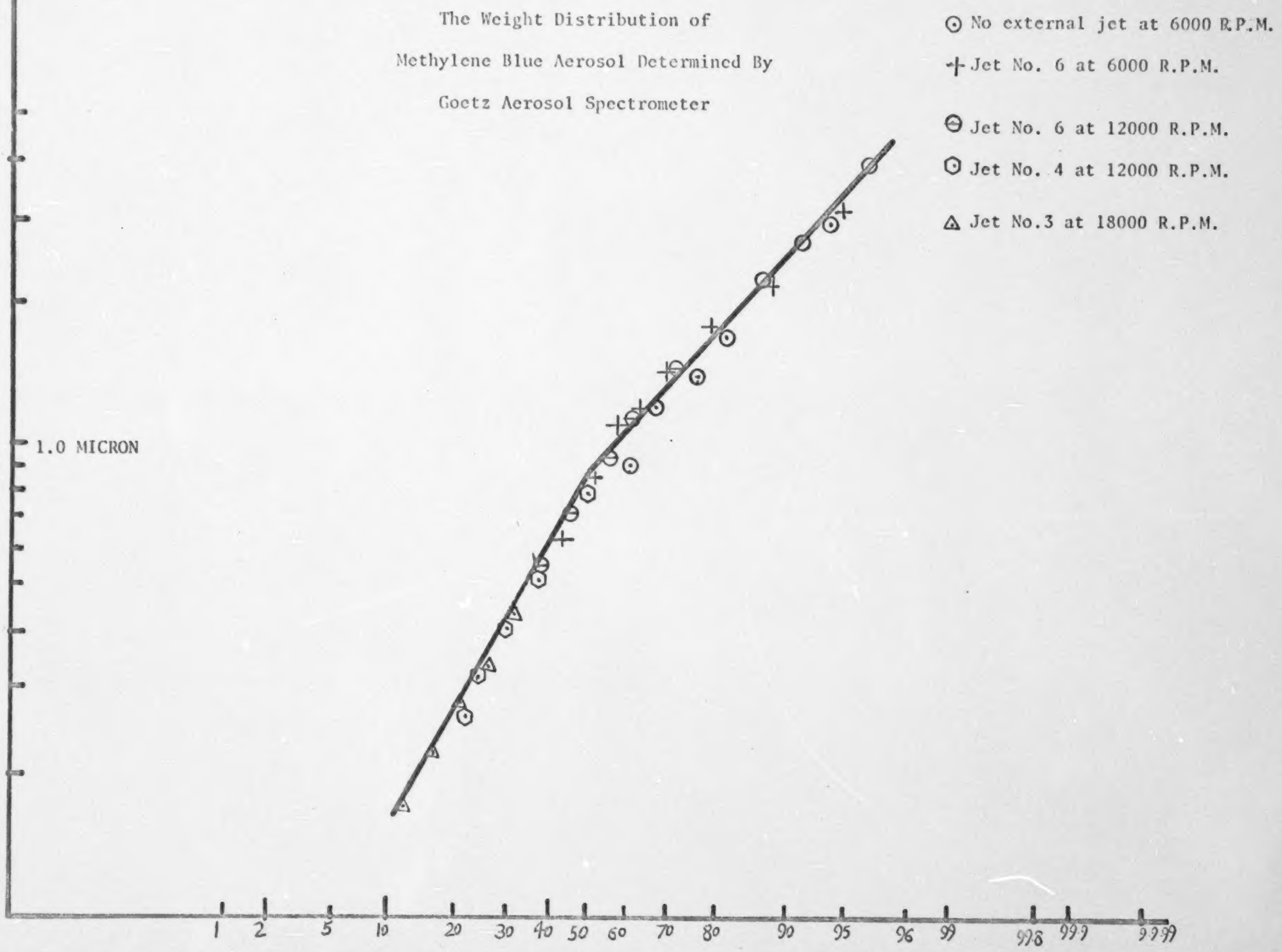

Figure 7

Collection Efficiency of the

Foam Column for Methylene Blue Aerosol

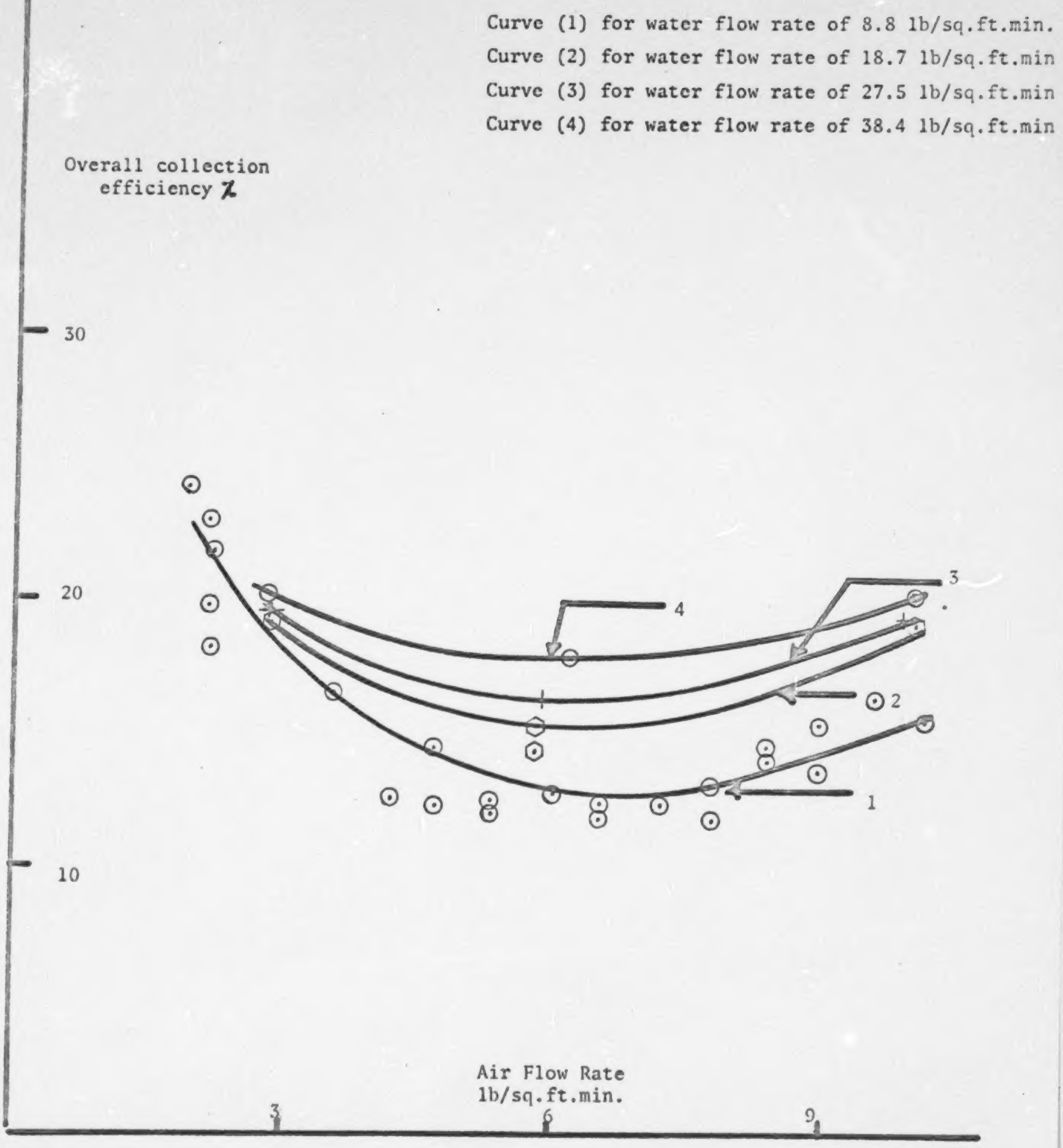

Curve (1) for water flow rate of 8.8 lb/sq.ft.min.
Curve (2) for water flow rate of 18.7 lb/sq.ft.min
Curve (3) for water flow rate of 27.5 lb/sq.ft.min
Curve (4) for water flow rate of 38.4 lb/sq.ft.min

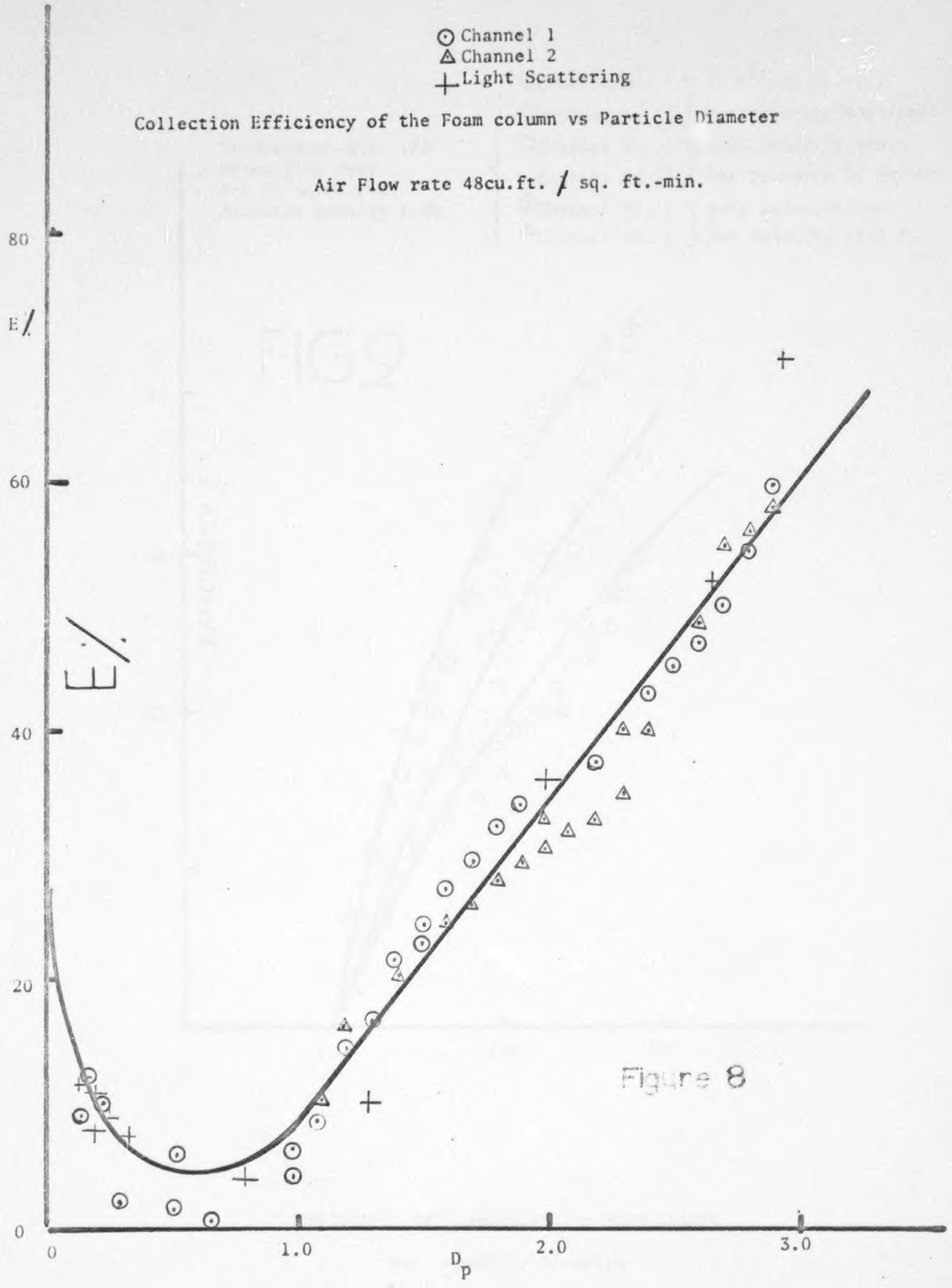
⊙ Channel 1
△ Channel 2
+ Light Scattering
Collection Efficiency of the Foam column vs Particle Diameter
Air Flow rate 48cu.ft. / sq. ft.-min.
80
E/
60
E%
40
20
0
0
1.0
2.0
3.0
D_p

Figure 8

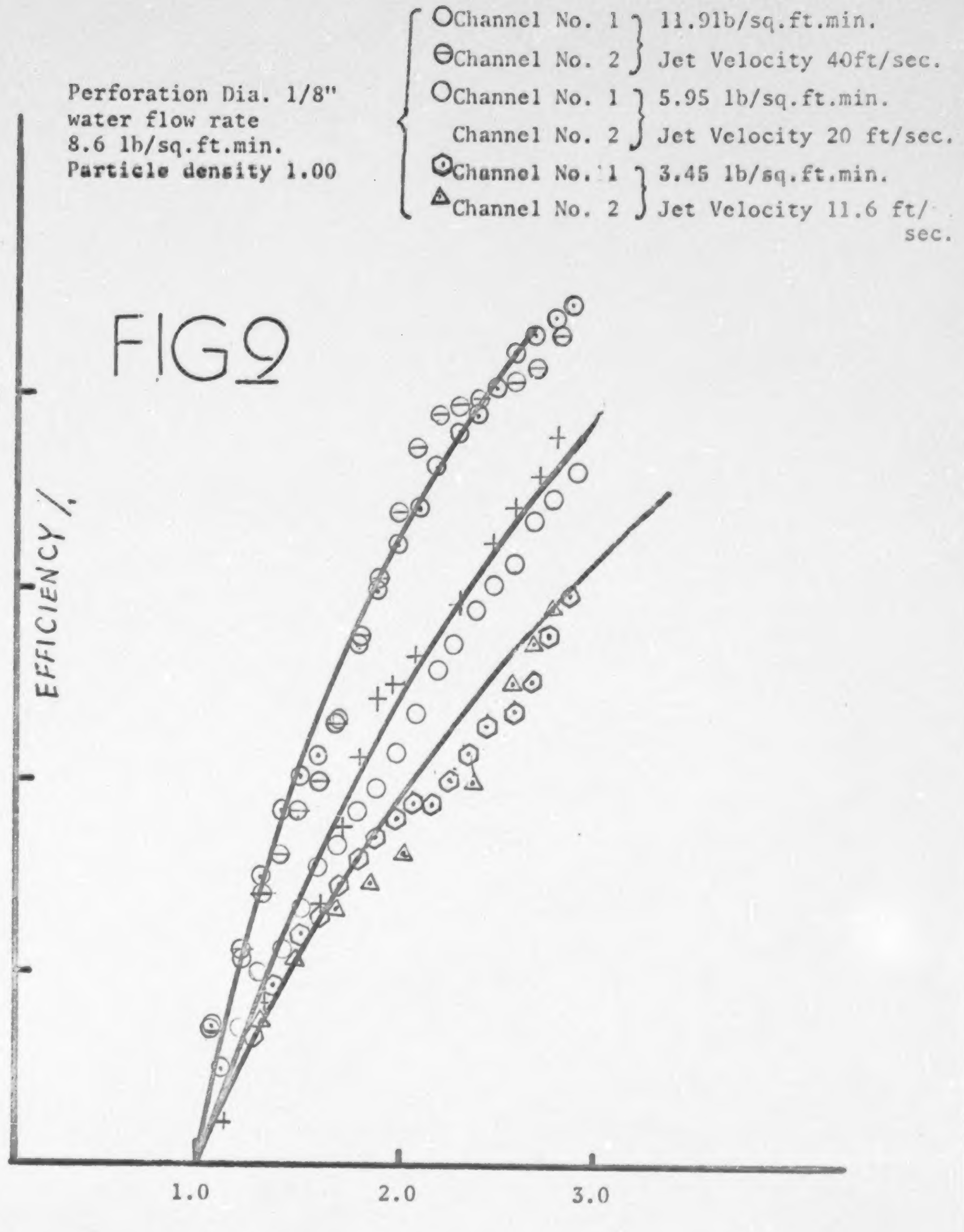

FIG 9

Collection Efficiency of the Foam Column

vs. Particle Diameter

Figure 10

Collection Efficiency of the Foam Column

vs.

Inertia Parameter

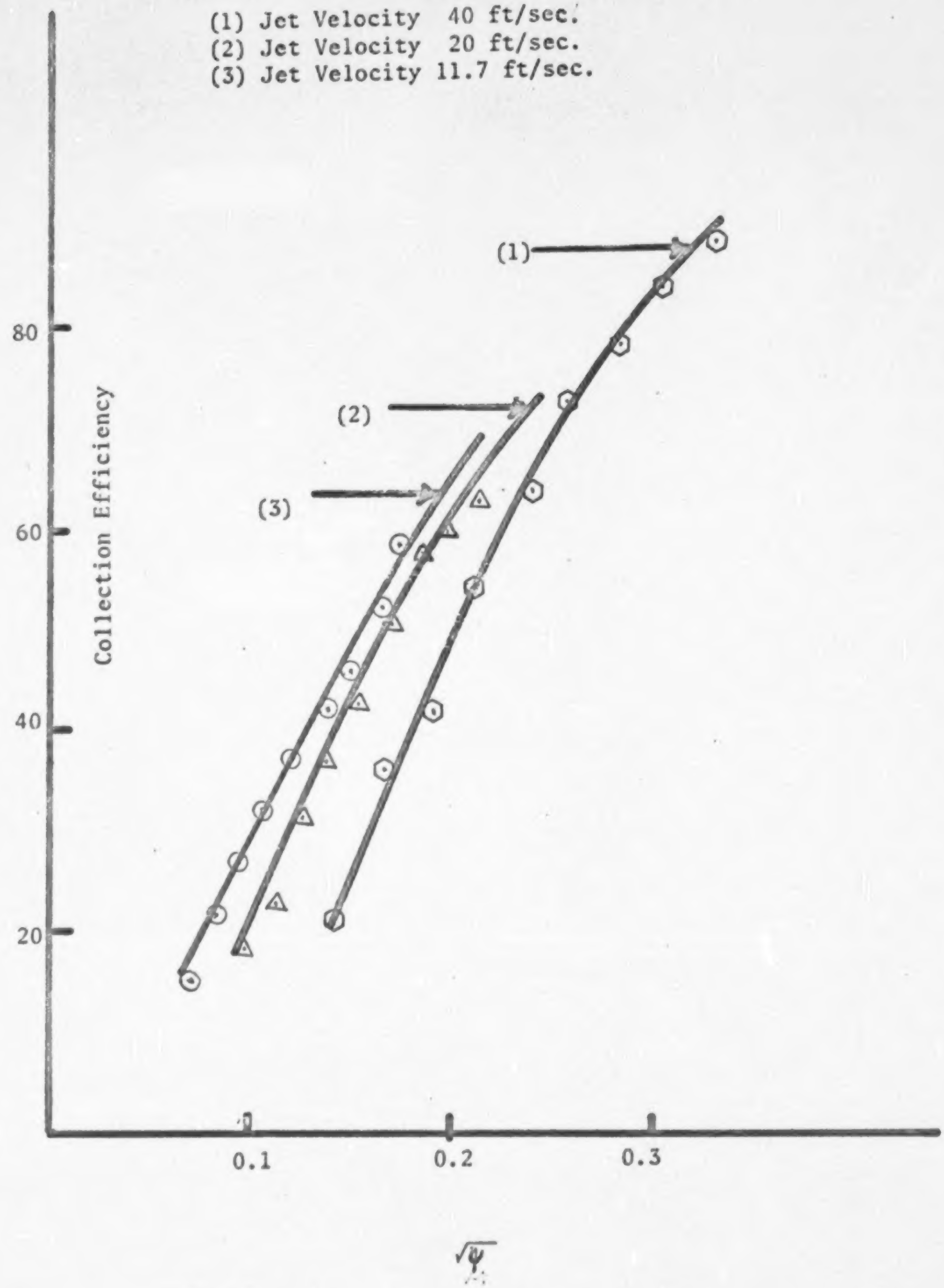

Figure 11

Collection Efficiency of the Foam Column
vs.
Particle Diameter

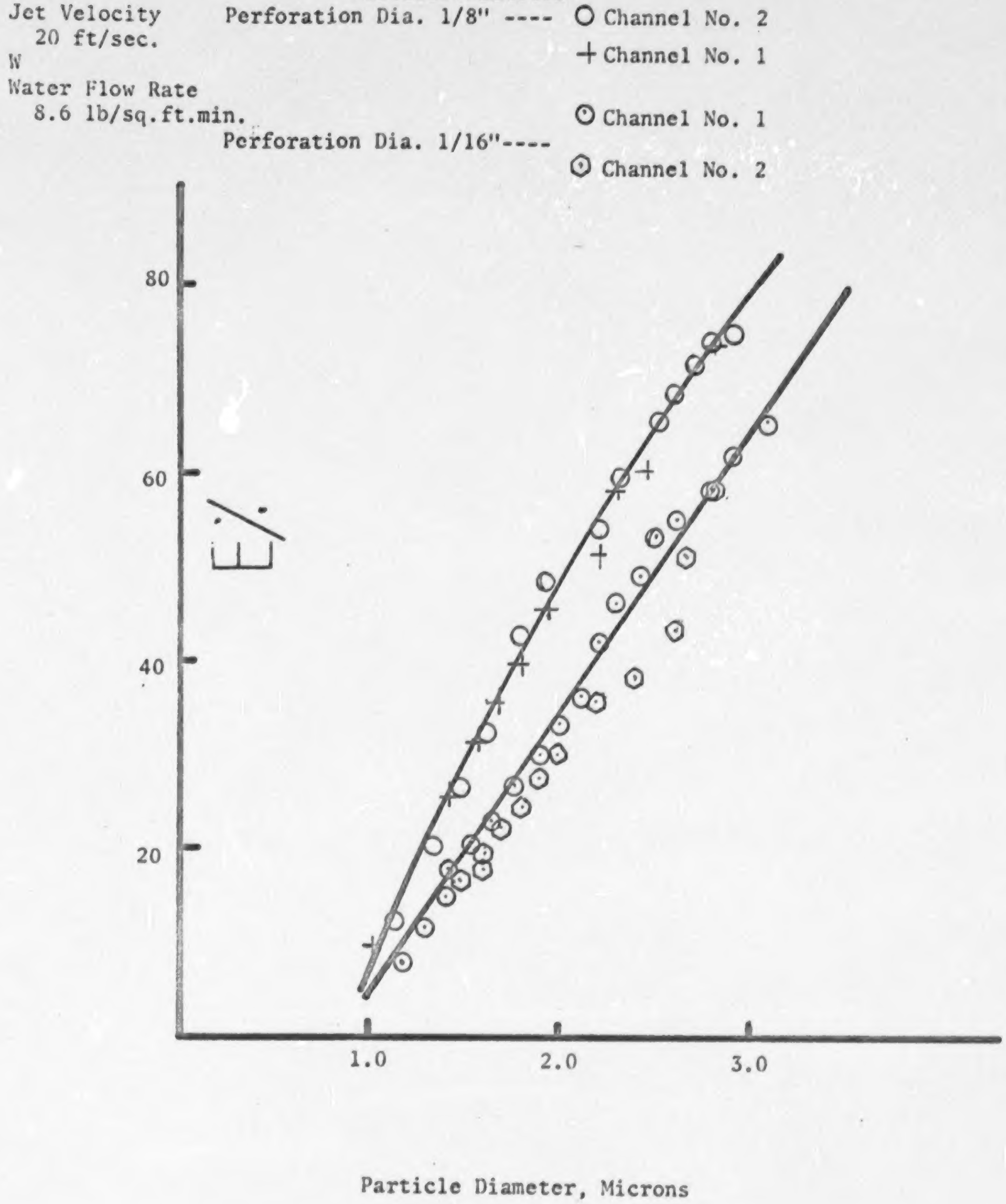

Figure 12

Collection Efficiency of the Foam Column
vs. Particle Diameter

Air Flow Rate 6 lbs/sq.ft.min.
Foam density o.5 {△ Channel 1, ⊙ Channel 2} 8.6 lb/sq.ft.min.
Foam density o.64 {⊙ Channel 1, + Channel 2} 42 lb/sq.ft.min.

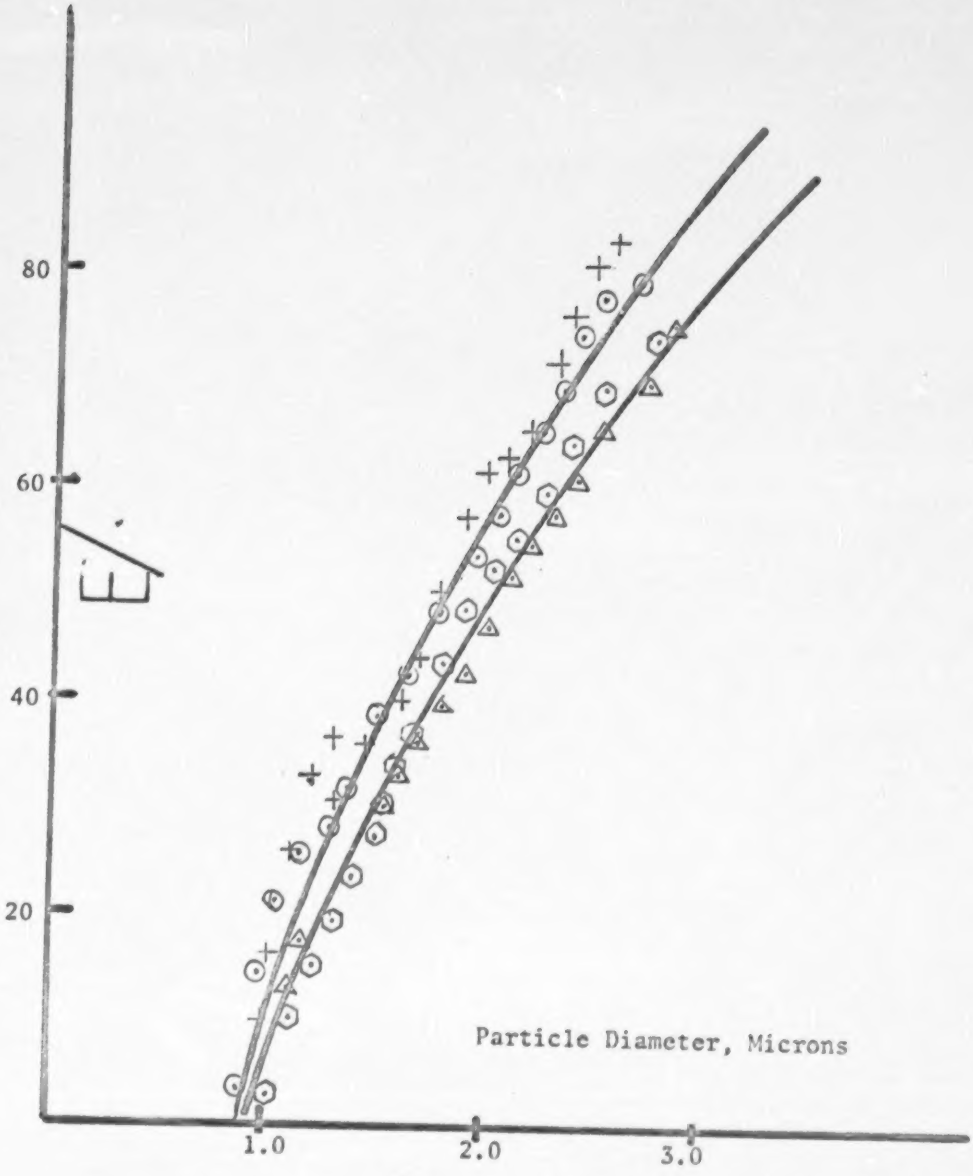

Figure 13

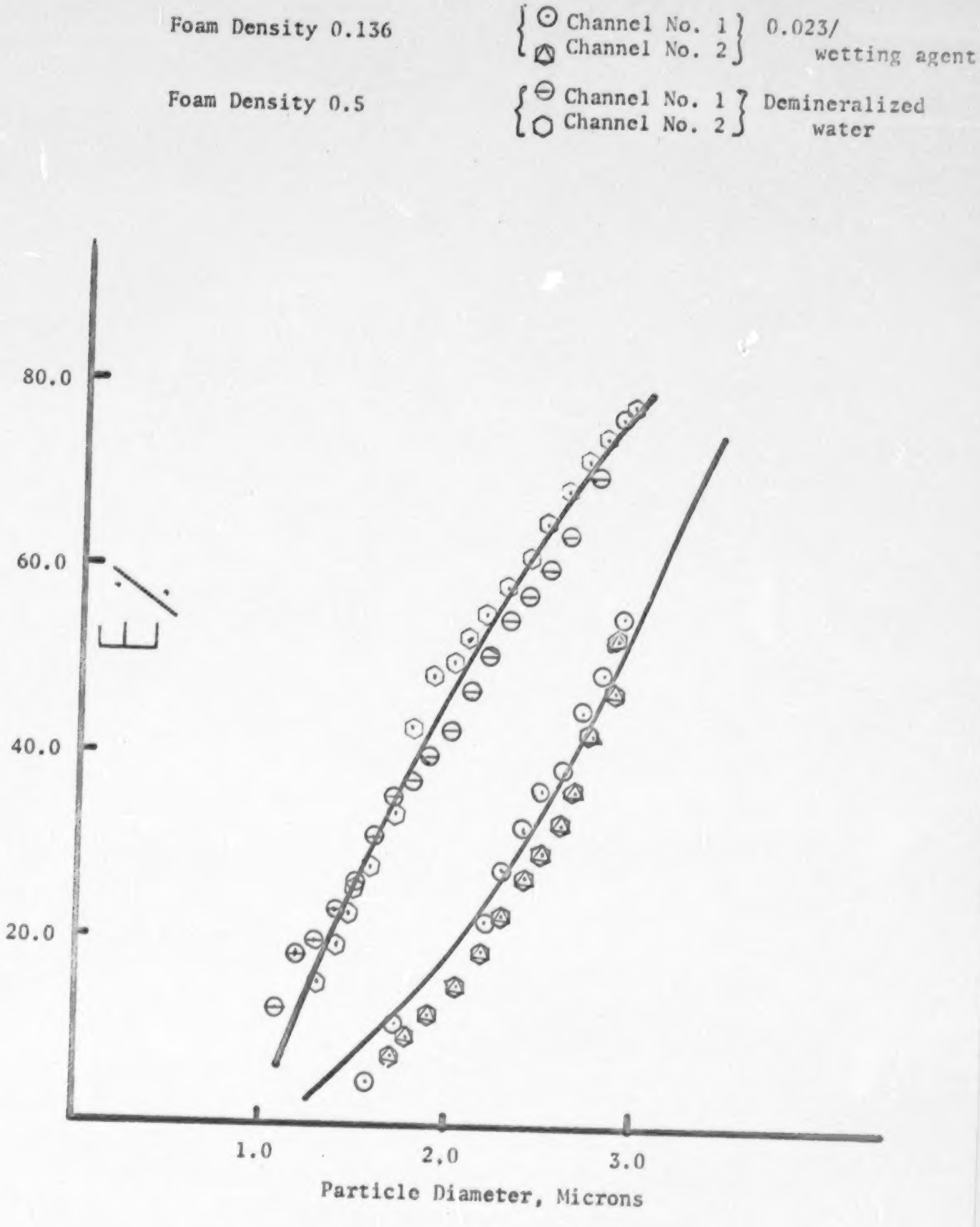

Collection Efficiency of Foam column
vs.
Particle Diameter

Figure 14

Collection Efficiency of the Foam Column vs. Inertia Parameter

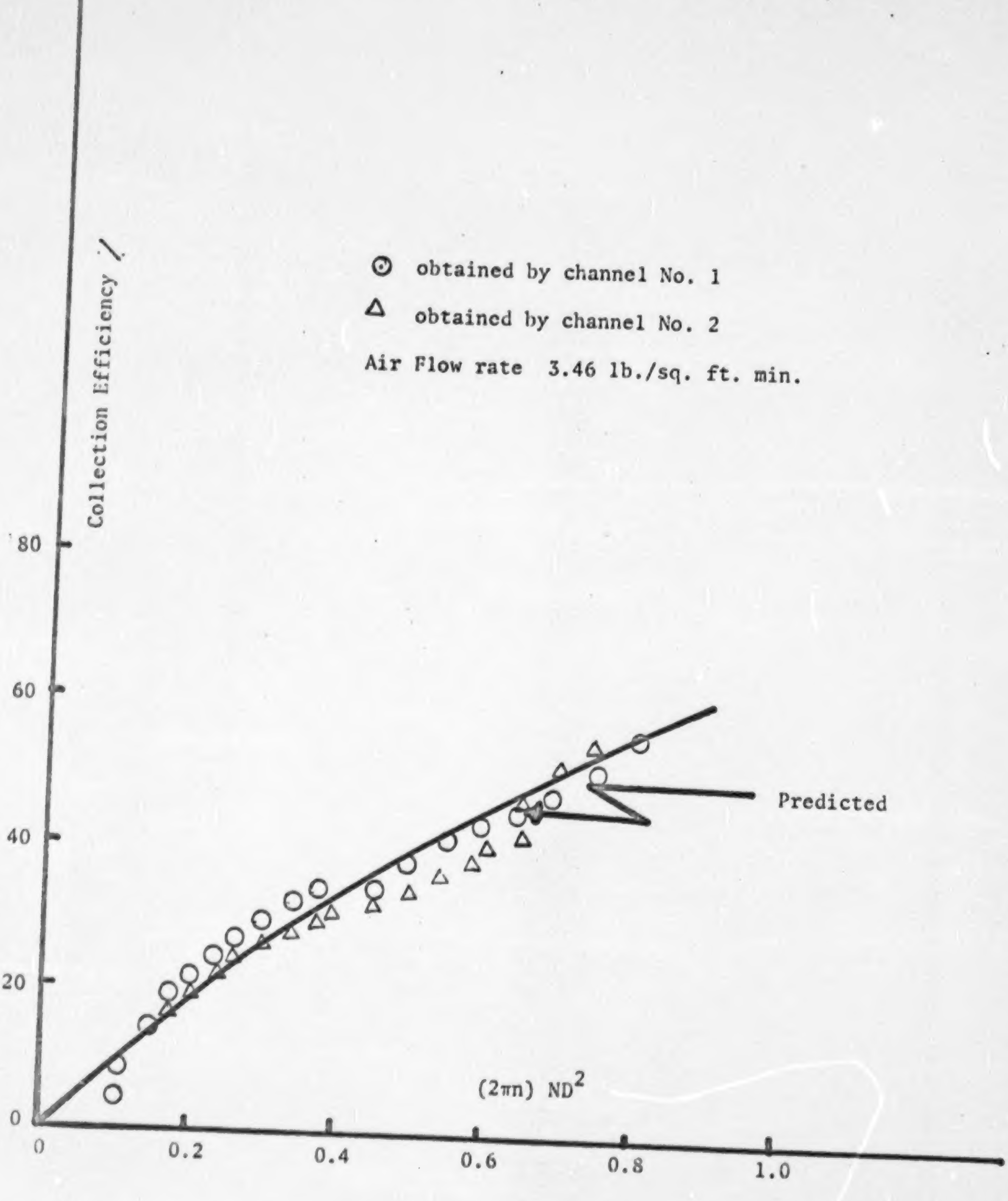

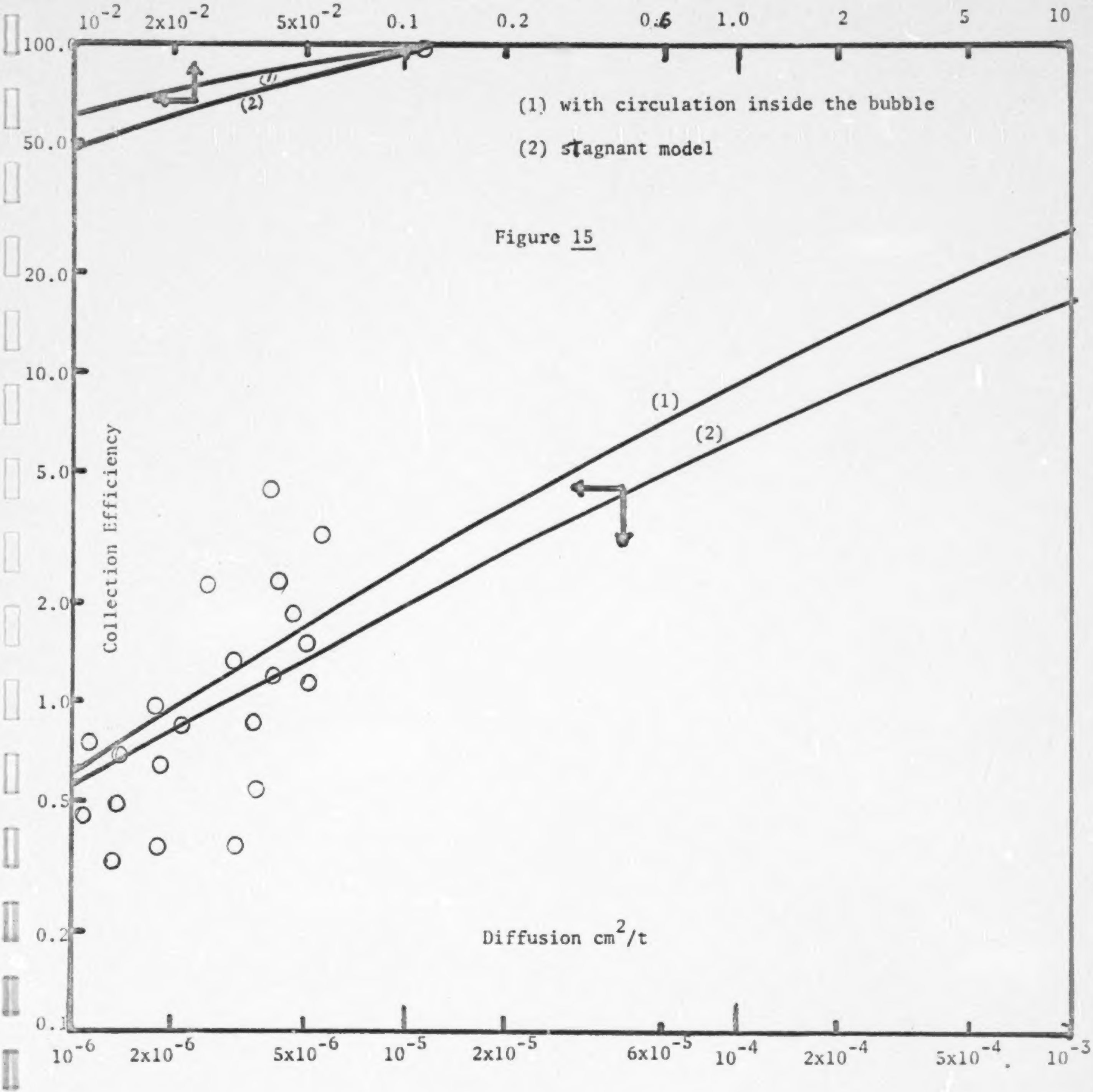
10^-2
2x10^-2
5x10^-2
0.1
0.2
0.6
1.0
2
5
10
100.0
50.0
20.0
10.0
5.0
2.0
1.0
0.5
0.2
0.1
Collection Efficiency
(1) with circulation inside the bubble
(2) stagnant model
(1)
(2)
Diffusion cm^2/t
10^-6
2x10^-6
5x10^-6
10^-5
2x10^-5
6x10^-5
10^-4
2x10^-4
5x10^-4
10^-3

Figure 15

Gas Sorption by Suspensions of Activated Carbon in Water

By: Dilip S. Mehta and Seymour Calvert

Presented at AIChE Meeting, Detroit, Michigan, 1966

ABSTRACT

Gas scrubbing by suspensions of adsorbent particles in liquids offers the advantages of high capacity, fluid handling, and inexpensive solvent losses. Capacity and mass transfer efficiency are reported for carbon dioxide, methane, propane, n-hexane, ethylene, acetone, trichloroethylene, butyl alcohol, amyl alcohol, benzene, and toluene sorption in activated carbon suspended in water. The data reported here were taken in small bubblers of 500 c.c. capacity. Solubility of the transferring component in water is the major factor affecting transfer rate.

Introduction

In recent years a demand has been placed on gas purification with the increasing realization of the effects of gaseous pollutants. These pollutants may simply be a source of nuisance or they may have detrimental effects upon human health, plants, animals, and materials (corrosion). Some of the important gaseous impurities are nitrogen oxides, sulfur oxides, carbon oxides, hydrocarbons, aldehydes and ketones, organic and inorganic acids, organic halides, ammonia, and special compounds specifically related to certain industries. The requirement of low level of these impurities in large volumes of low-pressure gas, with regard to air pollution abatement, spurs us to consider new approaches to gas purification.

This paper describes a preliminary investigation of gas scrubbing by suspensions of activated carbon in water. To our knowledge, this is the first time the use of suspensions of adsorbent particles in liquid has been investigated for gas scrubbing and hence is exploratory in nature.

The primary operation of the gas purification processes frequently falls into one of the following four categories:

1. Absorption into a liquid
2. Adsorption on a solid
3. Chemical conversion (reversible or irreversible) to another compound
4. Other processes, e.g. condensation, etc., for specific applications

There are problems and disadvantages associated with these methods. Easy handling of liquids for absorption is marred by its generally low capacity for physical sorption while exactly the opposite is true in the case of solids for adsorption. The separation of one constituent of a gas mixture may be effected by absorption in a liquor with which it undergoes a reversible or irreversible chemical reaction. In this case the advantage over a process involving physical absorption is much higher capacity, however, the disadvantages are corrosion problems, expensive solvent losses in regenerating the liquor, or the chemical cost for irreversible reaction.

The point of inception of the present research was the concept of combining the favorable characteristics of both types of systems. If the wet adsorbent can retain its hight adsorptive capacity, one can combine the advantages of the first two methods, i.e. easy handling, inexpansive solvent losses, and high capacity. Besides adsorption has the advantage of applicability to the removal of a wide variety of organic compounds.

An extensive body of literature exists for absorption and adsorption studies individually, yet little is known of adsorption and absorption as a combined process, i.e. "sorption" by suspensions. After the work of Findlay (1) in 1910, the study of sorption by suspensions has been reported only since 1951 (2, 3, 4, 5, 6) with most of the work reported from Hungary. Their study was with a viewpoint of improving the understanding of catalytic reactions.

OBJECTIVES

The objective of this research was to study and analyze the process of mass transfer as applied to gas sorption by suspension of adsorbent particles in liquid. Major factors of interest in this study are equilibrium relationships and rates of transfer. In gas transfer to suspension of adsorbent particles the solute gas first dissolves in the adsorbent and from liquid it is adsorbed by the adsorbent particles. Thus, there are transport steps from gas to interface, through liquid, from liquid to solid, and through solid. It is necessary that there be a useful adsorption capacity on the wet solid, but high equilibrium capacity does not necessarily ensure high rates. The rates and the factors affecting rates must be investigated.

Equilibria were determined in batch and in flow systems. Rates of sorption were measured in small bubblers in which gas is passed through a column of suspension. The choice of the bubbler was governed by the requirement of a simple system in which a comparative study of rates of sorption for a large number of gases could be made. The bubbler also provides some similarity to practical contacting devices such as sieve plates while allowing one to investigate the mechanism of transfer and the controlling factors. The effect of adsorbent concentration on the rates of sorption was investigated. This study included a number of organic gases and vapors to cover the range of solubility and adsorption.

MATHEMATICAL REPRESENTATIONS

In the discussion that follows, regarding the adsorption efficiency of a bubbler, we shall first investigate the transfer to the liquid and then take into account the presence of the adsorbent particles in liquid. Gas is dispersed through a sintered glass plate and bubbles in contact with the liquid tend toward equilibrium with the liquid at a finite rate. After a sufficiently long time of contact, equilibrium is reached and a limiting quantity of pollutant would have transferred from the gas to the liquid. In a short time of contact only a fraction, f, of this maximum mass would be transferred.

$$f = \frac{P_i - P_e}{P_i - P_1} \qquad (1)$$

In order to predict the intrinsic efficiency, f, of a bubbler we must take into account the physical behavior of bubbles in liquid. Though there exists a bubble size distribution and a residence time distribution of bubbles in a bubbler one can take an average bubble size and an average residence time because the distributions are narrow (7). If it is assumed that each bubble contacts liquid of constant average composition during its entire period of rise, t_r, the change of soluble component concentration in a bubble is given by:

$$\int_{P_i}^{P_e} \frac{d\,P_A}{(P_A - P_1)} = - \int_{o}^{t_r} \frac{P}{H\,M_B} \,.\, K_L \,.\, A \,.\, dt \qquad (2)$$

or $$P_e = e^{-\left[\frac{3RT}{Hr} \,.\, K_L \,.\, t_r\right]} \,.\, (P_i - P_1) + P_1 \qquad (3)$$

Therefore,

$$f = 1 - e^{-\left[\frac{3RT}{Hr} \,.\, K_L \,.\, t_r\right]} \qquad (4)$$

In the case of sparingly soluble gas overall mass transfer coefficient K_L can be identified with the liquid phase mass transfer coefficient K_L. The transfer coefficient from the interface into the liquid is described fairly well by Higbie's penetration theory as

$$k_L = \sqrt{\frac{2DU_B}{\pi r}}$$

The time of contact or surface renewal is taken as $(2r/U_B)$, the time required for a bubble to rise through one diameter of height.

When adsorbent particles are present in the liquid, the transfer of gas to the suspension can be viewed to take place in the following manner:

1. The solute gas diffuses from the bulk of the gas phase to the gas-liquid interface.
2. From the gas-liquid interface it diffuses to the bulk of liquid.
3. The diffused gas mixes in the bulk.
4. From the bulk of the liquid, through the liquid film surrounding the adsorbent particle, the dissolved gas diffuses to the particle surface.
5. Diffusion through the liquid filling up the pore to the pore internal surface.

For simplification, it is assumed that the presence of adsorbent particles is not going to affect the first two steps. Hence eqn. (4) is still valid and accounts for the first two steps. Instantaneous bulk mixing is assumed to eliminate step 3. The last two steps can be represented by the following equation.

$$N_A = AK_c \left[\frac{P_l}{H} - \frac{P_c}{H} \right] \qquad (5)$$

Eqn. (5) can be combined with the equation for the Freundlich type adsorption isotherm, such as,

$$V = a \, P_A^{\,n}$$

to give,

$$\frac{d\,P_c}{dt} = \frac{RT_l \quad P_c^{(1-n)}}{HP \;\; V_c \, . \, a \, . \, \rho \, . \, n} \, (AK_c) \, (P_l - P_c) \qquad (6)$$

The two rate equations, eqn. (4) and eqn. (6), along with the overall mass balance would complete the description of mass transfer to the suspensions. The overall mass balance is as follows:

$$\int_0^t (P_i - P_e) \, G \, dt = V_l \frac{RT_l}{HP} \, . \, P_l + P_c^{\,n} \, . \, a \, . \, w \qquad (7)$$

Equations (3), (6), and (7) are difficult to solve simultaneously due to nonlinearity, however, they can be written in a convenient form as given below and a computer solution of them can be obtained for given initial conditions.

$$\frac{dP_e}{dt} = f \, . \, \frac{dP_l}{dt} \qquad (8)$$

$$\frac{dP_1}{dt} = \frac{HP}{RT_1} \cdot \frac{1}{V_1} \left[G \cdot (P_i - P_e) + a\,(AK_c) \cdot \frac{RT_1}{HP}\,(P_1 - P_c) \right] \qquad (9)$$

$$\frac{dP_c}{dt} = \frac{RT_1}{HP} \cdot \frac{(AK_c)}{V_c . \rho . n} . \; P_c^{(1-n)} \; (P_1 - P_c) \qquad (10)$$

EXPERIMENTAL

General Method

Two techniques, batch and flow, were used to study equilibria. The batch method was used to determine the adsorption of carbon dioxide, propane, and butane on wet activated carbon at 1 atm. pressure. The equipment for the batch study is shown in Fig. 1. The amount of gas sorbed was decided by the amount of mercury displaced in the reservoir flask to maintain constant pressure. When equilibrium is reached, pressure does not change anymore. The amount absorbed by water can be calculated by using Henry's Law and subtracted from the total volume sorbed to obtain the volume adsorbed on wet activated carbon.

The solubilities (benzene, toluene, trichloroethylene), the adsorption isotherm (CO_2), and the rates of transfer (all the compounds) were measured in a bubbler by flow method. A known concentration of the pollutant was introduced in the bubbler at a constant flow rate and known total pressure. The concentration at the outlet was measured continually until, in the case of the equilibrium study, it reached about 99% of the inlet concentration. The results of the outlet concentration-transient allows the calculation of the sorption. The amount adsorbed by the liquid can be corrected to calculate the adsorption on wet adsorbent. Five 30 cc bubblers were used in series for the adsorption isotherm experiments and a 500 cc bubbler was used for the rest of the experiments. The five bubblers in series provided large contact areas and hence high efficiency so that equilibrium was achieved rapidly and the limitations of the analytical instrument overcome.

The method used for determining the adsorption isotherm of carbon dioxide requires special mention. The suspension was pretreated by bubbling air through it for twelve hours or more. This neutralized any basic groups present on carbon that may combine with carbon dioxide and provide added capacity above that of adsorption. Carbon dioxide concentration in the room was monitored to establish the base concentration. Experiments were performed in which pretreated suspension was stripped off carbon dioxide and then saturated with the room air to measure the adsorption capacity up to the carbon dioxide level of the room air.

Materials

Active carbon is the preferred adsorbent to remove organic vapors from air because of its selectivity for organic compounds. We selected the liquid phase application Nuchar C-190 as the adsorbent for most part of the studies. Two vapor phase application carbons, BPL12X30 and BPL28-48, were used only to compare the dry and the wet carbon adsorption capacities. Water was the logical choice as the inexpensive polar absorbent in combination with the nonpolar character of the adsorbent and the solute vapors. Some of the gases and vapors used in this study were carbon dioxide, methane, propane, butane, n-hexane, ethylene, trichloroethylene, acetone, butyl alcohol, amyl alcohol, benzene, and toluene. They cover a wide range of solubility and adsorption.

Gas Mixtures

Carbon dioxide, methane, and propane were obtained from the Matheson Company as standard gas mixtures (background nitrogen) in ppm range and were

3,000, 1,000, and 104 ppm respectively. All the other mixtures were prepared by the following method except for ethylene. Nitrogen from a nitrogen tank was bubbled through the organic liquid in a bubbler, whose vapor mixture was to be prepared. The outlet from the bubbler, which is nitrogen carrying the vapor of the organic liquid, is fed to an evacuated gas tank. The amount of nitrogen bubbled was governed by the vapor pressure of the organic liquid at the room temperature and the concentration of the organic vapor desired in the final mixture. Now the bubbler containing organic liquid was removed from the line and the tank containing organic vapor was pressurized with nitrogen to about 50 psig. This provided large enough volume of the mixture for the experiments.

Analytical Instruments

In all the experiments gas phase was analyzed. Carbon dioxide concentration was measured with the Infra Red Analyzer 215 of Beckman Instruments, Inc. It was calibrated by standard 3,000 ppm carbon dioxide mixture (100% response) and nitrogen (0% response) before each experiment. IR215 response to concentration is not linear. The calibration curve for it was obtained from the company and checked. For all the organic gases and vapors total hydrocarbon analyzer Model 109 from Beckman Instruments, Inc., was used. The instrument was calibrated, before each experiment, with nitrogen (for null point) and 104 ppm standard propane mixture at constant flow rates of air, hydrogen fuel, and sample. The concentration of various organic mixtures was decided by the comparison of the mixtures response to that of 104 ppm propane response and taking into account the effective carbon number of each compound.

RESULTS AND DISCUSSION

Solubility

The knowledge of the solubility of the solute gas component in the liquid is essential to predict the intrinsic efficiency in the bubbler. Solubility data for some of the organics was experimentally determined as it was not found in the literature. The solubilities were determined at only one concentration. Henry's Law constant was calculated from the experimental results of the amount of vapor absorbed in water and its partial pressure in the gas phase. It is assumed that in the low concentration range, in which this work is carried out, Henry's Law is valid.

Three runs were made in each case to check the reproducibility. Although the results were reproducible they may have an error as much as 5%, due to time-lag and adsorption in the total hydrocarbon analyzer. The results are given in Table 1.

TABLE 1

HENRY'S LAW CONSTANTS @ 25°C

Vapor	Partial Pressure atm.	H atm./(moles/cc)
Benzene	103.2×10^{-6}	$0.38 \times 10^{+4}$
Toluene	58.4×10^{-6}	$0.35 \times 10^{+4}$
Trichloroethylene	202.5×10^{-6}	$0.53 \times 10^{+4}$

Adsorption on Wet Activated Carbon

Adsorption of carbon dioxide, propane, and butane were measured on wet activated carbon at 1 atm. pressure. The measurements were made in the batch system. Two different types of carbon, BPL12x30 and BPL28x48 were used for carbon dioxide adsorption. The results are given in Table 2. Adsorption of carbon dioxide on dry carbon is taken from literature for comparison of dry to wet capacity. Although the activated carbons are different, they allow a rough comparison. It can be seen from Table 2 that the results of this study and that of Munemoris compare very well for carbon dioxide.

TABLE 2

Gas	Carbon	Carbon Condition	Adsorption cc/gm	% Capacity of wet to dry carbon	Reference
CO_2	Columbia	Dry	41.0	-	8
CO_2	BPL12x30	Wet	5.75	14.0	this study
CO_2	BPL28x48	Wet	5.34	13.0	this study
Propane	BPL28x48	Wet	68.2	-	this study
Butane	BPL28x48	Wet	140.0	-	this study
CO_2		Dry	33.5	-	2
CO_2		Wet	5.05	15.1	2

Comparison of the equilibrium data for propane and butane of this study with the adsorption on dry BPL4x10 of Grant (9) shows that the wet carbon capacity is roughly 70% that of the dry carbon capacity for propane and the two capacities are roughly equal for butane. It is interesting to note that 6.5 cc of propane and 2.0 cc of butane absorb in 100 cc of water and in contrast 68 cc of propane or 140 cc of butane absorb on 1 gm. wet activated BPL28x48.

The adsorption at 1 atm. has given us some idea of the differences between adsorption on dry activated carbon and wet activated carbon, but the form of adsorption isotherm must be known before the equations for the rates of transfer to suspensions can be used. From the viewpoint of air pollution the interest was mainly centered on the adsorption isotherm in the low pressure range.

Carbon dioxide was used in this study, although its adsorption is quite low because it can be used for comparisons in the future work with sieve plate column. Nuchar C-190 was the activated carbon as adsorbent. The data is shown in Figure 2 on log-log plot and is seen to fall on a straight line. This is a Freundlich type isotherm. It can be represented by the following equation

$$V = ap^n$$

where $a = 145$ and $n = 0.693$

Rates

In Figure 3 are given the results of the physical absorption and sorption of trichloroethylene. The ratio of the outlet to the inlet concentration is plotted against time as abscissa. It is noticed that the overall efficiency of physical absorption drops rapidly and approaches zero efficiency as water gets saturated. Whereas for sorption by 1% activated carbon Nuchar C-190 in 500 cc suspension, a high efficiency is maintained. These curves appear to be starting from zero penetration, or 100% efficiency, due to dead volume above the absorbing media.

Effect of the concentration of activated carbon is shown in Figure 4. A pseudo steady-state is reached quickly in each case. The straight lines observed in this plot can be extended back to zero time and we obtain "apparent initial efficiency" (AIE). At the AIE the concentration of the solute gas on the adsorbent is nearly zero and the concentration of the solute gas in the liquid is just enough to balance the rates of transfer between gas to liquid with that from liquid to solid.

The plots of AIE versus the concentrations of the adsorbent for benzene and trichloroethylene are given in Fugure 5. As the concentrations of the particles increases, we notice that the AIE increases, achieves a maximum at about 1 to 1.5% concentration and then starts decreasing. According to Figure 4 P_e is not changing with time during the initial period, i.e. $(dP_e/dt) = o$. Then from eqn. (8) $(dP_1/dt) = o$, if $(dP_e/dt) = o$. Also P_c is very nearly equal to zero. Hence eqn. (9) can be simplified as follows:

$$P_e = P_i \left[1 - \frac{f}{1 + G\cdot f\cdot \frac{HP}{RT_1 a} \frac{1}{AK_L}} \right]$$

Sufficiently high concentrations of particles in suspension will increase (AK_L) to the point where eqn. (11) approaches $P_e = P_i\ [1 - f]$. This implies that the AIE approaches the intrinsic efficiency. However, the maximum for the AIE is observed at about 1 to 1.5% concentration after which it starts decreasing. The decrease may be due to hydrodynamic factors. Changed hydrodynamics will affect the bubble size distribution and the residence time distribution. These distributions do directly affect the intrinsic efficiency of the bubbler for physical absorption. Hence, although the AIE may be very close to the intrinsic efficiency at high concentrations it may decrease due to the changes in the intrinsic efficiency itself.

The rate data for the sorption of all the other organics were taken at 1% activated carbon concentration. This should allow us to find the AIE that is closest to the intrinsic efficiency of the bubbler for that organic compound. The intrinsic efficiency for physical absorption under the hydrodynamic conditions prevalent at 1% will differ from that at 0% concentration. But the concentration and the hydrodynamic factors are opposing and 1%, from Fig. 5, still may be the optimum point to determine the AIE that would be closest to the intrinsic efficiency at 0%.

In Figure 6 are given the results of sorption for methane, propane, n-hexane, and ethylene. The physical absorption data for these hydrocarbons are not given as, except for the dead volume effect, the efficiency becomes zero too quickly to be measured. The results for physical absorption and sorption for toluene and amyl alcohol are shown in Figure 7. Butyl alcohol and acetone have very high solubility and 100% efficiency was obtained even for physical absorption in a 500 cc bubbler.. The results mentioned here are discussed later in this section.

A number of experiments were carried out to determine the intrinsic efficiency of the bubbler for physical absorption of carbon dioxide. Analysis of the results gave the value of f = 0.31. From equ. (4) we can see that changing of the solute gas in the gas phase would change only the solubility H and the diffusivity D. If the gases are sparingly soluble, we may say that the K_L has a square root dependance upon diffusivity. Hence,

$$f = 1 - e^{-\frac{0.371 \sqrt{D}}{H}} \qquad (12)$$

Eqn. (12) can now be used to predict the intrinsic efficiency for the physical absorption of various organics. The prediction should have a good agreement with the experimental AIE if our hypotheses about transfer mechanism is correct. Reliable data of solubility and diffusivity are, however, necessary to make meaningful predictions. Henry's law constants for propane and butane were calculated from the solubility data available in ref. (10). The solubilities of benzene, toluene, and trichloroethylene were determined experimentally and the

Henry's law constant for methane and ethylene are given in ref. (11). It is difficult to make reliable estimates of the diffusivity and where experimental diffusivity was not available it was taken as 1×10^{-5} cm^2/sec. Table 3 summarizes the results.

The results in Table 3 show that the prediction of the intrinsic efficiency puts us in the right range of the experimental efficiency. This leads us to an important conclusion that the solubility of the gas in liquid is the controlling factor for rates of transfer to suspensions. We can not achieve the overall efficiency of sorption higher than the intrinsic efficiency of the system for physical absorption in the liquid under the same hydrodynamic conditions. The presence of high capacity adsorbent particles maintains low concentration of the solute in liquid and thus, keep the efficiency close to the intrinsic efficiency.

SUMMARY AND CONCLUSIONS:

a. It has been shown that the controlling factor, for the rates of transfer to suspensions, is the solubility of the solute gas in water. The results of the study suggest that the overall efficiency of the system for sorption by suspensions can not be greater than the intrinsic efficiency of the system for physical absorption of the compound under the same hydrodynamic conditions.

b. The solubility of benzene, toluene, and trichloroethylene in water were determined at 25°C.

c. The absorption isotherm of carbon dioxide on wet Nuchar C-190 was determined in the range of 0 to 3×10^{-3} atm at 25°C.

d. The adsorption capacity of water can be increased to a great extent by addition of an adsorbent. In the presence of 2% (by wt.) activated carbon, the capacity of water increases by 0.2 times for carbon dioxide, by 21 times for propane, and by 142 times for butane at 1 atm. pressure and 30°C.

TABLE 3

PREDICTION OF THE EFFICIENCY

Compound	H	Reference	D	Experimental Efficiency (AIE)	Predicted Efficiency
Carbon Dioxide	$2.7 \times 10^{+4}$	11	1.77×10^{-5}	31%	-
Methane	$74.4 \times 10^{+4}$	11	1.8×10^{-5}	2.0%	1.35
Propane	$36.6 \times 10^{+4}$	10	n.a.	5.5	2.7
Butane	$116.2 \times 10^{+4}$	10	n.a.	≈0	0.8
n-Hexane	n.a.		n.a.	10.0	-
Ethylene	$20.5 \times 10^{+4}$	11	1.59×10^{-5}	2.5	4.75
Benzene	$0.38 \times 10^{+4}$	this study	1×10^{-5} A	87.0	86.2
Toluene	$0.25 \times 10^{+4}$	this study	1×10^{-5} A	88.0	88.3
Trichloroethylene	$0.53 \times 10^{+4}$	this study	1×10^{-5} A	76.8	75.8
Butyl Alcohol	n.a.			100.0	-

NOTE: n.a. = not available A = assumed

e. The overall efficiency for sorption goes through a maximum with the increase of activated carbon concentration. The increase is explained by a mathematical model for the rates of transfer and the decrease is suggested to be due to hydrodynamic factors.

f. Suspensions would give a high overall efficiency in a practical contactor for compounds with high intrinsic efficiency for physical absorption.

ACKNOWLEDGEMENT

The authors appreciate the financial support for this work under a grant from the Air Pollution Division of the U. S. Public Health Service.

NOMENCLATURE:

a - constant in Freundlich isotherm equation

A - area for transfer associated with liquid-carbon transfer

D - diffusivity of gas in liquid

f - intrinsic efficiency

G - flow rate of gas cc/sec.

H - Henry's Law constant

K_c - overall mass transfer coefficient-liquid to solid

K_L - overall mass transfer coefficient-gas to liquid cm/sec.

k_L - liquid phase mass transfer coefficient

M_B - moles of gas in one bubble

n - constant in Freundlich isotherm equation

N_A - rate of transfer, moles/sec.

P_i - partial pressure of solute gas in inlet to bubbler, atm.

P_e - partial pressure of solute gas in exit from bubbler, atm.

P_l - partial pressure of the solute gas, atm., that is in equilibrium with the concentration of the solute gas in liquid

P_c - partial pressure of the solute gas, atm., that is in equilibrium with the concentration of the solute gas on the solid

P_A - partial pressure of solute gas in the gas phase, atm.

P - total pressure of the gas

r - radius of the bubble

R - gas law constant

t - time, sec.

t_r - average residence time of a bubble in the liquid

T_1 - temperature

V, V_1, V_c - volume of gas adsorbed, volume of liquid, volume of solid - cc

w - gms. of carbon in liquid

ρ - density of carbon

BIBLIOGRAPHY

1. Findlay, A., and Greighton, J. M., J. Chem. Soc. (trans) 97-1, 536 (1910).
2. Munemori, Makota, Science Repts. Tohoku Univ., 35, 165-172 (1951)
3. Tibor, Erday-Gruz, and Nagy, F., Magyar Kemiai Folyoirat, 62, 395-400 (1956).
4. Nagy, F., and Schay, Greza, Magyar Kemiai Folyoirat, 64, 81-84, (1958).
5. Nagy, F., and Dezso, Moger, Magyar Kemiai Folyoirat, 65, 406-409, (1959).
6. Pozin, M. E., Kopylev, B. A., and Gulyaen, S. P., Trudy Leningrad Technal Inst. in Lensovesta, 43, 52-63, (1957).
7. Calvert, S., and Workman, W., Industrial Hygiene Journal, 22, 4, 318-324, (1961).
8. Ray, G. C., and Box, E. O., Jr., Ind. Eng. Chem., 42, 1314-1317, (1950).
9. Grant, R. J., Pittsburgh Coke and Chemical Company, Research and Development Department, Project No. 151-1002, Report No. 2, (1957).
10. Seidell, Atherton, "Solubilities of Organic Compounds," Third Edition, Volume II, D. Van Norstad Company, Inc., New York (1941).
11. Perry, John M., Editor, "Chemical Engineers Handbook", Third Edition, McGraw-Hill Book Co., Inc., New York, (1950).

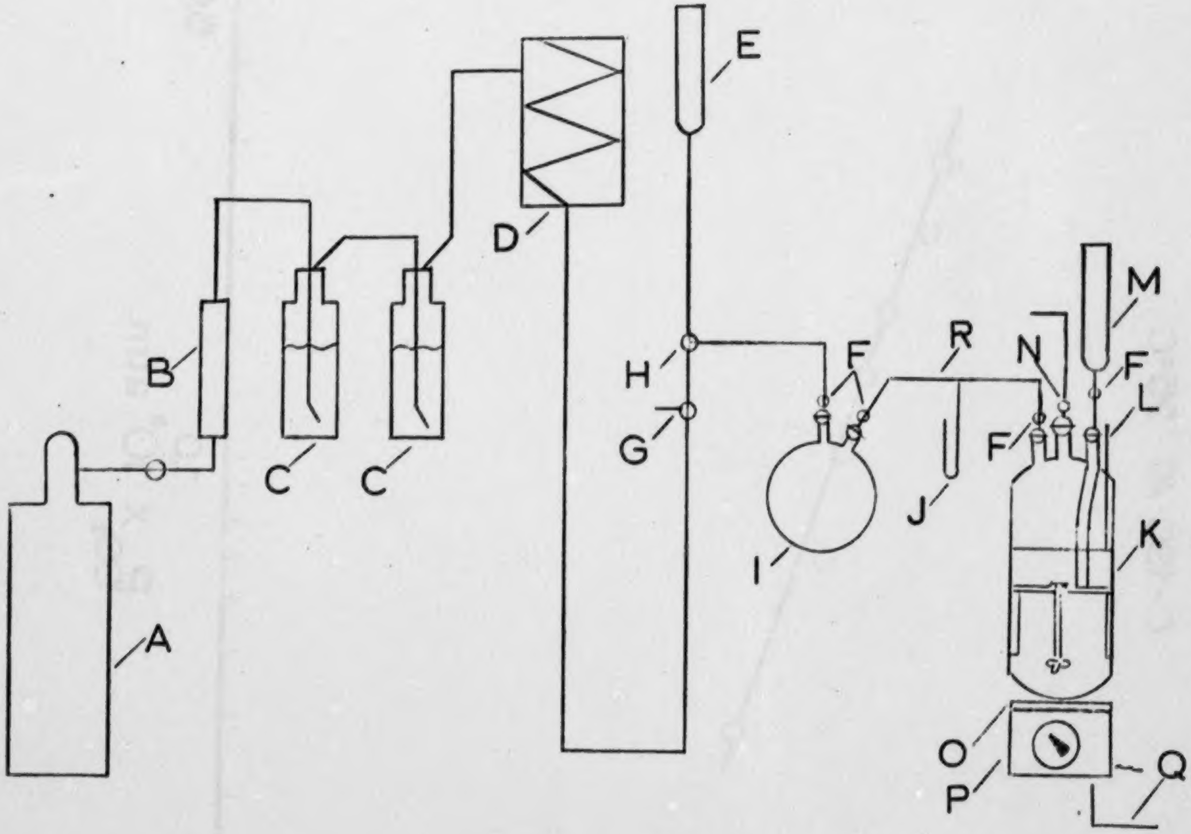

A
B
C
C
D
E
H
G
F
I
J
R
F
N
M
F
L
K
O
P
Q

Fig. 1
SCHEMATIC DIAGRAM

Fig. 2

ADSORPTION ISOTHERM OF CO_2 ON WET NUCHAR C-190 AT 25°C

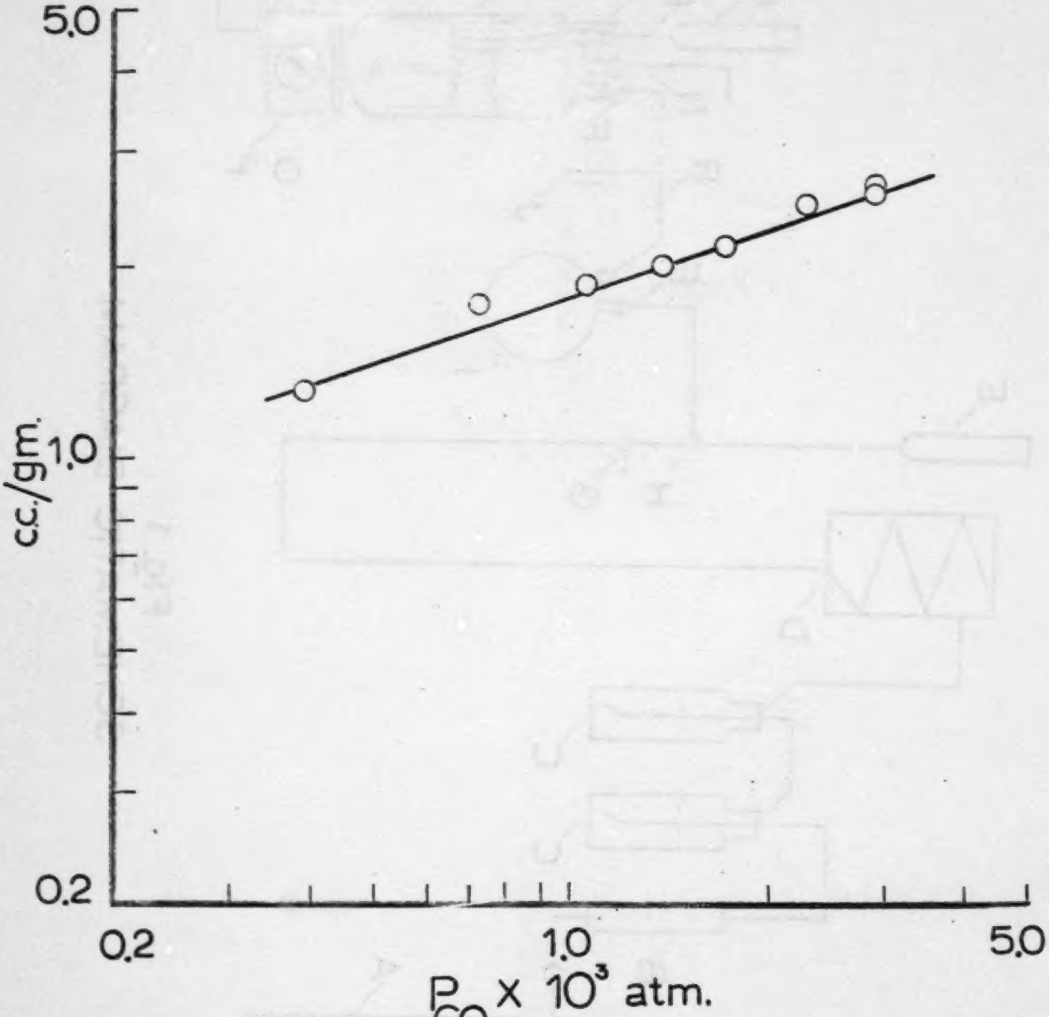

FIG. 3

UNSTEADYSTATE SORPTION OF TRICHLOROETHYLENE

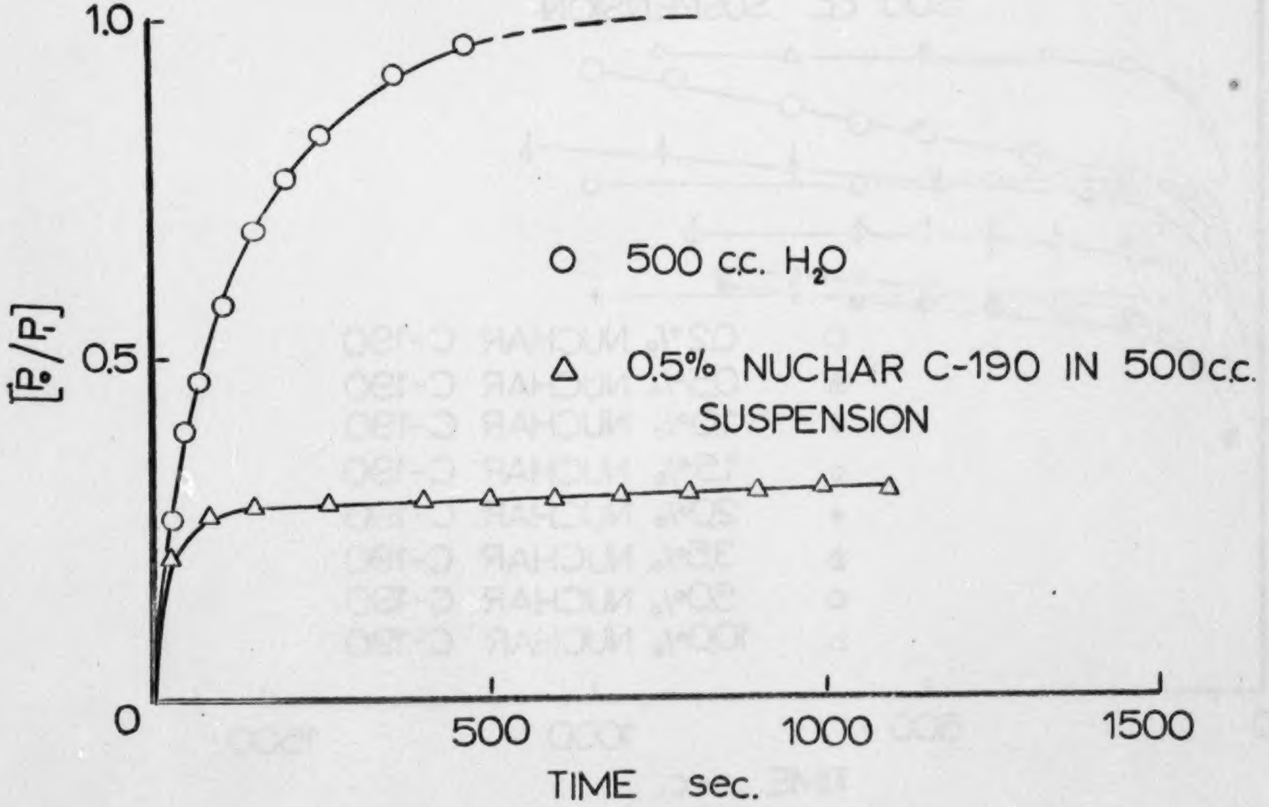

FIG. 4

EFFECT OF CONCENTRATION ON SORPTION OF TRICHLOROETHYLENE

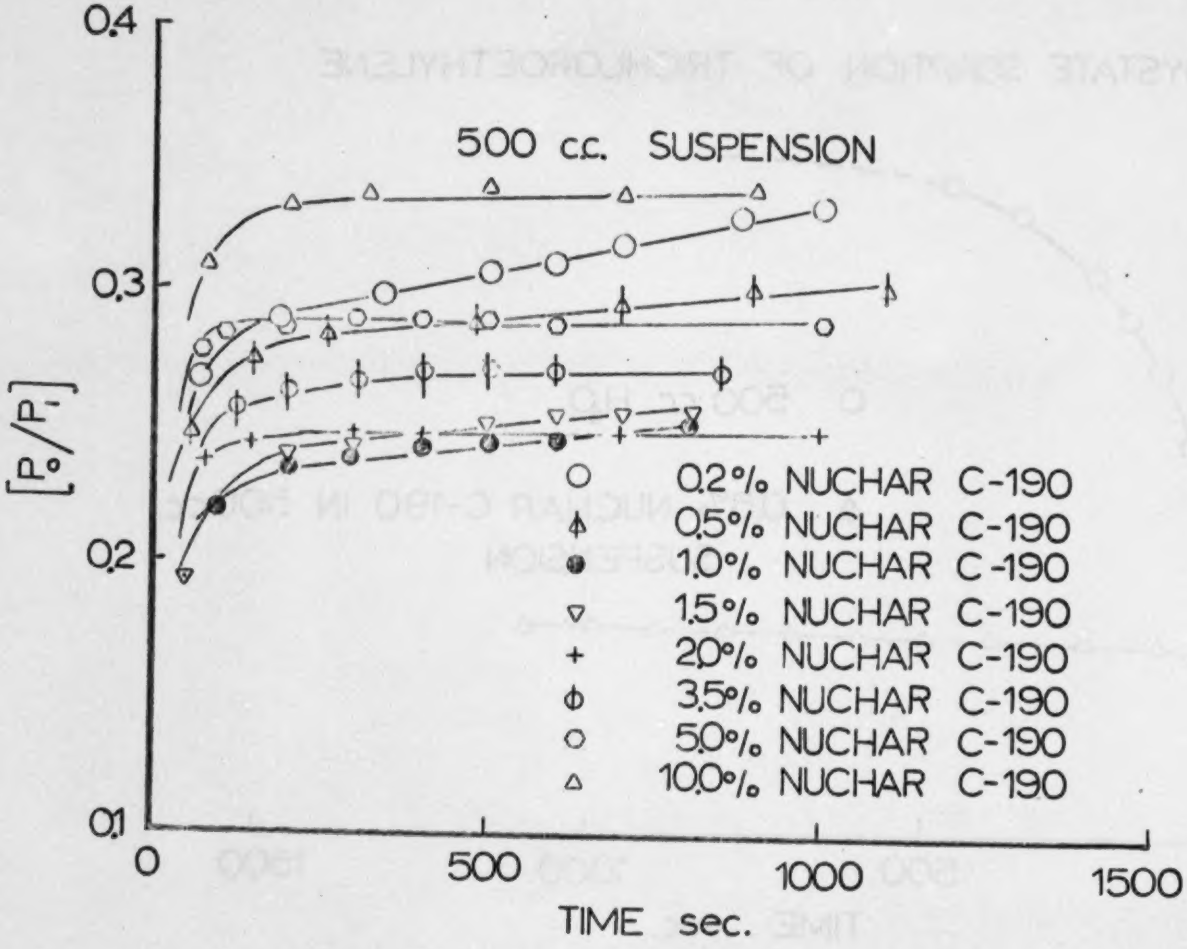

FIG. 5

EFFECT OF ADSORBENT CONCENTRATION
ON APPARENT INITIAL EFFICIENCY

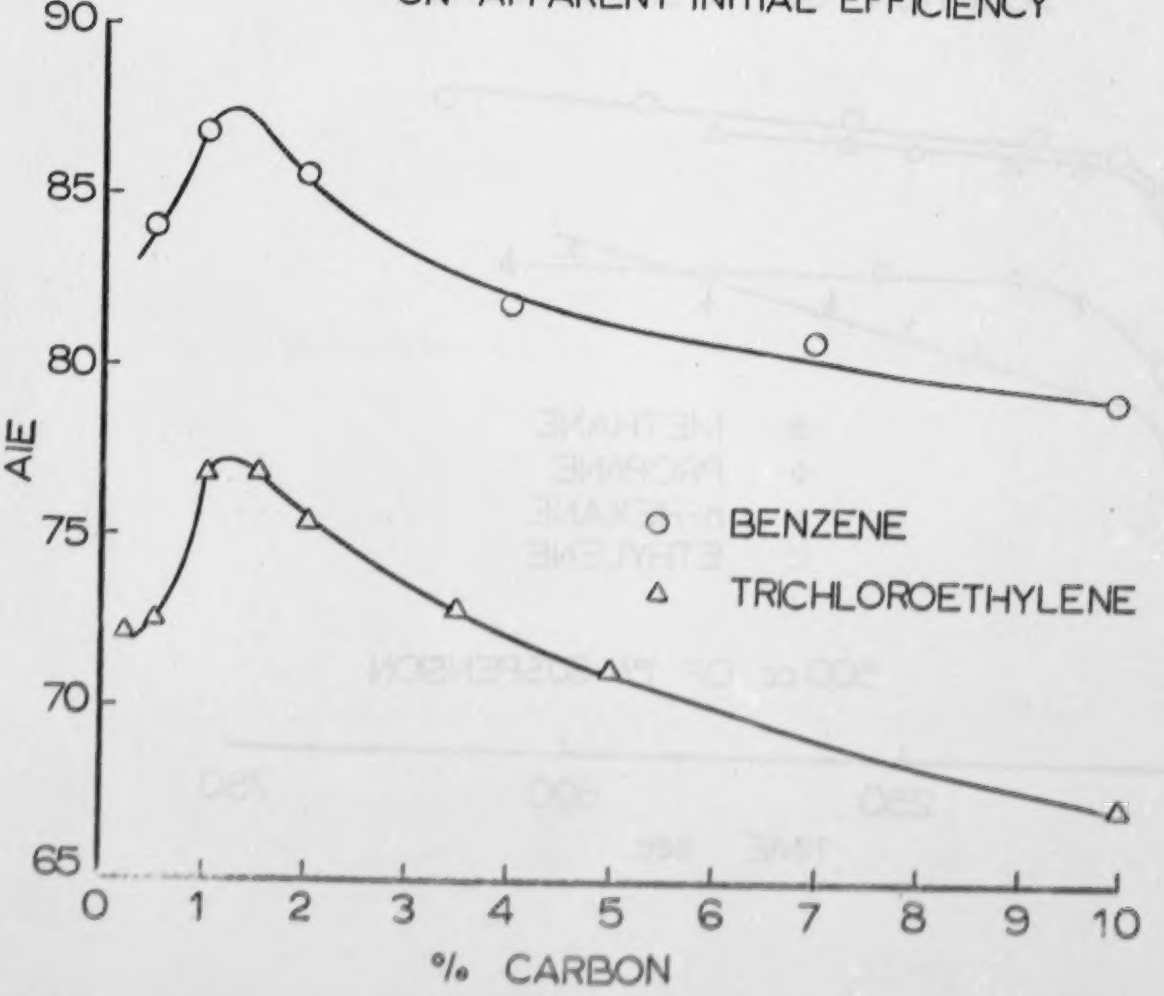

FIG. 6

SORPTION OF HYDROCARBONS

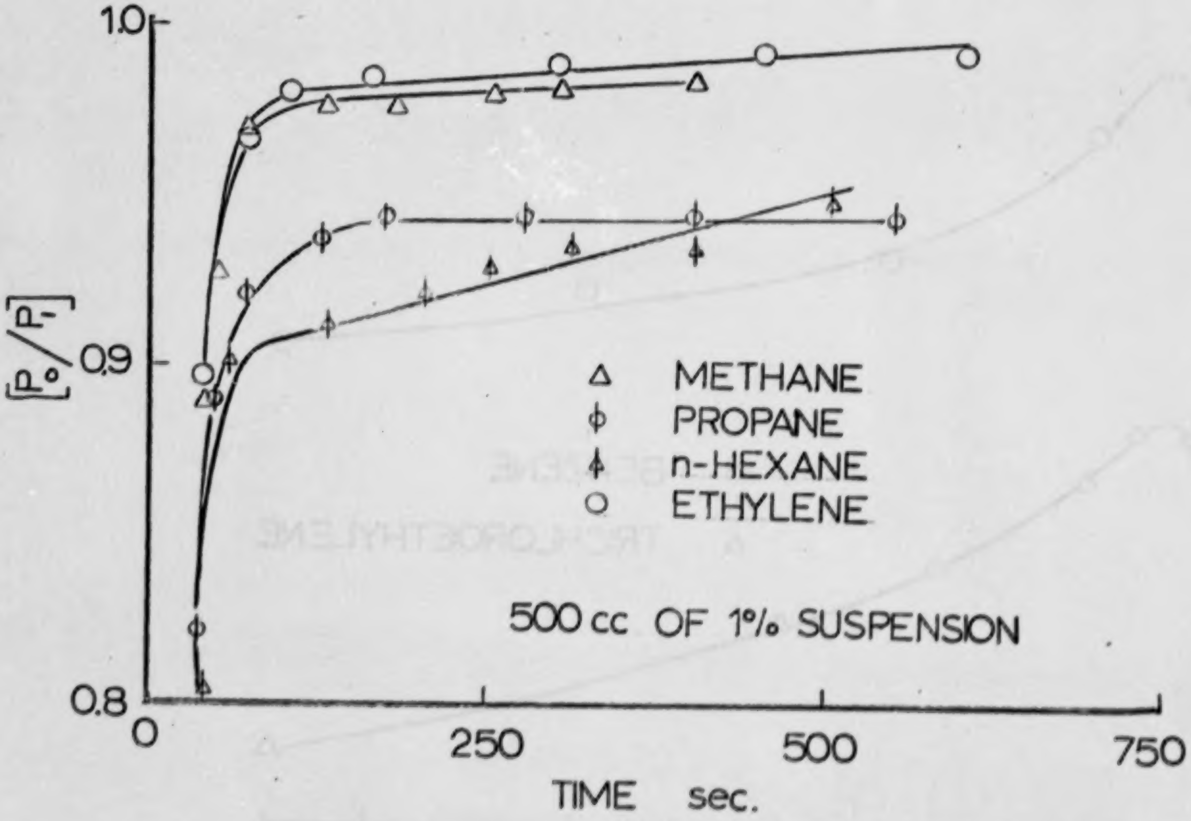

FIG. 7

SORPTION OF TOLUENE AND AMYL ALCOHOL

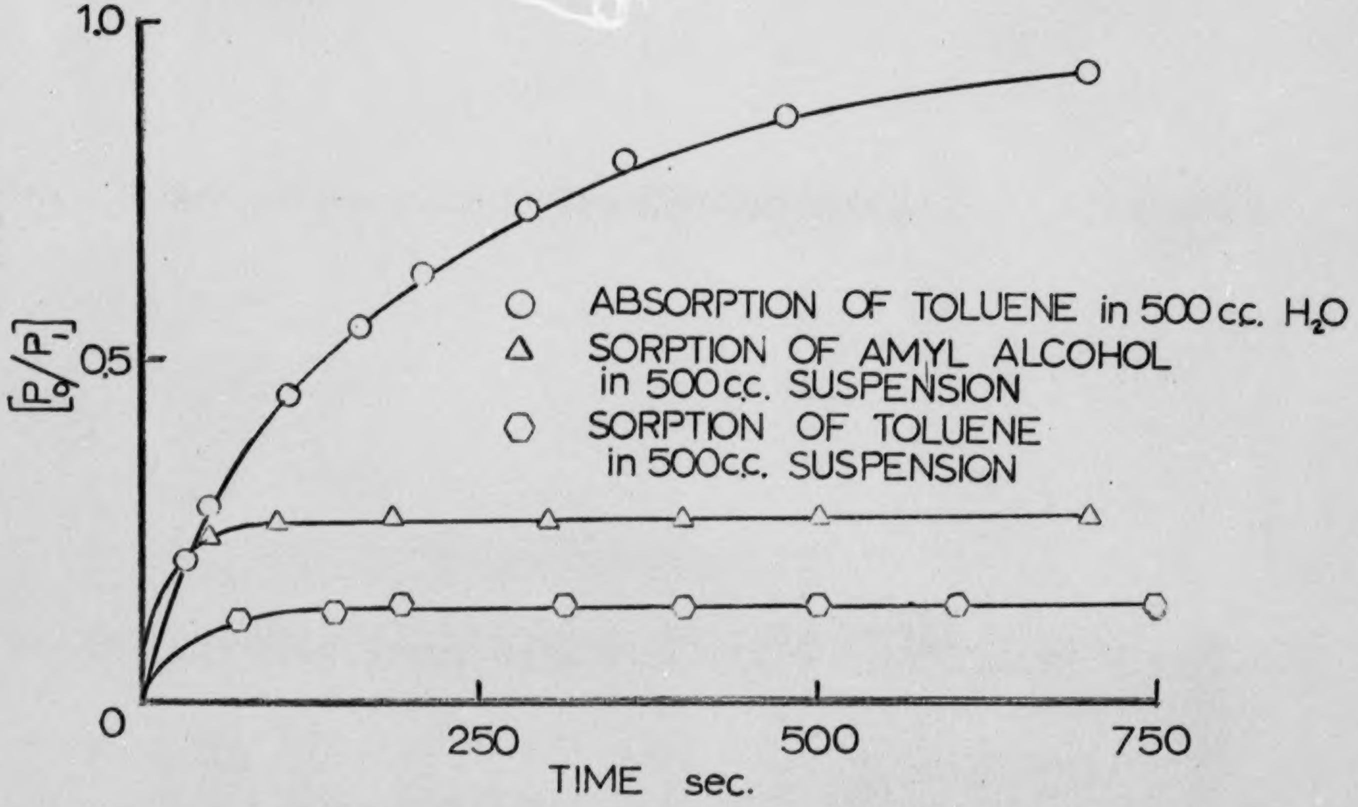

APPENDIX 7a

Absorption by Bubblers in Series

By: Dilip S. Mehta

Bubblers have been used widely for air analysis, in purification trains for gases in chemistry laboratories, and for other such purposes. The simplicity and convenience inherent in a bubbler led us to consider it for mass transfer studies. Comparative studies of efficiencies of sorption have been successfully carried out by us(1) in a bubbler. It was also thought that more than one bubblers in series might provide a good method of determining adsorption isotherm on wet activated carbon(1). Bubblers in series have been used for efficiency studies(2) and in air analysis. However, the analysis for the efficiency of bubblers in series, which can be of value in the understanding of the above mentioned work, is not available.

The purpose of this work was to develop generalized equation for the unsteady state absorption in n-similar bubblers in series. It was also decided to varify it experimentally.

Theoretical:

Intrinsic efficiency of a bubbler is defined as

$$f = \text{Intrinsic efficiency} = \frac{P_{n-1} - P_n}{P_{n-1} - P_{1n}} \qquad (1)$$

For similar bubblers the intrinsic efficiency would be the same provided they contain equal amounts of liquid and the flow rate of the gas is the same. This intrinsic efficiency would be(1)

$$f = 1 - e\left[- \frac{3RT}{H.r} \cdot K_L \cdot t_r\right] \qquad (2)$$

Figure 1 shows n-bubblers in series. Each bubbler is exactly similar to any other in all the characteristics. Amount of liquid in each bubbler is V c.c. Initially the concentration of the soluble component of gas is zero in the liquid. Now air, with the soluble component in constant concentration, is bubbled through this series of bubblers. Soluble component in air at inlet is in trace quantities.

Figure 1

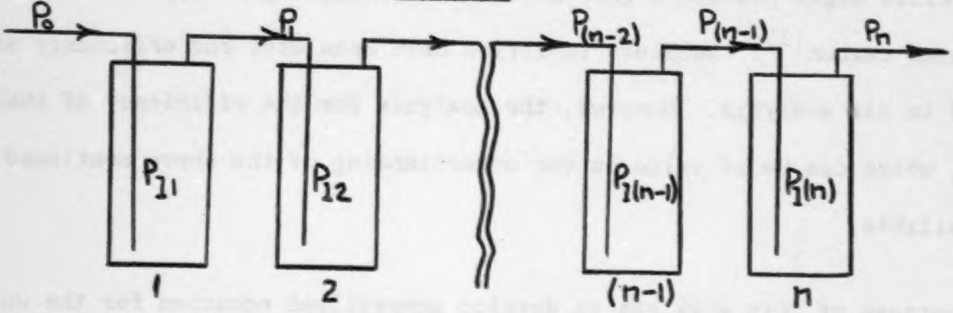

From equations (1) and (2) the following equation can be written:

$$P_n = A\,(P_{n-1} - P_{ln}) + P_{ln} \qquad (3)$$

where, $A = e^{-\left(\frac{3RT}{Hr} \cdot K_L \cdot t_r\right)}$

Similarly we can write equations for the concentration changes in the liquid.

$$dP_{ln} = \frac{HG}{RTV}\,(P_{n-1} - P_n) \cdot dt. \qquad (4)$$

Using equations (3) and (4) one can write the following set of equations

$$dP_{11} = \frac{HG}{RTV}\left[P_o f - P_{11} . f \right] dt \qquad (5)$$

$$dP_{12} = \frac{HG}{RTV}\left[P_o . A . f + P_{11} . f^2 - P_{12} . f \right] .dt \qquad (6)$$

$$dP_{13} = \frac{HG}{RTV}\left[P_o . A^2 . f + P_{11} . A . f^2 + P_{12} f^2 - P_{13} . f \right] dt \qquad (7)$$

....

$$dP_{1n} = \frac{HG}{RTV}\left[P_o A^{n-1} . f + P_{11} A^{n-2} f^2 + ... + P_{1(n-1)} f^2 - P_{1n} f \right] .dt \qquad (8)$$

Equation (5) can be solved and P_{11} obtained can be substituted in equation (6) to solve for P_{12}. Solving the equations this way until a general pattern is seen in the solution. The generalized solution can be written as follows.

$$P_{11} = P_o\left[1 - e^{-\frac{HG}{RTV} . ft.} \right] \qquad (9)$$

$$P_{1n} = P_o\left[1 - e^{-\frac{HG}{RTV}} - \left[e^{-\frac{HGft}{RTV}} \sum_{j=1}^{J=n-1} CijDj \right] \right] ; n>1 \qquad (10)$$

where, $Dj = \dfrac{\left[\frac{HGf}{RTV} . f . t\right]^j}{j!}$

$$Cij = \left[\sum_{i_j=1}^{i_j=(n-j)} A^{(i_j-1)} [i_j]^o \left[\sum_{i_{j-1}=1}^{i_{j-1}=i_j} [i_{i_0-1}]^p \left[\sum_{i_2=1}^{i_2=i_3} [i_2]^o \left[\sum_{i_1=1}^{i_1=i_2} [i_1]^o \right] \right] \right] \right]$$

and, $P_n = A\,P_{n-1} + P_{1n}\,f$ (11)

Although equation (10) and (11) are explicit they require lengthy computations for large numbers of bubblers. These equations were solved on the digital computer for the outlet concentration and for the overall average efficiency. Some of the results are plotted in Figure 2 and Figure 3.

Experimental:

Ethylene Oxide:

In order to utilize the above equations to predict the changes in concentrations with time one must know the intrinsic efficiency f, of a bubbler. J. C. Gage(3) has reported data for the concentration changes in the liquid phase when two bubblers are in series. These data are for absorption of ethylene oxide in water. From the data the following values were calculated.

$H = 1.94 \times 10^{2}$ (atm)/(mols/c.c.)

$P_o = 27.7 \times 10^{-6}$ atm.

$$\frac{G}{RT} = 0.341 \times 10^{-3} \quad \frac{(\text{mols})}{(\text{sec})\ (\text{atm})}$$

V = 10 c.c.

Time min.	$P_{11} \times 10^6$ atm	$P_{12} \times 10^6$ atm
1	9.02	2.2

2	15.18	7.26
4	23.1	13.2
10	27.7	25.7
20	27.7	27.7

One data point, P_{11} at 1 minute, was used to find intrinsic efficiency f=0.994. Now $P_{11}(t)$ and $P_{12}(t)$ can be predicted. The predicted curves and the experimental points are shown in Figure 4.

Carbon Dioxide:

Experiments were carried out for absorption of carbon dioxide in water in bubblers in series. Constant concentration carbon dioxide was introduced and the exit concentrations were measured continuously by infrared analyzer. In the desorption experiments water was saturated by constant concentration carbon dioxide mixture and then nitrogen was bubbled through it while exit concentrations were monitored. The results of this experimental work are given in Figure 5. It can be noticed that the desorption curves are mirror images of the absorption curves, indicating that the intrinsic efficiency for absorption and desorption is the same and that the mass transfer coefficients do not change.

The analysis of these results requires modification. This is due to the fact that the dead space above each bubbler is considerable and can not be neglected. Figure 6 is the correct representation of the situation instead of Figure 1.

Figure 6

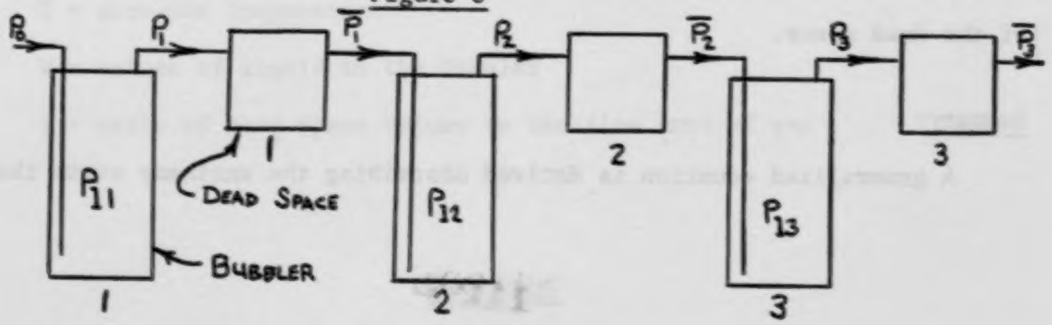

Equations have to be rewritten taking into account the dead space effect. If we assume this dead space to be a perfect stirred tank then for each bubbler and its dead space the following three equations can be written.

$$P_n = A\ \overline{P}_{n-1} + P_{1n} \cdot f \tag{12}$$

$$\frac{d\ (P_{12})}{dt} = \frac{HG}{RTV}\ (\overline{P}_{n-1} - \overline{P}_n) \tag{13}$$

$$\frac{d\ (\overline{P}_n)}{dt} + \frac{1}{\gamma}\ \overline{P}_n = \frac{1}{\gamma}\ P_n \tag{14}$$

Solutions for $\overline{P}_1$, $\overline{P}_2$, and $\overline{P}_3$ were derived. Final results are rather lengthy and only $\overline{P}_1$ is given here.

$$\overline{P}_1 = P_o\ (1-e^{-t/\gamma}) + (\frac{1}{\gamma})\ \frac{f.\ (P_{11}\ (t=o) - P_o)}{(\frac{1}{\gamma} - \frac{HG}{RTV} \cdot f)} \left[\overline{e}^{\ (\frac{HG}{RTV}\ t)} - \overline{e}^{\ (t/\gamma)} \right]$$

$$+ \overline{P}_1\ (t=o) \cdot \overline{e}^{\ (t/\gamma)}$$

From the data, one point was taken to calculate f. Then using that value of f ($f = 0.3$) $\overline{P}_1$, $\overline{P}_2$, and $\overline{P}_3$ were predicted for absorption and desorption. The predicted curves fall nearly on the top of the experimental curves and hence are not given in Figure 5. This also illustrates the remarkable success of the stirred tank assumption for the dead space and at the same time the importance of the dead space.

Summary:

A generalized equation is derived describing the unsteady state absorption in n-bubblers in series. The equation predicts the experimental data, taken from literature, accurately. The importance of dead space in a bubbler was shown and a method is given to take that into account.

Acknowledgement:

Mr. S. C. Jain's help in computer program is acknowledged.

Nomenclature:

A = 1-f

f = intrinsic efficiency

G = flow rate of gas c.c./sec.

H = Henry's Law constant

K_L = overall mass transfer coefficient - gas to liquid cm/sec

P_n = partial pressure of solute gas in exit from nth bubbler

P_{1n} = partial pressure of solute gas, atm., that is in equilibrium with the concentration of the solute gas in liquid in nth bubbler

$\overline{P}_n$ = partial pressure of the solute gas, in exit from the dead space of nth bubbler

r = radius of the bubble

R = gas law constant

t = time, sec.

t_r = average residence time of a bubble in the liquid

T = absolute temperature

V = volume of liquid in the bubbler

γ = ratio of dead space volume to the flow rate of gas

References:

1. D. S. Mehta and Seymour Calvert; "Gas Sorption by Suspensions of Activated Carbon in Water", to be presented at AIChE 61st National Meeting, December, 1966.
2. L. R. Roberts and H. C. McKee, Journal of the Air Pollution Control Association, Volume 9, Number 1, May, 1959.
3. J. C. Gage, Analyst, 85: 196 (1960).

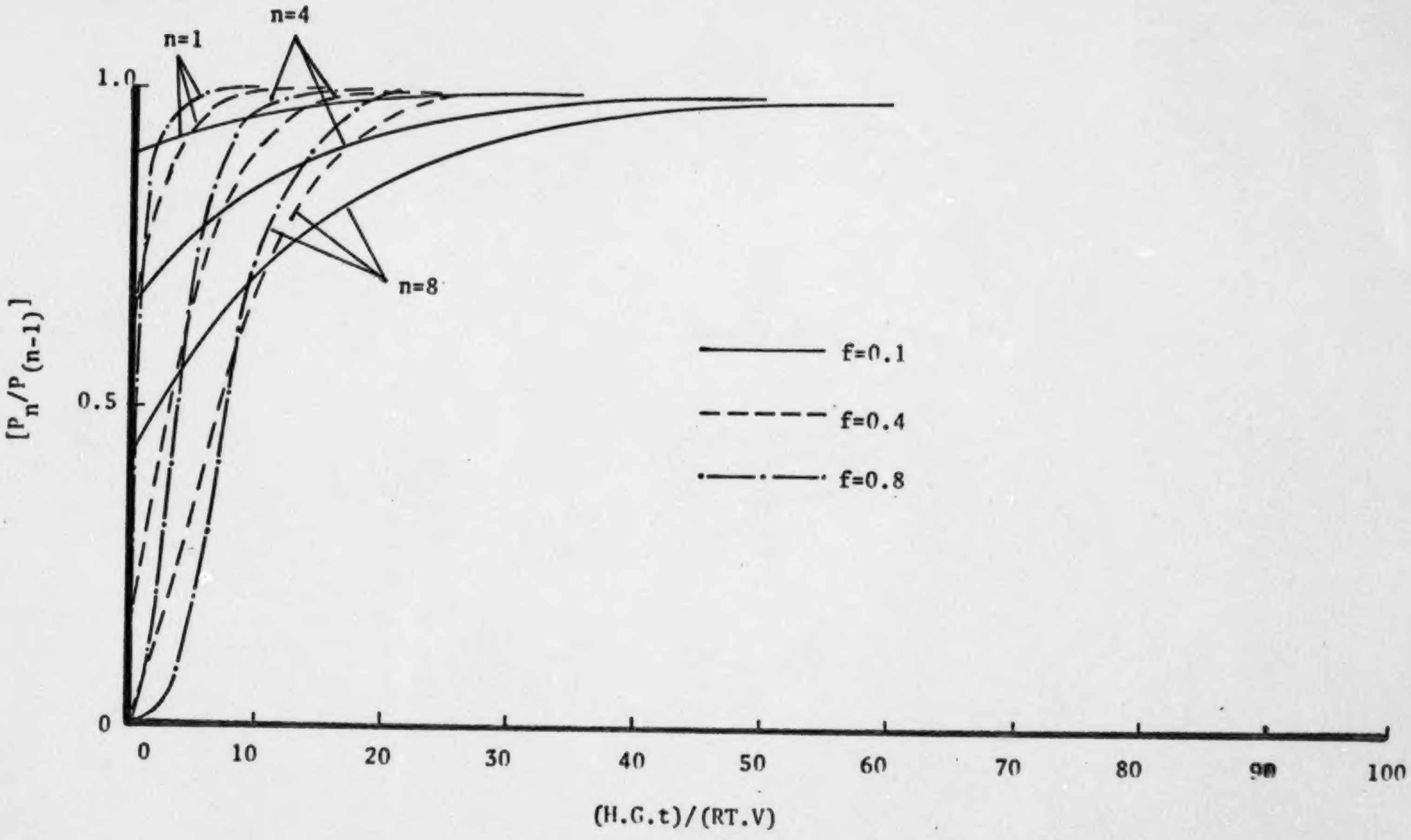
n=1
n=4
n=8
1.0
0.5
0
[$P_n/P_{(n-1)}$]
0
10
20
30
40
50
60
70
80
90
100
(H.G.t)/(RT.V)
f=0.1
f=0.4
f=0.8

Fig. 2

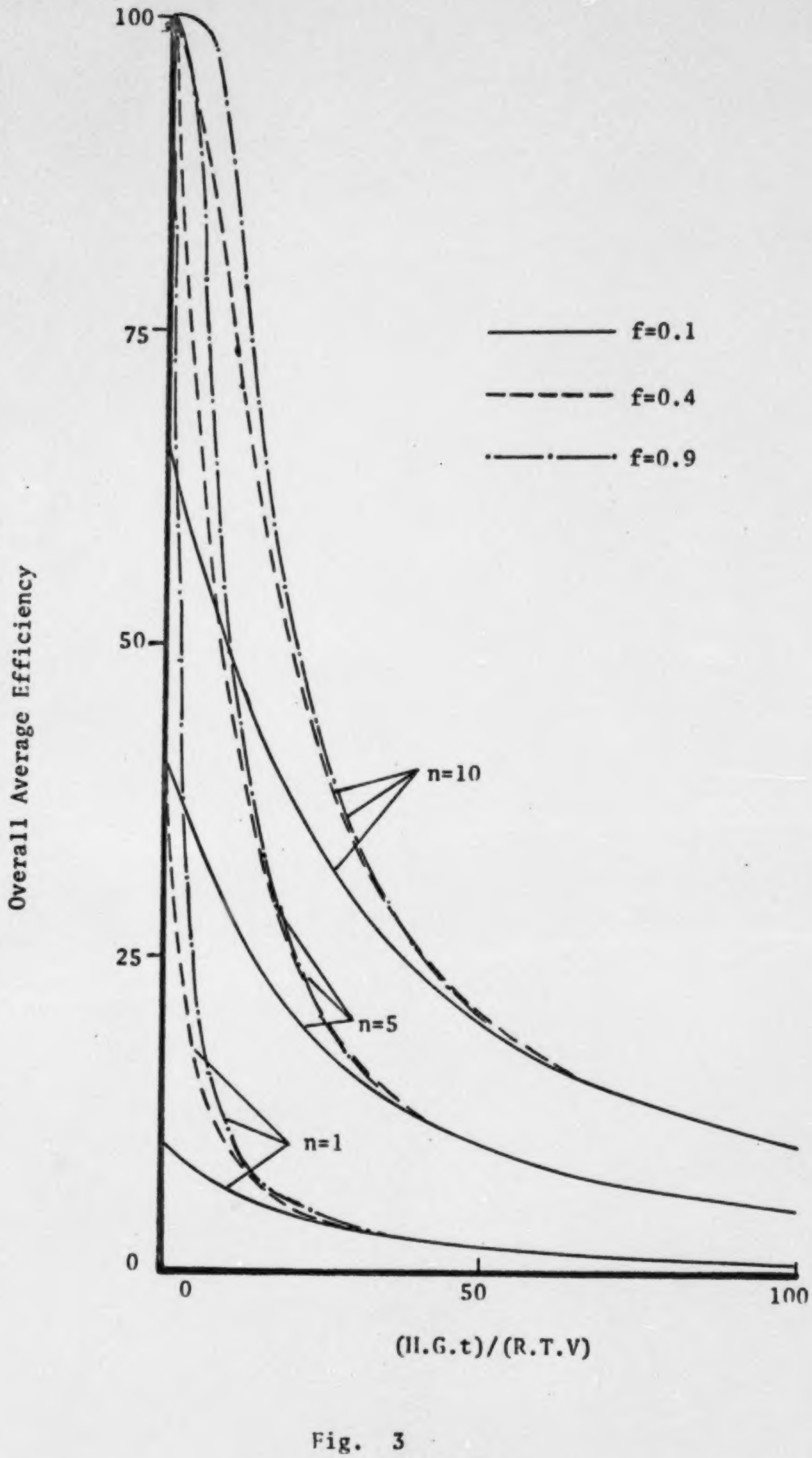
100
75
50
25
0
Overall Average Efficiency
0
50
100
(H.G.t)/(R.T.V)
f=0.1
f=0.4
f=0.9
n=10
n=5
n=1

Fig. 3

Absorption Of Ethylene Oxide
n-Bubblers In Series

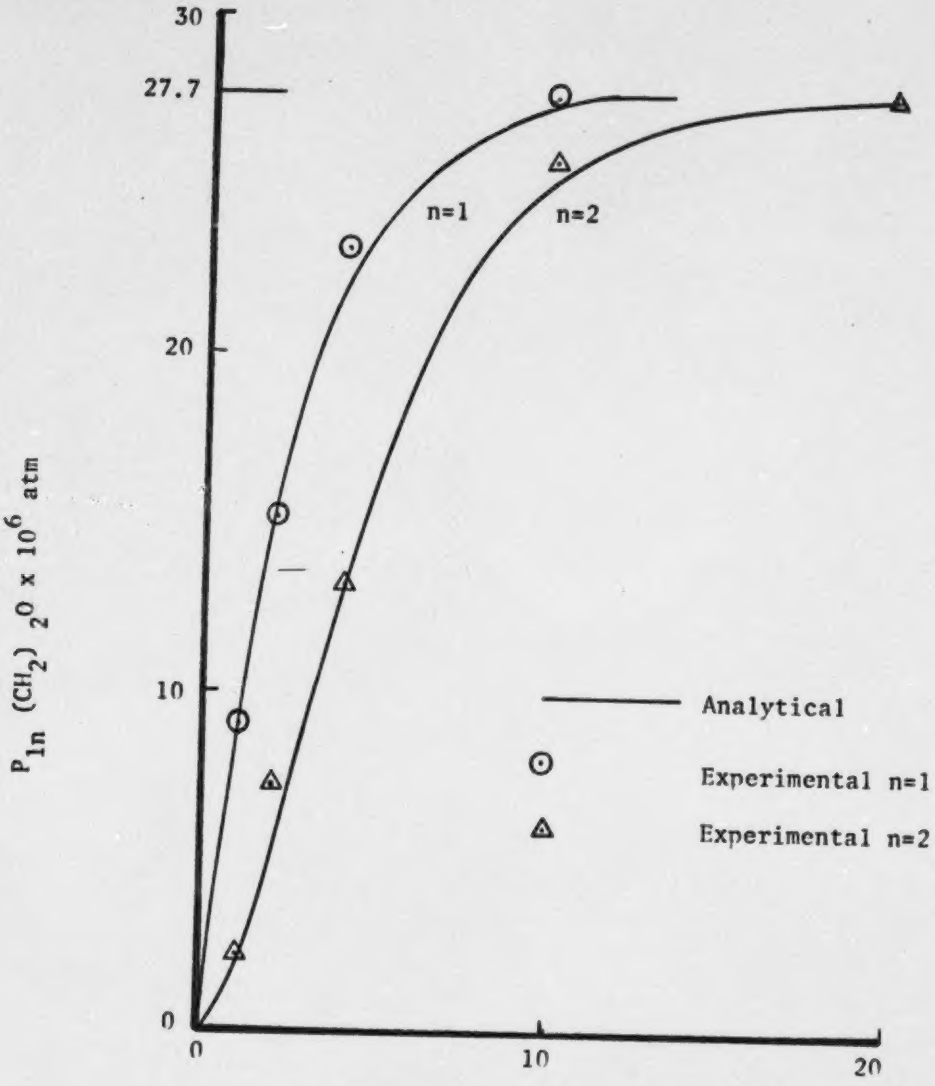

Fig. 4

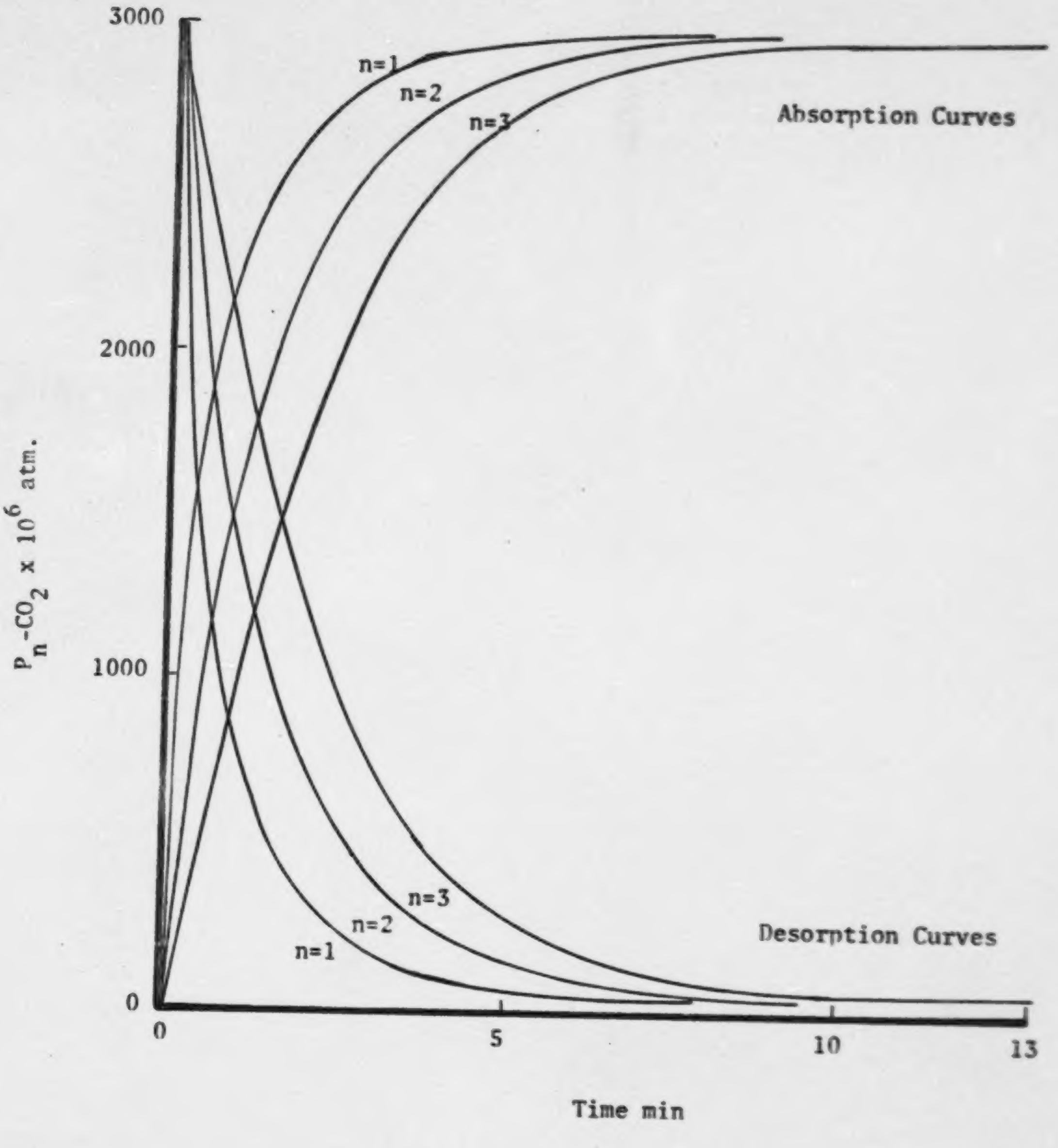

Experimental Absorption And Desorption Of CO_2
n-Bubblers In Series

Fig. 5

APPENDIX 7b

SORPTION BY SUSPENSIONS IN A SIEVE PLATE COLUMN

By: Dilip S. Mehta

Sorption by suspension is the absorption and adsorption of a gas by suspension of an adsorbent in a liquid. Previous equilibrium studies have made it evident that the capacity of a liquid for soluble gases can be increased greatly by the addition of a few percent of adsorbent. The rate studies in bubblers have shown that the controlling factor for the rates is the solubility of the gas in the liquid.

OBJECTIVE

The objective of the present work is to investigate the effectiveness of the suspension of activated carbon in a suitable practical contactor. This requires a comparative study of absorption and sorption under a wide range of system properties and operating conditions. Drop-through type (without downcomer) sieve plate column was chosen in this study due to its simplicity.

EXPERIMENTAL

A complicating factor in the study of plate efficiency is that either the gas- or liquid-phase physical properties or both may control the magnitude of the efficiency obtained. In determining the effect of system properties, it is desirable first to study the effect of gas-phase properties separately from that of liquid-phase properties by choosing special systems where either gas or liquid properties control. Thus the effect of the properties of one of the phases is eliminated from the measured efficiency. The vapors selected in this study were ethanol, methanol, acetone, and benzene. A high solubility gas would be gas-phase controlled with negligible resistance in the liquid phase. Methanol and ethanol fall in this category. Absorption of benzene is liquid-phase controlled due to its low solubility in water. Acetone has the solubility somewhere between these categories and in the absorption of acetone both phases would have appreciable resistance. These extensive studies in absorption are to characterize the column. The reliability of data is checked by the use of two different high solubility gases.

It was decided to use ethanol and benzene for the studies in sorption by suspension of activated carbon C-190 in water. This represents two different systems. Suspensions with one percent and five percent activated carbon were used for ethanol sorption while only one concentration was used in the case of benzene sorption. As has been mentioned this study is a comparative study of the efficiencies for absorption and sorption, and hence the design variables were not investigated. The operating variables were the flow rates of liquid and the gas. For benzene absorption the effect of these variables was not explored thoroughly due to analysis problems. The overall absorption efficiency for benzene is low and the change is the concentration between the inlet and the outlet gas is not very large to allow the effects of flow rates to be determined by our analytical method. The analytical instrument used is the total hydrocarbon analyzer and is described fully in Appendix 6.

Sieve plate column used in this study has one plate of two inches inside diameter. The plate has 5/32" holes on a triangular grid with pitch equal to 5/16".

Mixing of Vapors

In each experiment a constant concentration of the solute vapor (in hundreds of ppm range) in the background of air was provided to the column. The mixture was prepared in the following manner. Nitrogen was bubbled through the organic liquid of interest at the desired rate. Nitrogen containing the organic vapor from the outlet was mixed with the main stream of air. The mixture was passed through the rotometer and supplied to the column. A sample from inlet to the total hydrocarbon analyzer allows measurement of the concentration. The desired concentration can be achieved by control of the nitrogen flow rate. Figure 4 shows the set up for mixing.

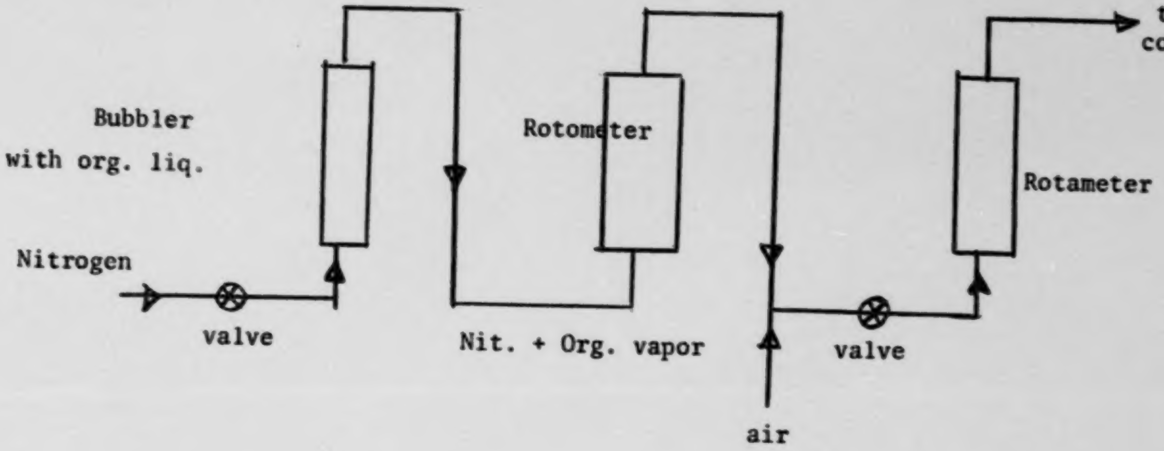

Figure 4

RESULTS AND DISCUSSION

The results of absorption of ethanol, methanol, and acetone by water are given in figures 1, 2, and 3 in terms of overall efficiencies. The vapor-phase Murphree efficiencies of these were calculated and are shown in Figures 5, 6, and 7. It can be noticed, both for the overall efficiency and murphree efficiency, that there is a great similarity in the efficiency curves for ethanol and methanol. The reason for this is the considerable similarity in the physical properties and solubilities of the two.

Effect of flow rates on absorption of benzene was not studied due to the reasons mentioned before. However, absorption efficiency was measured at $U_g = 0.76$ and 4.57 (ft./sec) and L = 1660 (lb)/(ft^2) (hr). Murphree efficiency was found to be about 10 percent. This value is an average value obtained after many runs.

The results of sorption by activated carbon suspension in water are given in Fig. 8 and 9. Two different concentrations were used for sorption of ethanol. In general it is seen that at 5% concentration the efficiencies are a bit lower than that at 1% concentration of the activated carbon. This is quite in agreement with the results of the bubbler study given in appendix 6. For both the concentrations the overall efficiency sorption curves are closer to the overall efficiency absorption curves rather than the Murphree efficiency absorption curves. This is obvious since for a high solubility gas it is a gas-phase controlled, with the presence of activated carbon affecting the efficiency hardly for any one plate.

Exactly the opposite is belived to be true in the case of low solubility gas such as benzene. Murphree efficiency absorption curve and the overall efficiency sorption curves for benzene are shown in Figure 9. The sorption curves are very close to the Murphree efficiency absorption curve. This is due to the presence of activated carbon as concluded in the bubbler study.

The above is only a short summary of results and conclusions. A detailed analysis is being made of the results.

CONCLUSION

In a practical contactor, such as a sieve plate column, the sorption efficiency would be somewhere between the overall and the Murphree efficiency of absorption. For a highly soluble gas the sorption efficiency would be closer to the overall efficiency while for a low solubility gas it would be closer to the intrinsic efficiency. This is our tentative conclusion until a critical examination is made of the results.

Absorption of Ethanol

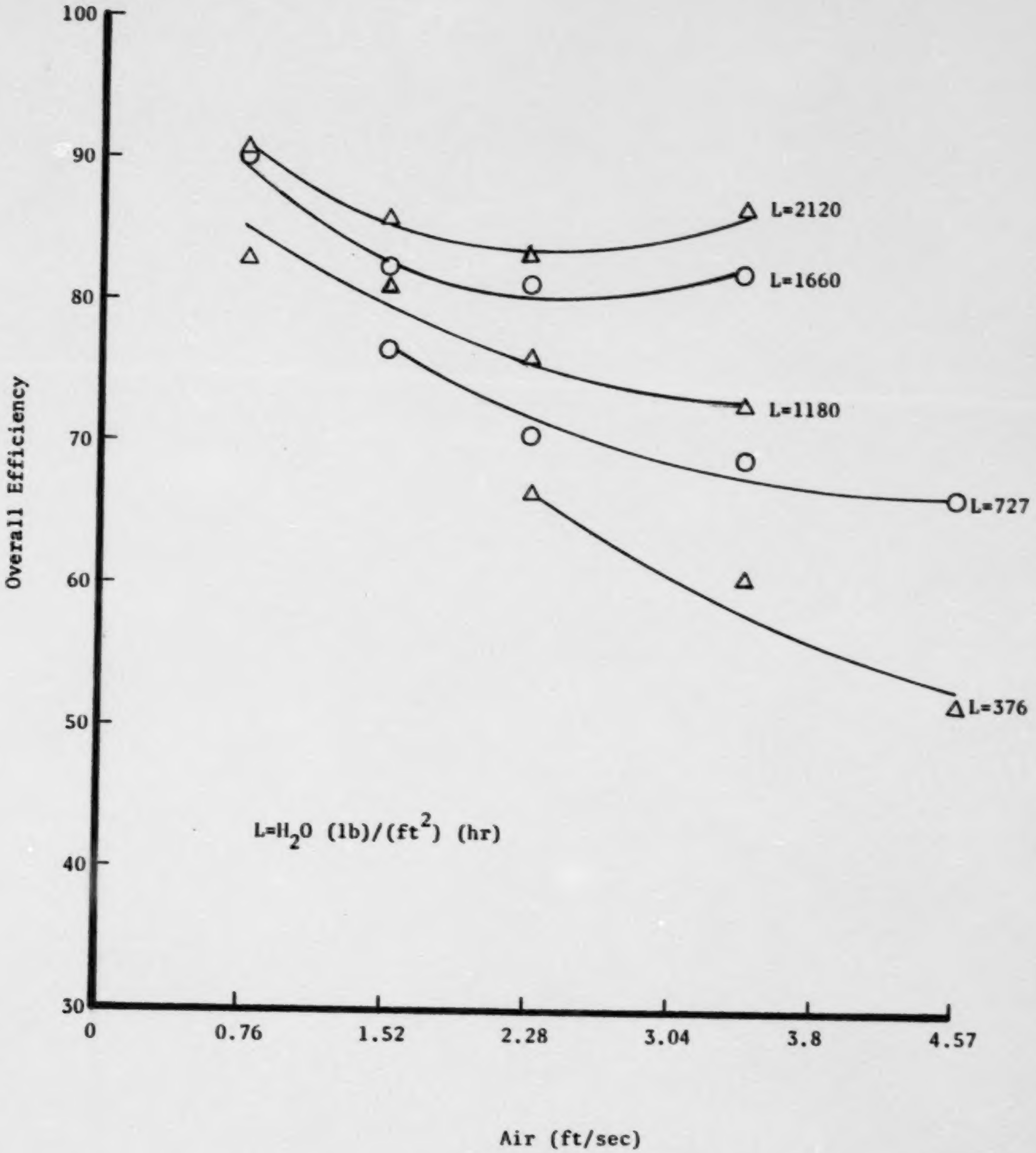

Fig. 1

Absorption of Methanol

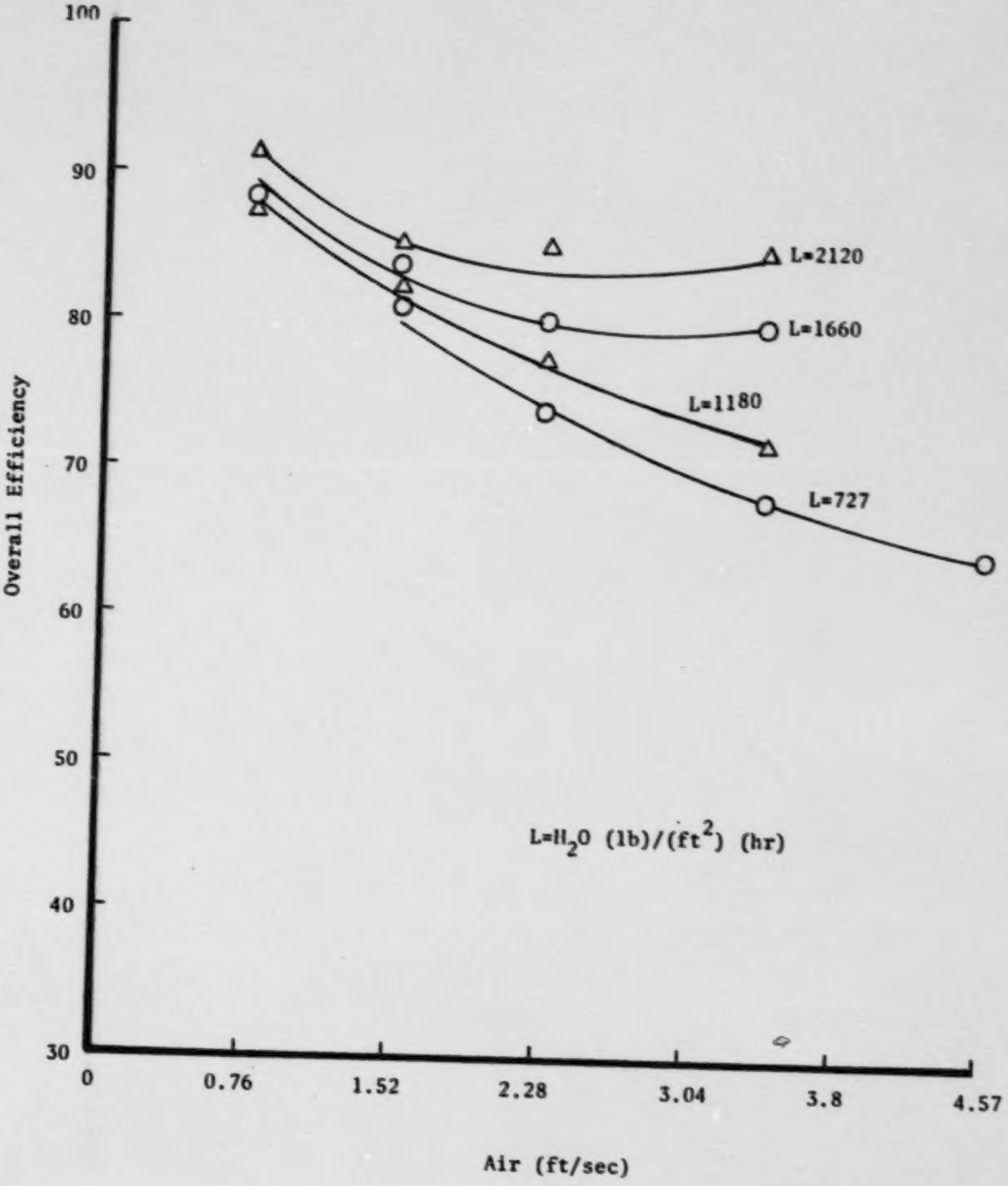

Fig. 2

Absorption of Acetone

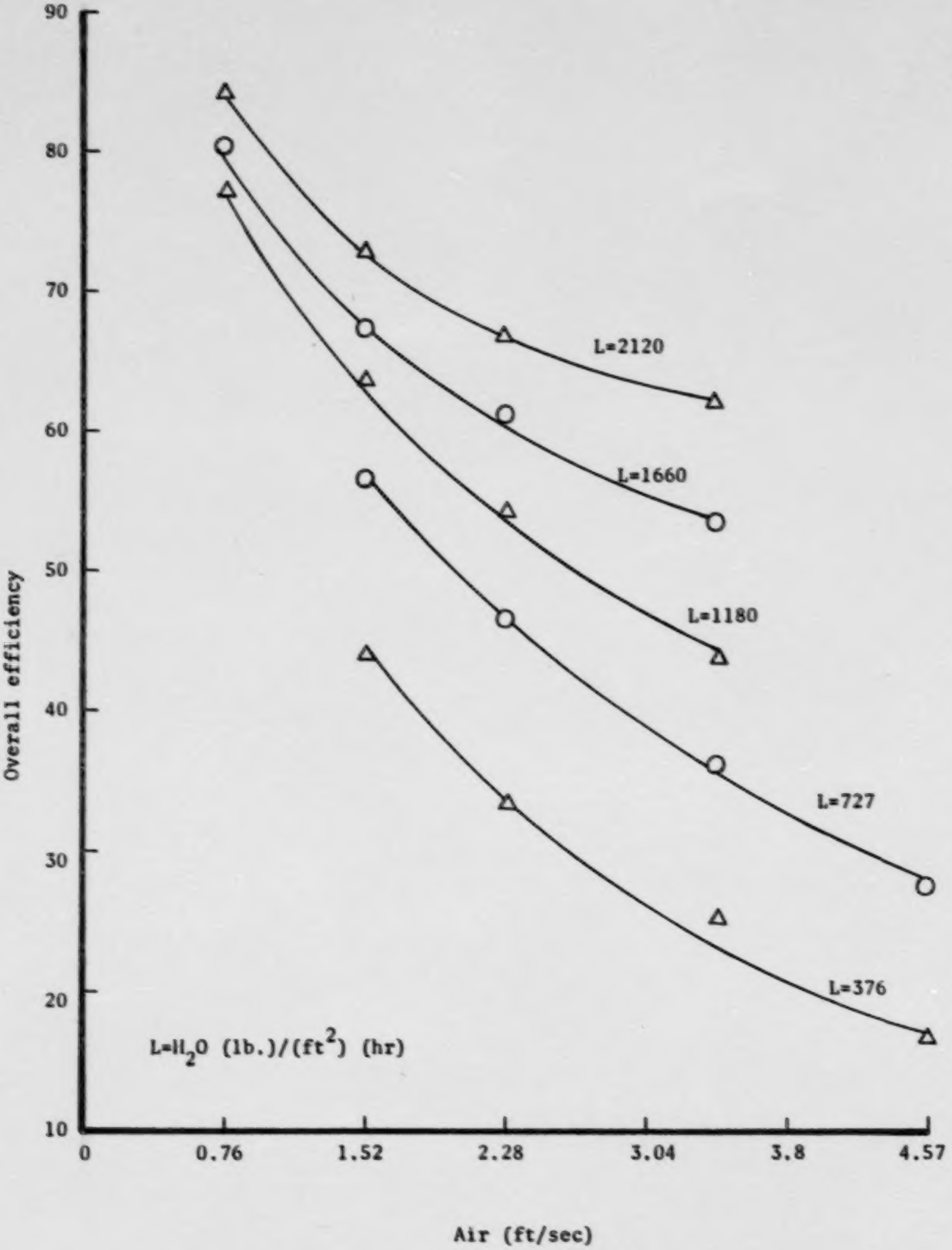

Fig. 3

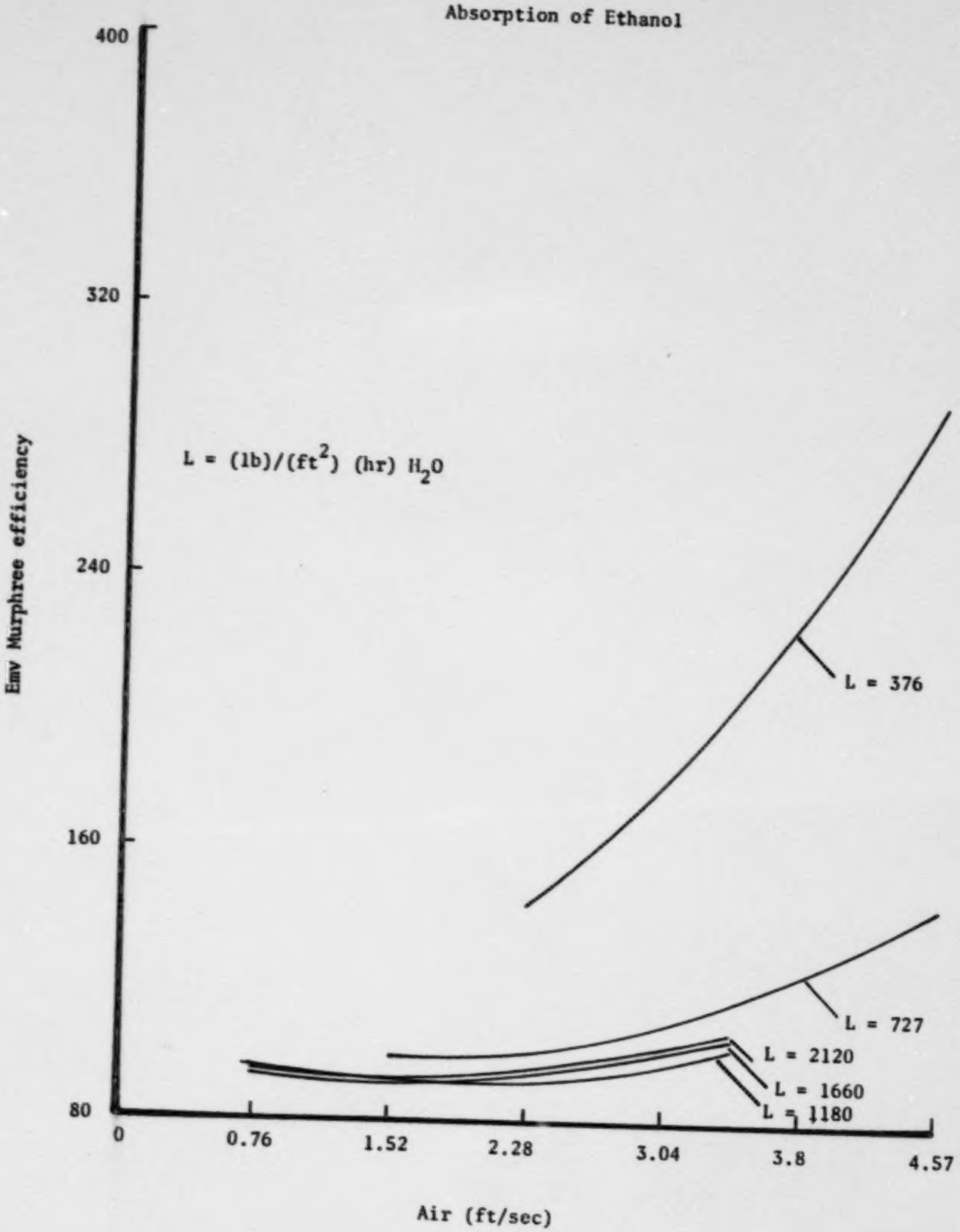
Absorption of Ethanol
400
320
240
160
80
Emv Murphree efficiency
L = (lb)/(ft^2) (hr) H_2O
L = 376
L = 727
L = 2120
L = 1660
L = 1180
0
0.76
1.52
2.28
3.04
3.8
4.57
Air (ft/sec)

Figure 5

Absorption of Methanol

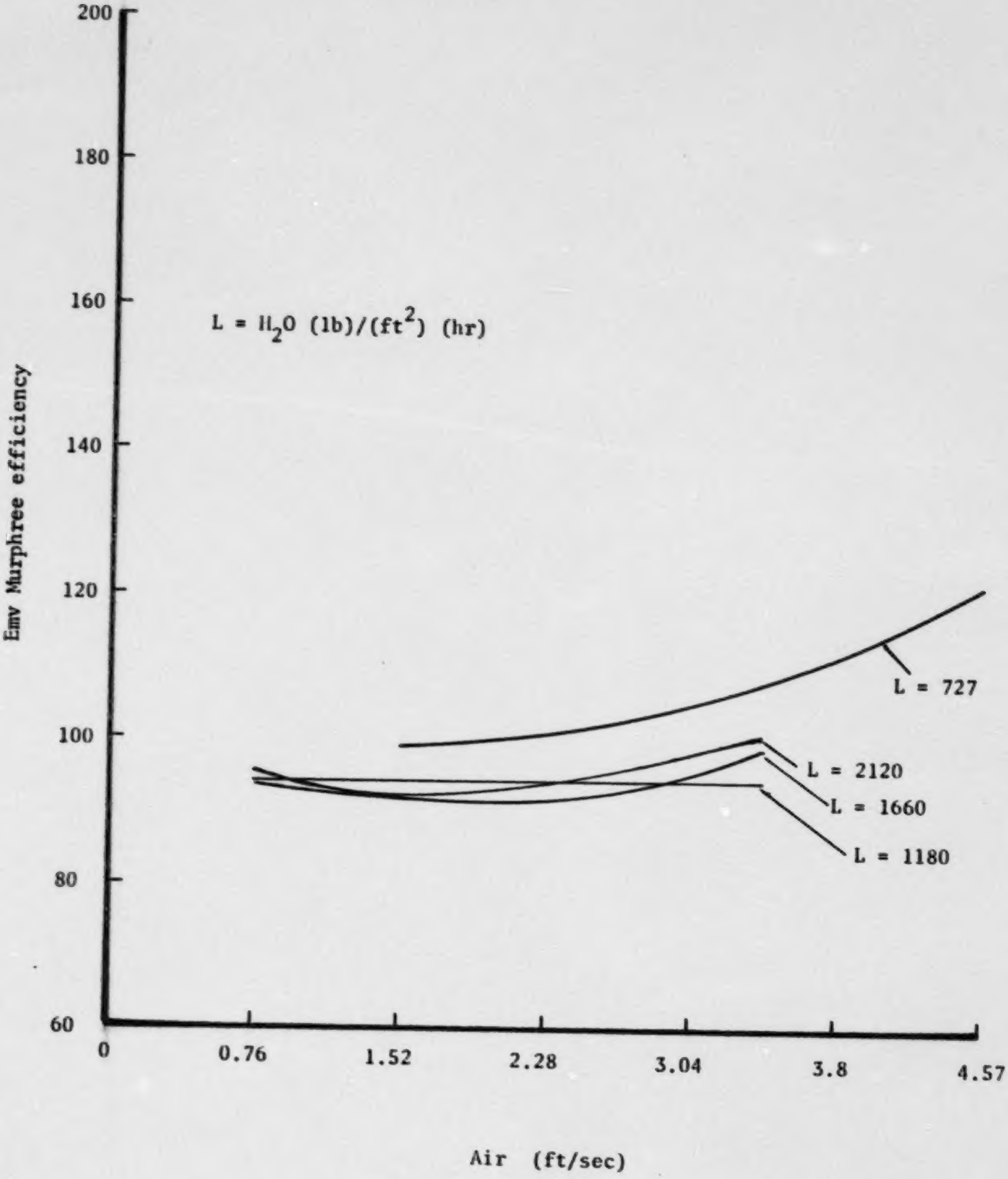

Figure 6

Absorption of Acetone

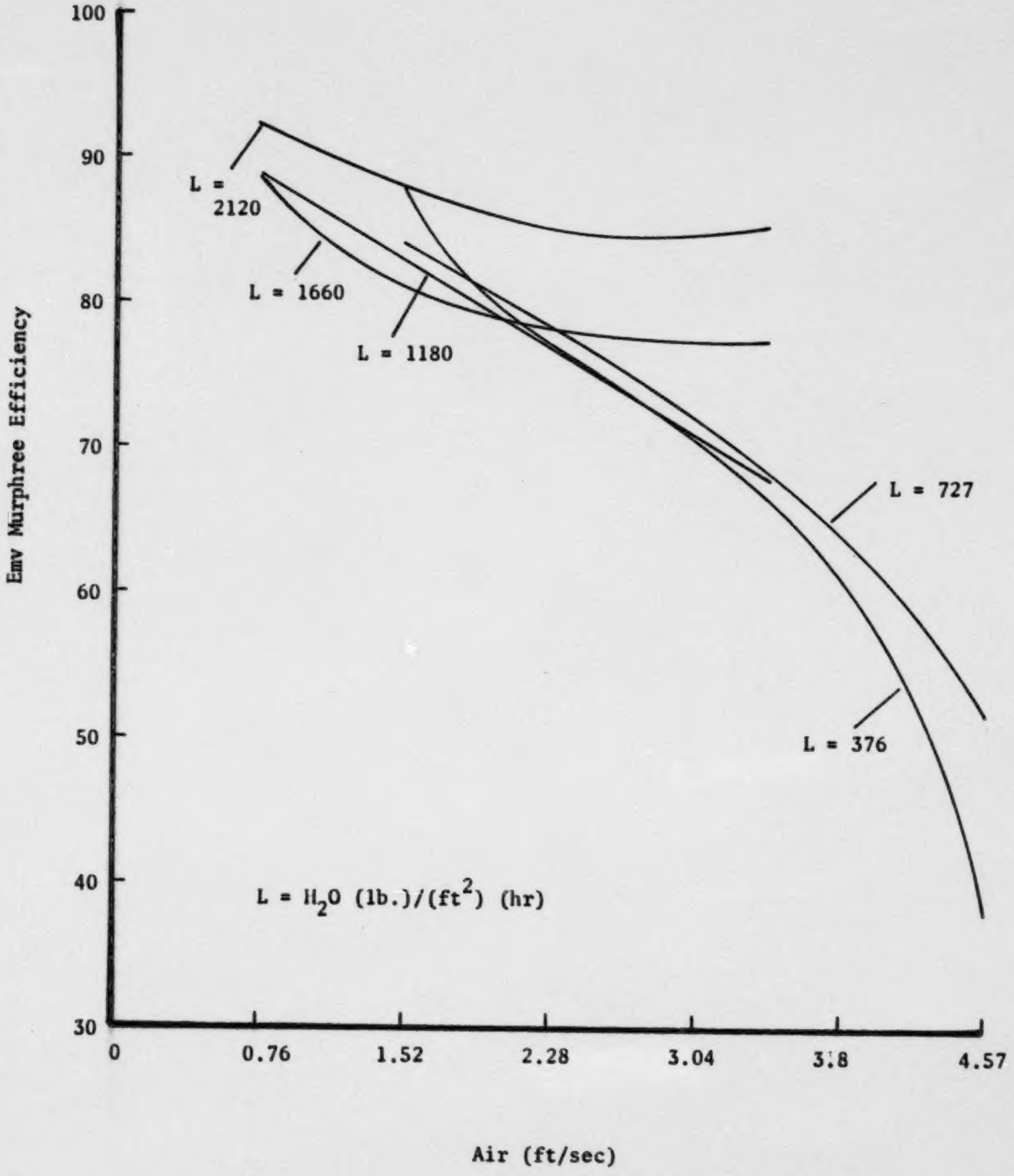

Figure 7

Sorption of Ethanol

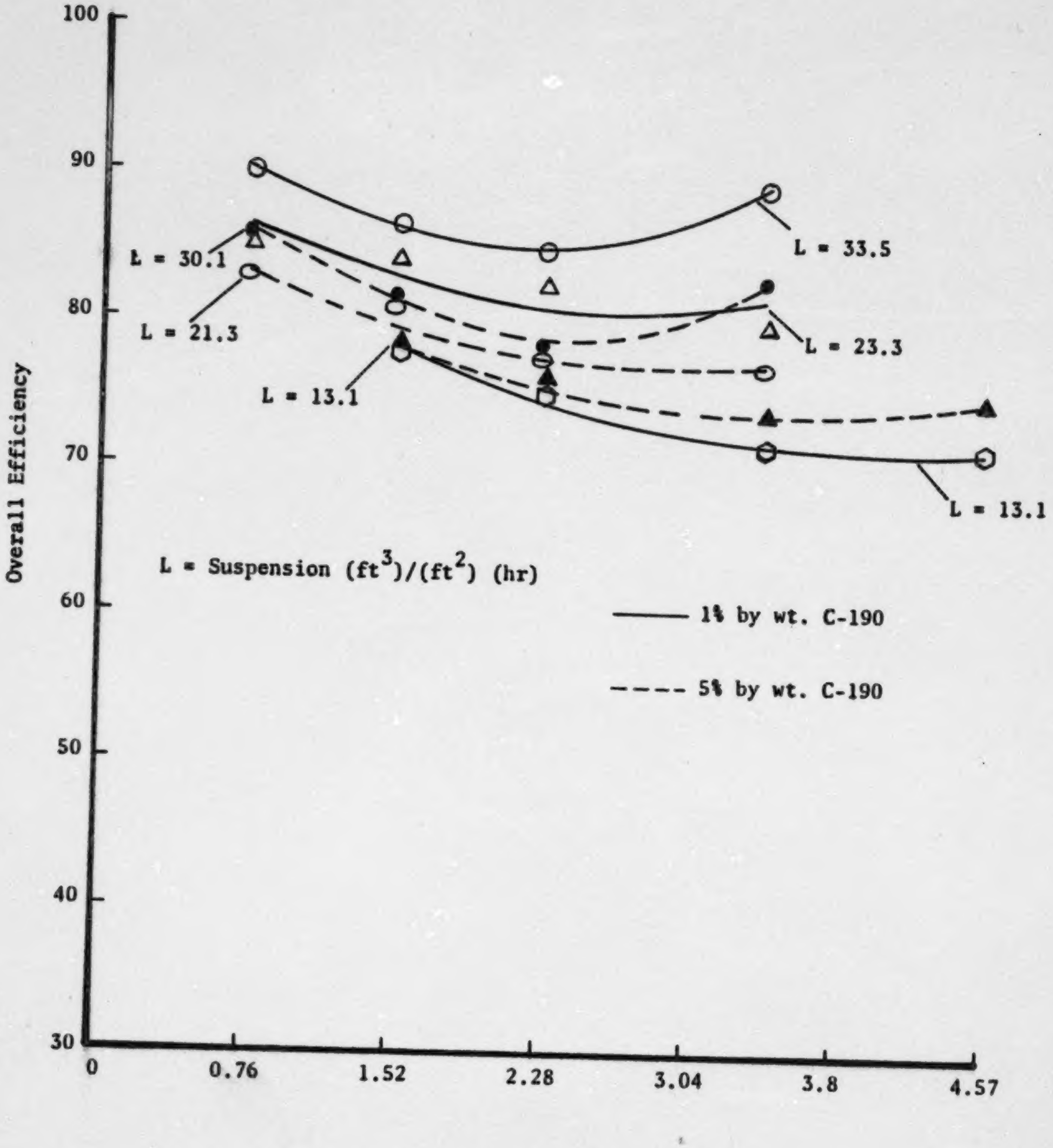

Figure 8

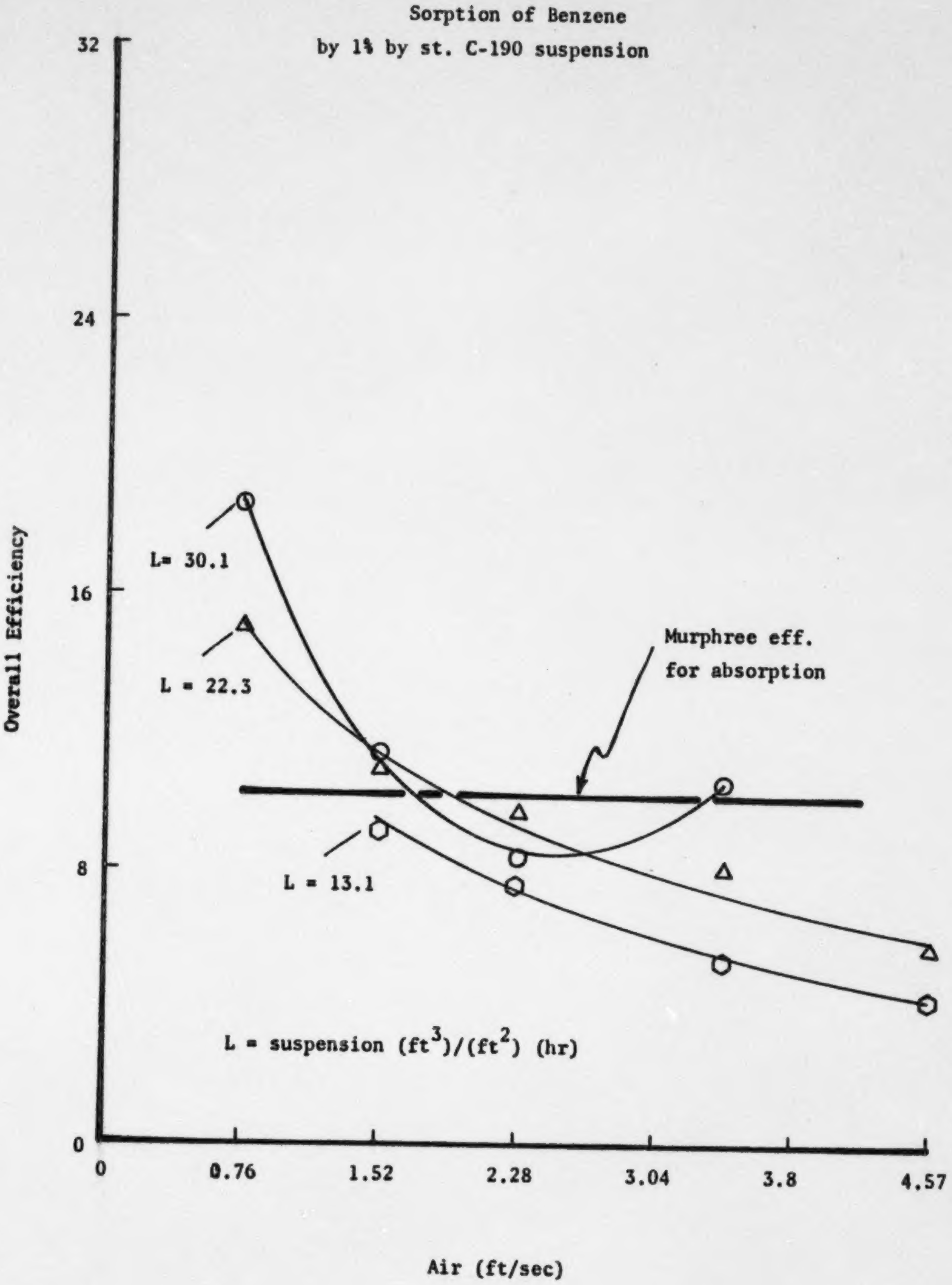

Sorption of Benzene
by 1% by st. C-190 suspension

Figure 9

APPENDIX 8

DEPOSITION OF PARTICLES FROM A TURBULENT STREAM BY MEANS OF THERMAL FORCE

By R. Lee Byers and Seymour Calvert

ABSTRACT

A theoretical model for the deposition of particles from turbulent streams by means of thermophoresis is presented. Predictions indicate that thermophoresis can be an effective mechanism for cleaning high temperature gases and that fouling rates of heat exchanger surfaces of simple geometry can be determined.

INTRODUCTION

Thermophoresis is the interaction between a dust particle and a steep thermal gradient which causes the particle to be accelerated down the gradient. The objectives of much theoretical and experimental investigation have been to define quantatively the phenomenon and use the mechanism as a means of particle collection. An air sampling device, the thermal precipitator, which is commercially available removes particles from air streams moving at rates ranging from 6-10 cc./min. The use of these samplers has been described in the literature (1, 2, 3). No known work has been done to determine the feasibility of using thermal force as a gas cleaning mechanism where it would be necessary to handle large quantities of gas. To determine such feasibility is the purpose of this work.

THEORY OF THERMOPHORESIS

Early observations of a dust-free space surrounding a hot body were made by Tyndall (4). He proposed that the dust-free space was due to the body heating the adjacent air causing it to rise, pulling the dust after it. Rayleigh (5) later performed some experiments and concluded that the curvature of the streamlines near the heated body exerted a centrifugal force on the dust particles causing them to be thrown away from the body. Aitken (6), and Lodge and Clarke (7) suggested that the motion of particles away from a hot body was caused by differential molecular bombardment of the dust particles in the vicinity of the body.

This latter explanation received further attention by Cawood (8). Considering a cylinder of gas, a length about twice the mean free path of the gas, whose axis is perpendicular to a hot surface, and whose radius is of the magnitude of the mean free path of the gas, Cawood concluded that a particle inside this cylinder would experience bombardment due to the motion of gas molecules parallel to the axis of the cylinder but would experience no net lateral bombardment.

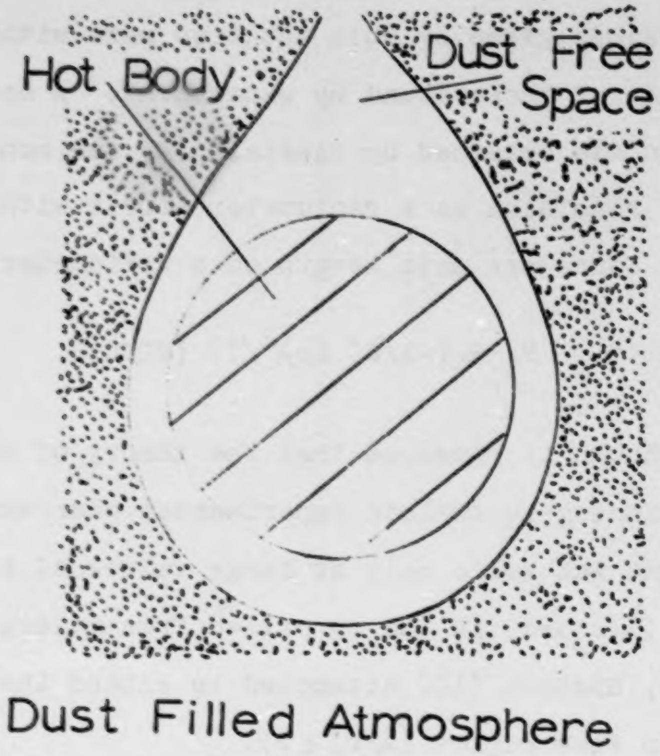
Hot Body
Dust Free Space
Dust Filled Atmosphere

Figure 1

Dust Free Space Surrounding a Hot Body

A force which a solid particle in the cylinder would experience away from the hot surface multiplied by the average velocity of gas molecules can be equated to the rate of energy flow through the cylinder. Reducing this to an equation Cawood obtained the following:

$$F_t = (-1/2)\ (p)\ (\lambda/T)\ (\pi r^2 p)\ (dT/dx) \qquad (1)$$

Values given by this equation were within an order of magnitude of those found by experiment. A more successful equation was obtained by Einstein (9) who considered thermal repulsion as a radiometer effect with the expression for the force per unit length on a radiometer vane being:

$$F_t = (-1/2)\ (p\lambda^2/T)\ (dT/dx) \qquad (2)$$

Though it appeared that the theory of thermal repulsion was beginning to explain experimental observations the agreement was valid only at large values of the Knudson number ($\lambda/r_p \gg 1$) in the so called free molecule regime. In 1929, Epstein (10) attempted to extend the theory to the slip flow regime ($\lambda/r_p < 1$).

Epstein considered both kinetic and hydroynamic aspects of flow of gas around a spherical particle and took into account the fact that the behavior of the particle in the gas would depend upon the ratio of heat transported through the interior of the particle to the heat received on its surface from molecular impacts. Three basic assumptions were made: (1) $\lambda/r_p \ll 1$ (for air at room temperature and atmospheric pressure for a 5 micron particle $\lambda/r_p = 0.0265$); (2) a uniform temperature distribution exists in the gas at a great distance from the particle; (3) and convective heat transfer to the particle is negligible compared to heat transfer by conduction.

The first step in calculations required solving for the temperature gradient over the surface of the particle. Using the thermal creep velocity, as defined by Maxwell (11), as a boundary condition the Navier Stokes equations were solved. By integrating over the entire surface the total force on the particle was obtained. The thermal force was then calculated as the component of the total force parallel to the direction of the temperature gradient. Epstein's final equation for the thermal force is given by

$$F_t = (-9\pi)\ (r_p)\ (\mu^2/\rho T)\ \left(\frac{k_g}{2k_g+k_p}\right)\ (dT/dx) \qquad (3)$$

Numerous experimental investigations have been carried out to test Epstein's equation. The data of Rosenblatt and LaMer (12) showed satisfactory agreement with the theory considering the assumptions used in its development. Additional support for the theory was given by the work of Saxtan and Ranz (13). However, results obtained by Shadt and Cadle (14, 15) cast some doubt on the Epstein theory particularly for aerosol particles of high thermal conductivity. As Equation (3) shows, when k_p becomes large the thermal force tends to zero. Yet, Shadt and Cadle found no such tendency in their experimental observations while using particles whose thermal conductivities ranged from 1.45×10^{-2} BTU/hr. ft.°R to 39.4 BTU/hr. ft.°R. In fact the thermal force on iron and sodium chloride particles was from twenty to thirty times greater than those predicted by Equation (3).

Several explanations (12) for the above discrepancy have been suggested. Brock (16, 17) has best been able to account for these differences by resolving the steady state Navier-Stokes equation subject to two corrections of the Epstein theory; (1) boundary conditions more suitable for the slip flow regime were used and (2) the continuum energy equation has been solved taking into account convective terms. Brock's equation has the form

$$F_t = \frac{(-12\pi)\,(\mu^2 r_p)\,(k_g/k_p + c_t\lambda/r_p)\,(c_{tm}\lambda/r_p)}{(1 + 3c_m\lambda/r_p)\,(1 + 2k_g/k_p + 2c_t\lambda/r_p)}\,(dT/dx) \quad (4)$$

Figure 2 (16) is given as a basis of comparison of Epstein's equation, Brock's equation and experimental points of Schadt and Cadle.

HYPOTHETICAL MODEL FOR PARTICLE DEPOSITION FROM A TURBULENT STREAM

It was conceived that a hot gas passing through an externally cooled tube might provide the necessary requirements for particle deposition. If turbulent flow were maintained the large thermal gradient which exists in the

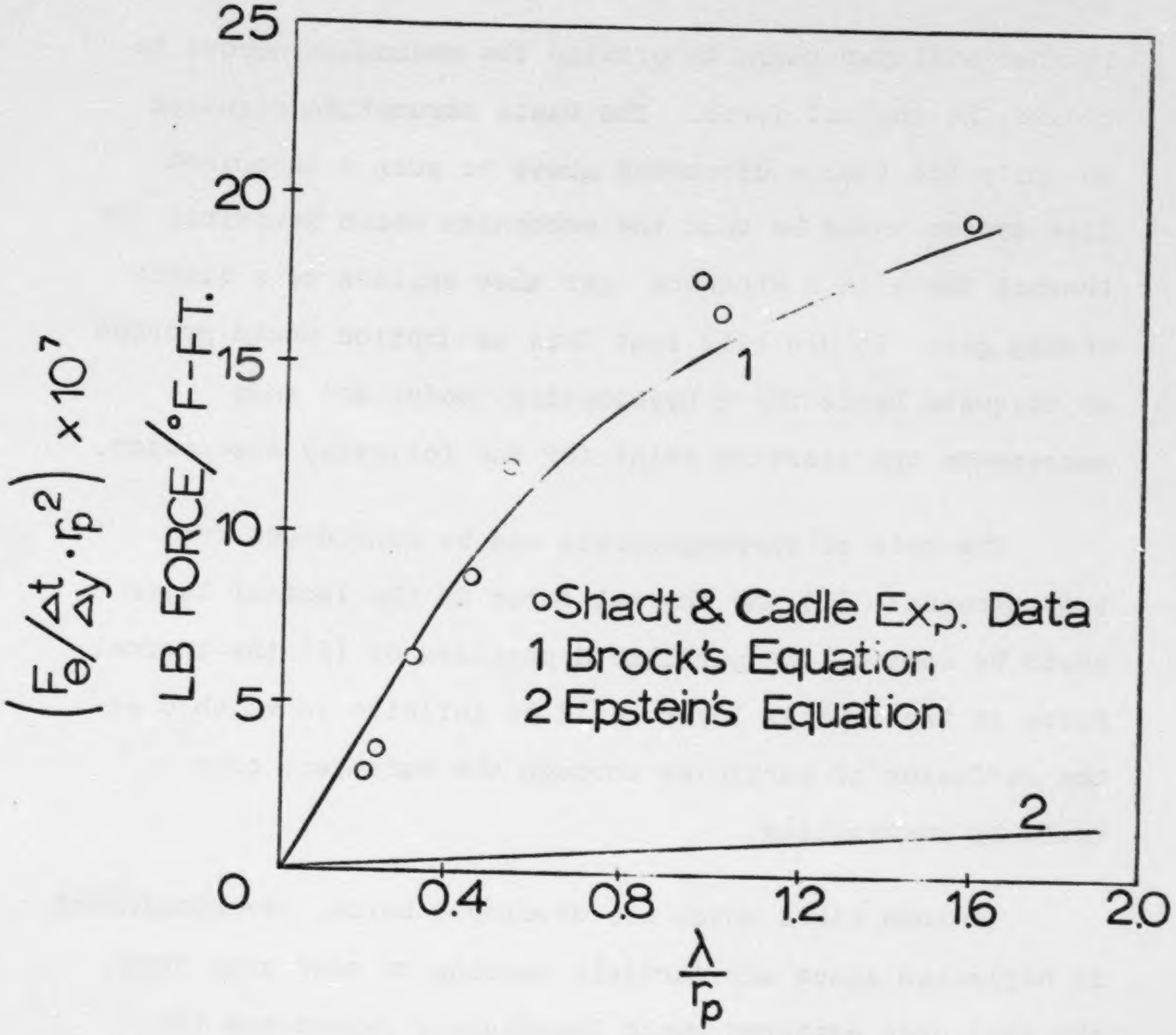

Figure 2

Thermal Force on Sodium Chloride Particles (Ref. 16), 0.44-0 micron diameter, T= 520° R laminar sublayer ought to provide the mechanism needed to create the thermal force. The basic assumption required to apply the theory discussed above to such a turbulent flow system would be that the mechanism which describes the thermal force in a stagnant gas also applies to a slowly moving gas. It was felt that this assumption would provide an adequate basis for a hypothetical model and thus represents the starting point for the following discussion.

The role of thermophoresis can be considered from two extremes: (1) the thermal force in the laminar layer could be controlling particle deposition or (2) the thermal force in the laminar layer could be infinite in which case the diffusion of particles through the turbulent core would be controlling.

In both cases which are developed below, re-entrainment is neglected since any particle tending to move away from the wall once captured would immediately experience the same thermal force which drove it to the wall.

THERMOPHORETICALLY CONTROLLED DEPOSITION

The thermal force controlling case is based on the following assumptions: (1) fully developed flow has been established, and (2) the concentration gradient in the turbulent core is flat (i.e. diffusion through this region is infinitely fast).

For steady state flow in a circular tube the equation of continuity has the general form

$$(1/r)\left[\partial(cv_r r)/\partial r\right] + (1/r)\left[\partial(cv_\theta)/\partial\theta\right] + \partial(cv_z)/\partial z = 0 \qquad (5)$$

Since concentration is a function of z alone, V_z is a function of radius alone, and the partial with respect to θ is zero the above equation reduces to

$$(c/r)\left[\partial(v_r r)/\partial r\right] + v_z(\partial c/\partial z) = 0 \qquad (6)$$

Multiplying through by $2\pi r$ and dividing by the cross sectional area of the tube leads to

$$2cv_r/r_t + \left[(\partial c/\partial z)/\pi r_t^2\right]\int_0^{r_t} 2\pi r v_z \, dr = 0 \qquad (7)$$

Upon integration with respect to r from $r = 0$ to $r = r_t$

$$2cv_r/r_t = (-\bar{V})\partial c/\partial z \qquad (8)$$

Rearranging and integrating again between the limits $C = C_o$ at $z = 0$ and $C = C$ at $z = L$ one obtains

$$\ln(c_f/c_o) = (-2v_r L)/(\bar{V} r_t) \qquad (9)$$

A particle moving in a viscous medium under the influence of a steady force attains a velocity proportional to the force

$$v_r = KF_t \tag{10}$$

The material and shape of the particle and medium determine the value of the mobility, K. Under certain conditions (18) in a homogeneous medium Stokes law applies and $K = (6\pi\mu r_p)^{-1}$. As the inhomogeneity becomes comparable with the size of particle (the slip flow regime, the mobility is given by

$$K = \frac{(1 + A\lambda/r_p)}{6\pi\mu r_p} \tag{11}$$

where A is the coefficient of slip (19).

Using Brock's equation for the thermal force and Equation (11), the velocity due to thermophoresis, v_r, is found. Substitution of v_r into Equation (9) the working equation is obtained:

$$\ln(c_f/c_o) = \frac{(-2L/\bar{V}r_t)}{} \; \frac{(1 + A\lambda/r_p)}{6\pi\mu r_p} \tag{12}$$

$$\frac{(12\pi^2 r_p)\,(c_{tm}\lambda/r_p)\,(k_g/k_p + c_t\lambda/r_p)}{(1 + 3c_m\lambda/r_p)\,(1 + 2k_g/k_p + 2c_t\lambda/r_p)} \quad (dt/dy)$$

The problem now is to determine dt/dy which is approximated as $\Delta t/\Delta y$. The temperature drop across the laminar sublayer is given by the Martinelli relation (20) written in the form

$$t_{y^+=5} - t_w = \frac{(q/A)_w N_{Pr} y^+}{c_p \rho (\tau_w/\rho)^{1/2}} \qquad (13)$$

The temperature gradient is assumed to be similar to the velocity gradient and is taken as linear through the test section. This assumption is valid for gas having a Prandtl number close to one. The rate of heat transfer to the wall is obtained from

$$(q/A)_w = h(t_b - t_w) \qquad (14)$$

where the heat transfer coefficient is given by the Dittus and Boelter equation

$$(hD/k)_b = 0.023\ (D\bar{V}\rho/\mu)^{0.8}\ (c_p\mu/k)_b^{\ 0.3} \qquad (15)$$

The fluid properties in Equation (15) are evaluated at the arithmetic mean bulk temperature, t_b.

The distance across the laminar sublayer is given by the universal velocity distribution

$$y = \frac{y^+ D}{N_{Re}(f/2)^{1/2}} \qquad (16)$$

The average value of $(t_{y^+=5} - t_w)$ along the test section divided by the average value of y gives the thermal gradient needed for substitution into Equation (12). With all quantities now determined the outlet concentration c_f can be found in terms of the inlet concentration, c_o.

DIFFUSION CONTROLLED DEPOSITION

If the rate of mass transfer by the thermal force is assumed to be much greater than that due to diffusion in the laminar layer the only resistance to mass transfer is in the turbulent core and buffer layer.

The rate of mass transfer in a turbulent stream is given by

$$N = (D_v + \varepsilon_g)\, dc/dy \qquad (17)$$

If it is assumed that fluid and particles behave similarly in the turbulent core, then $\varepsilon_g = \varepsilon_p$ where ε_p is the particle diffusivity (21). Lin, Moultan, and Putnam (23) have shown that the eddy diffusivity in the buffer layer is given by

$$\varepsilon_g = \varepsilon_p = \nu(y^+/5 - 0.959) \qquad (18)$$

Substituting from Equation (18) into Equation (17), taking D_v small compared to ε_g, and integrating between c = o at $y^+ = 5$ and $c = c_b$ at $y^+ = 30$ leads to

$$c_b = 24N/\left[\bar{V}(f/2)^{1/2}\right] \qquad (19)$$

The value of N is assumed constant in the buffer layer.

In the turbulent core the Reynolds analogy should hold so that

$$c_{ave} - c_b = \frac{N}{f/2(\bar{V})^2} (\bar{V} - V_b) \qquad (20)$$

The value V_b (23) is given by

$$V_b = 13.73\ \bar{V}(f/2)^{1/2} \qquad (21)$$

Substituting Equation (21) into Equation (20) and adding the result to Equation (19) gives, after rearrangement

$$k = N/c_{ave} = \frac{\bar{V}\ (f/2)}{\left[1 - 10.27\ (f/2)^{1/2}\right]} \qquad (22)$$

This equation permits the calculation of the mass flux at the wall.

CONCLUSIONS

Calculations based on the above model have been made to determine what collection efficiencies could be expected. The results shown in Figure 3 were obtained using a one foot test section, an average gas velocity of 120 ft./sec., and an inlet temperature of 925°R. The particle material used was silica whose thermal conductivity is 0.19 BTU/hr. ft.^{2} °F/ft.

Results showed that the thermal force is not greatly altered by using thermal conductivities up to 4 BTU/hr. ft.^{2} °F./ft. Collection efficiencies were not significiantly affected by particle diameter; for purposes of these calculations a 1.0 micron particle was used. The thermal force was calculated using Epstein's equation since it is more conservative of the two. When Brock's equation was used 100% collection efficiencies were predicted in all cases for the thermopheretically controlled model.

The curve representing the thermal force controlling case gives the best possible efficiencies; it represents the upper bound. The next best case would be when only diffusional resistance exists in the turbulent core. The worst possible condition that could exist is when diffusional resistance controls through each of the turbulent flow regimes; that is, the turbulent core, buffer layer, and laminar sublayer.

In conclusion, neither of these extremes are likely to exist. The most probable result will be a combination of (1) diffusional control in the turbulent core and buffer layer where any temperature gradient in the particle is quickly wiped out by the churning effect of the eddies, and (2) thermal forces controlling in the laminar layer. This resultant, shown in Figure 3, was obtained using an

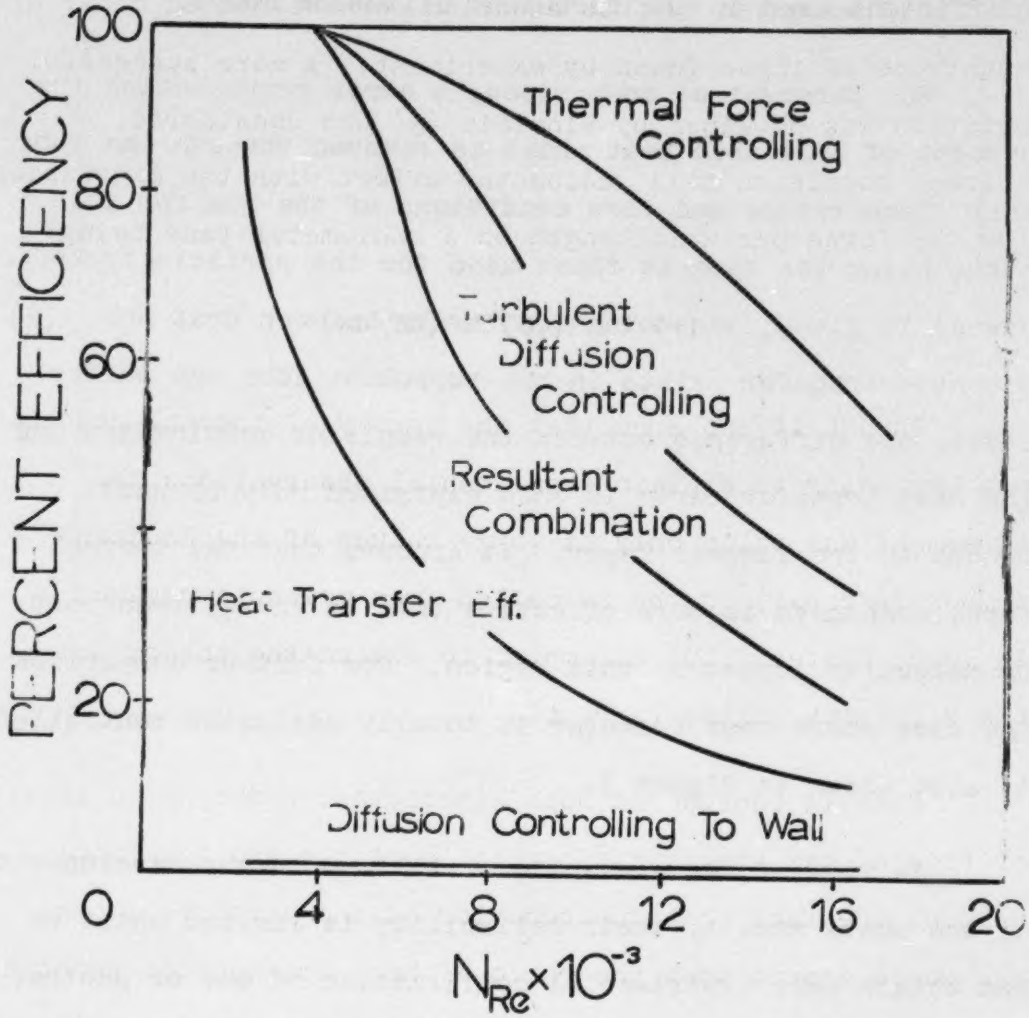

Figure 3

Collection Efficiency for Silica Particles, 1.0 to 5.0 micron diameter, T = 925°R

Equivalent mass transfer coefficient. This equivalent coefficient is a combination of a pseudo coefficient calculated from the thermal force controlling curve and the coefficient used in the turbulent diffusion curve.

For purposes of comparison, a curve representing the percent of available heat which is removed through the tube wall (temperature and flow conditions of the gas for this curve being the same as those used for the particle transfer cases) is given. Assuming similarity between heat and momentum transfer exists in the turbulent core and buffer layer, the difference between the resultant combination and the heat transfer curve is then explained only by what occurs in the laminar layer. It appears that the thermal force mechanism is more effective than is energy transport by molecular impact in this region. For further comparison the case where mass transfer is totally diffusion controlled is also shown in Figure 3.

In view of the assumptions utilized in the development of the above models, their reliability is limited until we can obtain some experimental confirmation of one or another. An experimental program presently under way is aimed at providing the necessary facts. For the time being it is possible to make design estimates which can show the feasibility of obtaining some desired level of particulate collection or the rate of fouling of heat exchanger surface due to the thermal force.

ACKNOWLEDGEMENT

This work is part of an Air Pollution Research Program sponsored by a grant from the Air Pollution Division of the United States Public Health Service.

NOTATION

A = coefficient of slip, taken as 1.0 in this case

c = concentration, particles/cu. ft.

c_{ave} = average concentration, particules/cu. ft.

c_b = concentration at outer edge of buffer layer, particles/cu. ft.

c_f = test section 'outlet' concentration, particles/cu. ft.

c_m = coefficient of viscous slip, 1.2

c_o = average inlet concentration, particles/cu. ft.

c_p = heat capacity BTU/lb.°F.

c_{tm} = temperature jump coefficient, 3.32

c_t = thermal velocity coefficient, 3,080 ft./hr. -°R.

D_v = molecular diffusivity, sq. ft./hr.

f = Fanning friction factor

F = force, lb. force

F_t = force, due to a thermal gradient, lb. force

g_c = Newton law of motion conversion factor, $\frac{(lb.)\ (ft.)}{(sec.)^2 (lb.force)}$

h = heat transfer coefficient, BTU/hr. sq. ft. °F.

K = mobility, lb./hr.

k = mass transfer coefficient, particles/(hr.) - (sq.ft.) - (unit concentration)

k_g = thermal conductivity of gas, BTU/(hr.) - (sq.ft.) - (°F/ft.)

k_p = thermal conductivity of particle, BTU/(hr.) - (sq.ft.) - (°F/ft.)

L = length of test section, ft.
m = mass of particle, lb.
N = particle transfer rate, particles/hr. sq. ft.
P = pressure, lb. force/sq. ft.
$(q/A)_w$ = heat flux at tube wall, BTU/hr. ft.^{2}
r_p = particle radius, ft.
r_t = tube radius, ft.
S = stopping distance, ft.
S^+ = dimensionless stopping distance, $S\bar{V}\rho/\mu$
T = absolute temperature, °R
t = temperature, °F
t_b = arithmetic mean bulk temperature of gas, °F
$t_{y^+=5}$ = temperature at edge of laminar sublayer, °F
t_w = tube wall temperature, °F.
$\bar{V}$ = average velocity, ft./hr.
V_b = velocity at outer edge of buffer layer, ft./hr.
v = velocity, ft./hr.
v_i = initial velocity, ft./hr.
v'_g = root mean square gas velocity, ft./hr.
$v_{r,O,z}$ = velocity components in cylindrical coordinates, ft./hr.
x = distance measured in direction of temperature drop, ft.
y = distance measured from wall, ft.
y^+ = generalized distance from wall
z = distance along path, ft.
$C_p\mu/k$ = Prandtl number

$D\bar{V}/$ = Reynolds number

hD/k = Nusselt number

ε_g = eddy diffusivity of gas, sq. ft./hr.

ε_p = eddy diffusivity of particle, sq. ft./hr.

λ = mean free path, ft.

μ = coefficient of viscosity, lb./hr. ft.

ν = kinematic viscosity, sq. ft./hr.

ρ = density, lb./cu. ft.

τ_w = shear stress at tube wall, lb. force/sq. ft.

LITERATURE CITED

(1) Kitto, P. H., J. Chem Metall. and Mining Soc., 284-306 (June 1952).

(2) Gordon, M. T. and Orr, Jr., C., Air Repair 4, 1-4 (May 1954).

(3) Fraula, H. C., British J. Indus. Med., 13, 196-201 (July 1956).

(4) Tyndall, J., Proc. Roy. Inst. 6, 3 (1870).

(5) Rayleigh, Proc. Roy. Soc., 34, 414 (1882); Nature 28, 139 (1882).

(6) Aitken, J., Trans. Roy. Soc. Edinburgh, 32, 293 (1884); Nature 28, 139 (1884).

(7) Lodge, O. J. and Clark, J. W., Phil. Mag. 17, 284 (1884).

(8) Cawood, W., Trans. Faraday Soc. 32, 1069 (1936).

(9) Einstein, A., Zwits f. Physik 27, 1 (1924).

(10) Epstein, P. S., Zwits f. Physik 54,537 (1929).

(11) Maxwell, J. C., Trans. Roy. Soc. (London) 170, 231 (1879).

(12) Rosenblatt, P. and LaMer, V. K., Phy. Rev. 70, 385-95 (1946)

(13) Saxton, R. L., and Ranz, W. E., Journal of Applied Physics, 23, 8, 917-923 (1952).

(14) Schadt, C. F. and Cadle, R. D., J. Coll. Sci., 12, 356 (1957).

(15) Schadt, C. F. and Cadle, R. D., J. Phys. Chem., 65, 1689 (1961).

(16) Brock, J. R., J. Coll. Sci., 17, 768 (1962).

(17) Brock, James R., "The Thermal Force on Spherical Sodium Chloride Aerosols," paper presented to the 39th National Colloid Symposium, Potsdam, N. Y., June 21-23, 1965.

(18) Millikan, R. A. *Electrons (+ and -)* University of Chicago Press, Chicago, pp. 95 (1935).

(19) Cunningham, E., *Proc. Roy. Soc.*, 83A, 357 (1910).

(20) Knudson, J. G. and Katz, D. P., *Fluid Dynamics and Heat Transfer*, McGraw Hill Book Company, Inc., New York (1958).

(21) Friedlander, S. K. and Johnstone, H. F., *Ind. Eng. Chem.*, 49, 7, 1151-56 (1957).

(22) Laufer, J., Natl. Advisory Comm. Aeronaut. Tech. Note 2954 (1953).

(23) Lin, C. S., Moulton, R. W., and Putnam, G. L., *Ind Eng. Chem.*, 45, 636 (1953).

APPENDIX 9

PROGRESS REPORT 1965-66

ON THESIS PROJECT
"Deposition of Particles from a Turbulent Stream By Means of Thermal Force"

Introduction

During the past year the thermophoresis project progressed from a stage of equipment design to a point of readiness for taking experimental data. The bulk of the time was thus spent in fabrication and construction of laboratory equipment. A smaller amount of time was devoted to writing a paper which was presented at the 58th National A.I.Ch.E. Convention in Dallas, Texas. A copy of that paper has been made a part of this report. The balance of the discussion here will be concerned with a description of the experimental apparatus.

Experimental Apparatus

A schematic flow diagram for the system is shown in Figure 1. The apparatus can be divided conveniently into three main function areas; 1) the aerosol generation section; 2) the aerosol treatment section; 3) and the collection section.

The aerosol generation section consists principally of a Wright Dust Feeder and an ionizer (Figures 2 & 3). A complete review (1) of the Wright Dust Feeder has been made. Briefly, it is a means for dry dust dispersion in which a knife blade scrapes a thin layer of dust from the bottom of a packed column of dust contained in a cap. A stream of dry air flowing radially inward just under the knife edge, carries the dust to the center of the knife blade, through a right angle turn and into a circular tube. This tube conducts the dust laden air to the outlet nozzle, the latter being fitted with a baffle to provide for deagglomeration. Immediately following the dust feeder ionized air is injected into the aerosol stream to provide for neutralization of charges generated when the dust particles are being dispersed. The characteristics of the ionizer are described in the literature (2).

The aerosol treatment section (Fig. 4) provides for a holding tank, dilution air, mixing, and heating. The holding tank gives a suitable residence time to allow for contact between ions and charged particles. Filtered dilution air is combined with the concentrated aerosol stream and mixing is accomplished in a baffled chamber. The aerosol enters an electric heater at room temperature and can be heated as high as 1000°F at flows rates up to 25 cfm.

The flow from the heater is split into two separate legs as it enters the collection section (Fig. 5). One leg contains a filter so positioned that the flow path from the heater to the filter is equivalent to the flow path between the heater and inlet to the test section in the second leg. Equal flow rates are maintained in the two legs by matching pressure drops. The test section in the second leg consists of a water jacketed, copper tube one foot long. The inside of this tube provides for the collection surface of the dust particles. The thermal gradient necessary for particle deposition is maintained by the cooling water removing heat from the hot aerosol through the copper tube wall. Immediately following the test section is another filter. Comparison of the samples (obtained from the inlet and outlet filters, in terms of mass and size distribution) will give to collection efficiency of the system.

Figure 6 shows the control panel for the equipment. Of particular interest here is the 24 channel Minneapolis Honeywell(Electronik 16). Twelve temperature points are monitored during test operations. The most significant temperature points are the copper tube wall temperatures and the axial temperatures of the gas stream in the test section.

Immediate Goals

Having a system that is operational and having selected several dusts (Fe_2O_3, TiO_2, $ZrSiO_4$) for test aerosols the next step is to determine a method of analysis for size distribution of the filter samples. Two methods are being considered; Goetz Aerosol Spectometer and the M.S.A. Particle Analyzer.

Once the analytical technique is established the ultimate goals of collection efficiency as a function of particle size, particle thermal conductivity, particle density, absolute aerosol temperature, and Reynolds number will then be in view.

References

1. Bursen, J. H., Iinoya Koicki, Orr, C.,"Particle Size Classfier for Subsieve Range," Review of Scientific Instruments, 34, 9, 1023-5, (1963)
2. Whitby, K. T., Mc Farland, A. R., Lundtren, D. A., "Generator for Producing High Concentrations of Small Ions," Tech. Report No. 12, Mech. Eng. Dept. University of Minnesota (1960)

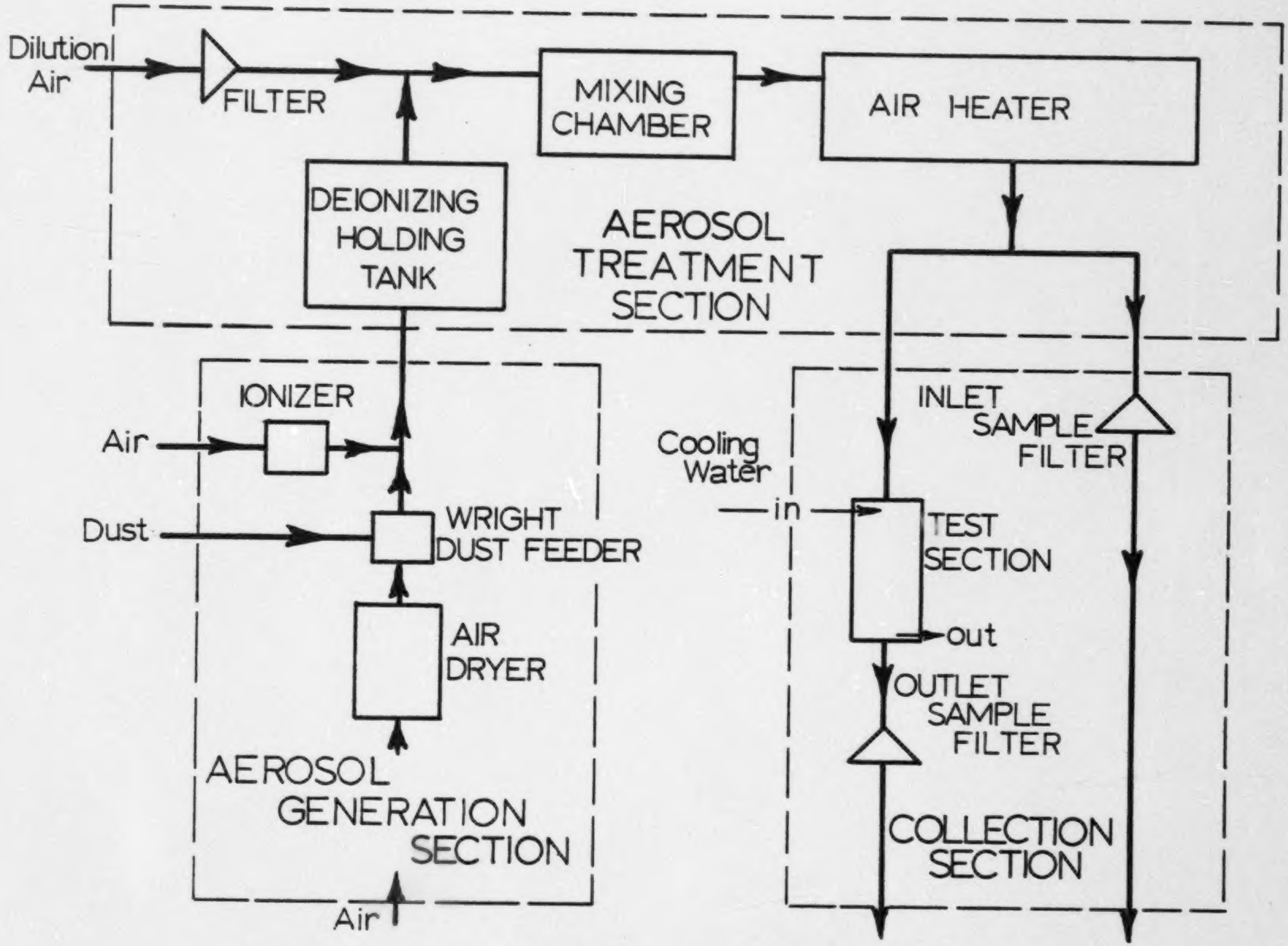
Dilution Air
FILTER
MIXING CHAMBER
AIR HEATER
DEIONIZING HOLDING TANK
AEROSOL TREATMENT SECTION
IONIZER
Air
Dust
WRIGHT DUST FEEDER
AIR DRYER
AEROSOL GENERATION SECTION
Air
Cooling Water
in
INLET SAMPLE FILTER
TEST SECTION
out
OUTLET SAMPLE FILTER
COLLECTION SECTION

FIGURE 1 SCHEMATIC FLOW DIAGRAM

Reproduced from
best available copy.

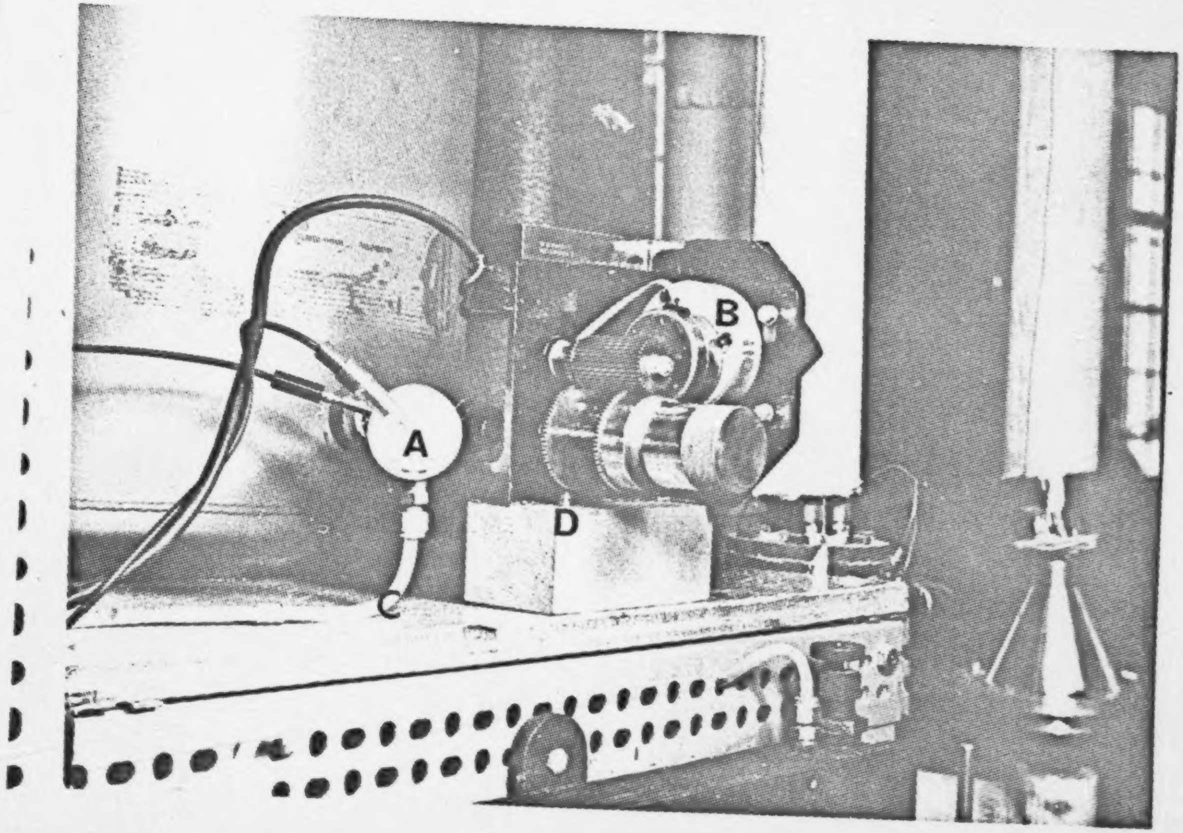

FIGURE 2. AEROSOL GENERATION SECTION, VIEW 1

A. Ionizer, B, Wright Dust Feeder,
C., D. Air Inlets.

Reproduced from best available copy.

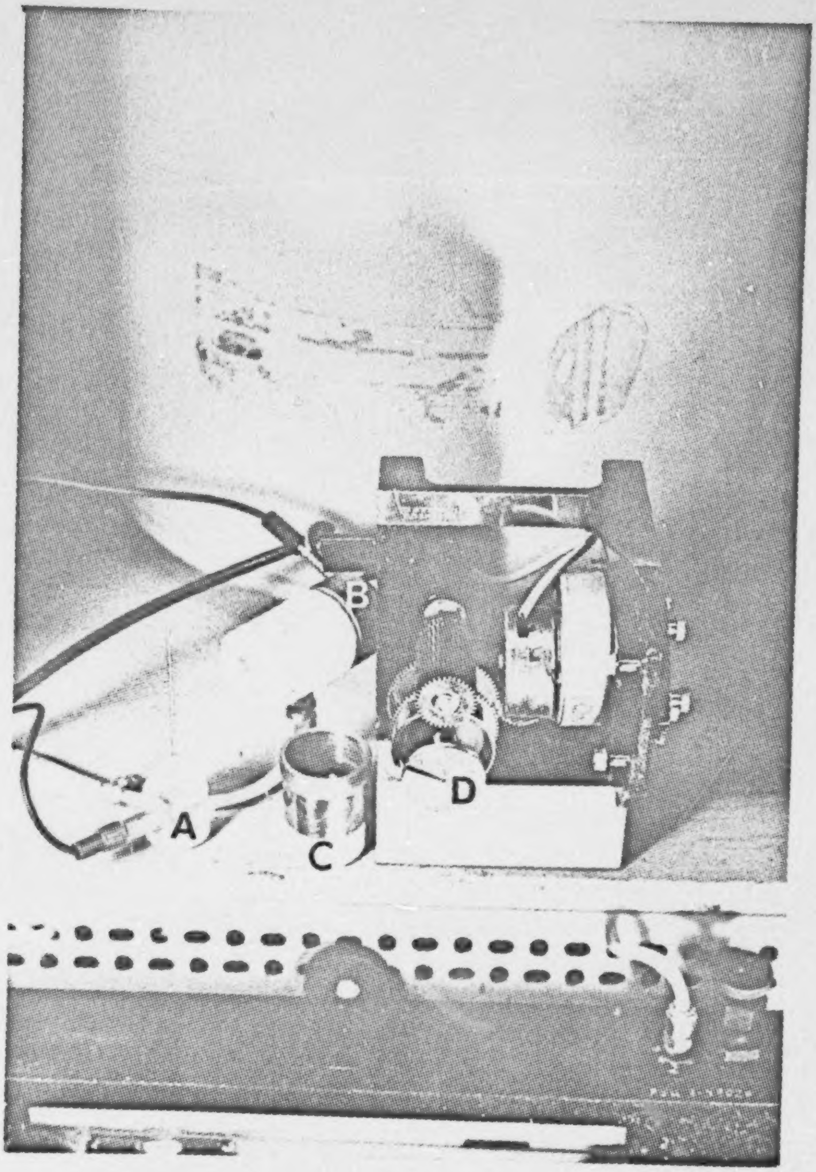

FIGURE 3. AEROSOL GENERATION SECTION, VIEW 2:

A. Ionizer Electrode (+); B. Ionizer Electrode (-); C. Dust Cap; D. Knife Blade.

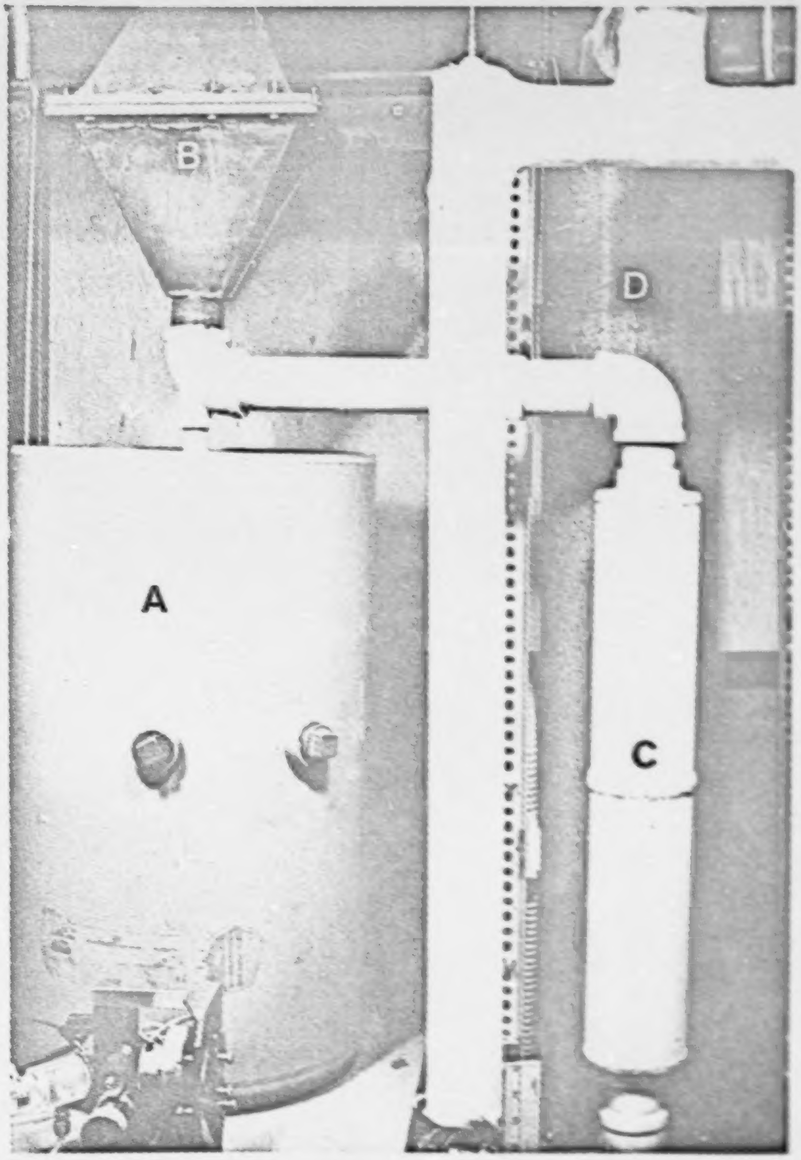

FIGURE 4. AEROSOL TREATMENT SECTION:
A. Deionizing Holding Tank;
B. Dilution Air Filter; C. Mixing
Tank; D. Air Heater

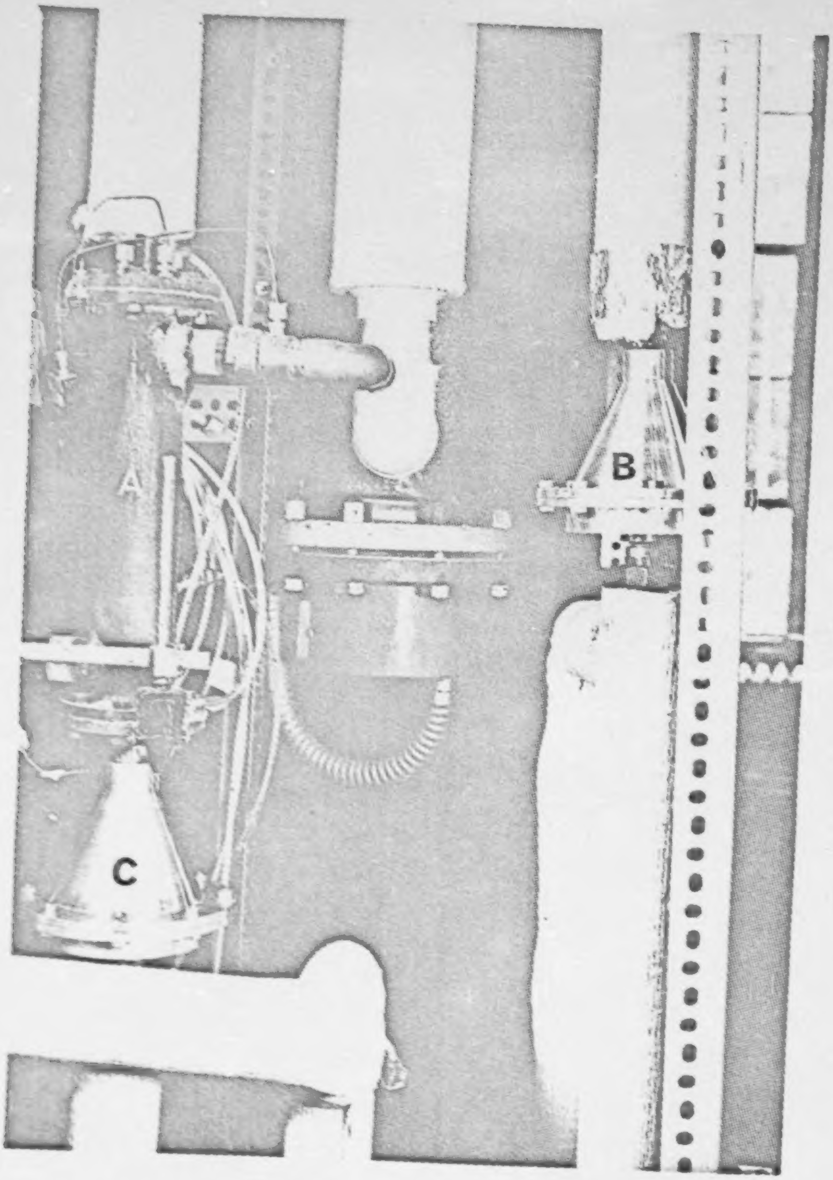

FIGURE 5. COLLECTION SECTION:

A. Test Section; B. Inlet Filter; C. Outlet Filter

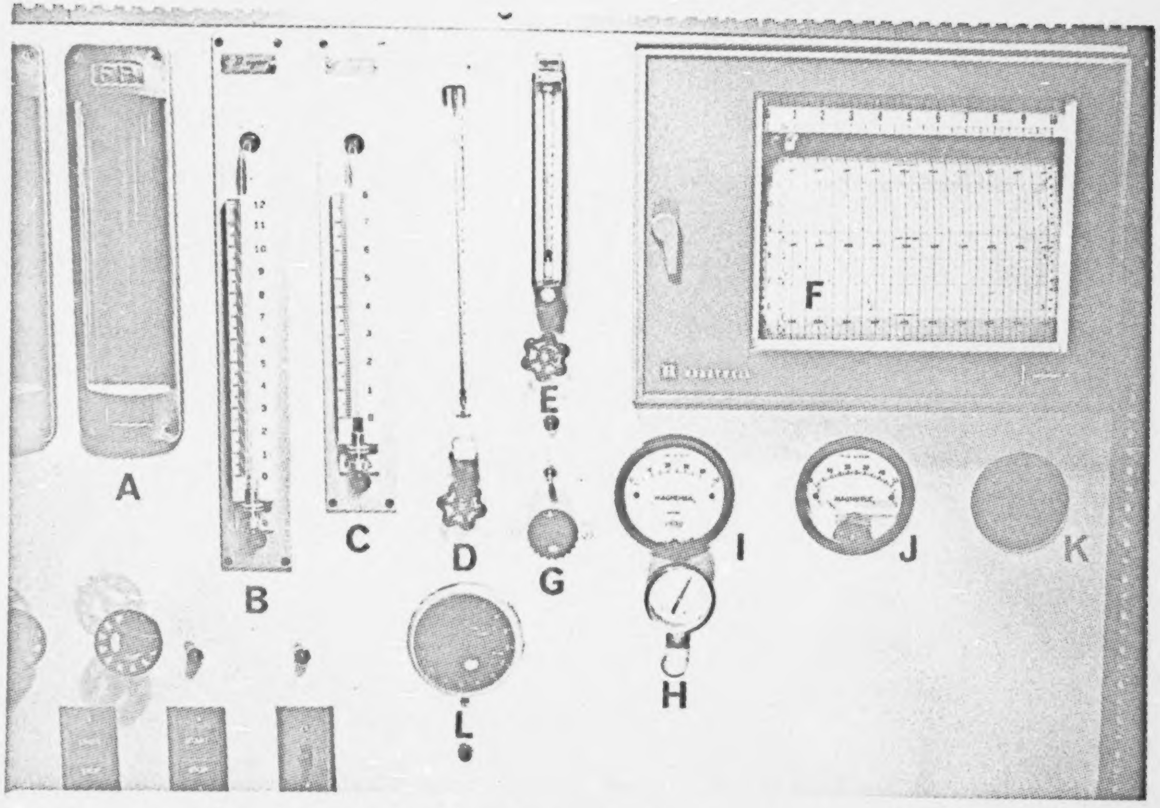

FIGURE 6. CONTROL PANEL:

A. Dilution Air Flowmeter;
B., C. Test Section Manometers;
D. Ionizer Flowmeter;
E. Wright Dust Feeder Flowmeter;
F. Temperature Recorder;
G. Pressure Regulator;

H. Metering Pressure Gage;
I, J. Filter Pressure Drop Gages;
K. Air Heater Control;
L. Ionizer Voltage Control

APPENDIX 10

PARTICLE COLLECTION IN SECONDARY FLOWS

By: Richard Barton

Secondary flows in conduits of irregular cross section (triangular, rectangular, etc.) and in curved conduits have been observed since before 1900. The quantitative effects these secondary flows have on particle collection, however, are not known. In order to understand and quantitatively determine these effects on particle collection, the laminar flow of an aerosol through a helical conduit of circular cross section is being studied.

The collection efficiency in helical conduits for low Reynold's numbers, where gravitational precipitation is dominant, is being determined both experimentally and analytically, and compared to the collection efficiency in a straight conduit.

The collection efficiency at high Reynold's number, where the inertia parameter is high, is also determined both experimentally and analytically.

The secondary flows in helical conduit, in general, diminishes particle collection because of the "mixing" effect and tendencies to diminish the effect of the dominate forces. The secondary flows produce smaller acceleration forces than gravity and the centrifugal force due to the conduit curvature. The circulation of the secondary flow does however, inhibit collection due to the gravitational and centrifugal forces.

To date, data has been obtained for two conduit diameters, two particle diameters, and four aspect ratios. Several models have been proposed to calculate the collection efficiency and particle trajectories have been computed to verify various assumptions.

Future work includes the study of particle collection in the diffusional range and the determination of transfer coefficients. Particle collection in larger conduit diameters and higher aspect ratios will also be investigated.

I. Introduction

The flow phenomena occuring in helical conduits has been studied by many researchers both analytically and experimentally since 1876 when the secondary flows were first observed. The secondary velocities are due to the radius of curvature which when coupled with the fluid's axial velocity creates centrifugal forces which in turn alter the axial velocity and produces secondary flows.

Analytical solutions and experimental results for the friction factor have been obtained for helical conduits in the laminar flow region. The most significant of the analytical treatments are by Dean, Adler, Cumming, and Truesdell [1, 2, 3, 4]. The first three solved the Navier-Stokes equations for low Reynold's numbers and low aspect ratios. Truesdell solved the equations numerically for high Reynold's numbers and high aspect ratios. Experimentally, the work by White[5] in the laminar range and Ito[6] in the turbulent range are the most significant.

An aerosol flowing through a helical conduit will also be influenced by the forces which produce the secondary flows and the secondary flows themselves. The particle collection phenomena will occur in three dimensions and the particle trajectories will be complex. For this reason, a helical conduit of circular cross section was selected to study the effects of secondary flows on particle collection. The extensive analytical and experimental research on helical conduits provides the secondary and axial flow velocities. These velocities can then be used to analytically determine trajectories or collection efficiencies and experimental work can be compared to the analytical work to determine the mechanisms involved in particle collection in secondary flow systems.

A helical conduit of circular cross section is used to qualitatively and quantitatively study particle collection in secondary flow systems.

II. Description of Helical Conduit

The helical conduit used is a copper tube of circular cross section coiled about cylinders of various diameters. Figure 1 illustrates the helical conduit's dimensions and defines the geometric ratio, the aspect ratio of the helical conduit. The axis of the conduit is placed in the vertical direction. All experimental and analytical work is conducted with the helix in the vertical position.

III. Description of Laminar Flow in Helical Conduits

The analytical determination of the secondary and axial flow velocities were first derived by Dean[1]. Cumming[3] refined the analytical methods to include conduits of elliptical cross sections. The velocity equations given below are from Cumming[3] for helical conduits of circular cross section. The equations are valid for low Reynold's numbers and low aspect ratios.

In the z direction

$$\frac{v_{fz}}{\overline{V}} = 2.0\ (1-x^2-y^2) + \frac{A\ (Re_f^{\,2})}{144}\left[\left[\frac{19}{40}\,(x^2+y^2)^{1/2} - (x^2+y^2)^{3/2} + \frac{3}{4}\,(x^2+y^2)^{5/2} - \frac{1}{4}\,(x^2+y^2)^{7/2} + \frac{1}{4}\,(x^2+y^2)^{9/2}\right]\frac{x}{(x^2+y^2)^{1/2}}\right]$$

In the x direction

$$\frac{v_{fx}}{\overline{V}} = \frac{A\ (Re_f)}{144}\Big(1-(x^2+y^2)\Big)\Big[(1.0-x^2-y^2)\ (4.0-x^2-3y^2) - 4.0\ y^2(4.0-x^2-y^2)\Big]$$

In the y direction

$$\frac{v_{fy}}{\overline{V}} = \frac{A\ (Re_f)}{72}\ (1-x^2-y^2)\Big[2.0\ (4.0-x^2-y^2) - (1-x^2-y^2)\Big]xy$$

where v_{fz} is the axial velocity,

v_{fx}, v_{fy} are the secondary flow velocities,

Re is the Reynolds number for flow in a straight conduit with the same pressure gradient as the helical conduit,

and $\overline{V}$ is the average axial velocity based on the above Re .

The primary and secondary velocities in helical conduits have also been computed by Truesdell[4]. The methods of computation were made using numerical methods. The velocities were computed for aspect ratios as high as 0.1 and Reynold's numbers as high as 1,000.0. The velocities can be computed from the data presented in reference 4.

The flow velocities are thus available for a wide range of Reynold's numbers. The availability of the flow velocities permits the particle trajectories to be calculated in both the gravitational precipitation region and the inertia impaction region.

The friction factor for helical conduits is summarized in reference 5. The equation, due to Prandlt, which best summarizes the experimental work, in the laminar region, is given by,

$$f = 18.5 \frac{A^{0.18}}{Re_f^{0.64}}$$

$$\Delta P = f \left(\frac{L_t}{D_t}\right) \left(\frac{\overline{V}^2}{2\ gc}\right)$$

The above equation was fit to experimental data using water as the fluid and is in good agreement with the experimental results over the following range of Re numbers and aspect ratios.

$$10^{1.6} < Re(A)^{0.5} < 10^{3.0}$$

The friction faction obtained using air was found to agree with the above equation (Figure 2). The critical Reynold's number for transition from the laminar region to the turbulent region is given by Ito[6] as

$$Re_{crit} = 2.0(A)^{0.32} \times 10^4$$

The critical Reynold's number for transition is higher for helical conduits compared to a straight conduit.

IV. Mathematical Model for Particle Collection

A. Particle Trajectories

Particle trajectories can be calculated once the carrier's velocity profile has been determined. Using Newton's law and equating the mass times the acceleration to the steady state drag forces and external forces a relationship can be found between the particle's acceleration and the forces acting on it. The steady state drag force is used. This assumption is reasonable as indicated by Fuchs[7]. The equations for the particle trajectories in helical conduits are given below in dimensionless form.

In the x direction

$$\frac{dV_{px}^*}{d_t^*} = -\frac{3}{8}\ C_D\ \left(\frac{\rho_a}{\rho_p}\ \frac{D_t}{D_p}\right)\ (\overline{V}_R^*)^2\ V_{Rx}^*\ + \frac{A}{(1+x)}\ \ (V_{zp}^*)^2$$

In the y direction

$$\frac{dV_{py}^*}{d_t^*} = -\frac{3}{8}\ C_D\ \left(\frac{\rho_a}{\rho_p}\ \frac{D_t}{D_p}\right)\ (\overline{V}_R^*)^2\ V_{Ry}^* - g^*$$

In the direction

$$\frac{dV_{pz}^*}{d_t^*} = -\frac{3}{8}\ C_D\left(\frac{\rho_a}{\rho_p}\ \frac{D_t}{D_p}\right)\ (\overline{V}_R^*)^2\ V_{Rz}^*\ - \frac{2.0\ A}{(1+x)}\ \ (V_{px}^*\ \ V_{pz}^*)$$

where

$$(\overline{V}_R^*)^2 = [\ (V_{px}^* - V_{ax}^*)^2 + (V_{py}^* - V_{ay}^*)^2 + (V_{pz}^* - V_{az}^*)^2]$$

$$V_{R\xi}^* = (V_{p\xi}^* - V_{a\xi}^*)$$

and

$$C_D = \frac{24}{Re_p} + \frac{4.8}{(Re_p)^{1/3}}$$

The subscripts designate the following

t refers to the helical conduit

p refers to the particle

a refers to the carrying fluid

ξ represents the three directions x, y, z

x, y, z represents the three coordinate directions shown in Figure 1.

The three simultaneous equations are not solvable analytically, but can be solved numerically using methods similar to Runge-Kutta[9] or Hamming[10]. The trajectories determined by the numerical methods provide the information needed to determine the collection efficiency in helical conduits.

The dimensionless equations indicate that the collection efficiency is a function of $(\frac{\rho_a}{\rho_p} \frac{D_t}{D_p})$, referred to as the obiedence parameter[8], Re_t, Re_p, A and g.

The above equations are valid for $Re_p < 3{,}000.0$. The equations can be simplified if $Re_p \ll 1.0$. For this case Stokes law for particle drag can be assumed. The particle acceleration can also be assumed equal to the fluid acceleration and the equations for the particle trajectories become

In the z direction

$$V_{pz}^* = V_{az}^* - 2.0\ (K)\ V_{az}^*\ (V_{ax}^*)\ A/(1+x)$$

In the x direction

$$V_{px}^{*} = V_{ax}^{*} + \frac{K\,(V_{az}^{*})^{2} A}{(1+x)} - K\,(a_{fx}^{*})$$

In the y direction

$$V_{py}^{*} = V_{ay}^{*} - K\,(a_{ay}^{*}) - K\,(g^{*})$$

where K is the impaction parameter based on the average axial fluid velocity and the conduit radius

and $a_{f\xi}^{*}$ is the fluid acceleration

The above equations were solved using the Runge-Kutta numerical methods on a digital computer. Typical trajectories are shown in Figure 3. The trajectories are valid only for small impaction parameter values. The trajectories are in the gravitational precipitation region.

B. Gravitational Precipitation in Straight Circular Tubes

The comparison of the collection efficiency in helical conduits to that in straight conduits of circular cross section requires the derivation of the collection efficiency due to gravity in straight conduits.

The following assumptions are made:

1. The fluid's axial velocity is given by

$$V_{az} = 2.0\,\overline{V}\left(1.0 - \left(\frac{r}{r_o}\right)^{2.0}\right)$$

2. Fluid velocities do not exist in the cross section of the conduit.
3. The particle axial velocity is equal to the fluid's axial velocity.
4. The particle drag due to gravity follows Stokes law.
5. The conditions are steady state.

The equation of continuity gives

$$\frac{\partial(n_p v_{px})}{\partial x} + \frac{\partial(n_p v_{py})}{\partial y} + \frac{\partial(n_p v_{pz})}{\partial z} = 0$$

where n_p is the particle concentration

since $v_{px} = 0.0$, v_{py} is a constant and v_{pz} is a function of the radius only the continuity equation reduces to

$$v_{py} \frac{\partial n}{\partial y} + v_{pz} \frac{\partial n}{\partial z} = 0$$

The solution of the continuity equation using the methods of characteristics gives that the particle concentration is constant over the area determined by the differential equation

$$\frac{v_{pz}}{v_{py}} dy = dz$$

Since $v_{pz} = v_{az}$ and $v_{py} = -v_t$, the terminal velocity of a particle in a gravity field, the differential equation above becomes

$$\frac{v_{az}}{-v_t} dy = \frac{2.0 \, \overline{V} \, (1 - x^2 - y^2) \, dy}{-\left(\frac{\rho_p \, g \, D_p^2}{18\mu}\right)}$$

Solving the above equation subject to the imposed boundary conditions and calculating the inlet and outlet concentration fluxes, the collection efficiency is found to be

$$\varepsilon = \frac{2}{\pi}\left[2\mu\sqrt{1-\mu^{2/3}} + \sin^{-1}(\mu^{1/3}) - \mu^{1/3}\sqrt{1-\mu^{2/3}}\right]$$

where

$$\mu = \left(\frac{3}{8}\,\frac{V_t L}{\bar{V} r_t}\right)$$

The above equation agrees with the equation given by Fuchs[7] for gravitational precipitation in a straight circular conduit.

C. Simplified Model of Collection in a Helical Conduit

The particle trajectories shown in Figures 3 and 4 indicate that unless large values of the impaction parameter occur the primary forces, the centrifugal forces produced by the coil's curvature and gravity, are largely cancelled by the circulation of the secondary flows. The only forces which tend to force the particles to the tube wall are due to the secondary flows acceleration. The secondary flows force the particles toward the wall until a position is reached where gravity and centrifugal forces precipitate the particles on the tube wall.

An idealized secondary flow can be assumed to simplify the description of the collection efficiency. The secondary flows streamlines can be assumed to be concentric circles in each half of the conduit cross section. The secondary velocities can further be assumed to be constant throughout. With these assumptions and the assumptions mentioned previously in IV-B, 3, 4, and 5, the collection efficiency can be derived by equating the drag forces and the inertia forces. The collection efficiency determined in this manner is

$$\varepsilon = 1.2 \times 10^{-12} \left(\frac{\overline{V}_s}{r_{te}}\right)^2 \left(\frac{\rho_p}{\mu_f}\right) D_p{}^2 \frac{L_t}{\overline{V}}$$

where V_s is the assumed secondary velocity

and r_{te} is an equivalent tube radius

It is not assumed that this equation can in itself predict the collection efficiency in helical conduits, but that it can be used to correlate the experimental data obtained to extend the data over a wider range of aspect ratios and Re numbers.

V. Experimental Equipment

A schematic of the experimental equipment is shown in Figure 5. The equipment includes an aerosol nebulizer, ionizer, holding chamber, mixing chamber, and light scattering sampling equipment. A description of each component follows.

a. Aerosol Generator

The particles used for the experimentation are uniform polystyrene beads. The beads are suspended in twice filtered distilled water and redispersed by a medical two fluid atomizer. The beads are subsequently dried, the surface charge is reduced, and the beads are mixed with filtered air.

b. Ionizer

The ionizer is similiar to the ionizer described in reference 11. The ionizer is used to reduce the high surface charge on the beads caused by the dispersion with the atomizer. The ionizer effectively reduces the charge on the beads to a charge normally found on beads. Uncharged particles are necessary to eliminate the space charging effects that occur in tubes at low Reynold's numbers and small diameters. Polystrene tubes have residual static voltages due to manufacturing and handling and these tubes cannot be used unless the inside is coated with a conductive material or the charged particles are eliminated. An investigation of particle collection in helical conduits thus requires a neutrally charged aerosol so that only the effects due to the fluids motion are studied.

c. Holding Chamber

The holding chamber provides the necessary time required for complete evaporation of any water remaining on the beads from dispersion. The holding chamber also provides the residence time required for the neutralization of the electrical charge on the particles.

d. Mixing Chamber

The mixing chamber provides the volume necessary to mix the particles and the filtered air. A baffle near the entrance provides a mixing mechanism so that the particles do not flow directly into the chamber. The aerosol samples are drawn from the chamber through the helical conduit or the sampling probe. The particle concentration is then determined using a light scattering system to indicate the concentration.

f. Sampling System

The sampling system used is a light scattering instrument which detects the light scattered in either the forward direction or at right angles. The source lamp is an automotive headlamp with a candlepower of 32.0. A photomultiplier tube, type IP21, is used to detect the light scattered. The photomultiplier's output is then indicated on an Aminco Photomultiplier Photometer. The particle concentrations used are low and the photometer indicates a voltage which is proportional to the particle concentration.

For small flow rates the entire aerosol is passed through the light scattering equipment. For high flow rates, only a fraction of the total aerosol is passed through the light scattering equipment.

VI. Results

Experimental results have been obtained for helical conduits of diameters 0.187 and 0.25 inches, aspect ratios from 0.0044 to 0.073, and particle diameters of 1.24 and 2.0 microns. The data obtained is primarily for high Reynold's numbers and are shown in figure 5. The experimental results for low Reynolds numbers are shown in figure 6. The charge particle effects, mentioned previously, affected the collection efficiency and these results are not included.

The data for low flow rates verifies that the secondary flows do indeed inhibit particle deposition due to gravitational precipitation. The high collection efficiencies for high flow rates may be due primarily to the first few turns of the helix when the secondary flows are developing. Further experimental data must be obtained to verify this effect quantitatively.

The analytical results obtained from the numerical solutions of the particle trajectories indicate that the secondary flows inhibit particle collection at low flow rates. The use of trajectories to determine collection has proved thus far to be very difficult due to the long computer time needed and small inaccuracies in the numerical computation methods.

VII. Conclusions

The analytical and experimental results taken to date indicate the effects of secondary flow on the collection efficiency of helical conduits. Experimentation will continue to obtain more quantitative information about these effects. Data will be obtained for different conduit diameters, larger aspect ratios, and different conduit lengths.

Future work also includes the study of particle collection in the diffusional range and the determination of the particle transfer coefficients in this range.

The analytical work with particle trajectories must be refined so that they may be compared to the experimental results thus extending these results over a wider range.

VII. Nomenclature

A. Dimensionless Parameters

A = aspect ratio - r_t/R_o

a^* = acceleration - $a\ r_t/\overline{V}^2$

f = friction factor

g^* = Froude number - $g\ r_t/\overline{V}^2$

C_D = drag coefficient

K = impaction parameter - $\rho_p\ D^2_p\ \overline{V}/18\ \mu_f\ r_t$

t^* = time - $\overline{V}\ t/r_t$

V^* = velocity - $v/\overline{V}$

x, y = directions in cross section of conduit referred to r_t

z = axial direction of conduit referred to r_t

ε = efficiency

B. Dimensional Quantities

a = acceleration - ft./sec.^{2}

D = diameter - ft. or microns

g = acceleration of gravity - ft./sec.^{2}

g_c = gravitational constant - lbm - ft./lbf - sec.^{2}

L = conduit length - ft.

n = concentration - number/ft.^{3}

ΔP = pressure difference - ft.

R_o = radius of curvature of helical conduit - ft.

t = time - seconds

r = radius - ft.

v = velocity - ft./sec.

v_t = terminal velocity - ft./sec.

$\overline{V}$ = average axial velocity - ft./sec.

μ = dynamic viscousity - lbm/ft. - sec.

C. Subscripts

a - refers to air

f - refers to the fluid

p - refers to the particle

t - refers to the conduit

x, y, z - refers to the coordinate directions

IX. References

1. Dean, W.R., "The Steamline Motion of Fluid in a Curved Pipe", Phil. Mag. (7), Vol. 5, 673ff (1928)
2. Adler, M., "Stromung in Gekrummten Rohen", Zeits. furAng. Math. und Mech, Band 14, 257ff (1934)
3. Cuming, H.G., "Secondary Flow in Curved Pipes", Aeronautical Research Council Reports and Memoranda No. 2880 (1952)
4. Truesdell, L. C., "Numerical Treatment of Laminar Flow Through Helical Conduits", Ph.D. Thesis, Case Institute of Technology (1963)
5. White, C.M., "Streamline Flow through Curved Pipes", Proc. Roy. Soc., Series A, Vol. 123, 645ff (1929)
6. Ito, H., "Friction Factors for Turbulent Flow in Curved Pipes", Trans. ASME, J. of Basic Eng., 123ff (June, 1959)
7. Fuchs, N.A., "The Mechanics of Aerosols", Pergamon Press, The MacMillan Company, New York (1964)
8. Dussorurd, J.L., "A Theoretical and Experimental Investigation of a Deceleration Probe for Measurement of Several Properties of a Drolet-Laden Air Stream", Naval Research Contract NSori - 07878, Massachusetts Institute of Technology, Cambridge, Massachusetts (1955)
9. Kunz, K.S., "Numerical Analysis", McGraw-Hill Book Co., Inc. New York, New York (1957)
10. Ralston, A., "Mathematical Methods for Digital Computers", John Wiley and Sons, Inc., New York (1960)
11. Whitby, K.T., McFarland, A.R., Lundgren, D.A., "Generator for Producing High Concentrations of Small Ions", Tech. Report No. 12, Mech. Eng. Dept., University of Minnesota (July 1960)

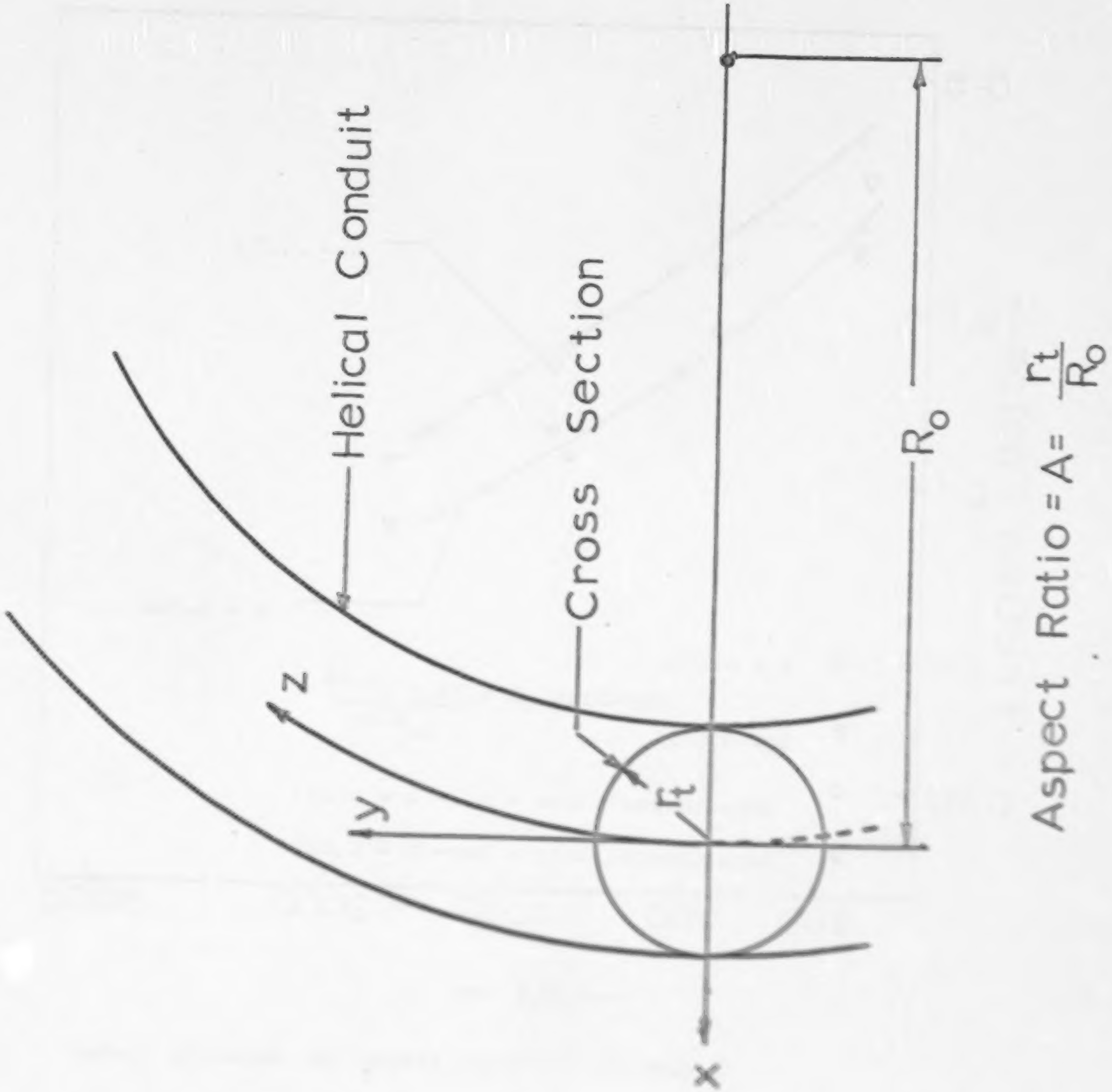
Helical Conduit
Cross Section
z
y
x
r_t
R_o
Aspect Ratio = A = $\frac{r_t}{R_o}$

Figure 1.- Helical Conduit Dimensions

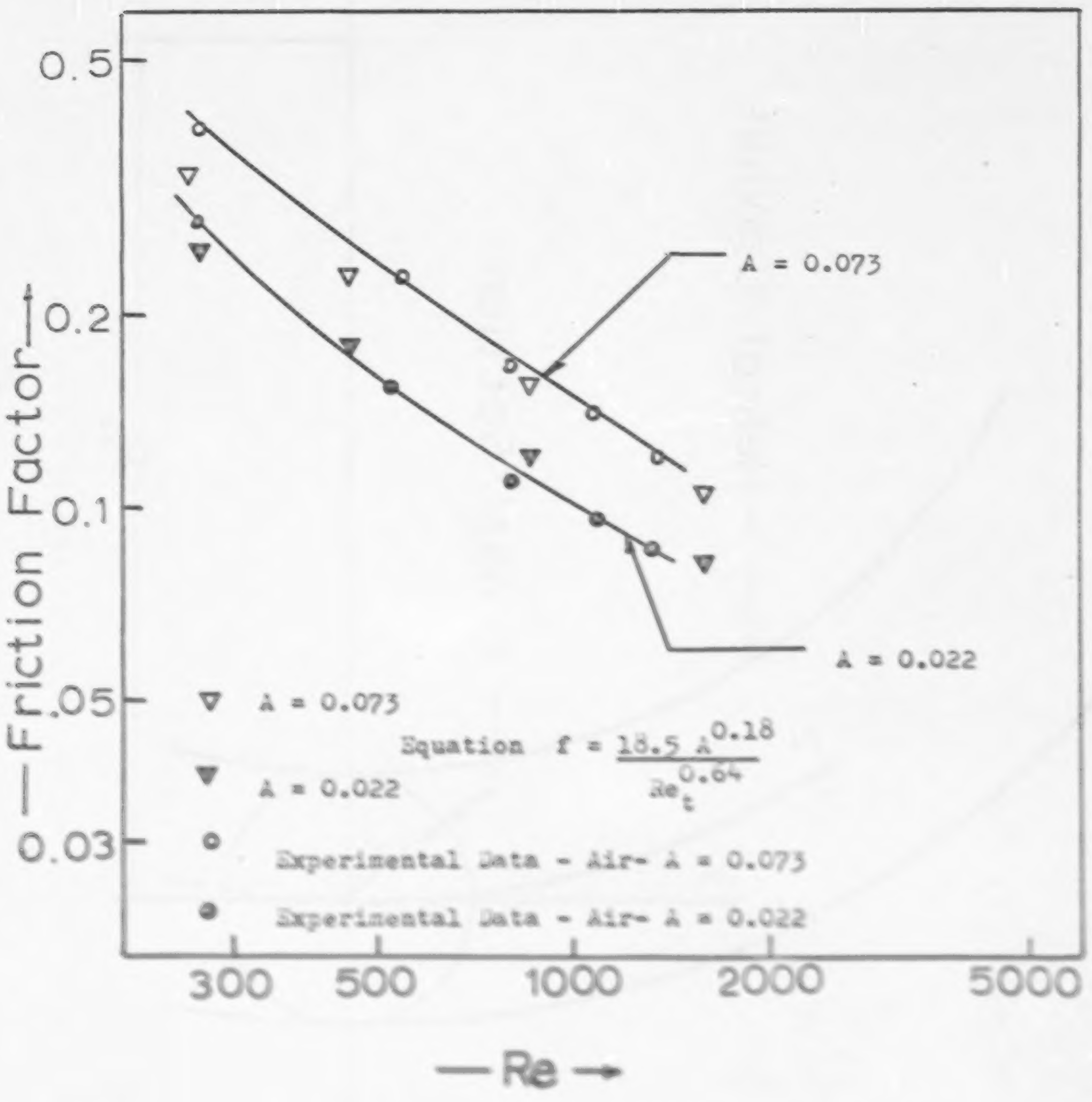

Figure 2. Friction Factor vs. Reynolds Number

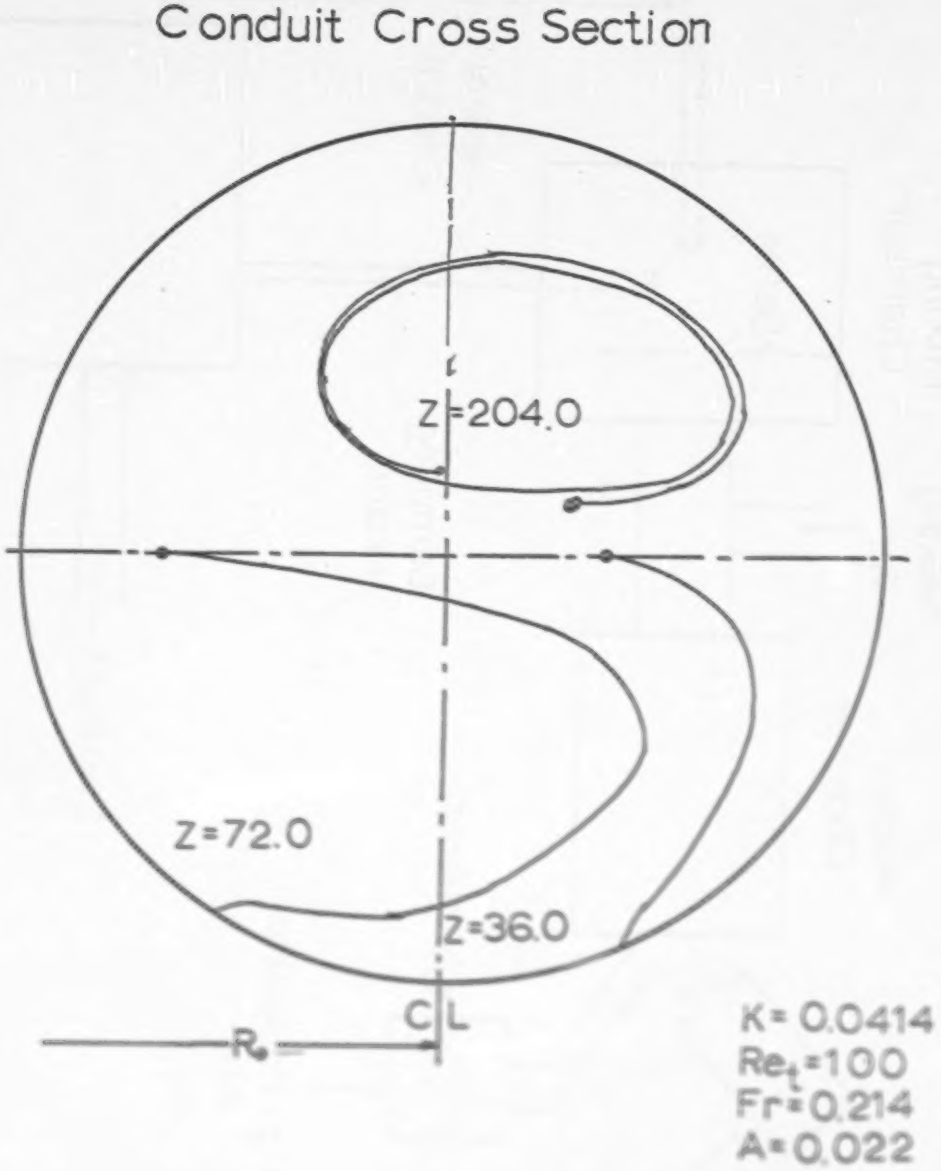
Conduit Cross Section
Z=204.0
Z=72.0
Z=36.0
C L
R₀
K= 0.0414
Re_t=100
Fr=0.214
A=0.022

Figure 3.. Particle Trajectories

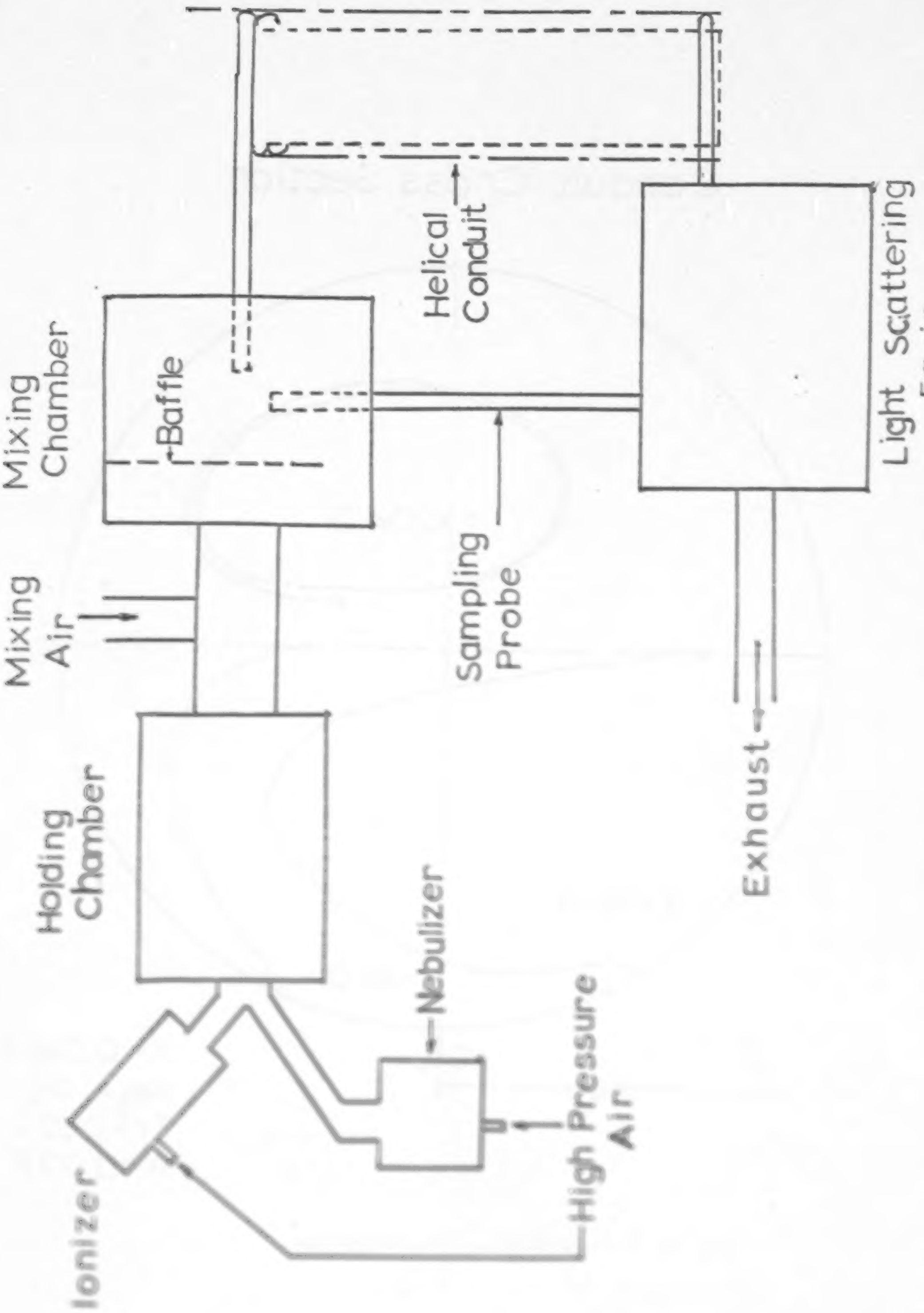
Mixing Chamber
Baffle
Helical Conduit
Mixing Air
Sampling Probe
Light Scattering Equip.
Holding Chamber
Exhaust
Nebulizer
High Pressure Air
Ionizer

Figure 4. Schematic of Experimental Equipment

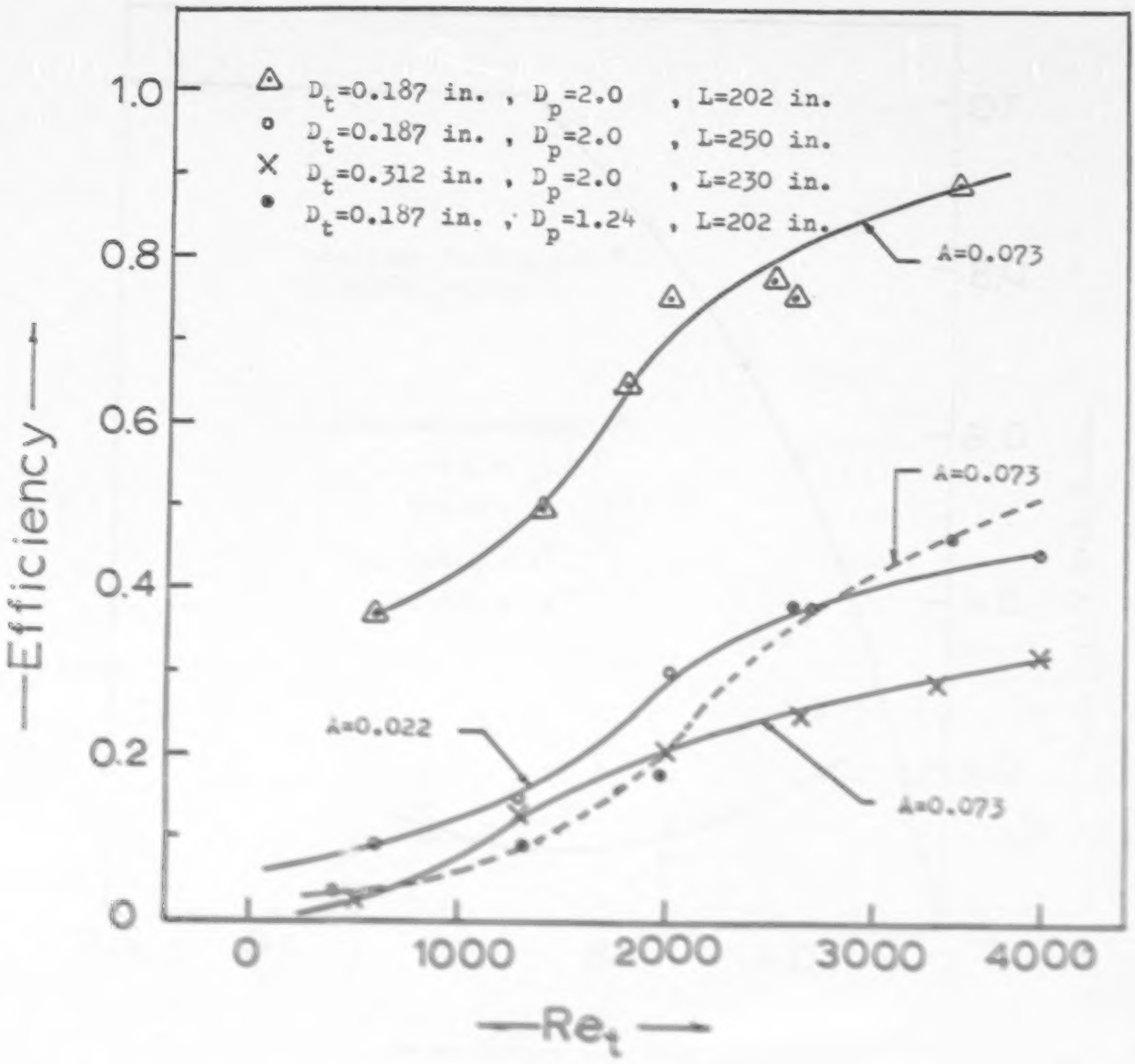

Figure 5. Collection Efficiency
High Re Numbers

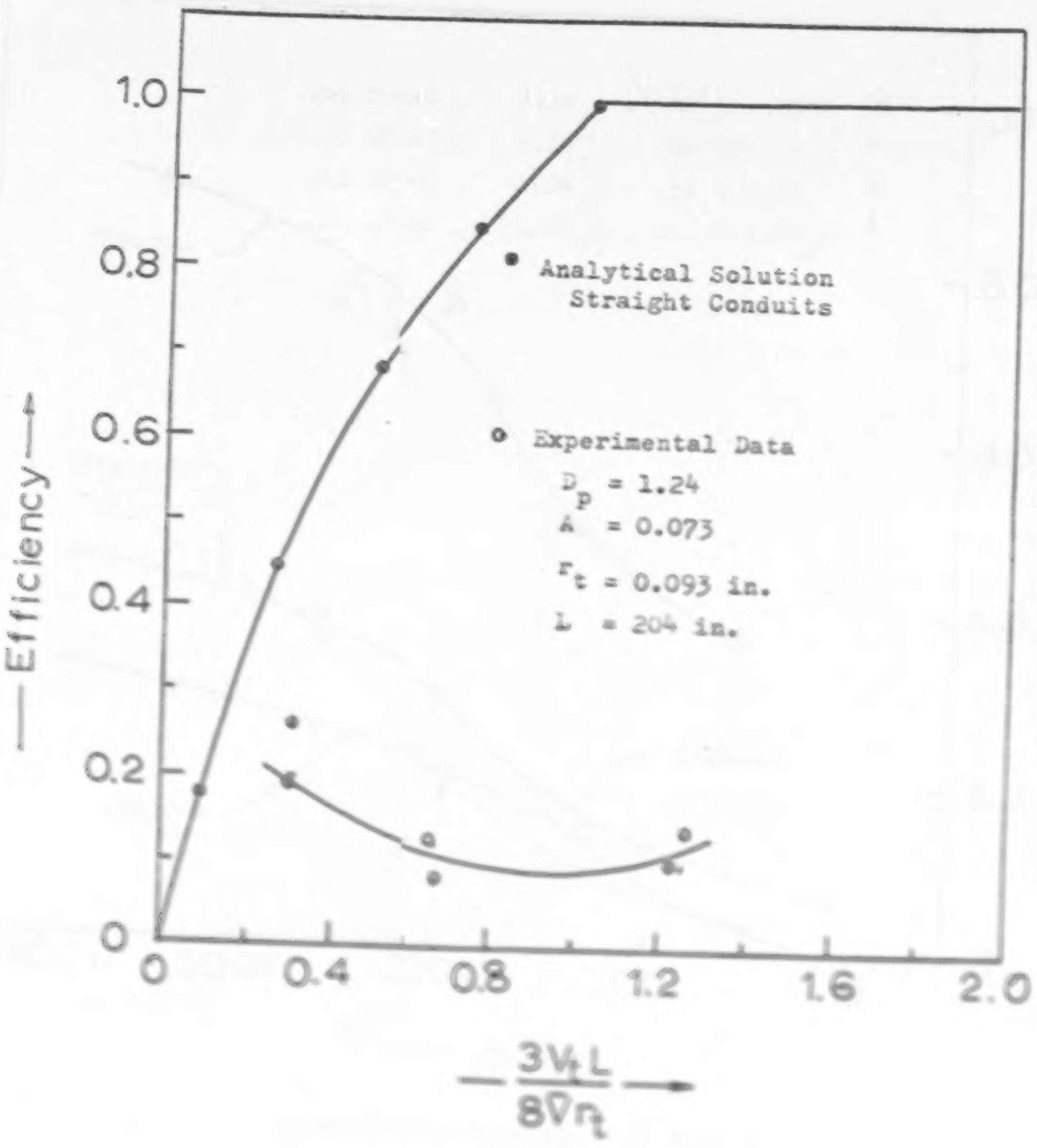

Figure 6. Collection Efficiency
Gravitational Precipitation

APPENDIX II

Aerosol Sampling with a Side Port Probe

By: Dale Lundgren and Seymour Calvert
Presented at AIHA Meeting, Pittsburgh, Pa., 1966

A most important consideration in determining particulate concentration in a gas stream is that of obtaining a true sample. This report describes an experimental investigation of a side port probe and a conventional sampling probe for obtaining aerosol samples from a duct. The basic study objectives were:

1. To determine the limitations of a side port probe; and
2. To present a method for predicting the anisokinetic sampling bias.

A side port probe is a straight section of tubing, positioned at right angles to the air flow direction, with which an aerosol sample is obtained by drawing in air through a side inlet or an end opening. Several different sizes of two basic side port probe configurations, shown in Figure 1, were studied and their performance compared with the commonly used probe configurations, also shown in Figure 1.

Use of a side port probe is of interest and importance because of the probe's simplicity and versatility. It requires only a simple circular opening of the probe diameter, to be inserted into a duct or plenum. Such considerations of simplicity are of greatest importance in industrial stack gas sampling and the like, where working conditions are far from convenient.

The merits of a side port probe were determined by comparing the side port probe with the straight inlet probe. This comparison was made on the basis of sampler bias where sampler bias is defined as the volumetric particle concentration determined from the probe sample divided by the actual volumetric particle concentration which existed in the gas stream.

Sampler bias can be divided into several parts in order to better illustrate the causes of bias or error. Anisokinetic sampling is the most common biasing factor. It is the concentration determination error due to unmatched sampler inlet and duct velocities and is illustrated in Figure 2.

If the sampling probe tip is blunt or if a side port probe configuration is used, there will be a biasing of the sample because of distortion of the flow field around the probe. With the straight inlet probe operating at isokinetic sampling velocities, there will be neither of the above biases; the side port probe, however, will always tend to be biased because of the flow field distortion effect.—The combined effect of anisokinetics and flow distortion is called the probe inlet bias, B_i, and defined as:

$$B_i = \frac{C_i}{C_o} \qquad (1)$$

Where:

C_i = volumetric particle concentration at the probe inlet

C_o = volumetric particle concentration in the gas stream

Other factors which affect inlet bias are duct turbulence, external force fields (such as electrical or thermal), probe misalignment and gravitational particle settling. These factors were assumed, or were caused by experimental design, to be zero except where noted.

Calculation of the volumetric particle concentration in a duct or an enclosed volume is based on the volume of gas sampled and the amount of particulate matter collected out by some device. If a section of tubing lies between the probe inlet opening and this collector, as is usually the case,

Reproduced from best available copy.

some particle matter will be lost to the tubing walls. This loss constitutes another bias and is referred to as the wall bias, B_w, where:

$$B_w = \frac{C_f}{C_i} \qquad (2)$$

Where:

C_f = volumetric particle concentration at the collector plane

Within the probe particles may be lost due to gravitational settling, diffusion, electrophoresis, thermophoresis, turbulence and inertial impaction. Under suitable conditions, any one of the above factors may cause an appreciable loss of particle matter; under the conditions of this experimental investigation, wall losses, except for inertial impaction, were kept as low as possible by design. Because inertial impaction is always present in the side port probe and in the straight inlet probe followed by a gradual bend, the normal stack gas sampling configuration, wall loss was investigated and described. The concept of inertial impaction loss in the side port probes is illustrated in Figure 3. Wall bias is of no concern if the concentration determination is based on an evaluation of the particle matter collected on both the probe inner walls and on the particle collection surface.

There have been more than a dozen articles published about sampling probes, isokinetic sampling and the like. There is, however, a great lack of experimental data on anisokinetic sampling in the micron particle size range.

Watson[2] in 1954 published a paper on anisokinetic sampling; his curves were drawn from four data points, two with 4 micron particles and two with 37 micron particles. Dennis, Samples, Anderson, and Silverman[3] used Cottrell precipitate and atmospheric dust to study sampling, both test dusts were too heterogeneous for determination of a sampling error vs. particle size relationship. An experimental study of Badzioch[4] utilized test dusts of 20 to 30 microns Stokes' mean diameter; while a study by Hemeon and Haines[5] involved dusts of 5 to 25 microns and larger. These dusts were rather coarse to be of much value to the industrial hygiene and air pollution fields.

Whiteley and Reed[6] pointed out the need for a simple and rugged sampling probe and reported on seven different probe designs. Two of these designs were straight side port probes of the type selected for use in this study. They obtained data for the side port probes using 150 microns diameter aerosols. These tests showed that the probes acted as approximately 100 per cent efficient impaction devices; the authors stated that the weight of the dust sampled varied only slightly with wide variations of sampling rate.

Vitols[1] was able to show that his theoretical anisokinetic sampling predictions fit the data of Whiteley and Reed and that of Hemeon and Haines. Because of a lack of experimental data for particles less than 10 microns, no correlation could be attempted in the micron diameter size range.

Experimental

Sampler bias for a side port probe and for a straight inlet probe was investigated experimentally using homogeneous test aerosols of various sizes from about 0.5 microns to 10 microns mass mean diameter. These tests were carried out at several duct velocities using various size probes to sample at velocities equal to, above, and below the duct velocity.

The range of variables covered by these tests are listed in Table I.

Aerosol Generation

Two different aerosol generation systems were used to generate test aerosols. Solid spherical dye particles with geometric standard deviations of about 1.15 were generated with a spinning disc generator[7] from uranine dye dissolved in an ethyl alcohol solution. Solid polystyrene particles having a geometric standard deviation of about 1.05 were generated with a two-fluid atomizer by nebulizing and evaporating a suspension of polystyrene beads in demineralized water. Aerosol samples for particle sizing with a light microscope were collected on membrane filters.

Sample Evaluation

Aerosol concentrations for all tests using uranine dye aerosols were determined by fluorometric measurements of the amount of dye collected on discs of high efficiency binderless glass filter paper; this procedure involves dissolving the dye from the filter in a known amount of water and measuring the fluorescence of the solution. Probe losses were determined by washing the inside of the sampling probe with known amounts of distilled water and making fluorometric measurements of the solution.

Aerosol concentrations determinations for the polystyrene bead aerosols involved use of the Royco Model 202 light scattering particle counter to count the number of beads, of the size being generated, in a known volume of air.

Table I

Range of Variables Investigated

Variable	Range
Particle Diameter - microns	0.5 to 10
Duct Velocity - fps	2 to 300
Probe Inlet Velocity - fps	0.2 to 300
Probe Inlet Diameter - inches	1/16 to 1/2
Velocity Ratio - Duct Velocity / Probe Inlet Velocity	0.1 to 15
Inertial Impaction Parameter - K	0.001 to 0.3

Test Procedure

The test equipment arrangement and airflow systems are shown schematically in Figures 4 and 5. For tests involving uranine dye aerosols the spinning disc aerosol generator was used. For each particle size and duct air flow rate, a set of tests were run with several probes simultaneously sampling at various flow rates. For each test, an isokinetic sample was taken with a sharp-edged straight inlet sampler probe to determine the true aerosol concentration. Aerosol concentration determined with the probes operating at anisokinetic flow rates were compared with the isokinetic sample from the straight inlet probe.

Tests which were run using polystyrene beads involved mixing uniform sized polystyrene latex spheres from Dow Chemical Company with distilled water and atomizing with a two-fluid atomizer. The liquid aerosol was mixed with an excess of dry air to assure complete evaporation of the water. Further dilution, with clean air, was used to obtain the desired test duct flow rates. Air used for atomization and dilution was dry, oil free and absolute filtered. Sampler bias was determined by comparing the concentration obtained at the test condition with that obtained isokinetically using a straight inlet probe.

Probe flow rates for all tests were determined using volumetric gas meters, corrected for pressure difference between the gas meter and the sampling probe inlet. All tests were run at standard temperature and pressure with filtered room air as the carrier gas. All test probes were made from clean, smooth tubing with no coatings inside to affect particle adhesion to the wall.

Experimental Accuracy

Estimated accuracy of the various measured or calculated values are listed in Table II.

191[illegible]

Table II

Test Data and Result Accuracy

Property	Estimated Accuracy
Particle Diameter	± 5%
Probe Diameter	± 5%
Velocity	± 5%
Velocity Ratio-R	± 10%
Impaction Parameter-K	± 20%
Concentration Ratio or Bias-B	
B = 1	± 2%
B = 1.25 or 0.75	± 5%
B = 1.5 or 0.5	± 10%

Results

There are several factors which affect sampler bias - particle size, shape and density; gas velocity, viscosity and (sometimes) density; and probe size, shape, orientation, and operation. Combining the above variables in different ways yields several dimensionless groups; the most important of these are: 1) inertial impaction parameter, K, and 2) velocity ratio, R. The parameters K and R are defined as follows:

$$K = \frac{C\rho_p V_o D_p^2}{18 \mu D_c} \qquad (3)$$

Where:

C = Cunningham correction factor - dimensionless (Fuchs[8])

$$= 1 + \frac{1.62 \times 10^{-5}}{D_p} + \frac{0.55 \times 10^{-5}}{D_p} \exp. (- 0.67 \times 10^{5} D_p)$$

ρ_p = particle density - gm/cc

V_o = duct velocity - cm/sec

D_p = particle diameter - cm

μ = gas viscosity - poise

D_c = probe inlet diameter - cm

$$R = \frac{V_o}{V_i} \qquad (4)$$

Where:

V_i = probe inlet velocity - cm/sec

As is quite often true in aerosol studies, the inertial impaction parameter is of primary importance.

Within the scatter of the experimental data, the probe inlet bias B_i can be described as a function of the parameters K and R over a range of sampling conditions. The side port probe internal wall loss or wall bias, B_w, due to inertial impaction can be described by the parameter K, where K is based on duct velocity V_o.

Sampling bias is divided up into probe inlet bias, B_i, and probe internal wall loss bias, B_w, and is discussed after the side port probe configuration and operational considerations of alignment.

Discussion of Side Port Probe Configuration

The two side port probe configurations tested are shown in Figure 6; the important probe dimensions are also shown. To determine the effect of probe alignment on sampling bias, several tests were run with the side port probes being positioned at various angles from 0° to 90° with the incoming air stream. Results for isokinetic sampling tests run at a duct velocity of 60 feet per second, using 1.3 micron diameter particles, are shown in Figure 7. A very definite effect of probe alignment is seen for the side inlet probes. With the 45° end opening probe there was essentially no detectable change in concentration until probe misalignments in excess of 30 degrees were reached.

To determine the optimum angle for the end opening probe, isokinetic sampling tests were run at 60 feet per second and 250 feet per second duct velocity using 1.3 micron diameter particles. Probes with end angles of 0 degrees, 22 1/2 degrees, 45 degrees, and 67 1/2 degrees were tested at the above conditions. Results for this series of tests are shown in Figure 8. From these test results it was concluded that the 45 degree angle inlet was near optimum, therefore, all other tests were run with an end opening probe angle of 45 degrees.

Discussion of Inlet Bias

Consider the two cases of anisokinetic sampling illustrated in Figure 2. In one case the sample will contain a disproportionately high concentration of particles and in the other a low concentration. If the particles of interest are of gas molecule size there will be no bias in either case; therefore, the problem is that of quantitatively describing the relation between sampling bias and the sampling variables - such as duct velocity, probe velocity, particle aerodynamic size - and the probe size and configuration.

The other extreme of inertialess particles are particles of great inertia: for this case the parameter K has a value much greater than one and only the projected probe inlet area, duct velocity and duct particle concentration affect particle collection rate (the probe acts as an impactor of 100% efficiency); this was experimentally shown by Whiteley and Reed^6.

Under all sampling conditions the side port probe's geometry will disturb the flow field and there will be a resulting sampling bias. If a side port probe is placed in an air stream, the air streamlines entering the probe's inlet would probably look something like those shown in Figures 9 and 10. Assuming the flow to be of the form shown, the number of particles entering the probe per unit time is:

$$(A_1 + A_2) V_i C_i = A_1 C_o V_o + A_2 C_o V_o \alpha_2 + A_3 C_o V_o (1 - \alpha_3) \quad (5)$$

Where:

A_1, A_2, A_3 = air sampling areas as shown in Figure 10

α_2 = fraction of particles entering probe from Area A_2

$1 - \alpha_3$ = fraction of particles entering probe from Area A_3

Reproduced from best available copy.

Assuming an incompressible fluid, Equation 5 becomes:

$$\frac{C_i}{C_o} = B_i = 1 + \frac{A_2\,\alpha_2 - A_3\,\alpha_3}{A_1 + A_3} \qquad (6)$$

If the case where $V_o = V_i$ (isokinetic sampling), area A_3 = area A_2 and:

$$B_i = 1 + \frac{A_2}{A_1 + A_2}\;(\alpha_2 - \alpha_3) \qquad (7)$$

Therefore, the inlet bias, B_i, will be greater than 1 for isokinetic sampling if α_2 is greater than α_3. The average velocity slightly upstream from the probe is lower in area A_3 than the velocity in area A_2: therefore, the impaction efficiency α_3 will be less than α_2 and the inlet bias will be greater than one even when the sampler inlet and duct velocity are matched. Impaction efficiency is also inversely dependent upon a characteristic dimension; this dimension is greater for area A_3 than for A_2 thereby further reducing α_2. The above can be extended to anisokinetic sampling conditions and will explain why the side port probe bias will always be a higher value than the straight inlet probe when both are operated at comparable conditions.

The impaction efficiency, α, is known to be a function of the parameter K, therefore sampler bias will be a function of the parameter K. Equation (6) shows the inlet bias to depend on both impaction efficiency and area ratios which in turn are determined by the velocity ratio V_o/V_i. Bias should therefore depend on both the velocity ratio and the impaction parameter.

The experimentally determined sampler inlet bias data can be fairly well described by just two dimensionless parameters; the impaction parameter K and the duct to probe inlet velocity ratio R. Figure 11 shows the relationship between sampler bias and velocity ratio for both side port probe configurations. Lines of constant K value are drawn in. Each data point shown is an average of several tests; the individual test data are tabulated in Table III. Figure 12 shows the same relationship for the straight inlet probe, again with constant K value lines drawn in. Each test result was plotted separately; these data are also contained in Table III.

Sampling bias is a function of both duct velocity and particle aerodynamic size; therefore, the bias for any set of anisokinetic sampling conditions can only be stated as a functional relationship involving particle size.

To better illustrate the effect of particle size and duct velocity on sampling bias, Figure 13 was prepared. This chart assumes standard temperature and pressure air, spherical particles of density one and a sampling probe of one centimeter diameter. The range of maximum interest is the K value range from 0.01 to 1.0; below 0.01 the sampling bias is low enough to be relatively unimportant; above 1.0 the sampling inlet bias is equal to the velocity ratio, therefore, quite easily determined if the velocities are known.

The data of Figures 11 and 12 have been replotted in Figures 14 and 15 with lines of constant bias drawn in. Sampler inlet bias for the K value range from 0.001 to 0.2 was experimentally determined by this study; the K value range from 0.2 to 1.0 was not covered and the bias vs K relationship presented in Figure 15 is an extrapolation for the straight inlet probe. A similar extrapolation was not attempted for the side port probe.

Table III

Experimental Data for Sampling Probes

Side Port Probes

K	R	B_i	D_p-microns	Probe Type
≈0.001	0.3	0.98	0.56	45° End Open
≈0.001	0.3	0.98	0.56	Side Hole
≈0.001	1.1	1.00	0.56	45° End Open
≈0.001	1.1	1.00	0.56	Side Hole
≈0.001	4.3	1.00	0.56	45° End Open
≈0.001	4.3	1.00	0.56	Side Hole
≈0.02	0.48	.94	1.3	Side Hole
≈0.02	0.95	1.02	1.3	45° End Open
≈0.02	1.5	1.03	1.3	45° End Open
≈0.04	0.15	0.67	2.7	Side Hole
≈0.04	0.72	0.97	2.7	Side Hole
≈0.1	0.48	0.82	4.5	45° End Open
≈0.1	0.48	0.83	4.5	Side Hole
≈0.1	0.64	0.95	5.2	45° End Open
≈0.1	0.64	0.81	5.2	Side Hole
≈0.1	0.94	1.12	4.5	45° End Open
≈0.1	0.94	1.06	4.5	Side Hole
≈0.1	1.04	1.04	4.9	45° End Open
≈0.1	1.04	1.05	4.9	Side Hole
≈0.1	1.9	1.18	4.6	45° End Open
≈0.1	1.9	1.22	4.6	Side Hole

Table III Continued

K	R	B_i	D_p-microns	Probe Type
≈0.1	1.9	1.31	4.6	45° End Open
≈0.1	1.9	1.30	4.6	Side Hole
≈0.2	0.63	1.12	9.2	45° End Open
≈0.2	0.63	1.14	9.2	Side Hole
≈0.2	0.88	1.25	9.2	45° End Open
≈0.2	0.88	1.24	9.2	Side Hole
≈0.2	1.86	1.50	9.2	45° End Open
≈0.2	1.86	1.72	9.2	Side Hole

Straight Inlet Probe

K	R	B_i	D_p-microns
≈0.005	0.25	0.98	1.3
≈0.005	0.30	1.00	1.3
≈0.005	5.	1.02	1.3
≈0.005	16.	1.05	1.3
≈0.02	0.29	.94	2.5
≈0.02	0.5	.95	2.5
≈0.02	1.4	1.05	1.3
≈0.02	2.0	1.07	1.3
≈0.02	2.2	1.07	1.3
≈0.02	3.3	1.10	1.3
≈0.02	3.9	1.09	1.3
≈0.02	4.3	1.07	2.5

Table III Continued

K	R	B_i	D_p-microns
≈0.02	4.4	1.07	2.5
≈0.02	4.9	1.08	1.3
≈0.02	5.5	1.10	1.3
≈0.02	15.4	1.10	1.3
≈0.04	0.20	0.57	1.3
≈0.04	0.25	0.66	1.3
≈0.04	0.35	0.88	1.3
≈0.04	0.51	0.96	1.3
≈0.04	0.71	0.99	1.3
≈0.04	1.41	1.09	1.3
≈0.04	2.05	1.10	1.3
≈0.04	3.1	1.12	1.3
≈0.04	4.0	1.13	1.3
≈0.04	5.2	1.14	1.3
≈0.08	0.21	0.49	1.3
≈0.08	0.35	0.58	1.3
≈0.08	0.50	0.86	1.3
≈0.08	0.80	0.98	1.3
≈0.14	0.20	0.19	2.7
≈0.14	0.25	0.32	2.7
≈0.14	0.35	0.64	2.7
≈0.14	0.47	0.59	2.7
≈0.14	0.65	0.90	2.7

Table III Continued

K	R	B_i	D_p-microns
≈0.14	0.74	0.93	2.7
≈0.14	1.4	1.17	2.7
≈0.14	2.0	1.23	2.7
≈0.14	3.2	1.33	2.7
≈0.14	4.0	1.45	2.7
≈0.14	5.1	1.42	2.7
≈0.32	0.21	0.25	2.7
≈0.32	0.35	0.35	2.7
≈0.32	0.49	0.63	2.7
≈0.32	0.70	0.79	2.7
≈0.32	1.65	1.30	2.7
≈0.32	1.95	1.43	2.7
≈0.32	2.3	1.76	2.7

Once a particle density and probe size have been picked and a chart similar to Figure 13 drawn, it is readily possible to determine the sampling inlet bias vs particle size for either the side port probe from Figure 14, or for the straight inlet probe from Figure 15. The procedure is to follow (vertically) a line of constant K, determined by the intersection of prescribed duct velocity and particle diameter, on either one of the sampling probe figures, and find the desired velocity ratio line; the inlet bias is then read from the figure. To illustrate this procedure, Figures 13, 14 and 15 were combined to form Figure 16. If, for example, one micron diameter particles in a 100 fps air stream were sampled at a side port probe inlet velocity of 25 fps, the sampling bias can be determined to be 1.05, or 5% in error, by following the dotted lines shown in Figure 16.

One important sampling consideration should be noted for the side port probe; if a sampling velicity ratio of about 0.7 is chosen, the inlet bias will contribute less than a 5% error to particle concentration over the K value range from 0 to 0.15; while at a velocity ratio of 1 (isokinetic) the error becomes about 20% at K = 0.15. With a side port probe or a blunt-edged probe of any type, slight undersampling (R<1) will contribute less error than isokinetic sampling, while oversampling (R>1) will serve to magnify the error.

Discussion of Wall Bias

Internal loss of particles in a probe can result from any one of several factors. For a side port probe, the most important of these is inertial impaction at the entrance. When air enters the probe it must change direction; a centrifugal force acts on the suspended particles causing all particles to move radially outward and causing some to impact out on the probe inner wall, as shown in Figure 3. The internal loss of particles due to impaction (which occurs in any probe with a curved section) is often times not accounted for in the analysis, therefore, it is important to consider the loss magnitude.

This impaction loss in the side port probe was determined for several sizes of probes using several sizes of test aerosols and several sampling velocities. The wall loss was correlated with the inertial impaction parameter K (based on tube diameter); a plot of the data is shown in Figure 17. Except for the points near the lower left hand corner (K = 0.02), the Equation:

$$B_w = 1 - 2K \tag{8}$$

fairly adequately describes the experimental data. This equation indicates a maximum loss (minimum wall bias) because the impacted particles are assumed to stick to the wall and not re-enter the air stream. At higher duct velocities and at high K values the particles will bounce off the wall, also when the probe inside surface becomes coated with particles, the material will begin to re-enter the gas stream.

Summary

Sampling biases for a side port probe and a straight inlet probe were determined and shown to be functions of two dimensionless parameters, the inertial impaction parameter K and the velocity ratio R.

Experimental results show that the side port probe can be used to obtain essentially representative samples under conditions of low impaction parameter values. Within the experimental accuracy, the biases for both side port probe configurations (the 45° end inlet and the side inlet) and for all three probe sizes (1/4, 3/16, and 1/2 inch outside diameter) had the same functional relationship and dependence on the parameters K and R.

If a maximum acceptable bias is specified for a sample, Figures 14 and 15 depict the conditions for sampling. If a sample is obtained under a set of known anisokinetic conditions the figures will depict the bias versus particle size relationship (through the parameter K).

Literature Cited

1. Vitols, V., "Theoretical Limits of Errors Due to Anisokinetic Sampling of Particulate Matter," APCA Journal, 16, 2:79 (1966).

2. Walson, H. H., "Errors Due to Anisokinetic Sampling of Aerosols," Amer. Ind. Hy. Assoc. Quart., 15, 1 (1954).

3. Dennis, R., Samples, W. R., Anderson, D. M., and Silverman, L., "Isokinetic Sampling Probes," Ind. Eng. Chem., 49, 294 (1957).

4. Badzioch, S., "Collection of Gas-Borne Dust Particles by Means of an Aspirated Sampling Nozzle," Brit. J. Appl. Phys., 10, 26 (1959).

5. Hemeon, W. C. L., and Haines, G. F., Jr., "The Magnitude of Errors in Stack Dust Sampling," Air Repair, 4, 159 (1954).

6. Whiteley, A. B., and Reed, L. E., "The Effect of Probe Shape on the Accuracy of Sampling Flue Gases for Dust Content," J. Inst. Fuel, 32, 316 (1959).

7. Whitby, K. T., Lundgren, D. A., and Peterson, C. N., "Homogeneous Aerosol Generators," Int. J. Air & Water Pollu., 9, 263 (1965).

8. Fuchs, N. A., "The Mechanics of Aerosols," P. 27, The Macmillan Co., New York (1964).

Figure 1 Sampling Probe Configurations
Figure 2 Anisokinetic Sampling
Figure 3 Impaction Loss in a Side Port Probe
Figure 4 Test Equipment Arrangement for Dye Aerosols
Figure 5 Test Equipment Arrangement for Atomized Beads
Figure 6 Side Port Probe Dimensions
Figure 7 Sampling Bias vs. Probe Alignment
Figure 8 Sampling Bias vs. Probe Inlet Angle
Figure 9 Schematic of Flow into Side Port Probe
Figure 10 Area Nomenclature for Side Port Probe
Figure 11 Side Port Probe - Bias vs. Velocity Ratio
Figure 12 Straight Inlet Probe - Bias vs. Velocity Ratio
Figure 13 Relationship Between K, Dp & V
Figure 14 Side Port Probe - Velocity Ratio vs. K
Figure 15 Straight Inlet Probe - Velocity Ratio vs. K
Figure 16 Composite Figure for Bias Determination
Figure 17 Wall Loss vs. K for Side Port Probe

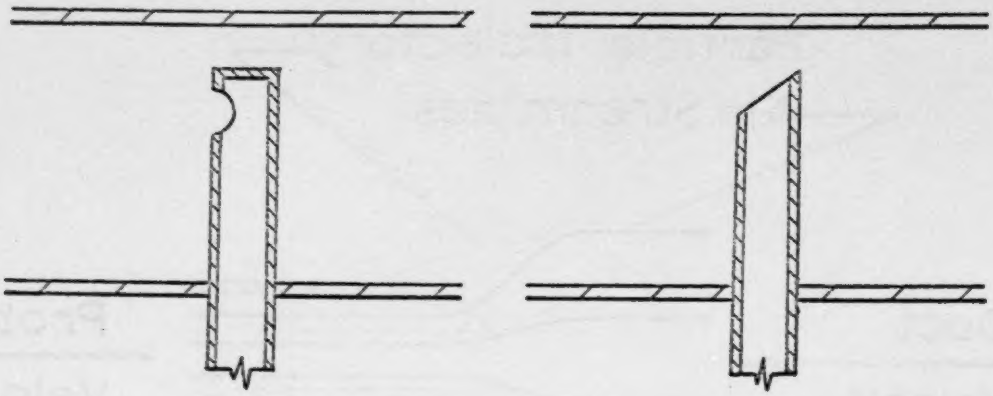

a) SIDE PORT PROBES

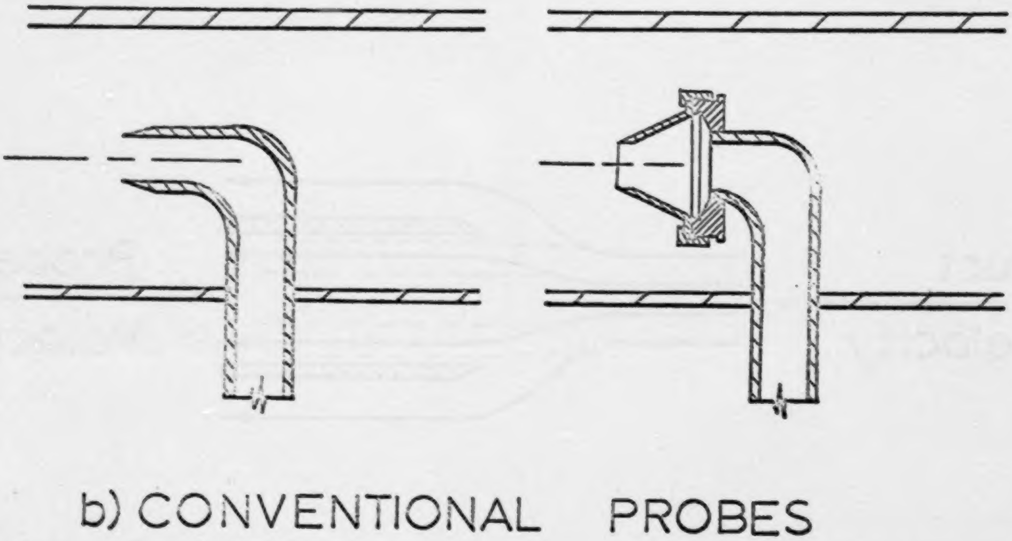

b) CONVENTIONAL PROBES

Figure 1 Sampling Probe Configurations

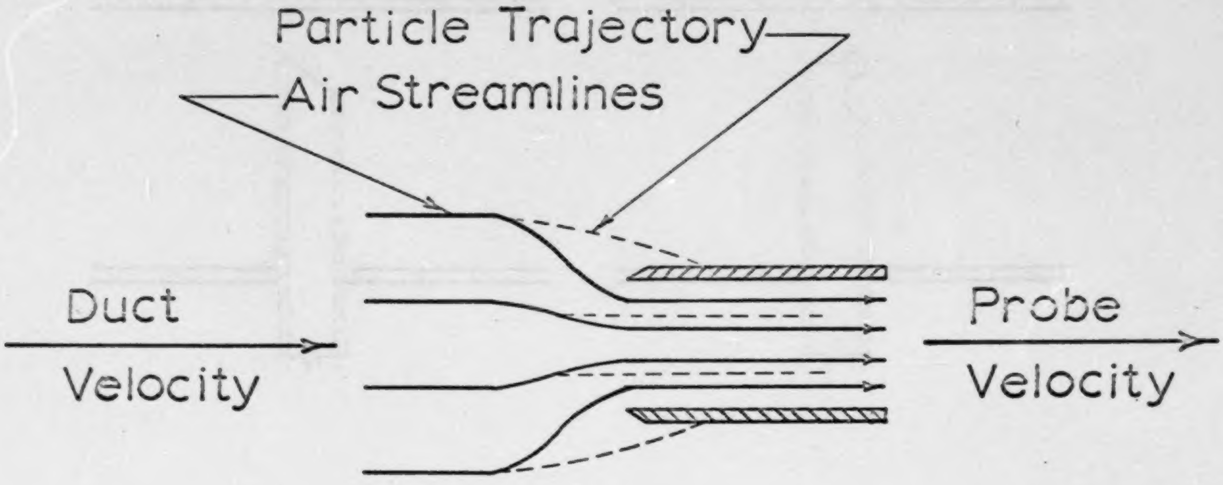
Particle Trajectory
Air Streamlines
Duct
Velocity
Probe
Velocity

a) DUCT VELOCITY < PROBE VELOCITY

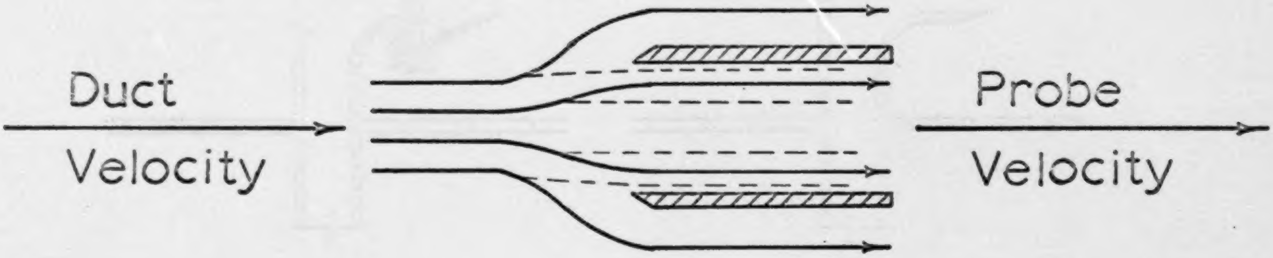
Duct
Velocity
Probe
Velocity

b) DUCT VELOCITY > PROBE VELOCITY

Figure 2 Anisokinetic Sampling

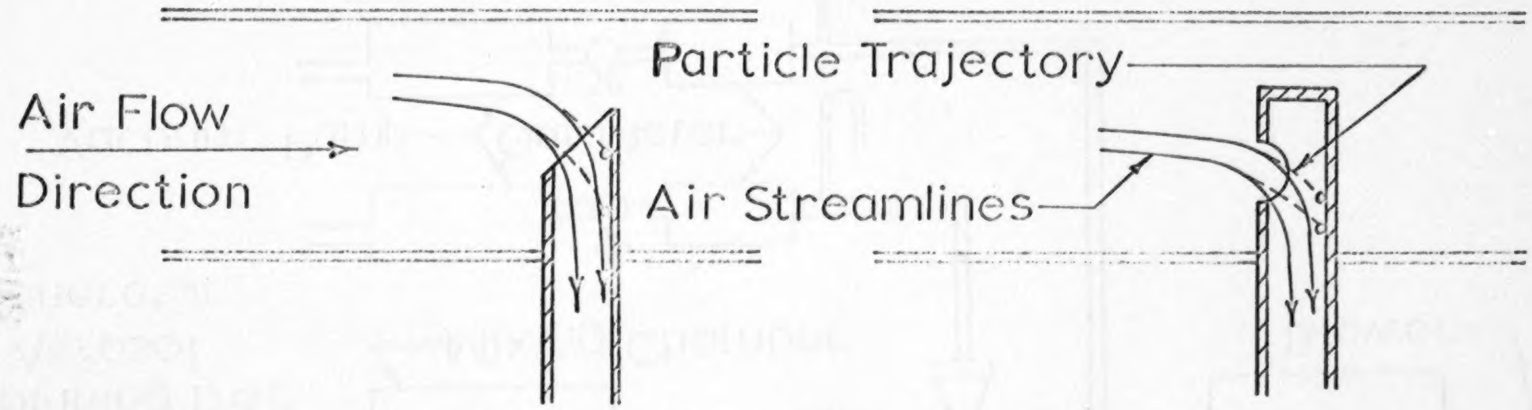
Air Flow
Direction
Particle Trajectory
Air Streamlines

Figure 3 Impaction Loss in a Side Port Probe

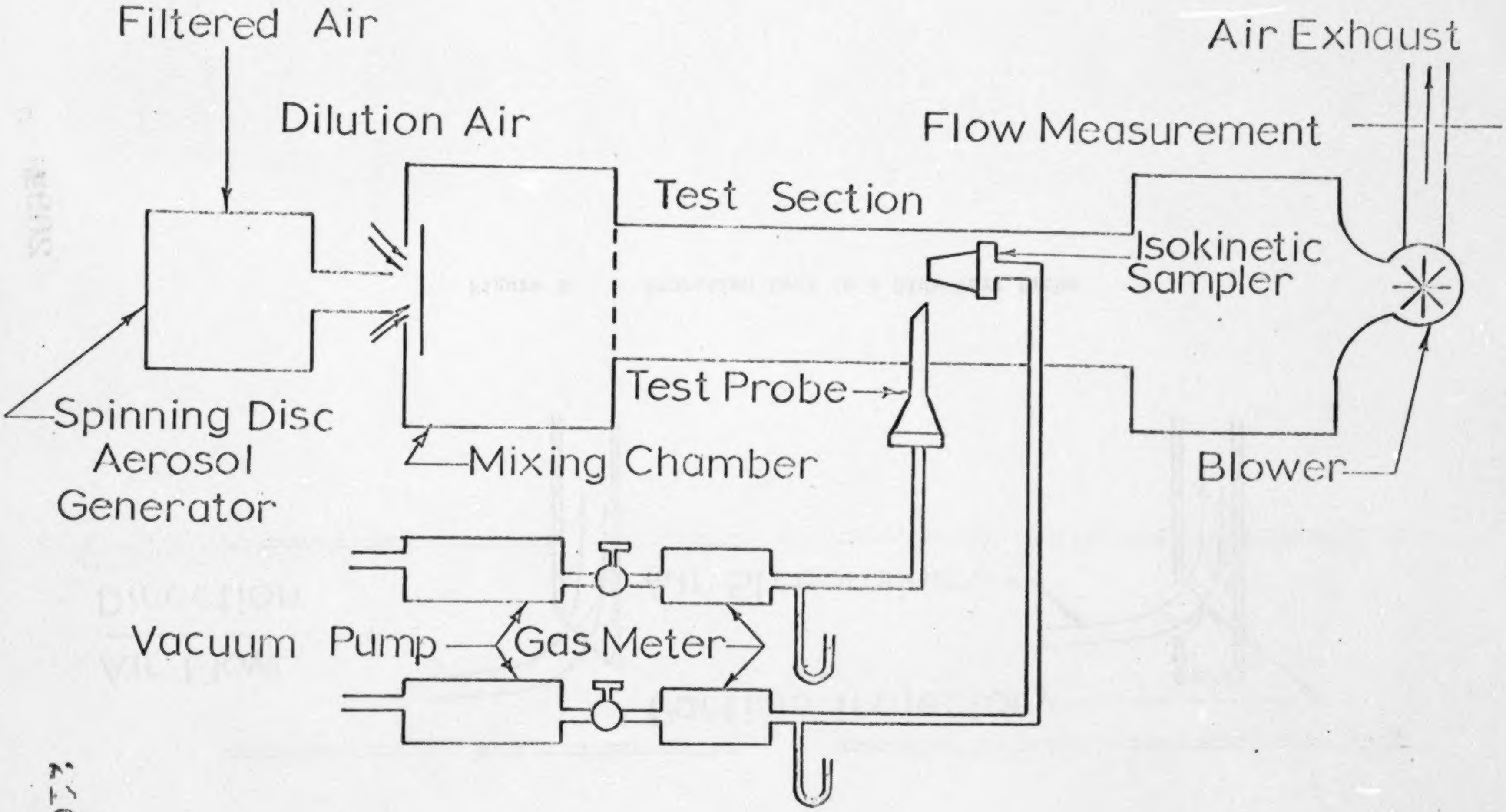
Filtered Air
Dilution Air
Air Exhaust
Flow Measurement
Test Section
Isokinetic Sampler
Test Probe
Spinning Disc Aerosol Generator
Mixing Chamber
Blower
Vacuum Pump
Gas Meter

Figure 4 Test Equipment Arrangement for Dye Aerosols

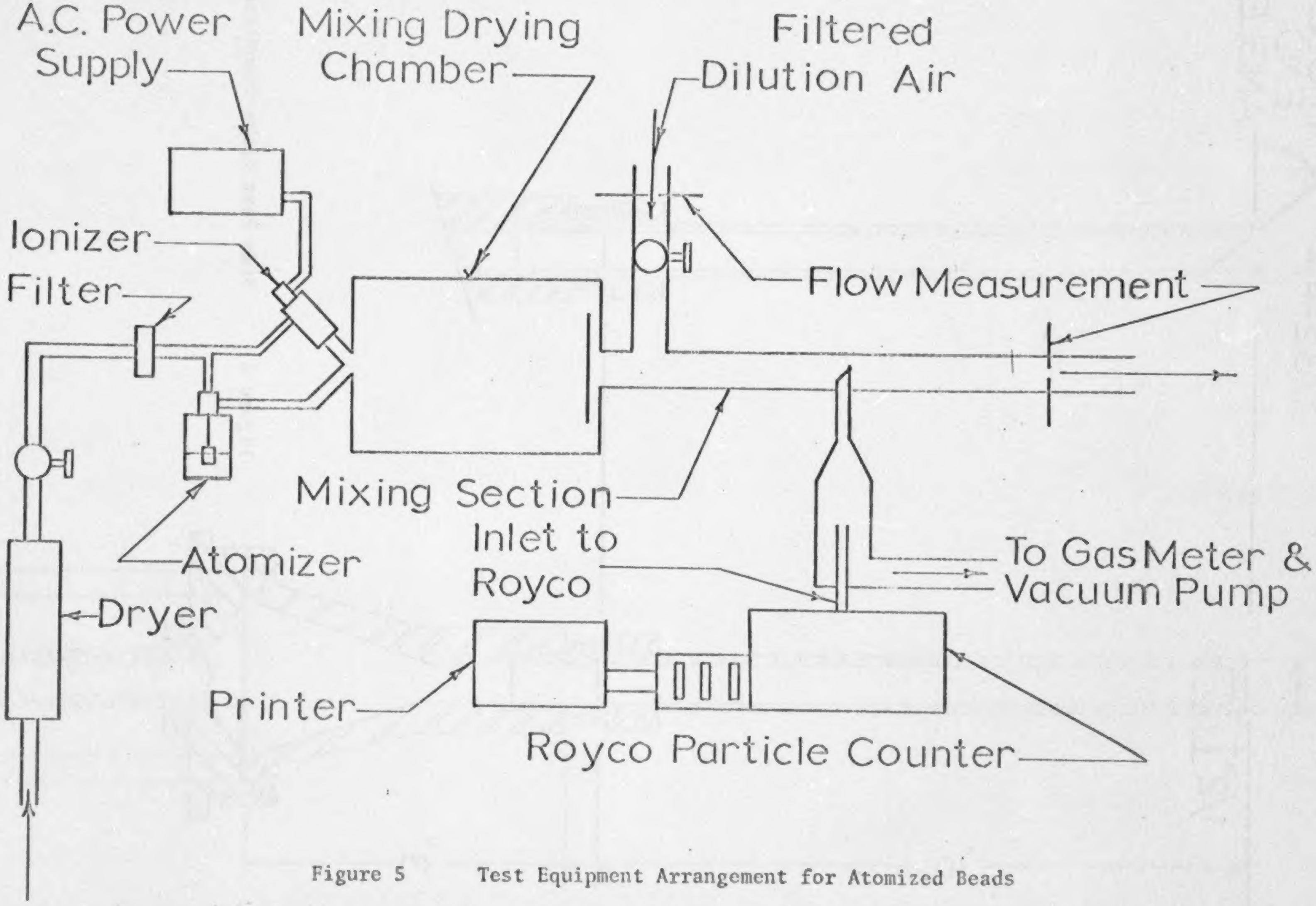
A.C. Power Supply
Mixing Drying Chamber
Filtered Dilution Air
Ionizer
Filter
Flow Measurement
Mixing Section
Inlet to Royco
To GasMeter & Vacuum Pump
Atomizer
Dryer
Printer
Royco Particle Counter

Figure 5 Test Equipment Arrangement for Atomized Beads

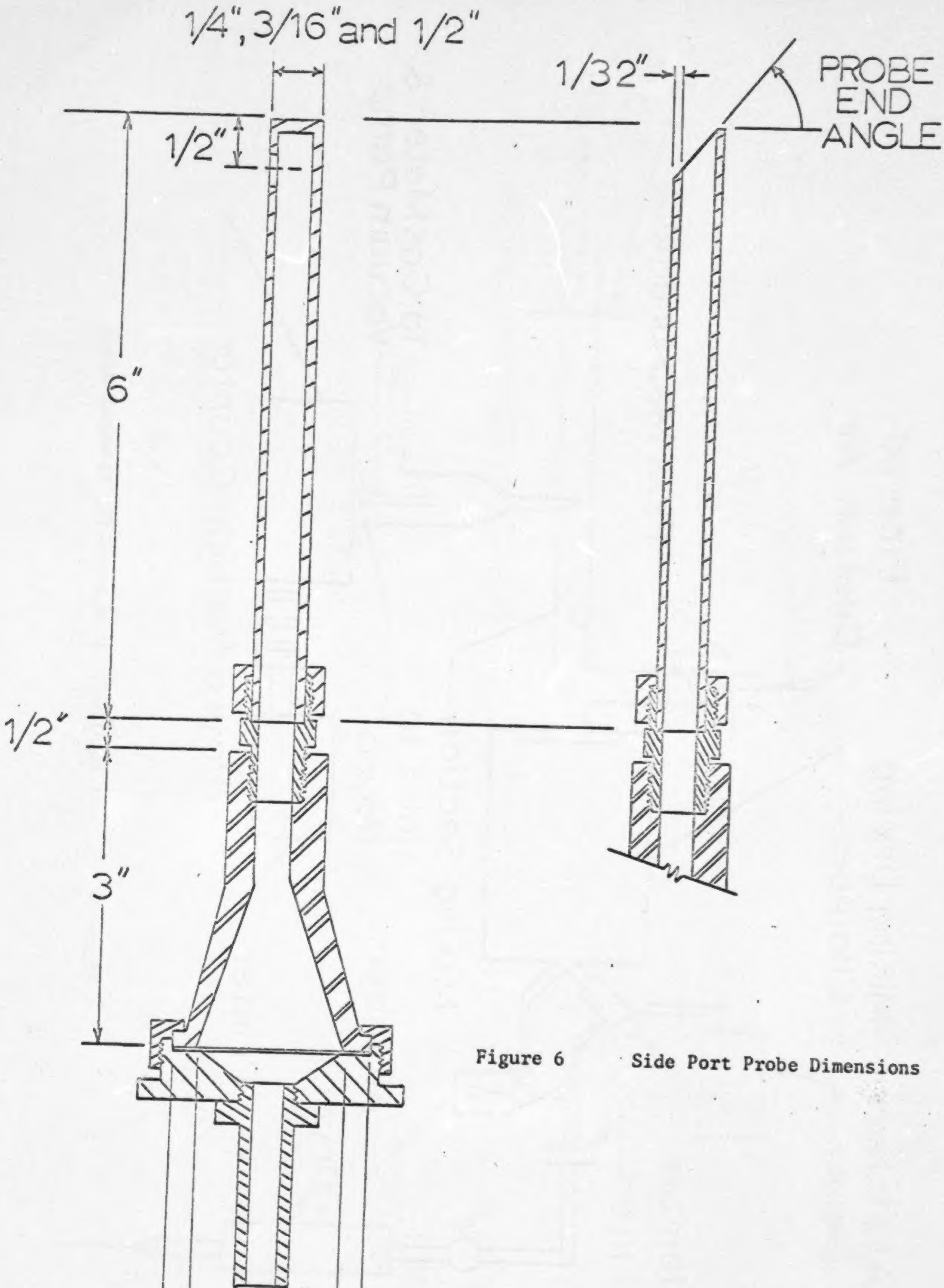
1/4", 3/16" and 1/2"
1/2"
6"
1/2"
3"
1 1/2"
2"
1/32"
PROBE
END
ANGLE

Figure 6 Side Port Probe Dimensions

Figure 7 Sampling Bias vs. Probe Alignment

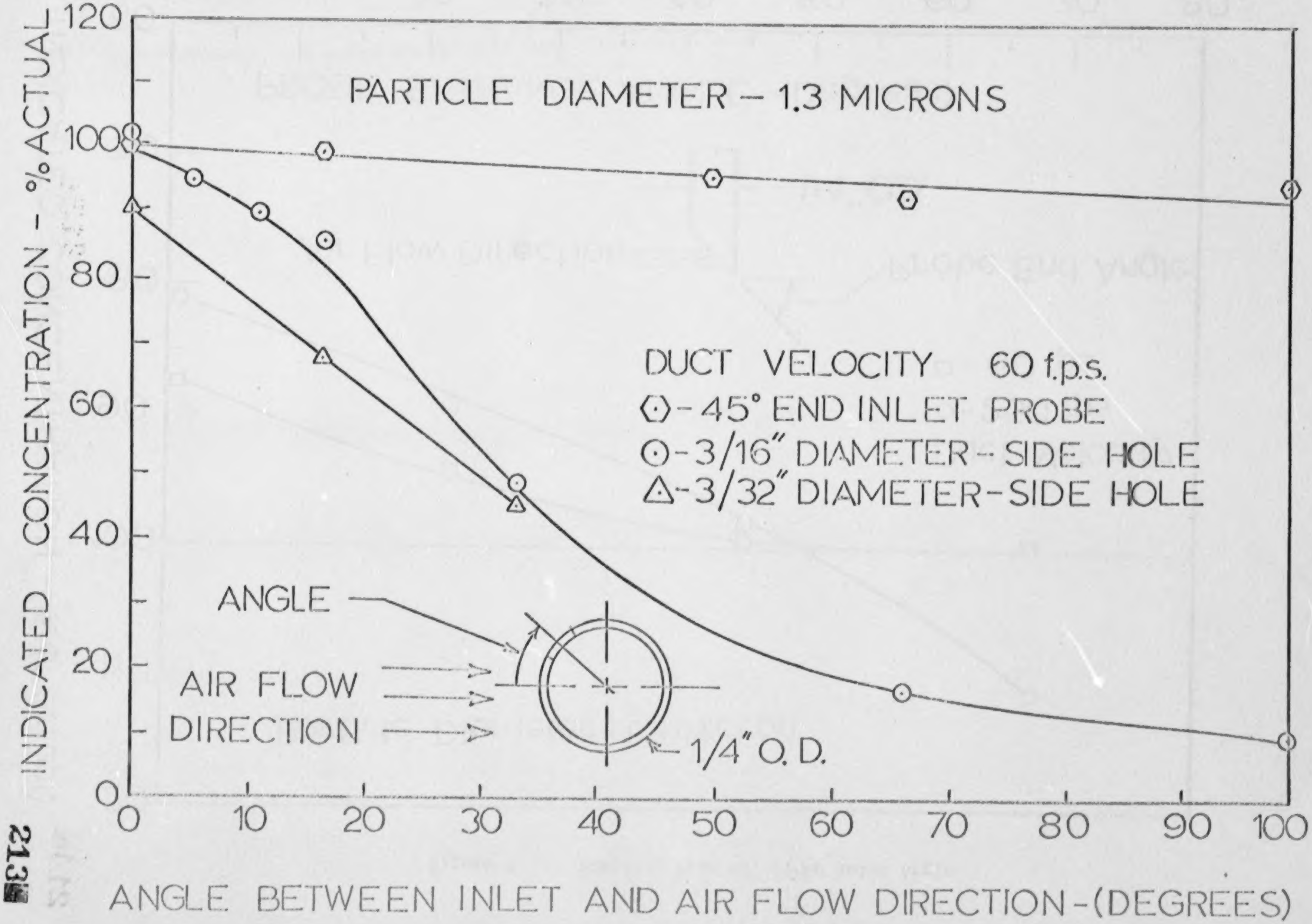

Figure 8 Sampling Bias vs. Probe Inlet Angle

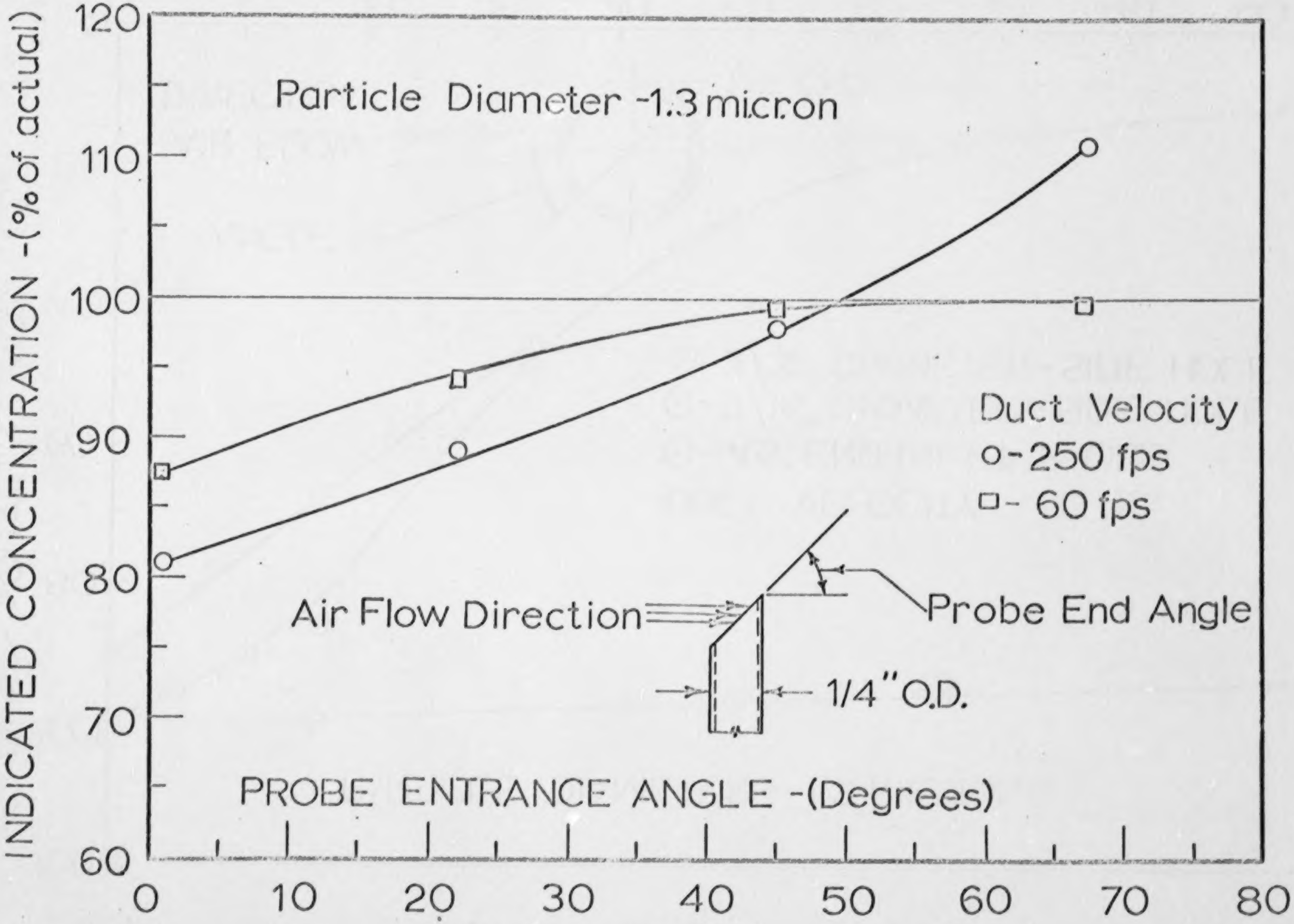

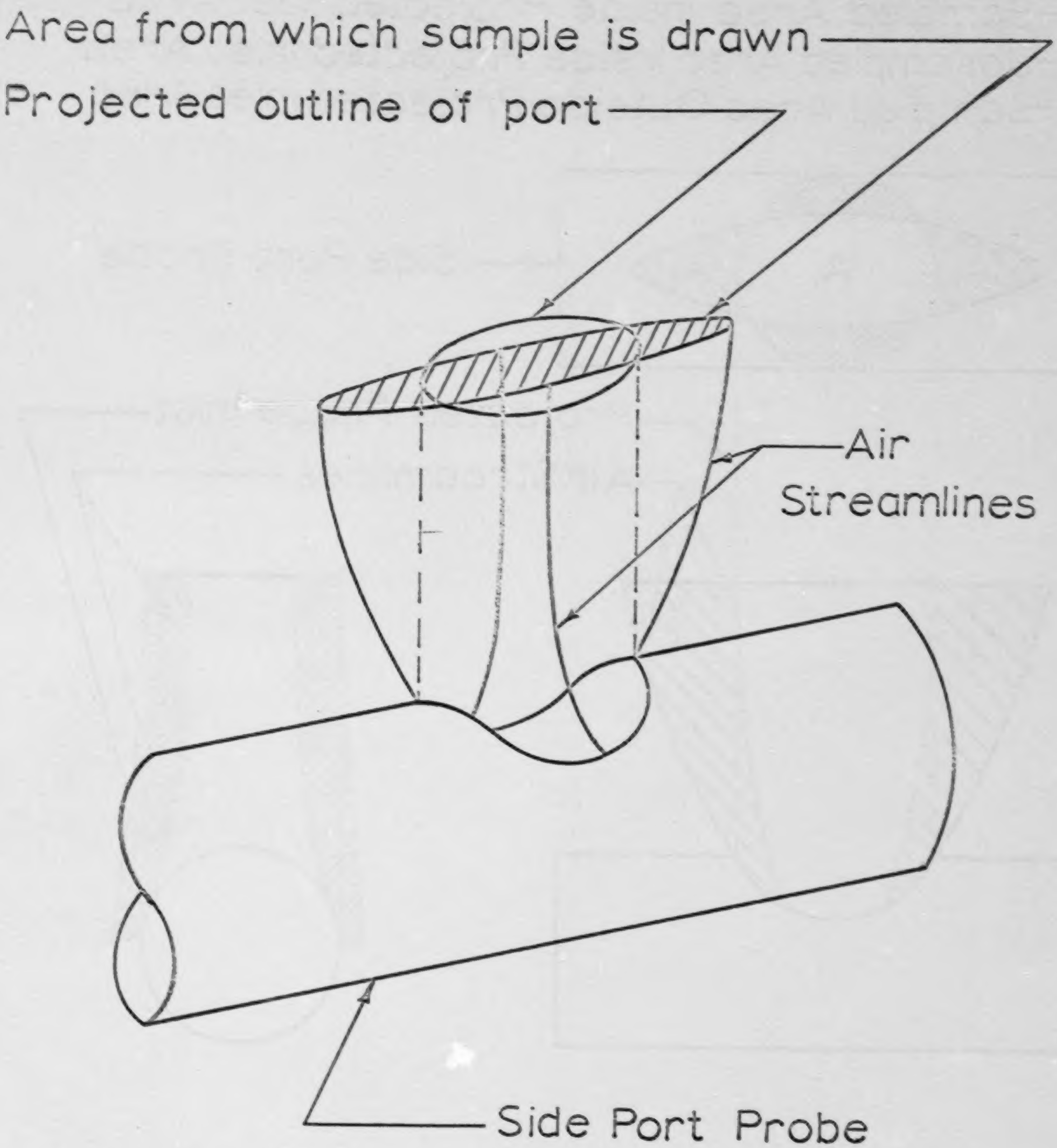
Area from which sample is drawn
Projected outline of port
Air Streamlines
Side Port Probe

Figure 9 Schematic of Flow into Side Port Probe

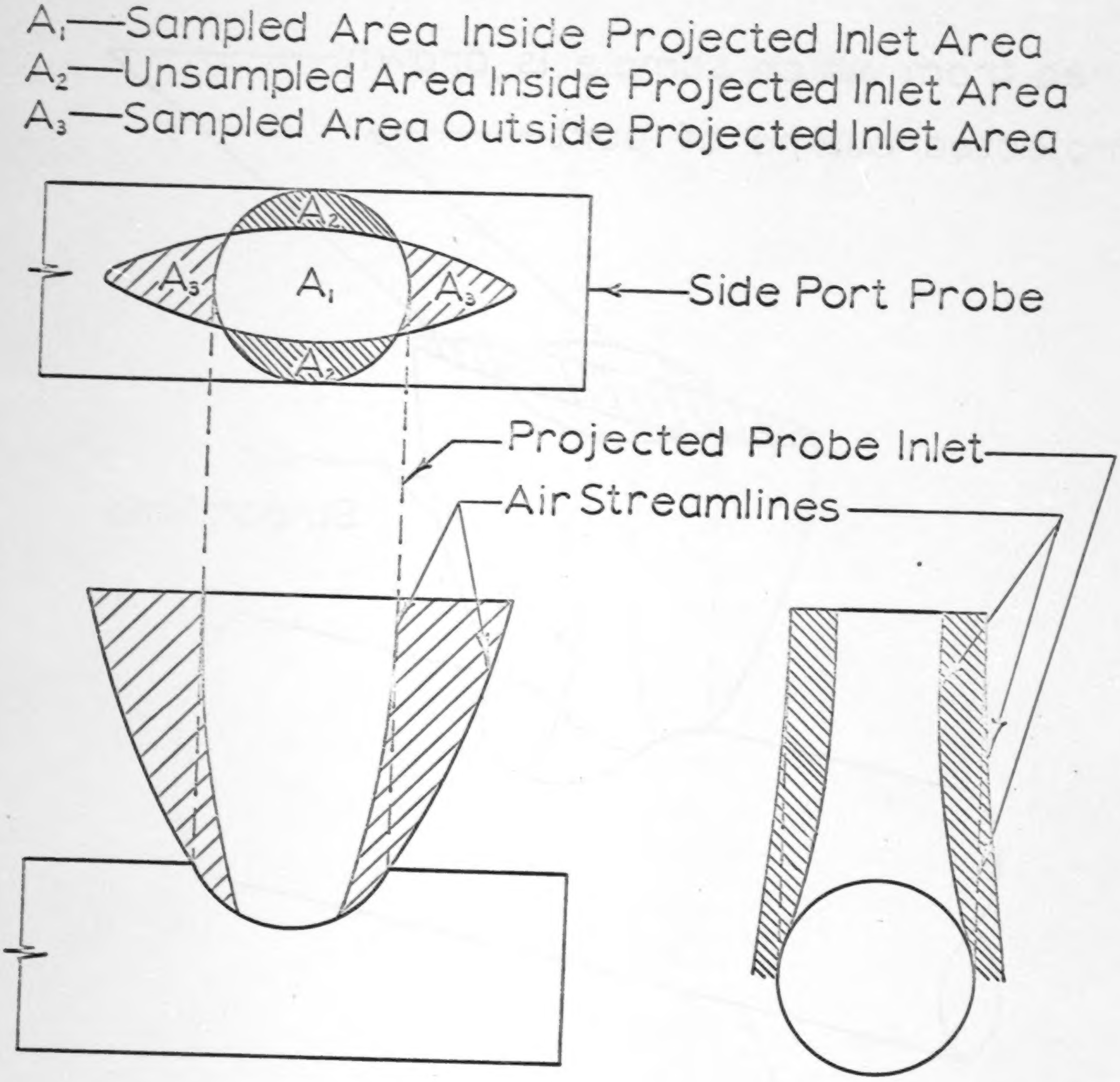
A1—Sampled Area Inside Projected Inlet Area
A2—Unsampled Area Inside Projected Inlet Area
A3—Sampled Area Outside Projected Inlet Area
A2
A3
A1
A3
A2
Side Port Probe
Projected Probe Inlet
Air Streamlines

Figure 10 Area Nomenclature for Side Port Probe

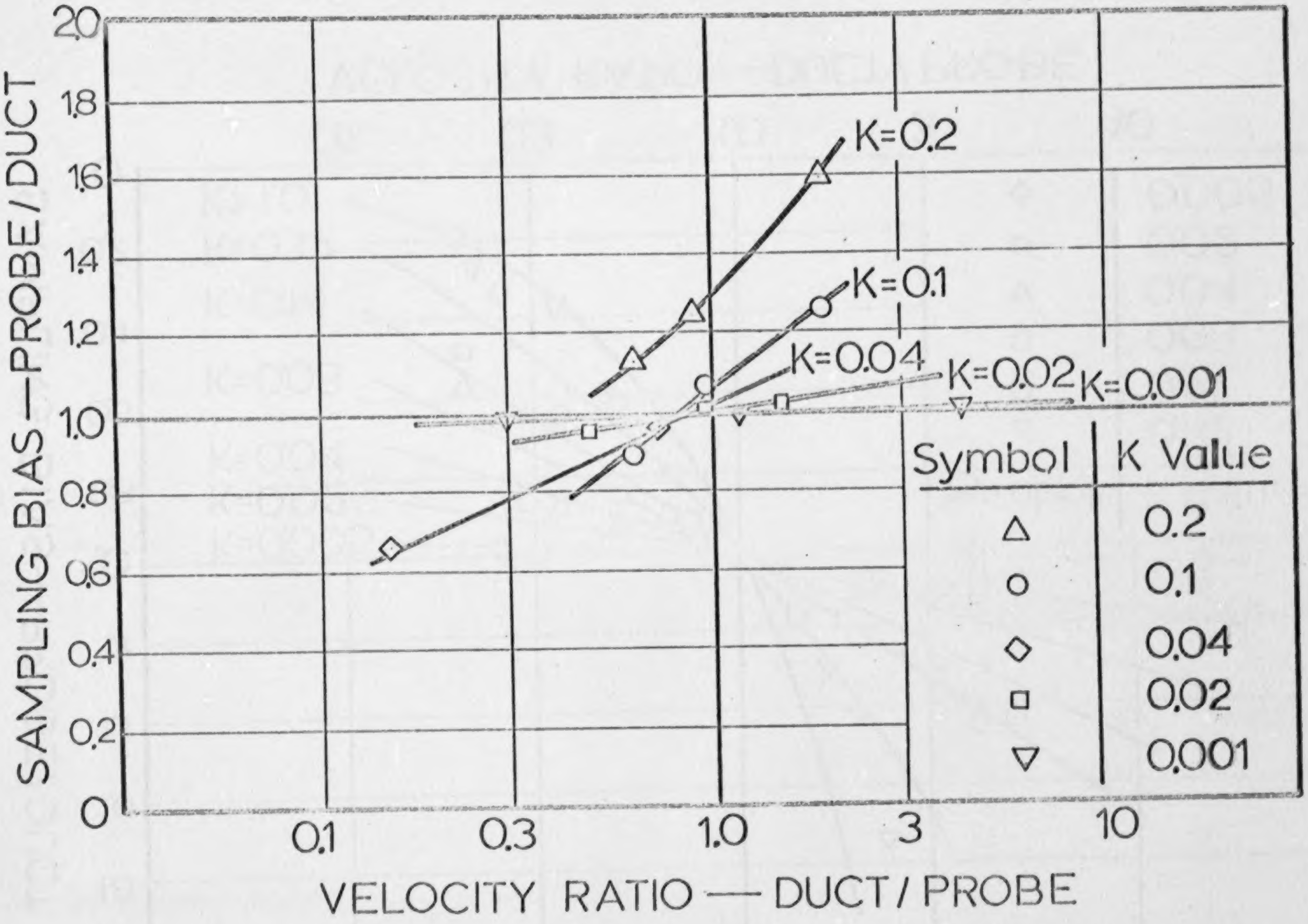

Figure 11 Side Port Probe - Bias vs. Velocity Ratio

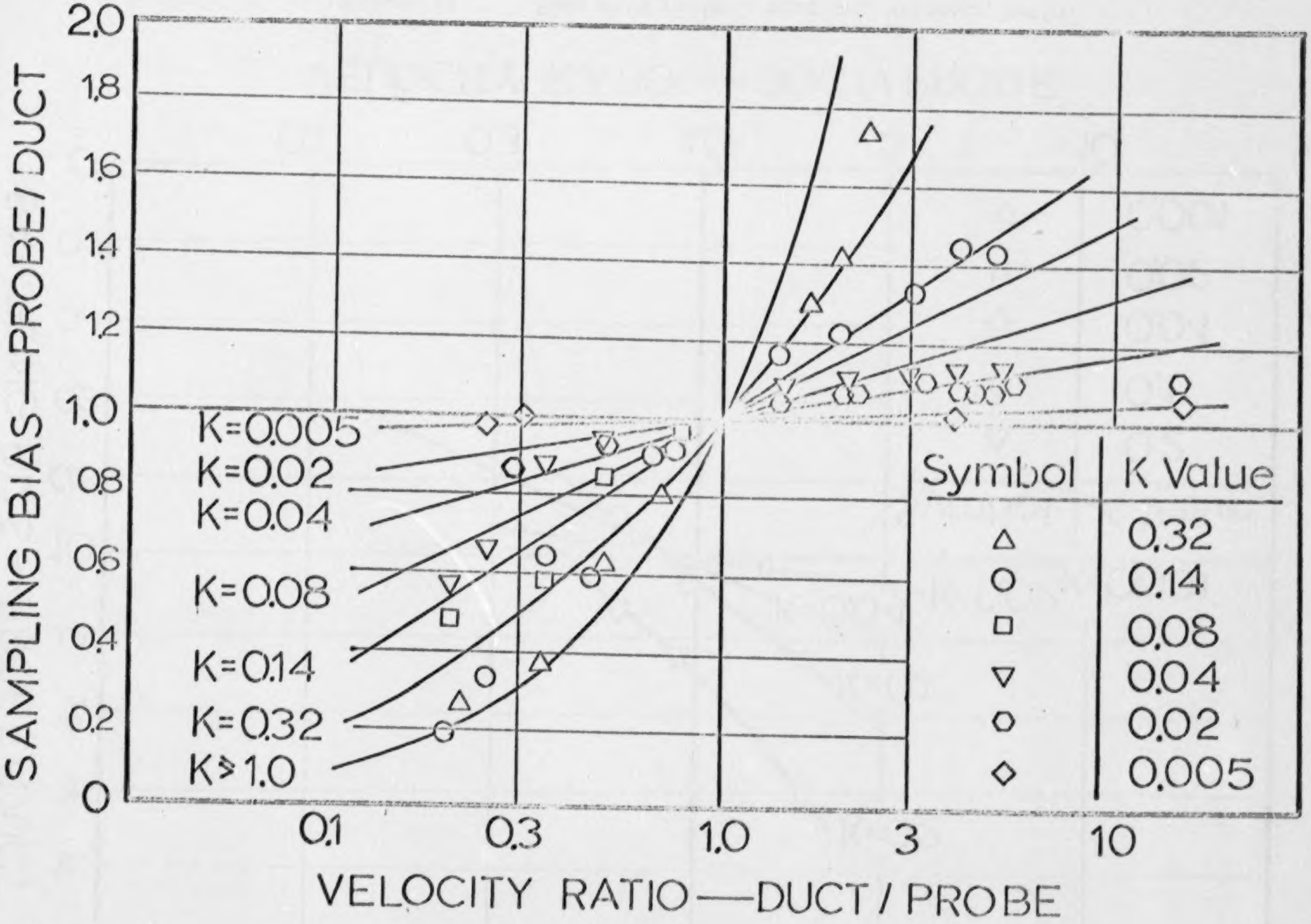

Figure 12 Straight Inlet Probe - Bias vs. Velocity Ratio

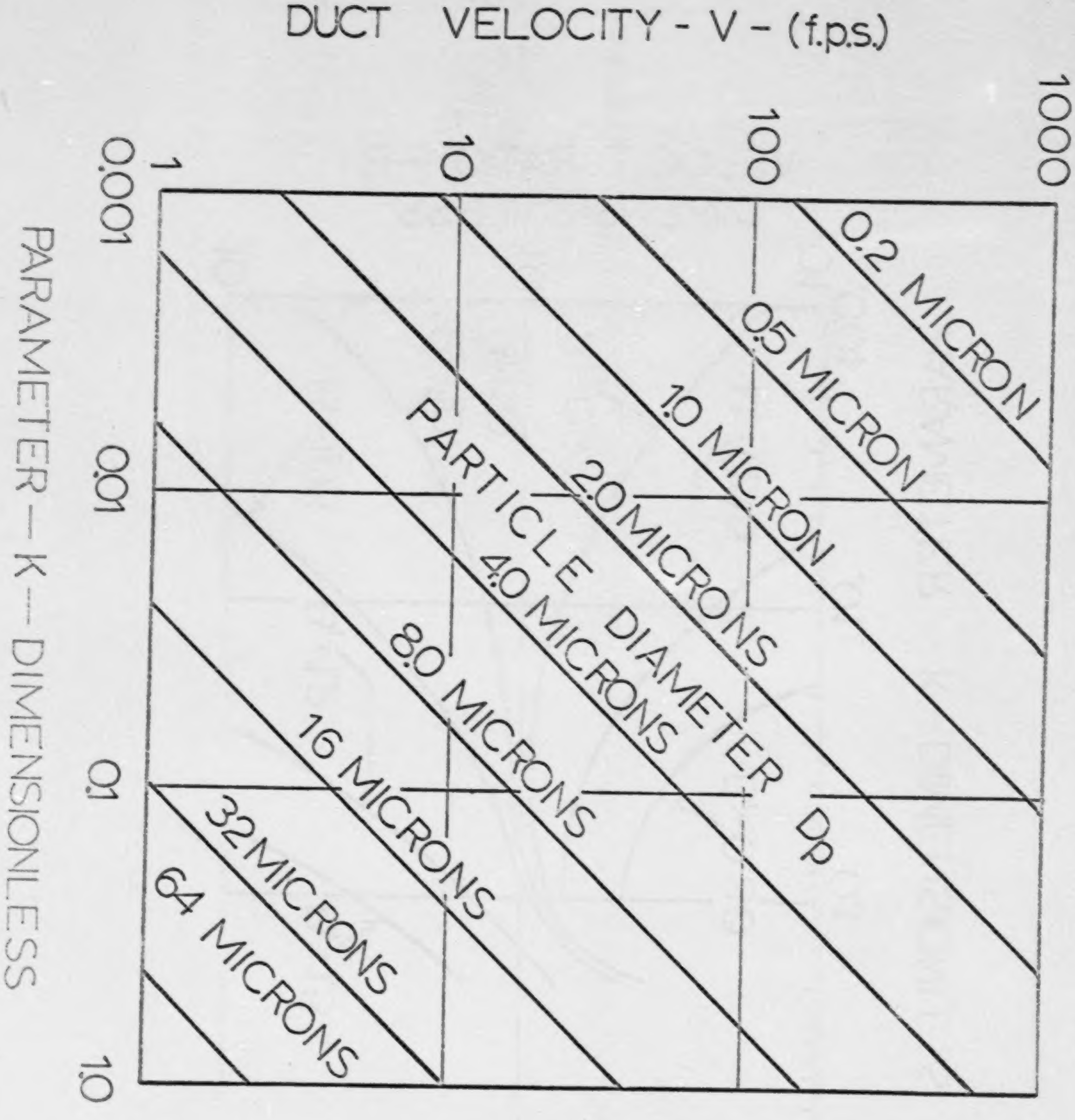

Figure 13 Relationship Between K, Dp & V

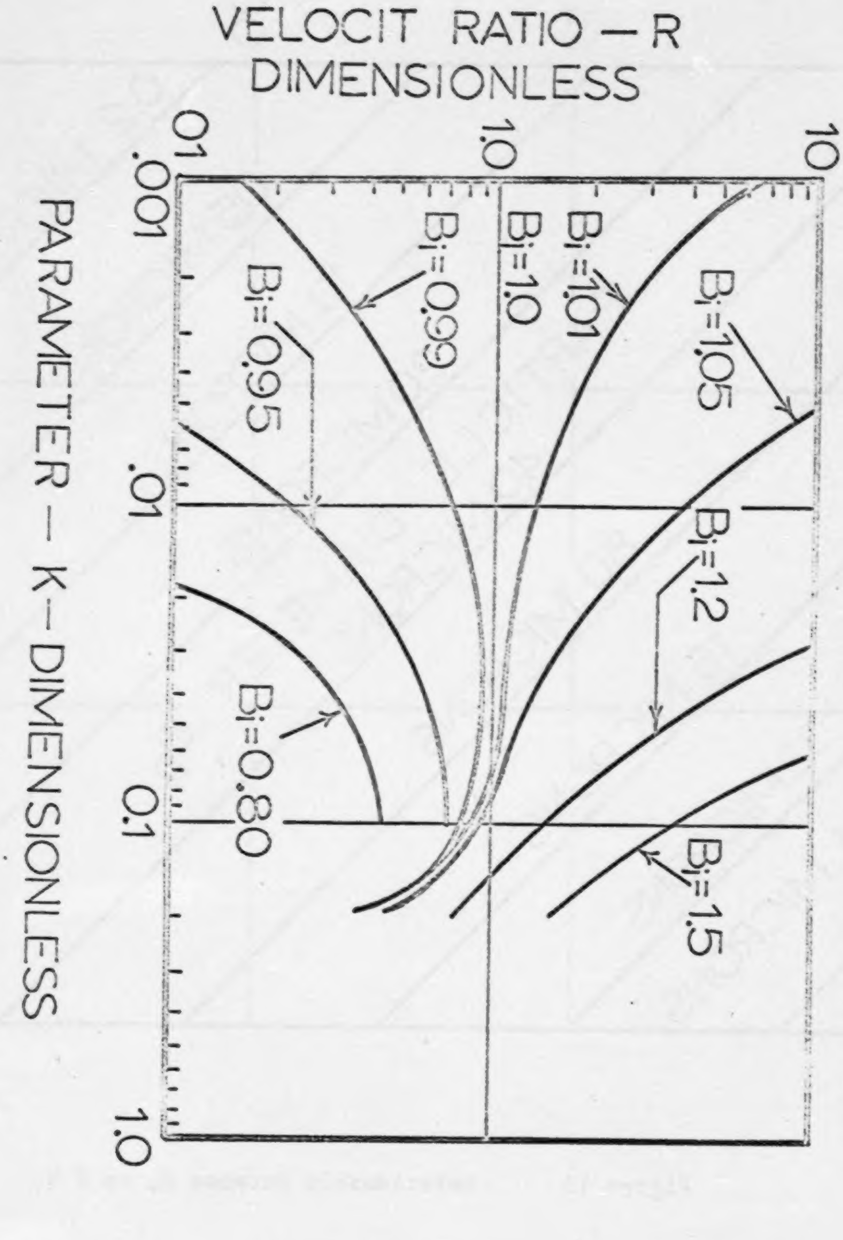

Figure 14 Side Port Probe - Velocity Ratio vs. K

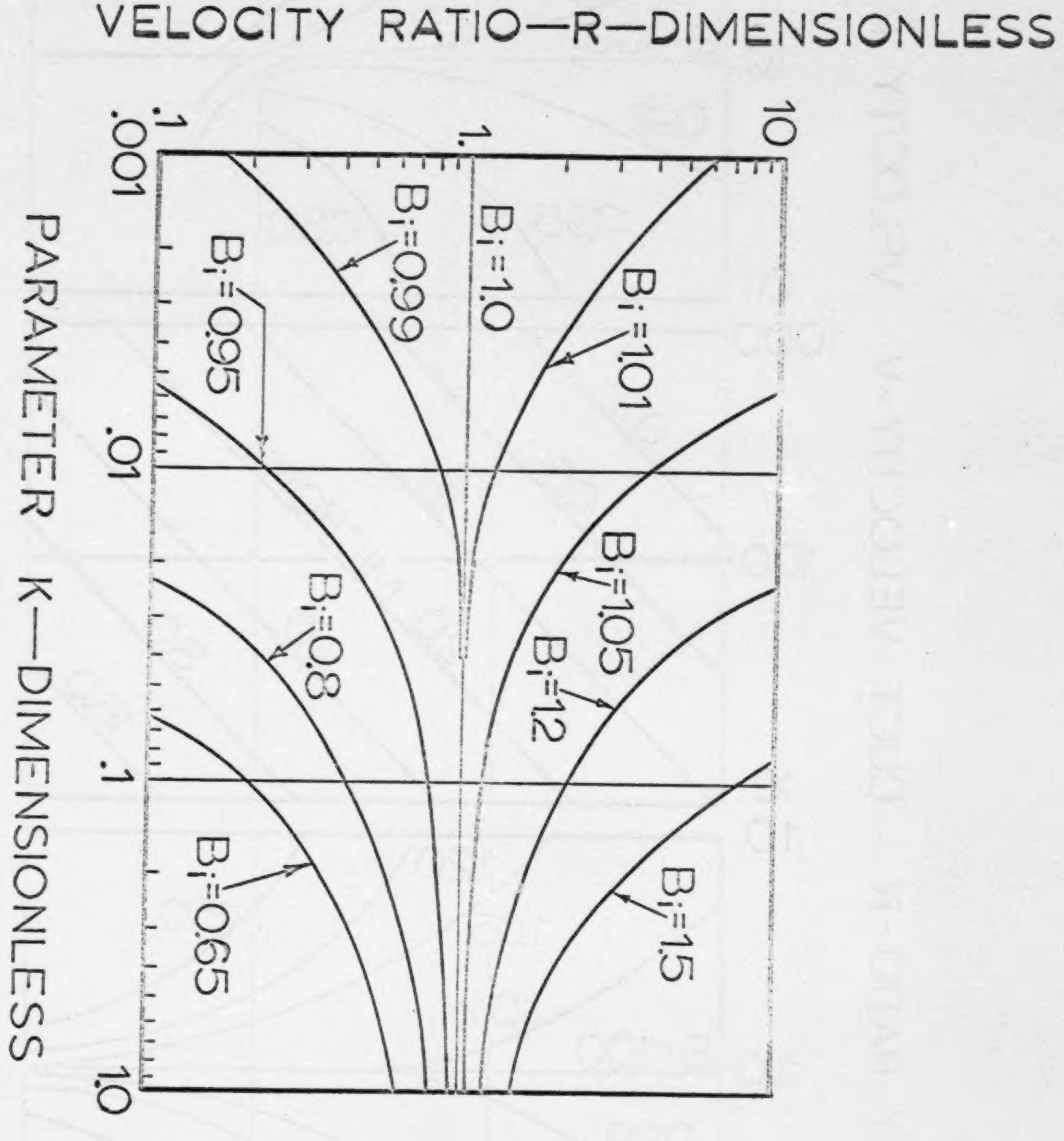

Figure 15 Straight Inlet Probe - Velocity Ratio vs. K

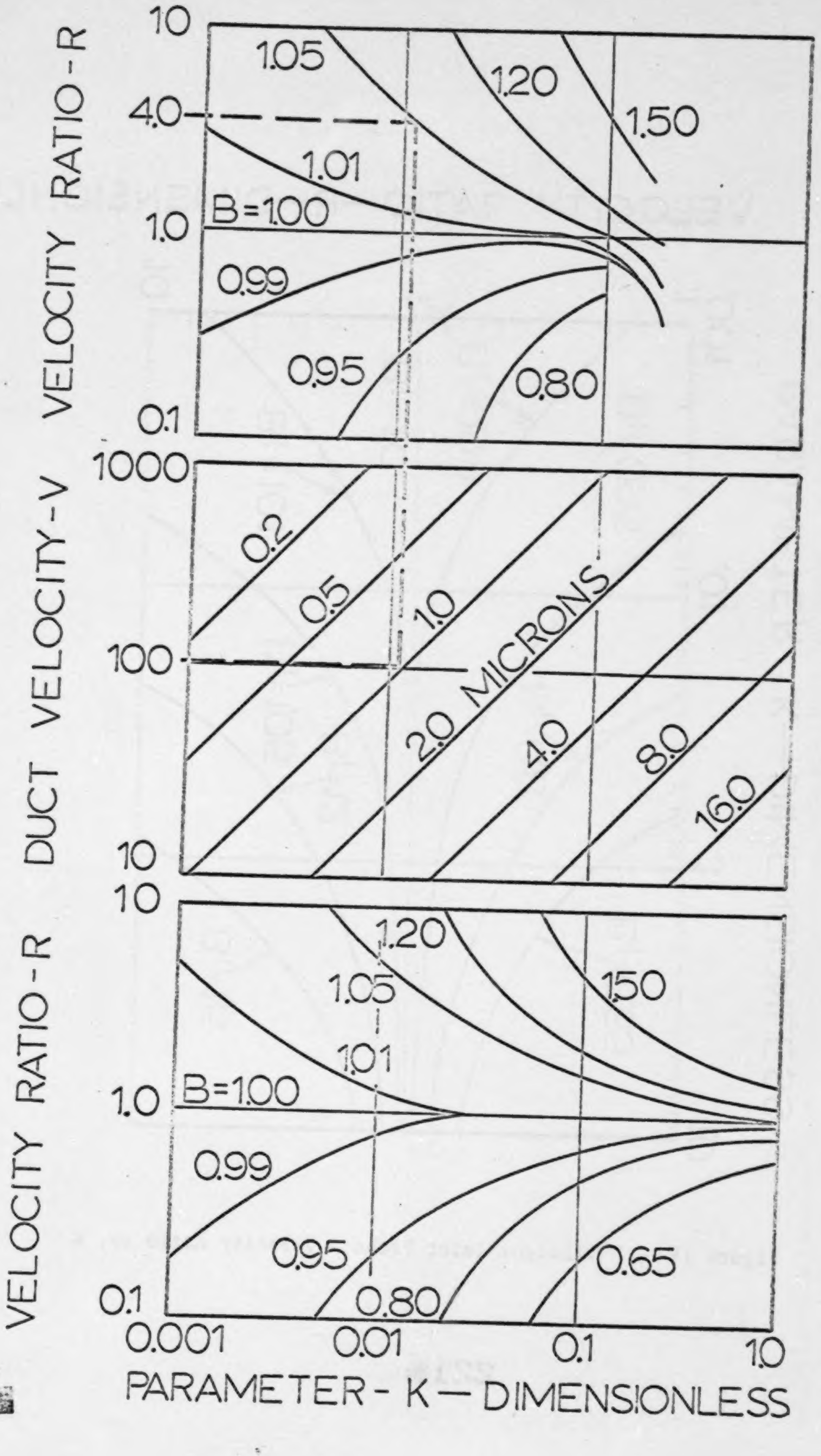

Figure 16 Composite Figure for Bias Determination

Figure 17 Wall Loss vs. K for Side Port Probe

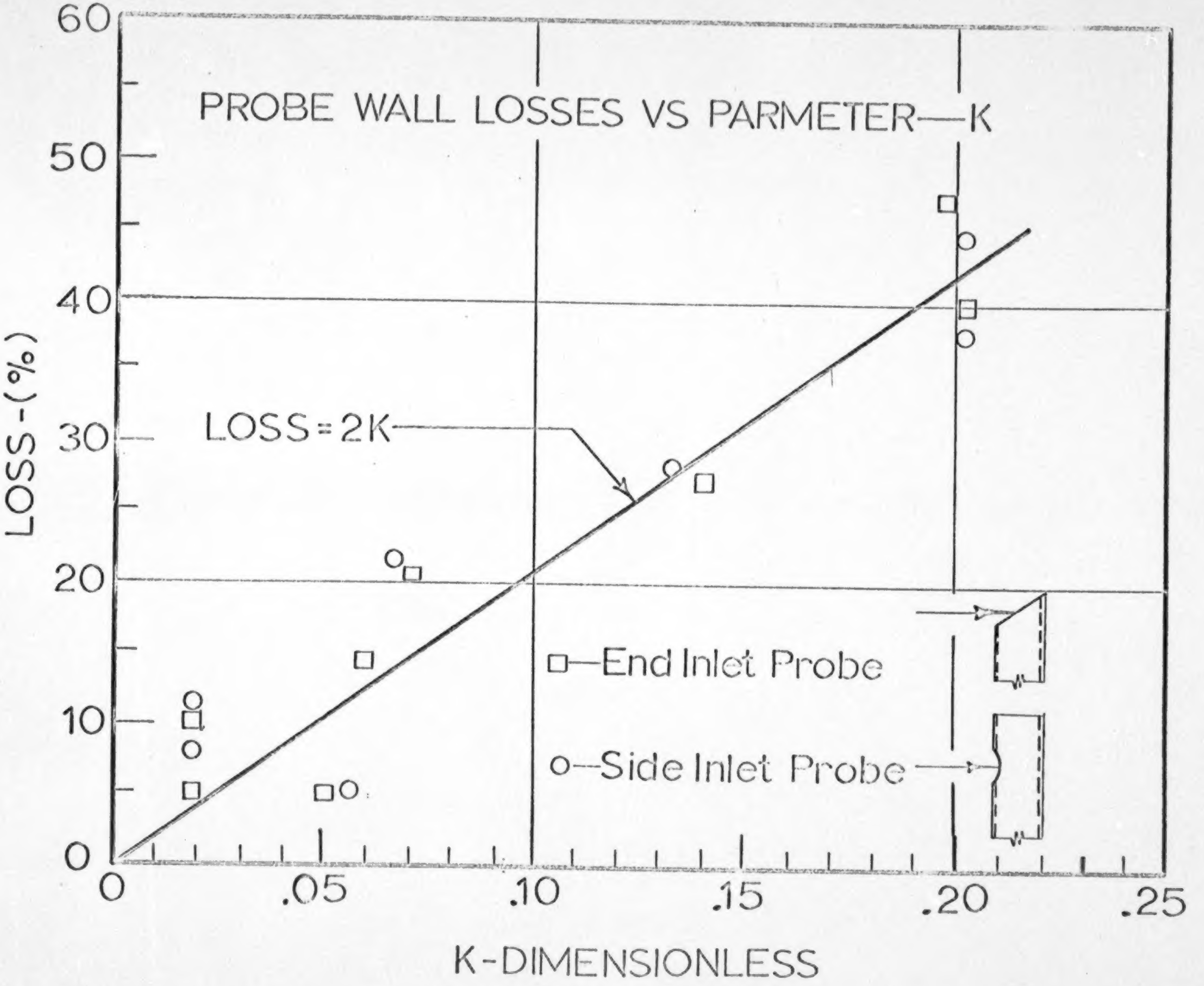

APPENDIX 12A

file

Seymour Calvert
Center for Air Environment Studies
University Park, Pennsylvania

GAS ABSORPTION IN A RIBBON-GRID COLUMN

Fay Fun
E. I. du Pont de Nemours & Company, Inc., Wilmington, Delaware, and
Seymour Calvert
Pennsylvania State University, University Park, Pennsylvania

Preprint 37e

Presented at the
Symposium on Selected Papers—Part III
FIFTY-SIXTH NATIONAL MEETING
San Francisco, California
May 16-19, 1965

AMERICAN INSTITUTE OF CHEMICAL ENGINEERS
345 East 47 Street, New York, New York 10017

50 cents

GAS ABSORPTION IN A RIBBON-GRID COLUMN

Fay Fun* and Seymour Calvert**
Case Institute of Technology

INTRODUCTION

Packed columns for gas liquid contacting has long been known of their lack of flexibility in operation. It is therefore that columns larger than ten inches in diameter were infrequent a decade ago. The design of packing materials has been concerned primarily with providing as much contacting area as possible. Such area is generally facilitated by spreading the streams over solid packing surfaces. Conventional columns are thus necessarily of high specific packing surface, low void space and small open cross-sectional area. The prices paid for substantial mass transfer are high pressure drops, and limited flow capabilities. In spite of this inherent disadvantage, packed columns are today reported to give good service in all sizes comparable with other types of contacting equipment. Although the majority of improvement has been made along the logic of conventional film contacting theory, a number of new packing designs have shed light on the application of different concept. Notably among the new packings are

---

* Present address: E.I. DuPont DeNemours & Co.,
Wilmington, Delaware

**Present address: Pennsylvania State University,
University Park, Pennsylvania

the PANAPAK(15,16) and SPRAYPAK(3,10,11). They were claimed to be of high efficiency and of large throughput capabilities and yet of small pressure drops. A major feature of these packings is their dependence upon free surfaces. The contact between gas and liquid is achieved across skins of dispersed liquid bodies which are either only supported on the periphery by the packing elements or completely free from contact with any solid surface. Relieving the packing element from providing the basic contact area, a spraying mechanism makes possible the use of minimum amount of packing material and a loose and hollow structure to reduce pressure drop, increase flow capacity and maintain the absorption efficiency. The efficiency reported for the Panapak and Spraypak shows that the free surfaces created in a loosely packed column is as good as the solid-adhering surface in a conventional dense structure.

An aged freely falling drop, under normal conditions such as in a conventional spray tower, is relatively inefficient for mass transfer. However, vigorous motions and turbulence can promote the drop to many times higher efficiency. The recognized desirable conditions are various modes of oscillatory movement and internal circulatory currents(1,4,5,6,8,12,21). In the case of drop oscillation, notable increase in efficiency was observed when the vibratory velocity of a drop exceeded the displacement velocity(1,4,8,21).

In the case of internal circulation, a sharp rise of absorption rate was reported when the circulation Reynold's number was greater than 50(6). The onset of oscillation and above critical internal circulation is followed immediately after a drop disengaging a solid substrate. Garner and Lane(5) have obtained ratio as high as 80 of the effective diffusivities in a drop disengaging from a forming nozzle to that of a similar stagnant drop. In the same experiment, the unusually high ratio decayed rapidly to a value of 2.2 and remained thereafter during the drop's lifetime.

For supported drops, the onset and sustaining of these motions can best be assisted by means of external disturbances in the form of mechanical vibration, collision with other drop or abrupt burst of the surrounding medium. A supported drop in a steadily flowing medium of moderate speed generally does not manifest significant oscillation or circulation(1). The energy required to generate and sustain such modes is so small that they become very attractive means to activate the otherwise less efficient fragment of liquid. For a population of liquid fragments, a grid of thin solid elements can serve to achieve this purpose.

DESCRIPTIONS OF THE RIBBON-GRID COLUMNS

The ribbon-grid packings are composed of individual trays of parallel straight ribbons laid on a supporting ring. A packed section is a number of such rings stacked together with the ribbon elements of one tray being perpendicular to that of the adjacent rings. The rings are separated with spacers from $\frac{1}{4}$ inch to 1 inch apart. The stacked unit fits tightly into a 4-inch section of glass pipe. The glass pipe is then used as the packed section of the absorption columns. Figures 1 and 2 are different views of a packed section. Six configurations of the tray design with the combination of nine columns were studied. The characteristic dimensions of these columns are shown in Table 1.

The experimental column consisted of a 1-ft length of 4-inch glass pipe as the packed section. A 6-inch length straight glass pipe was immediately above and below the packed section. Inlet and outlet of fluid streams were facilitated by a standard 4-inch tee at both end of the straight section. The liquid distributor consisted of six radially extended manifold each fitted with eight 18 gage hypodermic needles approximately 1/2-inch long. The needles produced droplets which fell a distance of eight inches before reaching the top layer of packing grid. Air and water were used for flow experiments. The air stream was contaminated with solute gas in the absorption experiments.

The ribbon-grid packing is noted for its low packed density. Over 98 per cent of the total column is occupied by free space as compared to 20 to 70 per cent in conventional type packed columns. The specific packing surface of a column is also very small. All six columns studied have specific packing surfaces only 20 per cent of a column packed with 3/8 inch stoneware Raschig rings.

FLOW PHENOMENA

In general, the liquid distributor feeds drops of liquid into the packed section. Such a population of drops comes into reaction with the ribbons of the first tray and emerges as another population of droplets. The new population is in several aspects distinctively different from the original population. A small fraction of the new population may consist of older aged drops that have escaped reaction with the ribbons. The majority of the droplets has now a different molecular content as a result of the mixing produced in ribbon-drop reaction. The drops are young and fresh. Theypossess some modes of motion that are seldom present in drops of older age. In the first few trays, the mean size of the new population is also smaller. Similar events take place in the trays following the first. The packed section is now filled with freshly generated droplets. The molecular content of the drops is mixed at the end of their short life between the trays. Each drop experiences an intensified activity of gross and molecular agitation. Such modes of motions as lateral oscillations, surface contraction and expansions, internal circulations and skin renewals are greatly promoted.

The above paragraph is only a general statement pertaining to the overall theme of events in the column. The actual drop to drop, drop to ribbon interactions are

TABLE I. COLUMN CHARACTERISTICS

Column Designation	No. of Trays T	Width of Ribbon W, In.	Thickness of Ribbon X, In.	Ribbon Spacing S, In.	Tray Spacing h, In.	a_v ft^2/ft^3	ϵ	α
A-20	20	1/16	0.032	1/4	1/2	9.928	0.991	0.8588
A-15	15	1/16	0.032	1/4	1/2	9.928	0.991	0.8588
A-10	10	1/16	0.032	1/4	1/2	9.928	0.991	0.8588
A-5	5	1/16	0.032	1/4	1/2	9.928	0.991	0.8588
B-31	31	1/16	0.032	1/4	1/4	19.259	0.983	0.8588
C-16	16	1/8	0.0089	1/4	1/2	13.381	0.995	0.7960
D-15	15	3/8	0.0089	3/8	1/2	10.160	0.996	0.7315
E-16	16	1/4	0.016	3/8	1/2	15.355	0.981	0.6892
F-9	9	1/4	0.016	3/8	1	8.029	0.990	0.6892

too complicated for a clear cut description. Again in rather general terms, a drop meeting a ribbon produces the following results. A large drop may disintegrate into smaller drops due to the impaction. A medium drop may spread and adhere to the surface of a ribbon. A small drop may sometimes be bounced off the ribbon. By way of high speed cinematography, taken with a 16-mm Fastax camera at up to 4,400 frames per second, it was ascertained that only the medium sized drops in the range of 3 to 8 mm diameter constituted the bulk of the droplet population. Such a drop will spread along the surface of a ribbon and will merge with the liquid already on the ribbon. Mixing of the molecular content of droplets is chiefly accomplished in this fashion. The pools of liquid bodies so formed on a ribbon element will grow or drip subject to dynamic equilibrium of forces. Drop to drop interactions are present mostly in the form of collision and coalescence followed by almost immediate disintegration. However, the frequency of drop to drop interaction is far less than the drop to ribbon interactions.

Since the bulk of the dispersed liquid exists in the ribbon column in the form of either a free drop floating in the open space or supported globules sitting on the ribbon surfaces, we shall concentrate onthe behavior of these two categories of liquid bodies. Several items are of interest in the discussion. 1, The ratio of free drops to supported globules. 2, The ratio of wetted versus unwetted ribbon surface. 3, The proportion of the fraction of a supported body on top the ribbon to that beneath the ribbon. 4, The size and shape of supported liquid bodies.

Gas and liquid rates have pronounced effects upon these items. At low liquid flow, distinctive drops were observed of spheroidal or ellipsoidal shapes. The ribbons were only partly wetted at different spots with such drops. Supported drops were slightly fewer than floating drops by number but were of larger size. The drip points and wetted points were identical along a ribbon and moved about at a slow pace. Increasing gas flow resulted in a decrease of pendant portions of the drop and pushed it more toward the top of a ribbon. Surface rippling and gross drop vibration became more prominent and the drip points moved about at an increased tempo. At even higher gas flow, supported drops grew larger in volume restricting more of the open cross-section for gas passage and resulted in numerous breaking-ups. Above the flooding velocity, such breaking-ups caused excessive entrainment in the effluent gas stream. Liquid could only find ways to channel down along the wall of the column. The shape of supported liquid was more spherical at low flow but became more and more irregular and elongated behind the ribbon with the increase of flow rate.

228

229

Liquid rate has more pronounced effect to the flow phenomena than gas rate. By increasing the liquid flow, the liquid bodies began to show more irregular shapes. The ratio of floating and supported drops diminished rapidly. At moderate liquid flows the supported liquid first became more elongated along the length of a ribbon with drip points oscillating between the extremes of the elongated body. The neck of the drip point also extended farther away from the supporting ribbon and eventually reached the next tray. A continuous dripping passage was so established sometimes bridging two to four trays. The ribbon surface was wetted more completely than before.

Looking at a single ribbon, one could see a very thin film of liquid covering the entire ribbon with frequent bumps or pools bulging out indicating the receiving or dripping locations. At even higher rate of liquid flow, one chunk of liquid on one ribbon would become so large as to touching another chunk on an adjacent ribbon. Such horizontal bridges increased in number as the liquid flow. Further increase of liquid flow brought about a flooded column even at relatively low gas flow. At high liquid rate, flooding took place in the form of a liquid filled column bubbling vigorously by the gas forcing its way up. The aerated liquid height increased sharply until the column was completely flooded and unoperable.

Gas flow had same effect at higher liquid flow as at lower flow, except the result was magnified greatly by the high liquid flow. The most prominent effect was the decrease in the volume of the floating drops with corresponding increase of liquid volume as continuous bridges between trays as well as between ribbons.

PRESSURE DROPS AND FLOODING VELOCITIES

The pressure drops of the columns investigated can be represented by the data contained in Fig. 3. The effect of gas rate shows a general pattern similar to conventional packings such as rings and saddles. Loading and flooding are prominently demonstrated at high liquid flow by the breaking points of the pressure curves. At low liquid rate, however, the onset of these phenomena is rather obscure, the determination of which has required visual observation. Dry pressure drops of the columns can be represented by straight lines on logarithmic coordinates. When compared to conventional packings, the ribbon columns show considerably lower pressure drops. Figure 4 is such a comparison.

The dry pressure drop of the ribbon column can be considered to consist of losses due to sudden contraction, enlargement and friction in the packed section.

$$\Delta P' = \Delta P_c + \Delta P_e + \Delta P_f \qquad (1)$$

The contraction and expansion losses can be estimated by the method of Perry(13). A drag coefficient of 2.2 can be used to predict the frictional pressure drops. This coefficient was reported by Delany et. al.(2) for flow past single, thin rectangular cylinders. Thus the predicted pressure drops is given by

$$\Delta P' = \left[(ab+1) - (a+2)\alpha + 3.2\alpha^2 - 2.2\alpha^3\right] \cdot \frac{G^2}{2g_c\alpha^2\rho_G} \qquad (2)$$

230

where $a = 0.40$, $b = 1.25$, for $\alpha < 0.175$;

and $a = 0.75$, $b = 1.00$, for $\alpha > 0.175$.

This type of estimation, although crude, has been used by several authors(9). The ratio of observed to estimated pressure drops, was found to bear a certain relationship with the column dimensions. By means of stepwise regression, an equation is arrived at which the ratio can be correlated within ±20 per cent in the range of gas rates from 500 to 7,000 lb./ft.²hr.

$$\psi = 0.745\left(\frac{W}{S}\right)^{0.9} G^{1.17} \alpha^{0.17} \qquad (3)$$

Thus, it is possible to estimate the actual pressure drops by the use of the following relation.

$$\Delta P = \psi \Delta P' \qquad (4)$$

The origin of discrepancies in the estimated pressure drop to the actual value is inherent in the assumptions involved in arriving at a prediction. For example, the ribbon-grid is a structure of many ribbons rather closely spaced. The interference among these ribbons will contribute to a major deviation to the drag coefficient used in Eq. (2). The ratio, ψ, is a necessary factor to account for nonidealities as this. The use of a constant as the drag coefficient in Eq. (2) is not entirely justified. Probably this is the reason that gas rate, G, should enter into the expression of Eq. (3). McAllister(9) has used a similar empirical factor for perforated columns.

Liquid flow contributes to more pressure drops by way of two mechanisms. The presence of liquid in a column necessarily reduces the cross-sectional area available for gas passage. The restrictions bring about intensified turbulence in the gas stream. The liquid bodies also cause more frictional losses. Judging from the mass transfer results, the frictional loss is controlling below the loading point. Near and above the loading point, liquid holdup in the grids causes rapidly increasing losses due to turbulence and restrictions. A plot of the ratio, A_L, of wet to dry pressure drops is presented in Figure 5 for the six columns investigated.

Flooding velocities in the ribbon columns can be correlated by Lobo's method(7). Provided a modified porosity factor is used, the data points fall nicely on the curve reported by Sherwood et. al. for small diameter packed columns(19). Figure 6 shows the correlation. The modified porosity factor, $\mathcal{E}$, is necessary because the usual factor, a_v/ϵ^3, is no longer adequate an expression for geometrical similarity among the ribbon columns. It is a product of the conventional factor multiplied by a factor governed by the packing dimensions. The modified porosity factor is defined in Equation (5) and is given in Figure 7 as a function of column characteristics.

$$\mathcal{E} = \phi(a_v/\epsilon^3) \qquad (5)$$

The ribbon grid column has larger throughput capabilities than other packings. This is particularly so for gas flow. A comparison of the gas rates at flooding points is shown in Table II. The ribbon-grid columns of this study are capable of handling two to four times higher gas flows than conventional 1 inch Raschig rings.

TABLE II. GAS HANDLING CAPACITY AT FLOODING POINT
(Liquid Rate = 10,000 lb./hr.ft^2.)

Columns	Flooding Gas Rate lb./hr.ft^2.	Per cent Handling Capacity**
1 in. Raschig Rings*	680	100
A	2,500	368
B	2,700	382
C	1,900	279
D	3,000	441
E	1,850	272
F	2,200	308

*Data of Ref. 18.

**Based on 1 in. Raschig as 100 per cent.

231

ABSORPTION RESULTS

Absorption of carbon dioxide by water is generally considered as a purely liquid phase controlled system.(18) This system was used for determining the liquid phase resistance in the ribbon columns. Samples of the inlet gas carrying air stream and both liquid streams were taken and analyzed by means of volumetric titrations. The sample was neutralized in excess barium hydroxide. The excess was back titrated to an end point with dilute hydrochloric acid. The outlet gas composition was obtained by a material balance. The overall number of transfer units, N_L', were calculated and corrected to 25°C with a correction factor:

$$\exp\left[0.0203\left(25^\circ C - \frac{t_{L,1} + t_{L,2}}{2}\right)\right]$$

in which the constant 0.0203 is the average of three reported values(14,17,20).

Figure 8 is a representation of a typical absorption result. Liquid rate seems to have little effect on the rate of absorption. The combination of very low gas flow and high liquid rate shows a trend of decreasing the amount of absorption. The gas stream under this condition does not possess the necessary kinetic energy to uniformly distribute itself through the liquid. The unstable condition results in excessive liquid and gas channeling which in trun lowers the contact efficiency.

232

Gas rate alone always produces better efficiency by promoting droplet motions and turbulence.

The absorption of ammonia gas by water was used for the gas phase resistance controlling experiments. The overall number of transfer units, N'_{OG}, was calculated based on analysis of all four inlet and outlet streams of air and water. The compositions were analysed by titrating with hydrochloric acid and sodium hydroxide . The number of transfer units so obtained was not corrected for temperature since it is little affected by small changes of temperature (18). Although the ammonia system is not purely gas phase resistance controlled, its finite liquid phase resistance can be estimated from the carbon dioxide results. The data reported in this paper are overall number of transfer units.

The effects of gas and liquid rates are depicted in Figure 9. For a typical column, such as in Fig. 9, the absorption is almost directly proportional to liquid rate and inversely proportional to gas rate in the normal operating range below the loading point. Above the loading point, higher liquid flow induces sever channeling in the column resulting in a decrease of efficiency. The gas and liquid flows exert generally similar effect in the ribbon columns to columns packed with conventional rings or saddles, although there are discrepancies at the extreme end of the

operable range.

All absorption data can be correlated by the familiar expressions:

$$N'_L = a\,G^b/L^c \qquad (6)$$

and

$$N'_{OG} = d\,L^e/G^f \qquad (7)$$

The constants and exponents in these formulas are shown in Tables III and IV. Most data fall within ±10% of the prediction of the equations. The few that show a maximum spread beyond this range are believed to have been caused by faulty conditions existed in the column when the runs were made.

TABLE III CONSTANTS IN EQUATION (6)

$$N'_L = a\,\frac{G^b}{L^c}$$

L=500-7000 lb./hr.ft.^{2} G=500-2000 lb./hr.ft.^{2}

COLUMN	a	b	c	Maximum % Deviation
A-20	0.7073	0.0	0.190	7.39
A-10	0.8656	0.136	0.090	-4.99
A-5	0.0901	0.203	0.066	-6.08
B-31	0.6029	0.0	0.194	7.48
C-16	0.0225	0.514	0.204	-26.96
D-15	0.4697	0.0	0.163	15.94
E-16	0.7090	0.147	0.105	-5.13
F-9	0.6820	0.110	0.107	-6.48

TABLE IV CONSTANTS IN EQUATION (7)

$$N'_{OG} = d\,\frac{L^{e}}{G^{f}}$$

L=500-7000 lb./hr.ft.^{2} G=500-2000 lb./hr.ft.^{2}

COLUMN	d	e	f	Maximum % Deviation
A-15	23.438	0.232	0.466	6.88
A-10	0.0781	0.293	0.430	10.34
A-5	0.0585	0.301	0.417	-5.55
B-31	0.0265	0.488	0.718	-20.62
C-16	0.0441	0.377	0.541	6.45
D-15	0.0716	0.300	0.529	-18.20
E-16	0.0732	0.301	0.511	8.67
F-9	0.0428	0.383	0.696	-10.32

DISCUSSION AND CONCLUSION

The amount of mass transfer in a packed column is a function of the packed height.

$$N'_{OG} = \int_0^Z \left[K_y a(1 - y)_m / G\right] dZ \qquad (8)$$

Under conditions that all the quantities within the bracket are independent to the height, Z, a linear relationship exists between the number of transfer unit and the height.

$$N'_{OG} = \left[K_y a(1 - y)_m / G\right] Z \qquad (9)$$

However, actual conditions in a column do not always warrant the validity of this linearity. Especially in the initial length of a packed section, where the flow pattern has not been fully developed, both the transfer coefficient and the contact area vary with the height. Such deviation is negligible for a relatively long or tall column. For short columns, it will show up more prominently. In this study, a noticeable effect was observed. The curves shown in Figures 10 and 11 indicate that the rate of increase in absorption is relatively slow in the first few trays. When more trays are added to the column, the rate of increase becomes faster and finally resides at a constant value.

One may visualize the population of drops coming to the first tray to be different from the population of drops coming to the 20th tray, for instance, because they are

233

from different origins; one from the distributor and the other from the 19th tray. Interactions between the drops and the ribbons at the first tray produce a new population of drops which begin to show some similarity to the population from the 19th tray. They are still not quite identical because part of the original population has failed to interact with the ribbons. After several trays, probably between the fifth and the tenth tray, the population has undergone so many changes and has been in the grid for so long that it has reached an equilibrium with the environment in the ribbon structure.

From there on, the population of drops will experience the same changes passing every tray that it does not make any difference whether it now comes from the 11th or the 19th tray. The variations in absorption rate in the initial trays arise undoubtedly from this type of changes. It is to be noted that such changes principaly changes the mixing and turbulence inside the liquid phase. Less an effect is expected on the gas phase. That, the ammonia absorption curves in Figure 11 show more of a linearity than the curves in Figure 10 for carbon dioxide , verifies this expectation.

To compare the absorption efficiency of a ribbon

column, the equilibrium efficiency of a tall column must be used. The equilbrium efficiency is estimated by the slope of a curve in Figure 10 or 11 at the data point corresponding to the largest number of trays. A comparison is made to evaluate the relative effectiveness of the ribbon column to conventional columns. Figures 12 and 13 present the results. The liquid phase efficiency of the ribbon column is slightly lower than rings and saddles but competible with drip tiles and wood grids. The gas phase efficiency of the ribbon column is greater than all types of conventional packings presented.

The size and spacings of the ribbons are important dimensions of the ribbon grid and is expected to show profound influences to the contacting efficiency. This investigation has not found any correlatable patterns. From a factorial analysis of the variances, the most influential factor seemed to be the fractional free cross section, α . The gas phase was again less affected than the liquid phase. Regressional analysis showed that the overall gas phase transfer unit , N'_{OG}, was proportional to the 0.62th power of α , while the liquid phase transfer unit, N'_{L}, was proportional to the 5.13th power. The thickness of the ribbons studied showed little if any effect. Increasing the tray spacing generally decreased the absorption.

The study of the ribbon-grid column was carried out to show that a packing element does not require large specific surface nor is it preferred to orient the surface in any particular manner, i.e., parallel to the streams; and that a loosely packed column of simple structure is to be preferred to a densely packed column. A primary objective of packing design is to activate the fluid element for all its mass transfer potential.

Many gas cleaning operations in the industry demand low pressure drops, large volume of flow and high efficiency. The ribbon column should find its way for applications easily by way of its commentable performances. The simplicity of its structure should lend itself particularly suitable for system that fouls or contains solids.

ACKNOWLEDGEMENT

This work was financed by the United States Public Health Service, Research Grant S-84. Mr. Edward Emmer helped in the computer program for regressional analysis.

NOMENCLATURE

a_v - Specific packing surface, ft^2/ft^3 .
A_L - Ratio of wet to dry pressure drops.
g_c - Gravitational constant, $lb_m/lb_f/ft/sec^2$.
G - Mass flow rate of gas, $lb_m/hr.ft^2$.
h - Tray spacing, in.
H - Height of a transfer unit(end effect excluded), ft.
K_y - Gas phase mass transfer coefficient,
L - Mass flow rate of liquid, $lb_m/hr.ft^2$.
N' - Number of transfer units(end effect included).
ΔP - Observed pressure drop, in. H_2O.
$\Delta P'$ - Pressure drop predicted by Equation(1).
S - Edge to edge spacing between ribbons, in.
t - Temperature, °C.
T - Number of trays.
W - Width of ribbon, in.
X - Thickness of ribbon, in.
Z - Height of a packed section, ft.

GREEK LETTERS

α - Free cross section / total cross section.
$\mathcal{E}$ - Modified porosity factor, Eq. (5).
ϵ - Fractional void space.
ψ - Pressure drop correlation factor, Eq. (4).
ϕ - Flooding rate correlation factor, Eq. (5).
ρ - Density, lb_m/ft^3.
μ - Viscosity, centpoise.

BIBLIOGRAPHY

1. Constan, G. L., Ph.D. Thesis, Case Inst. Tech., (1961).
2. Delany, K., and Sorenson, N. E., NACA TN3038, (1953).
3. Ellis, S.R.M., Barker, P.E., and Hodgson, W.S., Trans. Inst. Chem. Engrs. (London), 38, 267 (1960).
4. Finlay, B. A., Ph.D. Thesis, Univ. of Birmingham, Edgbaston, Birmingham, England, (1957).
5. Garner, F. H., and Lane, J. J., Trans. Inst. Chem. Engrs., 37, 162 (1959).
6. Groothius, H., and Kramer, H., Chem. Eng. Sci., 4, 17, (1955).
7. Lobo, W. E., Friend, L., Hashamall, F., and Zeuz, F., Trans. Am. Inst. Chem. Engrs., 41, 693 (1945).
8. Martinelli, R. C., and Boelter, L. K. M., Proc. of the 5th Inter-national Congress of Applied Mechanics, 578 (1958).
9. McAllister, R. P., McGinnis, P. H., Jr., and Plank, C. A., Chem. Eng. Sci., 9, 25 (1958).
10. McWilliams, J. A., Pratt, H. R. C., Dell, F. R., and Jones, D. A., Trans. Inst. Chem. Engrs., (London), 34, 17 (1956).
11. McWilliams, J. A., and U. K. Atomic Energy Authority, Brit. Patent 729587 (1953).
12. Pano, A., M.S. Thesis, Case Inst. Tech., (1962).
13. Perry, J. H., "Chemical Engineers' Handbook", 3rd ed., McGraw-Hill Book Co., New York, (1950).
14. Pigford, R. L., and Pyle, C., Ind. Eng. Chem., 43, 1649 (1951).
15. Scofield, R. C., Chem. Eng. Prog., 40, 405 (1950).
16. Scofield, R. C., US Pat., 2470652, (1949).
17. Sherwood, T. K., and Holloway, F. A. L., Trans. Am. Inst. Chem. Engrs., 36, 39 (1940).
18. Sherwood, T. K., and Pigford, R. L., "Absorption and Extraction", McGraw-Hill Book Co., New York, (1952).
19. Sherwood, T. K., Shipley, G. H., and Holloway, F. A. L., Ind. Eng. Chem., 30, 765 (1936).
20. Sweeney, T. L., Ph.D. Thesis, Case Inst. Tech., (1962).
21. Tessin, W., and Jacob, M., Trans. A.S.M.E., 75, 473(1953).

FIGURE 1

Looking Down a Ribbon-grid Column

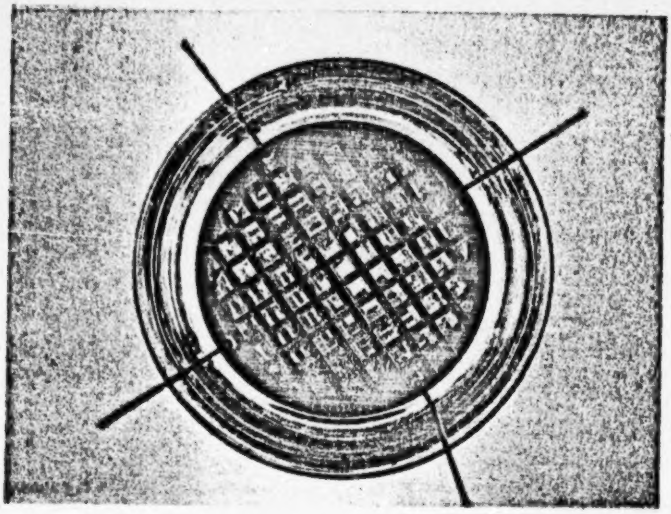

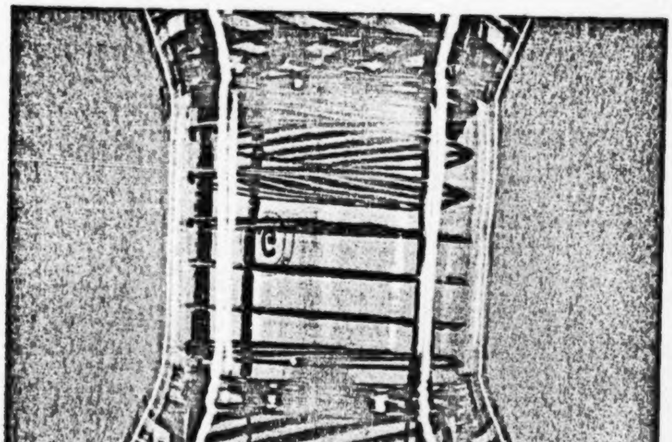

Side-view of a Packed Section

FIGURE 2

FIGURE 3

Pressure Drops of Column B-31

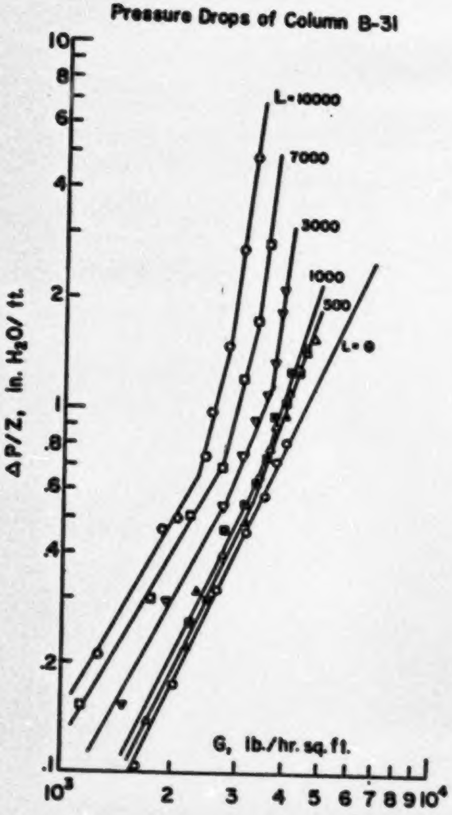

FIGURE 4

Comparison of Dry Pressure Drops

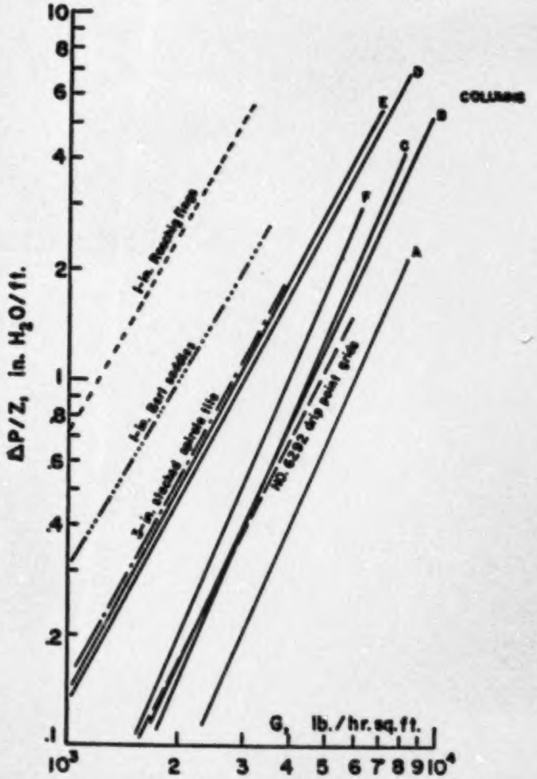

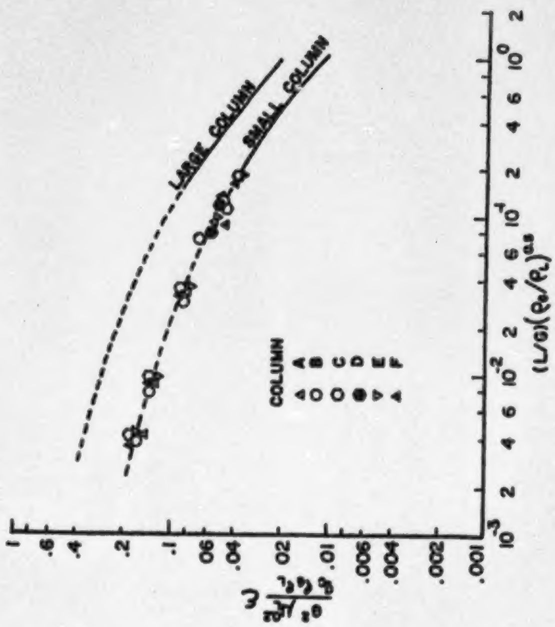

FIGURE 6

FLOODING VELOCITY CORRELATION

FIGURE 5

EFFECT OF LIQUID RATE ON PRESSURE DROPS

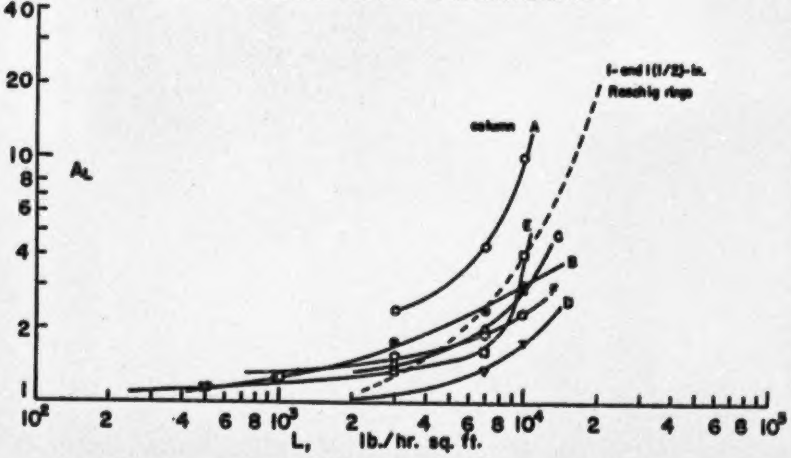

FIGURE 8

Effect of Gas Rate on CO_2 Absorption
Column E-16

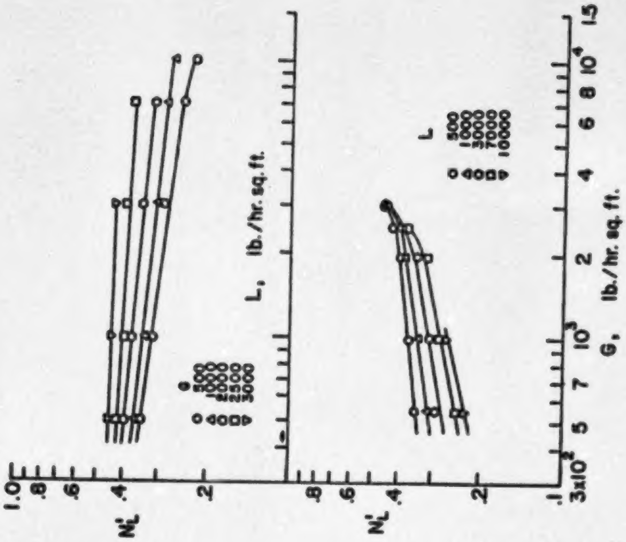

FIGURE 7

Flooding Velocity Correlation Factor

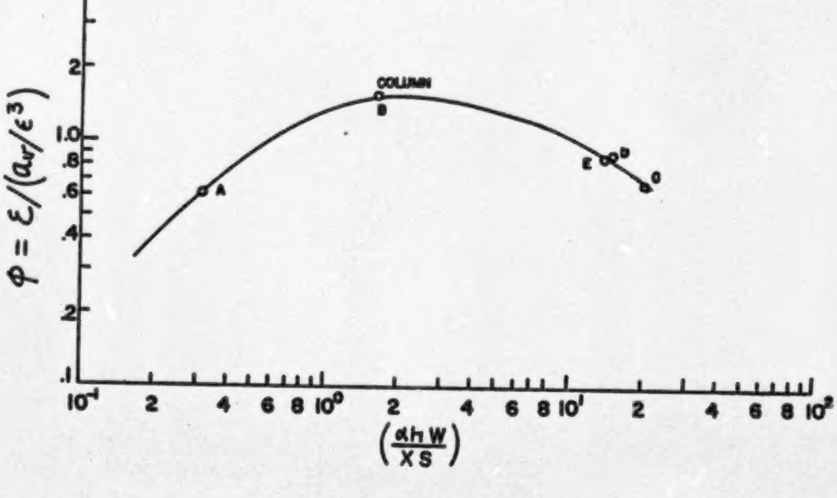

FIGURE 10

EFFECT OF PACKED HEIGHT

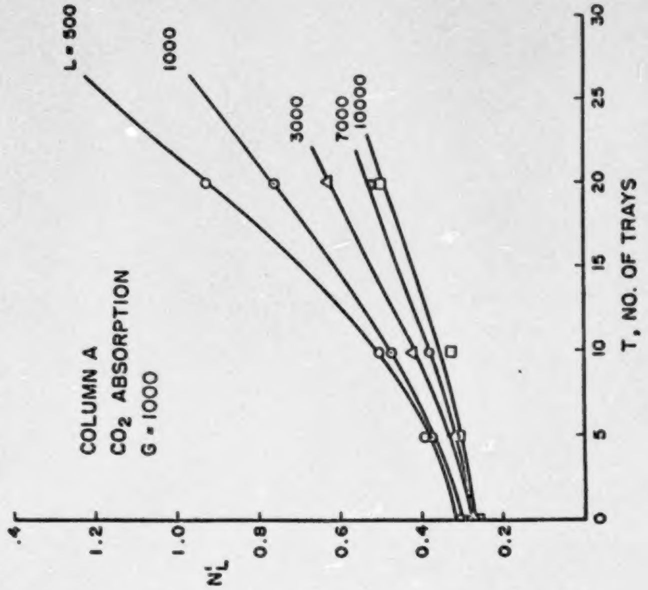

FIGURE 9

Effect of Flow Rate on NH_3 Absorption

Column E-16

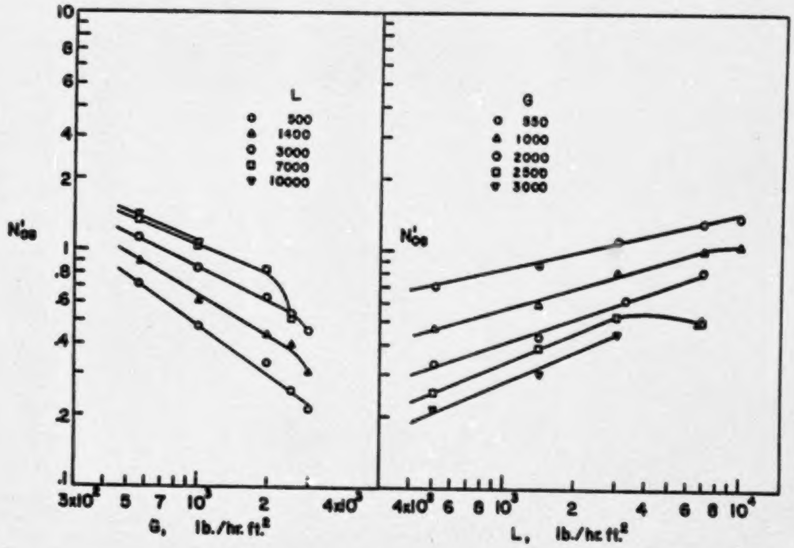

FIGURE 11

EFFECT OF PACKED HEIGHT

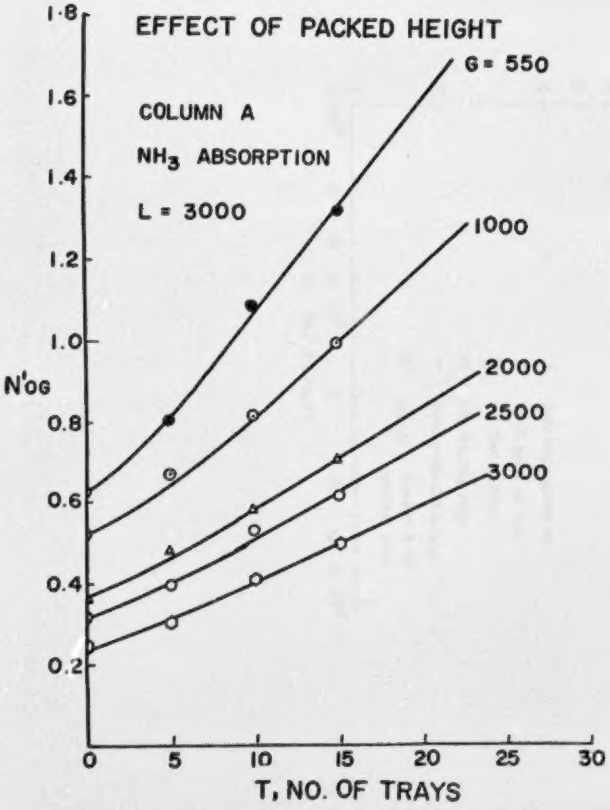

FIGURE 12

Comparison of Liquid-phase Controlled Absorption

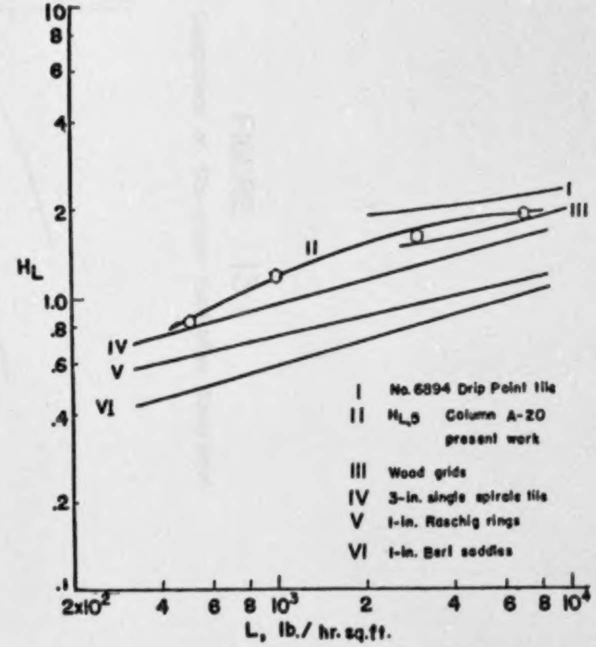

FIGURE 13

Comparison of Gas-phase Controlled Absorption

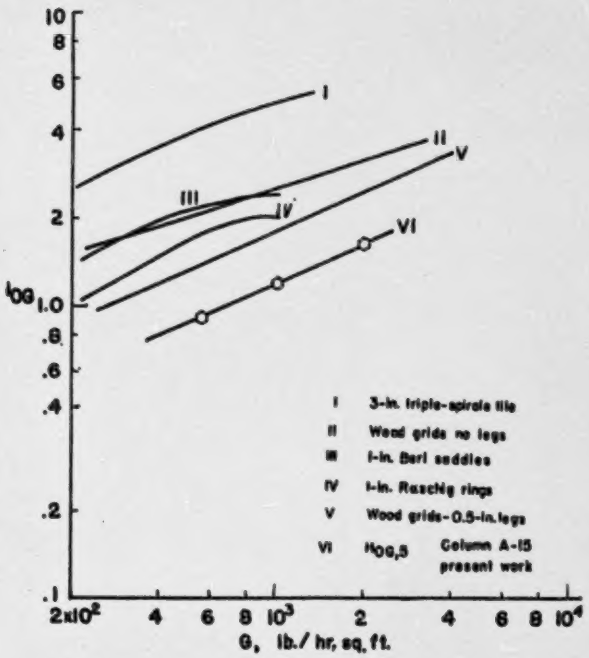

APPENDIX 12B

Mass Transfer in Horizontally Moving Stable Aqueous Foams

EUGENE Y. WEISSMAN and SEYMOUR CALVERT
Case Institute of Technology, Cleveland, Ohio

An efficient gas absorption device has been developed based on a stable aqueous foam moving in a horizontal duct, with a gas-liquid interaction that causes only negligible pressure drops.

The study of a liquid-phase and a mostly gas-phase-controlled system has indicated that their mass transfer performance can be predicted. This is based on hydrodynamic data for flowing foams, obtained in a preliminary study published elsewhere.

The influence of geometry, foaming solution properties, and surfactant-caused interfacial resistance are included in the analysis.

Foaming systems have lately been receiving increased attention for heat and mass transfer applications owing to the large interfacial areas they offer from relatively low amounts of liquid.

Work on gas-bubble columns was reported as early as 1950 by Shulman and Molstad (*40*). Additional work of both practical and theoretical interest has since been published (*11, 15, 16, 39*).

The use of foam rather than bubble assemblies is apparently reported only since 1955, when Helsby and Birt (*13*) found greater efficiencies of absorption of carbon dioxide in foam columns than in packed columns. Metzner and Brown (*21*) published their findings in the area of mass transfer in foam columns in 1956, stressing the disadvantage of high pressure drops and applicability limited to unconventional situations. Since then, the field has become more and more active (*5, 8, 10, 17* to *20, 22* to *28, 31* to *36, 41* to *43, 45*) but the investigations were limited to the technique of countercurrent contacting on sieve plates with correspondingly large operating pressure drops. This is particularly the case for highly intensified gas-liquid contacting, that is high flow rates and pure liquids (no surfactants added). Such dynamically stable foams collapse below a critical gas flow rate.

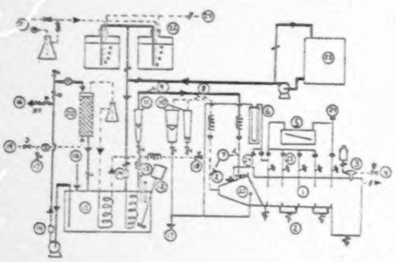

Fig. 1. Diagram of the experimental installation. (1) The foam-apparatus; (2) drain and liquid sampling points; (3) antifoam spray assembly; (4) 100 lb. per sq. in. g. air source; (5) inclined-tube manometer filled with specific gravity 0.827 red oil; (6) U-tube manometer (two of them; one filled with water, the other one with mercury); (7) thermometer with 0.2°C. subdivisions; (8) Wet- and dry-bulb thermometer; (9) dial thermometer; (10) gas rotameter; (11) liquid rotameter; (12) stirrer assembly; (13) Fenwal thermo-switch and thermometer with 0.1°C. subdivisions; (14) strainer; (15) constant-temperature bath; (16) from or to jacket of Ross-Miles apparatus; (17) line drain; (18) regulating vent; (19) blower air supply; (20) air humidifier; (21) atmospheric air and carbon-dioxide supply; (2) feed bottles; (23) solution preparation tank; (24) vent; (25) connections for pressure measurement and gas sampling.

Symbols: globe valve; gate valve; needle valve; ⊗ check valve; ⊗ toggle valve; screw clamp or quick-acting pinch-cock; solenoid valve; heating tape; centrifugal pump; —— liquid line; - - - - gas line, ——— pressure measurement line.

Some different approaches have also been published. Workman (*48*) reported on sieve plate arrangements with and without egg crate supports for the froths that were formed. Ungemach (*43*) published a brief note on an inclined baffled tube arrangement, and an application to heat exchange (*29*) is under study.

This paper treats the gas desorption from a moving aqueous foam. In the present case, however, the foam has been generated by pretreatment of the liquid phase (water) with a small amount of a surface-active agent (saponin)* prior to contacting with a gas phase. Thus, a suitable surface activity has been induced in the liquid, and high rates of momentum transfer are no longer necessary for the obtention of a stable foam.

APPARATUS AND PROCEDURE

The desorption of carbon dioxide from water (liquid-phase controlled system) and of ammonia from water (almost gas-phase controlled) were studied under identical sets of operating conditions and geometries. The stripping gas was air [containing 350 p.p.m. carbon dioxide (*46*)]. It also made the solution foam and was presaturated with water at the run temperature (30°C.).

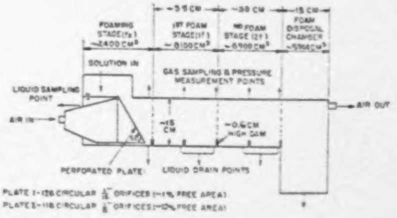

Fig. 2. Schematic representation of foam apparatus showing the division by stages.

Eugene Y. Weissman is with the General Electric Company, Lynn River Works, Lynn, Massachusetts. Seymour Calvert is at The Pennsylvania State University, University Park, Pennsylvania.

* Saponin is an extract of naturally occurring glucosides, nonionic in character, and known to produce very stable slow-draining foams. An 0.2% concentration by weight was found to be the minimum amount permitting good operation of the foam apparatus over a wide range of gas and liquid flow rates while not affecting the equilibrium relationships carbon dioxide-water and ammonia-water (*46*).

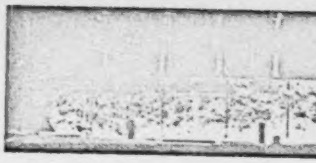

Fig. 3. Apparatus in operation (⅛-in. plate holes, 5 std. cu. ft./min. air, 1,050 cc./min. liquid).

Apart from offering the advantage of better control of the experimental conditions, desorption also yields truer measurements of the diffusional rates of mass transfer. Thus, it was found (*46*) that both carbon dioxide and ammonia increase the surface tension of the solution when absorbed in it. As a result, the apparent measured rate of absorption would also include the contribution of convection currents tending to restore the decreasing surface tension gradient in the liquid, in a direction perpendicular to the interface (*1, 2, 12*) with the lowest surface tension at the interface. Conversely, during desorption this surface-tension equilibrium is not disturbed.

The complete experimental installation is described schematically in Figure 1. The foam apparatus and its various stages, defined and investigated separately during this work, is represented in Figure 2, while Figure 3 is a photograph of the apparatus in operation.

With this setup the only pressure loss occurred at the perforated plate. No measurable pressure drop could be detected, owing to the moving foam column, over the entire practical range of gas and liquid flow rates. The pressure drops throughout the plate are minor (maximum 5 cm. water) because the apparatus must operate at low gas flow rates (in this case, up to 30 cm./sec.) for efficient foam operation.

In a typical run, after the gas stream had been brought to the desired temperature and humidity and the foaming solution had been readied in the constant-head vessels, the two streams were metered into the apparatus at the desired flow rate. The measurements were started only after the liquid stream was at the gas temperature. By that time at least fifteen apparatus volumes of foam had passed through the duct.

Flow rates, pressures, and temperatures were recorded and liquid and gas samples collected. Each apparatus stage was considered individually. Gas sampling was subsequently discontinued as it did not yield average concentrations representative of the foam stage under study. The liquid samples did so, since they were the result of the draining of the totality of foam cell lamellae in a given foam column section (stage).

In addition to various combinations of gas and liquid flow rates and plate geometries, the influence of the following physical parameters (in carbon dioxide solutions) was also studied:

1. Surface tension (at constant bulk viscosity and specific gravity), by varying the saponin content from 0.10 to 0.75% by weight, which is 0.25% above the critical micelle concentration (*46*). The corresponding surface tension change was from 44.5 to 36.6 dynes/cm.

2. Bulk viscosity (at constant surface tension and specific gravity), by adding to a 0.2% saponin solution from 0.1 to 0.2% by weight of Natrosol 250,* giving a corresponding viscosity change from 0.8 centipoises for 0% Natrosol to 5.5 centipoises for 0.2% Natrosol solutions.

Carbon dioxide in the saponin containing liquid samples was determined by first stripping it out with carbon dioxide-free air and then absorbing in Ascarite and Anhydrone.

Pure water-carbon dioxide solutions were also analyzed by excess treatment with barium hydroxide in the presence of barium chloride and backtitration with hydrochloric acid in the presence of phenol-phthalein as an indicator. An alternative method, also used, was the measurement of electric conductivity of the aqueous sample.

Ammonia liquid samples were titrated with hydrochloric acid in the presence of a mixed indicator (methyl red + methylene blue) with a correction factor obtained from blank saponin containing samples.

Surface tensions were determined with the Du Nouy ring method (*4*), bulk viscosities by Ubbelohde viscometry, foaminess and foam stability by the Ross-Miles method (*3, 37, 38*), and specific gravity by hydrometry with temperature correction.

On separate runs the following foam characteristics were also determined: interfacial areas, by photography; fractional liquid hold ups, by a technique based on an instantaneous stopping of the gas and liquid flow rates after steady operating conditions had been attained, and measurement of the amount of liquid collected from the killed foam section in each stage.

A detailed description of the equipment and experimental procedure has been given elsewhere (*46*).

ESTIMATION OF THE RATES OF MASS TRANSFER

In essence, the foam results from crosscurrent contacting of a liquid phase with a gas phase. And even after it has been generated and moves along the duct, this crosscurrent interaction continues in the sense that the gas moves horizontally forward and liquid drains out of the foam lamellae, downward. In addition, a portion of the gas phase continues to exist as an independent phase even after the flowing foam has been generated. This portion channels through the moving foam column at a faster rate than the column itself. The channeling becomes more pronounced as the flow rates decrease towards their critical values below which no effective foam can be obtained.

The arbitrary division of the foam column into two stages (Figure 2) has a mechanistic justification. Thus the first foam stage is the active part, as indicated by its intense draining and marked contribution to the overall transfer process, and the second foam stage is already spent, passive from the same points of view (*46*).

An added clarification of the mechanisms occurring in the foam apparatus requires a further subdivision of the foaming stage into three zones:

1. The plate zone (p) where the downflowing layer of foaming solution is contacted by gas passing through the perforations. In general, high fractions of the incoming liquid drain out of this zone without apparently foaming at all.

2. The bubble formation zone (b), taken as a slice of the foaming stage parallel to the plate and of a thickness equal to the radius of an average bubble being formed (taken as equal to half the pitch). It is here that the bubbles form, grow, and coalesce into a stable foam.

3. The foam zone (f) which is similar in character to the foam stages that follow downstream. It represents the downstream end of the foaming stage.

The integrated rate expressions for mass transfer in a liquid-phase controlled system and in a gas-phase controlled system are, respectively:

$$N = \frac{\rho_L}{M_w} K_{Lc} A (X - X^*) \qquad (1)$$

and

$$N = \frac{\rho_G}{M_A} K_{Gc} A (Y^* - Y) \qquad (2)$$

The material balances yield

$$N = (\lambda_i)_{ave} (X_i - X_o) \text{ and } N = \bar{\gamma}(Y_o - Y_i) \qquad (3, 4)$$

Both systems obey Henry's law in the range of concentrations and pressures under consideration and are sufficiently dilute to warrant the assumption of a straight operating line and of the following approximation for the overall number of transfer units:

---

* Natrosol 250 is a hydroxyethylated cellulose, nonionic in character.

$$N_{toL} = \int_{X_1}^{X_2} \frac{dX}{X - X^*} = \frac{X_2 - X_1}{(\overline{X - X^*})} \text{ and}$$

$$N_{toG} = \int_{Y_2}^{Y_1} \frac{dY}{Y^* - Y} = \frac{Y_1 - Y_2}{(\overline{Y^* - Y})} \qquad (5, 6)$$

Utilizing Pozin's simplified and yet sufficiently accurate expression for the magnitude of the average driving forces $(\overline{X - X^*})$ or $(\overline{Y^* - Y})$ in crosscurrent flow (*30*) and rearranging, one obtains

$$N_{toL} = \frac{\rho_L}{M_w} \frac{A K_{LG}}{(\lambda_i)_{stage}} = \frac{X_i - X_o}{\dfrac{X^*_i - X^*_o}{2} - \dfrac{X_o - X_i}{\ln\left(\dfrac{X_i^* - X_i}{X_i^* - X_o}\right)}} \qquad (7)$$

$$N_{toG} = \frac{\rho_G}{M_A} \frac{K_{GG} A}{\overline{\gamma}} = \frac{Y_o - Y_i}{\dfrac{Y_i^* - Y_o^*}{\ln\left(\dfrac{Y_i^* - Y_i}{Y_o^* - Y_i}\right)} - \dfrac{Y_i - Y_o}{2}} \qquad (8)$$

where the left-hand side of Equations (7) and (8) is used for the predictions and compared with the experimental right-hand side.

Equation (7) can be further simplified by noting that $X_i^* \approx 0$, $X_o^* \approx 0$, and one finally obtains

$$N_{toL} = \frac{\rho_L}{M_w} \frac{A K_{LG}}{(\lambda)_{stage}} \approx \ln\left(\frac{X_i}{X_o}\right) \approx N_{tL} \qquad (9)$$

The mass transfer coefficients have been evaluated by means of the penetration theory (*14*):

$$K_{LG} = \left(\frac{4D_L}{\pi}\right)^{0.5} \frac{1}{t^{0.5}} \qquad (10)$$

for carbon dioxide desorption, and

$$K_{GG} = \left(\frac{4D_G}{\pi}\right)^{0.5} \frac{1}{t^{0.5}} \qquad (11)$$

for Ammonia desorption.

The corresponding penetration times t have been derived based on the mechanisms of gas-liquid interaction as observed in the various postulated stages and zones of the apparatus. Space considerations preclude a detailed presentation of the analysis, already available elsewhere (*46*). The results are outlined below.

Peneration times *t* for various situations

Carbon dioxide desorption

Plate zone—see discussion below regarding N_{tf}.

Bubble formation zone—

$$t_b = \frac{\rho_L}{M_w} V_b \left(\frac{\mathcal{L}_f}{\overline{\lambda}_b}\right) \qquad (12)$$

Foam zone
First foam stage
Second foam stage

$$t = \frac{\rho_L}{M_w} S_p l' \left(\frac{\mathcal{L}}{\lambda_A}\right) \qquad (13)$$

Ammonia desorption

Plate zone—

$$t_{pr} = 2.96 \times 10^{-4} \pi \left(\frac{\mu_L M_w}{g \rho_L^2}\right)^{0.333} \frac{P}{T} \frac{N_h d_h^2}{(b \sin \phi)^{0.333}} \left(\frac{\lambda_i^{0.333}}{G_r}\right) \qquad (14)$$

Bubble formation zone—

$$t_b = 4.10 \times 10^{-4} pS \frac{P}{T} \left(\frac{1}{G_r}\right) \qquad (15)$$

Foam zone
First foam stage
Second foam stage

$$t = 8.20 \times 10^{-4} l'S \frac{P}{T} \left(\frac{1 - \mathcal{L}}{G_v}\right) \qquad (16)$$

Several adjustments, in the form of correction factors, are necessary before the prediction equations for N_t, the number of transfer units, can be used.

One of them, general to both the liquid and the gas-phase controlled systems, is due to the physico-chemical interfacial resistance to mass transfer caused by the surfactant (Saponin) molecules preferentially adsorbed at the interface. It has been shown (*9, 44, 46*) how the following expression is sufficiently accurate to be used as the appropriate correction factor:

$$\exp\left[-\frac{(\sigma - \sigma_s)\omega}{R'T}\right]$$

It is based on the fact that the chemical potentials of the solute (transferring component) at the interface and in the bulk of the solution (with or without surfactant) differ by the amount

$$\sigma\omega$$

A second correction factor, applicable only to the liquid-phase controlled system, is necessary in order to account for the finite thickness of the liquid foam films (*6*). It is defined as the ratio of the approach to equilibrium in a finite system, such as this, to that of a semi-infinite one (as for the penetration theory):

$$\frac{(M_t/M_\infty)_\phi}{(M_t/M_\infty)_z} \qquad (18)$$

In this case, whether one is dealing with a hollow sphere in the bubble formation zone or a plane sheet in the foam column between two adjacent foam cells, one obtains for the semi-infinite case

$$\left(\frac{M_t}{M_\infty}\right)_z = 2.257 \left[\frac{D_L t}{(\delta')^2}\right] \qquad (19)$$

where

$$\delta' = 2 \frac{\mathcal{L}}{a} \ (46, 47) \qquad (20)$$

For the finite case the following solutions can be derived (*6bis*):

For the bubble formation zone

$$\left(\frac{M_t}{M_\infty}\right)_\phi \approx 1 - \frac{384\,(a')^2}{\pi^2[48(a')^2 + (\delta'_f)^2]} \exp\left[-4\pi^2 \frac{D_L t_b}{(\delta'_f)^2}\right] \qquad (21)$$

where

$$a' = \frac{2.51}{a\mathcal{L}^{0.01}} \ (46, 47) \qquad (22)$$

For the foam zone and stages

$$\left(\frac{M_t}{M_\infty}\right)_\phi \approx 1 - 0.811 \exp - \left[9.86 \frac{D_L t}{(\delta')^2}\right] \qquad (23)$$

Finally, the gas-phase controlled system, also requires a second correction factor which takes into account the gas-channeling effect. It is given by

$$\left(\frac{\overline{v}_H}{u_H}\right)^{0.5} \qquad (24)$$

where

$$\overline{v}_H = \frac{M_w}{\rho_L} \frac{\overline{\lambda}}{S\mathcal{L}} \qquad (25)$$

$$u_{\mathcal{H}} = \frac{1{,}218.8}{S} \frac{T}{P} \frac{G_v}{(1-\mathcal{L})} \qquad (26)$$

This corrects accordingly the value of the mass transfer coefficient predicted by means of a penetration time based on $u_{\mathcal{H}}$ (see tabulation of t expressions, above).

The resulting expressions for the prediction of the overall number of transfer units are:
For liquid-phase controlled systems

$$N_{tfo} \approx N_{tb} + N_{tf}{}^{*} \qquad (27)$$

$$N_{tb} = \beta_0 \left[1 - \left(\frac{61.44}{75.72 + \mathcal{L}_f^{2.02}} \right) \exp\left(-\beta_1 \frac{a_f^2}{\mathcal{L}_f \bar{\lambda}_b} \right) \right] \qquad (28)$$

where

$$\bar{\lambda}_b = \lambda_{tf} = \lambda_t - \lambda_{\Delta fo} + \lambda_{\Delta f} \qquad (29)$$

$$\beta_0 = \text{const} = 17.96 \frac{\rho_L}{M_w} \exp\left[-\frac{(\sigma - \sigma_s)\omega}{R' T} \right] \qquad (30)$$

$$\beta_1 = \text{const} = 0.526\, D_L V_b \qquad (31)$$

$$\lambda_{\Delta f} = (\alpha_1 \mathcal{L}_{1f} - \alpha_2 \mathcal{L}_{2f}) \left[\left(\alpha_1 \frac{V_f}{V_{1f}} \right) \left(\frac{\lambda_\Delta}{\mathcal{L}} \right)_{1f} - \left(\alpha_2 \frac{V_f}{V_{2f}} \right) \left(\frac{\lambda_\Delta}{\mathcal{L}} \right)_{2f} \right] \qquad (46, 47)$$

$$\alpha_1 = \frac{l_f + 2l_{1f} + l_{2f}}{l_{1f} + l_{2f}}, \quad \alpha_2 = \frac{l_f + l_{1f}}{l_{1f} + l_{2f}} \qquad (32)$$

$$N^{(a')}_{tf,1f,2f} = \beta \frac{a\mathcal{L}^{0.01} \lambda_\Delta}{\lambda_{tf,t1f,t2f}} \left[1 - 0.811 \exp\left(-\beta_2 \frac{a}{\lambda_\Delta \mathcal{L}^{1.01}} \right) \right] \qquad (33)$$

where $N_t^{(a')}$ has been obtained by taking $l' = a'$ (see above tabulation of expressions for t):

$$\beta = 0.398 \frac{V}{(S_B S_t)^{0.5}} \exp\left[-\frac{(\sigma - \sigma_s)\omega}{R' T} \right] = \text{const} \qquad (34)$$

$$\beta_2 = 6.192 \left(\frac{\rho_L D_L}{M_w} \right) S_B = \text{const} \qquad (35)$$

$$N^{(Z)}_{tf,1f,2f} = \frac{\beta' \lambda_\Delta}{\lambda_{tf,t1f,t2f}} \left[1 - 0.811 \exp\left(-\beta_3 \frac{a^2}{\mathcal{L} \lambda_\Delta} \right) \right] \qquad (36)$$

where $N_t^{(Z)}$ has been obtained by taking $l' = Z$ (see above, tabulation of expressions for t):

$$\beta' = \frac{V}{ZS_B} \exp\left[-\frac{(\sigma - \sigma_s)\omega}{R' T} \right] = \text{const} \qquad (37)$$

$$\beta_3 = 2.465\, (S_B Z) \left(\frac{\rho_L D_L}{M_w} \right) = \text{const} \qquad (38)$$

For gas-phase controlled systems

$$N_{tfo} = N_{tp} + N_{tb} + N_{tf} \qquad (39)$$

$$N_{tp} = \mathcal{D}_p \frac{\lambda_t}{G_r^{0.5}} \qquad (40)$$

where

$$\mathcal{D}_p = \text{const} = 8.56 \times 10^{3} \left(\frac{D_G P}{R^2 T} \right)^{0.6} \left(\frac{M_w \mu_L}{g \rho^2_L} \right)^{0.287}$$

$$\frac{N_h^{0.5}}{(b \sin \phi)^{0.287}} \exp\left[-\frac{(\sigma - \sigma_s)\omega}{R'T} \right] \qquad (41)$$

$$N_{tb} = \mathcal{D}_b \frac{a_f}{G_r} \left(\frac{\bar{\lambda}_b}{\mathcal{L}_f} \right)^{0.5} \qquad (42)$$

where $\bar{\lambda}_b$ is given by Equations (29) and (32) above:

$$\mathcal{D}_b = 81.63 \frac{P}{RT} \left(\frac{M_w D_G}{\rho_L} \right) \frac{V_b}{(pS)^{0.5}} \exp \left[-\frac{(\sigma - \sigma_s)\omega}{R'T} \right] = \text{const} \qquad (43)$$

$$N_{tf,1f,2f} = \mathcal{D} \frac{a}{G_r} \left(\frac{\bar{\lambda}}{\mathcal{L}} \right)^{0.5} \qquad (44)$$

where $\bar{\lambda}$ is an arithmetic average of the incoming and outgoing flow rates:

$$\mathcal{D} = 57.72 \frac{P}{RT} \left(\frac{M_w D_G}{\rho_L} \right)^{0.5} \frac{V}{(l'S)^{0.5}} \exp \left[-\frac{(\sigma - \sigma_s)\omega}{R'T} \right] = \text{const} \qquad (45)$$

with l' taken equal to l
Finally

$$(N_t)_{\text{apparatus}} = N_{tp} + N_{tb} + N_{tf} + N_{t1f} + N_{t2f} \qquad (46)$$

All the prediction expressions outlined above are usable if sufficient knowledge is available on the characteristics of flowing foams (say $\mathcal{L}$, a, λ_Δ, $\frac{v_H}{u_{\mathcal{H}}}$ as a function of λ_t, G_r, $l_1, \ldots_n$). This information has been obtained in preparation to the present work and is reported elsewhere (*46, 47*).

RESULTS AND DISCUSSION

It has been shown that there exists an interrelationship between the basic flow and position parameters, with their dependent foam flow characteristics, and the prediction expressions for rates of desorption. This determines the change properties of, say N_t, as a function of either the liquid flow rate entering the apparatus† or the gas flow rate.

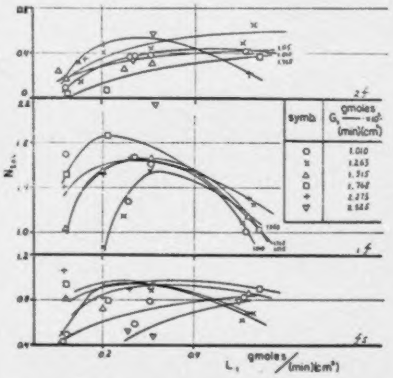

Fig. 4. N_{tol} vs. the liquid flow rate entering the apparatus, parameter: G, 1/16-in. perforations.

---

* N_{tf} cannot be added to the sum as it is based on a different liquid flow rate. At any rate, it assumes negligible values (for a contact length taken as $\frac{z_p A'_e}{A'_p}$).

† It might be worth re-emphasizing that, in the case of flowing foams, there is a distinct difference between the liquid flow rate entering the apparatus and the successively decreasing liquid flow rates entering any arbitrary foam stage in a downstream direction, due to foam drainage.

If one plots N_t vs. either of these two flow variables, a set of exponential curves is obtained that exhibits maxima in many instances.* This holds true for both liquid- and gas-phase controlled systems and for any position within the apparatus, and is illustrated in Figure 4 chosen from the many available sets of data (*46*).†

A few experimental results showing actual concentrations measured at various points within the apparatus are tabulated below in order to exemplify some typical separation performances:

System: CO_2-H_2O (0.2% Saponin)

d_s, in.	L, g. moles / (min.) (sq. cm.)	G, g. moles / (min.) (sq. cm.) × 10^2	X_1	X_2	X_3	X_4
			moles CO_2 / mole water × 10^4			
1/16	0.204	1.26	3.805	1.486	0.620	0.539
1/8	0.307	4.04	3.689	1.747	0.571	0.343

System: NH_3-H_2O (0.2% Saponin)

d_s, in.	L, g. moles / (min.) (sq. cm.)	G, g. moles / (min.) (sq. cm.) × 10^2	Y_1^*	Y_2^*	Y_3^*	Y_4^*
			mm. Hg			
1/16	0.205	1.52	2.537	2.396	2.236	2.223
1/8	0.299	4.04	2.429	2.281	2.114	2.060

The predicted rates of mass transfer are compared with the experimental values in Figure 5.

The agreement in the case of ammonia desorption is good except at the low end of the range of gas and liquid flow rates. At this extreme the characteristics of moving foams might change drastically before a complete decay occurs. This would account for the lack of agreement.

For carbon dioxide desorption the experimental values tend to fall between the low (based on contact length = Z) and the high (based on contact length = a') predictions in the case of the active first foam stage. Only the low predictions are of any consequence for the inactive second foam stage, and the increased scatter is probably due to the higher experimental inaccuracy (very low concentrations to be measured).

The complexity of processes occurring in the foaming stage is also evident from the figure. Here, the experimental results range from lower than the lowest predicted values (at the critical end of flow rates range below which the foam decays rapidly) to higher than the highest predicted values [at the other end of the range, where the hydrodynamic regime is highly intensified and increased gas channeling contributes to more mixing in the liquid phase (*46, 47*)]. It is felt that at least part of the blame is to be laid on the difficulty of accurate assessment of interfacial areas in the foaming stage (*46, 47*) and on the nature of assumptions used for the physical model and the integration of the individual zone predictions into an overall figure for the stage.

The mass transfer performance in any stage of the apparatus, for a given flow rate, will depend also on the types of plate perforations (geometry), in line with what was reported on the characteristics of flowing foams (*46, 47*).

If the gas velocities through the plate perforations are about equal, that is if the superficial gas velocities in the duct stand in a ratio of about 1:4 (in this case), similar numbers of transfer units are obtained at the foaming stage, particularly for ammonia desorption. This is to be expected, since the mechanism of mass transfer in essentially gas-phase controlled systems will depend directly on the gas velocity (which determines the penetration time). Also, at least two of the three zones of the foaming stage, namely the plate and bubble formation zones, will perform according to the gas velocity through the perforations rather than through the duct.

For carbon dioxide desorption, where the agreement is less good, the dependence on gas flow rate can only be indirect, that is in terms of the flow characteristics of the bubble formation zone (drainage, interfacial areas, etc.).

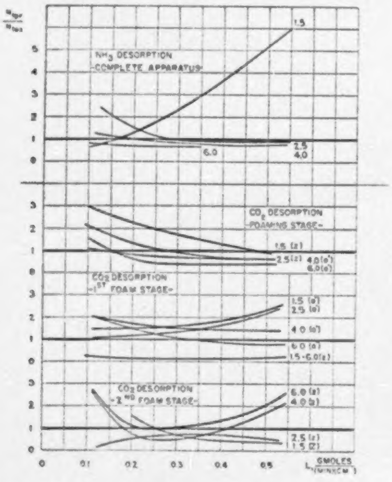

Fig. 5. Graphical representation of prediction accuracy-Parameter: G, $\dfrac{\text{g. moles}}{\text{(min.)(sq. cm.)}} \times 10^2$ (in brackets: contact length on which N_{tpr} is based).

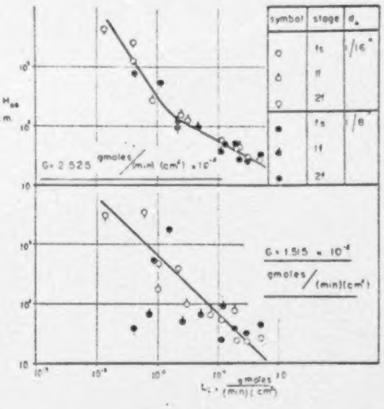

Fig. 6. H_{OG} vs. the liquid flow rate entering any stage, Parameter: G.

---

* Here and in what follows it should be noted that correlations and presentation of results vs. a liquid-to-gas flow rate ratio were not found applicable. This, too, is due to the peculiar flow characteristics of aqueous and continuously draining foams. These can be markedly different at low and at high liquid and gas flows with the result that identical L/G values are related to different mass transfer data depending on the absolute magnitudes of the flow rates in question.

† Tabular material has been deposited as document 8252 with the American Documentation Institute, Photoduplication Service, Library of Congress, Washington 25, D. C., and may be obtained for $1.25 for photoprints or $1.25 for 35-mm. microfilm.

Considering now the relationship between the overall height of a transfer unit (rather than the number of transfer units) and the liquid flow rate entering any given stage (rather than the apparatus), one observes a log-log type of correlation trend particularly for the case of ammonia desorption. This is illustrated in Figure 6. Although this fact is interesting, the prediction equations that have been developed based on the liquid flow rate entering the apparatus (and thus easy to determine and control) have a more practical significance. One notices that at higher gas flow rates differences in the plate geometry are no longer evident, and the scatter of the data is much reduced. Conversely, a break point appears at $L_i \approx 2 \times 10^{-2}$ g.moles/(min.)(sq.cm.) (the same value also in the case of carbon dioxide desorption). Below this flow rate a higher rate of increase of H_{OG} with decrease in L_i is obtained which is to be expected, since:

$$\lim_{L_i \to O} H_{OG} = \infty$$

Figure 7 indicates a straight-line correlatibility between bulk viscosity or surface tension and the carbon dioxide desorption performance. These two physical parameters are important factors in any foaming system (*46, 47*).* An increase in surface tension brings about an increase in the rate of transfer (particularly for the first foam stage, which also has the main transfer role). The undesirable fact that for a higher surface tension foams are less stable and the corresponding starting solutions are less foamable is more than offset by the following factors:

1. Small resistance to diffusion since the surfactant-determined interfacial resistance term is exponentially dependent on the surface tension gradient between a solution and the same solution with surfactant added to it. Thus, a higher surface tension of the foaming solution (that is less surfactant) decreases the gradient and, with it, the magnitude of the interfacial resistance term.
2. The drainage rates from any given stage increase with an increase in surface tension (*46, 47*); this leads to shorter liquid-gas contact times and higher rates of desorption.
3. The resulting lower foam stability is conducive to a more intensified process of decay with more foam bubbles bursting in a given volume of the duct. More mixing or a shorter gas-liquid contact length is the result with the same consequence as above.

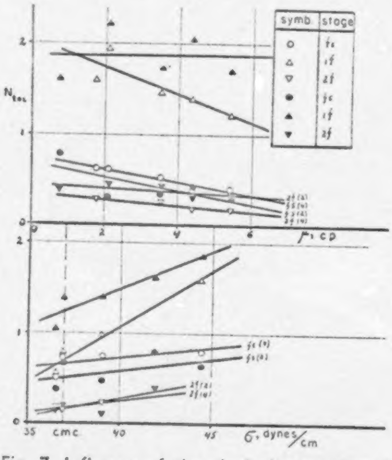

Fig. 7. Influence of the physical properties of the foaming solution on N_{tol} (1/16-in. perforations) (clear points—2.02×10^{-2} g.moles air/(min.)(sq. cm.), 0.316 g.moles water/(min.)(sq. cm.), black points—1.01×10^{-2} g.moles air/(min.)(sq. cm), 0.312 g.moles water/(min.)(sq. cm).

In conclusion, the limit to higher mass transfer rates appears to be the highest surface tension, that is lowest concentration of surfactant, at which a solution will produce a flowing foam. In the present case this limit has been attained at $\sigma \approx 45$ dynes/cm., corresponding to approximately 0.1% Saponin by weight.

An exactly opposite effect is obtained when the bulk viscosity of the solution increases for the reasons outlined in points 2 and 3 above.

COMPARISON WITH OTHER DATA

A direct comparison with other types of equipment utilizing foams or froths, or conventional hardware such as packing is made difficult by the following reasons:

1. The data reported in the literature for foam, froth, or gas-bubble columns refer to countercurrent operation at flow rates considerably in excess of those used in the present work. Such relatively high flow rates would be unpractical anyway, owing to foam decay problems in this case.
2. The present paper deals with the rather unusual situation of a decreasing liquid flow rate (as a function of the position in the apparatus) caused by foam drainage. The data available for comparison are all, of course, reported for a constant liquid flow rate.

Figure 8 compares some data in terms of the overall height of a transfer unit based on the liquid phase vs. the air flow rate. The considerable discrepancy in liquid flow rates is obvious, although use has been made only of the data that were obtained in the present work at the highest liquid flow rates. It is apparent that the other data for H_{OL} are higher with some exceptions in the case of the inactive second foam stage.

CONCLUSIONS

1. It has been shown that a workable mass transfer device can be operated, based on a horizontal column of a stable aqueous foam in motion. This foam can readily be generated over a certain range of gas-liquid flow rate combinations, and its formation and existence are the result of an induced surface activity in the liquid phase (by addition of 0.2% by weight of Saponin). There are no energy requirements other than those necessary for the flow of gas through a perforated plate, where the foam is produced, and through the empty duct that is to be filled by the moving foam.

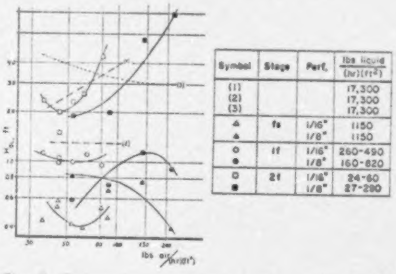

Fig. 8. Comparison with other data. (1)— Reference 27—adsorption of carbon-dioxide by surfactant-treated water, porous plate columns. (2)—Reference 40—desorption of carbon-dioxide from water in gas bubble columns (porous plate)—extrapolated curve. (3)—Cooper, C. M., et al., *Trans. Am. Inst. Chem. Engrs.*, 37, 979 (1941)—same liquid flow rate as (1); adsorption of carbon dioxide by water; packed column with 2-in. Raschig rings—interpolated data.

---

* See second footnote on page 360.

2. After a certain length of travel in the downstream direction, during which the foam films are continually losing their liquid content by drainage, a foam becomes inactive with resulting low drainage rates and separation efficiencies.

3. At a given gas flow rate, different foam flow behavior results for different plate geometries. In this case this refers to a ratio of nearly 1:4 in the percent free area. In turn, differences are caused in the mass transfer performance. The only cases where some similarities are observed correspond to equal gas velocities based on the plate free area at the foaming stage. These similarities are apparently due mainly to the plate and bubble formation zones that are expected to be susceptible to the gas velocity through the perforations rather than to the superficial gas velocity in the duct. Indeed, a higher degree of similarity in performance is obtained for ammonia desorption, where the dependence on the gas flow is direct (as per the prediction theory outlined in this paper) rather than in terms of foam characteristics, as for carbon dioxide desorption.

4. The mass transfer performance of stable foams in movement becomes better as their foamability and foam stability decrease. This situation corresponds to an increase in surface tension (for a betterment in performance) and continues up to the point beyond which no more moving foam can be generated.

This characteristic may be approximated by a linear relationship between σ and N_{tOL}. It is explainable on the basis of the analytical model for predictions of mass transfer rates and in terms of the foam flow correlations reported elsewhere (*46, 47*).

5. The mass transfer performance of stable foams in movement becomes poorer as the bulk viscosity of the foaming solution increases, and this change can also be described by a linear correlation and explained as for point 4 above.

6. Some types of foam equipment, all of them based on countercurrent contacting in vertical towers, have already been studied and their efficiencies and/or rates of mass transfer found generally superior to those of conventional types of hardware (packed towers, for instance).

The moving foam systems studied in the present work exhibit sometimes similar but generally significantly better mass transfer performances when compared with the other types of foam equipment, while operating at much lower liquid flow rates (one order of magnitude or more) and lower gas flow rates. This, and also the negligible pressure drop ascribable to the interaction of the gas and liquid streams, should compensate for the disadvantage of larger volumes of equipment per unit flow rate (as compared with countercurrent tower operation).

7. The various parameters and criteria for a moving foam interact in such a way that if one expresses the performance (say N_t or η) as a function of liquid flow rate or of gas flow rate only, a maximum is exhibited in many instances.

8. The height of a transfer unit appears to be correlatable exponentially, with a certain degree of scatter, in terms of the incoming liquid flow rate to any foam stage (at any longitudinal position in the duct). This is particularly the case for gas-phase controlled systems and higher gas flow rates. Thus, an alternative way of defining mass transfer performances would be available. However, it is believed that a definition based on the liquid flow rate entering the apparatus is more practical from the standpoint of its applicability to predictions.

Below a given value of incoming liquid flow rate, identical for the cases of ammonia and carbon dioxide desorption (because their foam flow behavior is identical), the curve of H_{OL} or H_{OG} vs. L_i exhibits a break. This break characterizes a certain stage of foam decay that has been reached, beyond which rapid deterioration occurs in the mass transfer performance with, at the limit, $H_{OL} = H_{OG} = \infty$ (for $L_i = 0$).

9. An analysis of the hydrodynamics of moving foams and of the mass transfer occurring in them is possible by means of a distinct definition of a foaming stage, where the foam is generated, and of several foam stages of an arbitrary length, composing the moving foam column. The foaming stage, in turn, is definable as a composite of several distinct zones, each one with its specific performance and behavior: the plate zone, where the foam generation is started by cross current gas-liquid interaction; the bubble formation zone, where bubbles are formed, grow, and and coalesce into a stable, true, foam; and the foam zone, which is the upstream end of the moving foam column.

10. The mass transfer performance of moving stable aqueous foams can be defined and predicted, for both a liquid- and a gas-phase controlled system, in terms of three basic parameters: gas flow rate, liquid flow rate entering the apparatus, and longitudinal position in the duct. These parameters act interdependently either directly, as an independent variable, or indirectly, in terms of the characteristic foam criteria: fractional liquid holdup, interfacial area, drainage flowrate, gas channeling.

The predictions are based on a model of crosscurrent interaction between the phases whether within the moving foam or at the foam source (where it is generated), and on several correction factors: An interfacial resistance term of a physico-chemical nature, due to the presence of surfactant in the solution, a term accounting for the finiteness of the liquid medium in which transfer occurs, and, a term accounting for the gas channeling effects in the moving foam column.

ACKNOWLEDGMENT

The authors gratefully acknowledge financial support of this work by the U.S. Public Health Service, Research Grant No. AP 00024-05.

NOTATION

A = area of mass transfer sq.cm.
A' = area of given geometry sq.cm.
a = interfacial area, sq.cm./cc. of given volume
a' = average foam cell (bubble) size, cm.
B = the slope, in linear correlation
b = width of rectangular duct, cm.
D = diffusivity, sq.cm./sec.
d_h = diameter of plate perforation, cm.
$\mathcal{D}$ = constant in Equations (40) to (45)
F = intercept, in linear correlation
G = molar gas flow rate, g.moles/(min.)(sq.cm. duct cross section)
G_s = standard volumetric gas flow rate, std. cu.ft./min.
g = acceleration of gravity = 980.1 cm./sec.^{2}
H = height of a transfer unit, cm.
K_c = overall mass transfer coefficient based on a driving force in g.moles/cc., cm./sec.
L = molar liquid flow rate entering the apparatus = sum of measured outflowing liquid streams, g.moles/(min.) (sq.cm. duct cross section)
l = (horizontal) length of given stage, cm.
l' = characteristic gas-liquid contact length, in any direction, cm.
$l_{1,\ldots,n}$ = longitudinal coordinate, cm.
$\mathcal{L}$ = fractional liquid holdup, cc./cc. apparatus section
M = molecular weight
M_t = amount of component transferred per unit area in time t, g.moles
M_∞ = amount of component transferred per unit area in time $t = \infty$, g.moles
N = rate of mass transfer, g.moles/sec.

N_h = number of plate perforations
N_t = number of transfer units
P = ambient pressure, mm.Hg
p = pitch of perforated plate, cm.
R = gas constant = 62,363.3 (mm.Hg) (cc.)/(g.mole) (°K.)
R' = Boltzmann constant = 1.3804×10^{-16} erg./(°K.) (molecule)
r_1 = internal radius of hollow sphere, cm.
r^2 = square of the correlation coefficient
S = cross-sectional duct area (perpendicular to horizontal direction of flow, sq.cm.)
S_B = cross section parallel to bottom of duct, sq.cm.
S_L = cross section parallel to lateral duct sides, sq.cm.
$s_{y.x}$ = standard error of the estimate (7)
T = absolute temperature, °K.
t = penetration time, sec.
u = gas velocity (in general), cm./sec.
V = volume of given apparatus section, cc.
v = liquid velocity (in general), cm./sec.
X = liquid-phase concentration, moles/mole water
Y = gas-phase concentration, moles/mole air
Z = height of duct, cm.
z = travel distance of downflowing liquid, cm.

Greek Letters

$$\alpha_1 = \frac{l_f + 2l_{1f} + l_{2f}}{l_{1f} + l_{2f}}, \quad \alpha_2 = \frac{l_f + l_{1f}}{l_{1f} + l_{2f}}$$

β, β', etc. = constants in Equations (30), (31), (34), (35), (37), (38)
γ = molar gas flow rate, g.moles/sec.
δ' = average thickness of foam cell film (lamella), cm.
η = stage efficiency defined as $(X_i - X_o)/(X_i - X_o^*)$ or $(Y_o - Y_i)/(Y_o^* - Y_i)$, fraction of unity
λ = molar liquid flow rate, g.moles/sec.
μ = viscosity, poises
ρ = density, g./cc.
σ = surface tension, dynes/cm.
ϕ = angle of plate with respect to horizontal, deg.
ω = area of solute molecule at the interface, sq. cm.

Subscripts

A = air
app = apparatus
b = bubble formation zone
ex = experimental
f = foam zone
fs = foaming stage
$1f$ = first foam stage
$2f$ = second foam stage
G = gas phase
H = in a horizontal direction
$\bar{H}$ = based on the fractional gas holdup
i = incoming flow or concentration to any defined section of the apparatus (note: i used alone indicates inlet to the apparatus as a whole, that is to the plate zone) (λ_i)
L = liquid phase
OG = overall, based on the gas phase
OL = overall, based on the liquid phase
o = outgoing flow or concentration from any defined section of the apparatus
p = plate zone
pr = predicted
W = water
Δ = draining out
σ = based on the plate free area
ϕ = based on a finite medium
Σ = based on a semi-infinite medium

Superscripts

(bar) = average
$*$ = equilibrium (interface)

LITERATURE CITED

1. Anderes, G., Ph.D. thesis, No. 3101, Zurich, Switzerland (1961).
2. ———, *Chem. Ing. Tech.*, **34**, 597-602 (1962).
3. *ASTM Test No. D1173-53*, adopted 1954.
4. *ASTM Standard D1331-56*, adopted 1956.
5. Calderbank, P. H., and M. B. Moo-Young, *Chem. Eng. Sci.*, **16**, 39-54 (1961).
6. Calvert, S., and G. Kapo, *Chem. Eng.*, **70**, 99-104 (February, 1963); also *ibid.*, 105-110 (March, 1963).
6^bis^. Crank, J., "The Mathematics of Diffusion," Oxford at ruary, 1963); also *ibid.*, 105-110 (March, 1963).
7. Crow, E. L., et al., "Statistics Manual," pp. 156 et seq., Dover Publications, New York (1960).
8. Drouhin, R., *Génie Chim.*, **85**, 23-29 (1961).
9. Defay, R., and I. Prigogine, "Surface Tension and Adsorption," vol. 2 of the Treatise of Thermodynamics, in French ed., Desoer, Liège, Belgium (1951).
10. Drozdov, N. P., et al., *J. Appl. Chem. (USSR)*, **33**, 2572-2575 (1960).
11. Fesenmeyer, H., Ph.D. thesis, No. 3066, Zurich, Switzerland (1960).
12. Grassmann, P., and G. Anderes, *Chem. Ing. Tech.*, **31**, 154-155 (1959).
13. Helsby, F. W., and D. C. P. Birt, *J. Appl. Chem. (London)*, **5**, 347-352 (1955).
14. Higbie, Ralph, *Trans. Am. Inst. Chem. Engrs.*, **31**, 365-389 (1935).
15. Houghton, G., et al., *Chem. Eng. Sci.*, **7**, 26-39 (1957).
16. Johnson, A. I., and C. W. Bowman, *Can. J. Chem. Eng.*, **36**, 253-261 (1958).
17. Kadlas, P., and S. Veseley, *Chem. Prumysl.*, **10**, 565-571 (1960).
18. Kuzminykh, I. N., *Khim Prom.*, 234-237 (1956).
19. ———, and A. I. Rodionov, *J. Appl. Chem. (USSR)*, **29**, 1433-1438 (1956).
20. *Ibid.*, **32**, 1523-1528 (1959).
21. Metzner, A. B., and L. F. Brown, *Ind. Eng. Chem.*, **48**, 2040-2045 (1946).
22. Mochalova, L. A., and M. K. Kishinevsky, *J. Appl. Chem. (USSR)*, **28**, 25-33 (1955).
23. *Ibid.*, **29**, 193-198 (1956).
24. *Ibid.*, **31**, 525-533 (1958).
25. *Ibid.*, 1007-1012.
26. Mukhlenov, I. P., *ibid.*, 1328-1333.
27. ———, and E. S. Tumarkina, *ibid.*, 1635-1642.
28. Mutzenberg, A., *Chem. Ing. Tech.*, **34**, 542-546 (1962).
29. Poll, A., and W. Smith, *Trans. Inst. Chem. Engrs.*, **40**, A93-A97 (1962).
30. Pozin, M. E., *J. Appl. Chem. (USSR)*, **25**, 1097-1105 (1952).
31. ———, and B. A. Kopylev, *ibid.*, **30**, 383-389 (1957).
32. *Ibid.*, 31, 375-380 (1958).
33. Pozin, M. E., and E. Y. Tarat, *ibid.*, 1318-1327.
34. Pozin, M. E., et al., *ibid.*, 838-846.
35. *Ibid.*, **32**, 1027-1032 (1959).
36. *Ibid.*, pp. 1033-1038.
37. Ross, J., and G. D. Miles, *Oil and Soap*, **18**, 99-102 (May, 1941).
38. Ross, J., et al., *U. S. Pat. 2,315,983* (Apr. 6, 1943).
39. Ruckenstein, E., *Rev. Chim. (Bucharest)*, **12**, 97-98 (1961).
40. Shulman, H. L., and M. C. Molstad, *Ind. Eng. Chem.*, **42**, 1058-1070 (1950).
41. Tarat, E. Y., *J. Appl. Chem. (USSR)*, **34**, 1846-1851 (1961).
42. ———, and S. A. Bogatykh, *ibid.*, 1788-1791.
43. Ungemach, M., *Chem. Ing. Tech.*, **33**, 632 (1961).
44. Vignes, A., *J. Chim. Phys.*, **57**, 999-1005 (1960).
45. Vlcek, V., et al., *Intl. Chem. Eng.*, **2**, 216-220 (1962).
46. Weissman, E. Y., Ph.D. thesis, Case Institute of Technology, Cleveland, Ohio (1963).
47. ———, and S. Calvert, to be published.
48. Workman, W. L., Ph.D. thesis, Case Institute of Technology, Cleveland, Ohio (1963).

Manuscript received March 16, 1964; revision received November 4, 1964; paper accepted November 18, 1964. Paper presented at A.I.Ch.E. Pittsburgh meeting.

APPENDIX 12C

Reprinted from A.I.Ch.E. JOURNAL, September 1965

Gas Absorption in a Fin-Wall Conduit

THOMAS L. SWEENEY and SEYMOUR CALVERT

Case Institute of Technology, Cleveland, Ohio

Gas absorption and pressure drop were studied in a fin-wall conduit; a fin-wall conduit is a rectangular duct with fins placed on two internal walls perpendicular to the axis of flow. Pressure drop data were obtained with the air-water system. Gas absorption data were obtained with the air-ammonia-water system, and were corrected for the expected liquid-phase resistance by the use of oxygen desorption data. The pressure drop per transfer unit is on the order of 0.05 in. of water per transfer unit.

Gas-liquid contacting devices that accommodate a wide range of liquid and gas rates at a low pressure drop, and that handle particulate-bearing gases have wide application. The purpose of this paper is to present mass transfer and pressure drop characteristics of one such device: the fin-wall conduit.

The fin-wall conduit is a rectangular duct with transverse fins attached to one or more internal walls; it is shown in Figure 1. Three attractive qualities of this device prompted its study: the vortex flow patterns between the fins, the open construction, and the reproducibility of its critical dimensions.

Figure 2, which was obtained in a water tunnel with the aid of lycopodium powder, shows typical single-phase flow patterns between fins; flow is from left to right. In turbulent flow, the formation and the form of these vortex patterns depend only on the ratio of fin spacing to fin height. Visual studies indicate that there is a rapid exchange of material between the mainstream and the vortices. The rotational velocity of a vortex, by visual observation, increases with increasing mainstream velocity.

A small part of the volume of a fin-wall conduit, 2 to 5%, is occupied by fins; the other 95 to 98% is open. This suggests that the fin-wall conduit may be capable of handling large volumes of gas, which will make it useful in the wet scrubbing of gases that contain particles.

The fin-wall conduit has few important dimensions; these are the fin spacing, the fin height, and the distance between fin walls. By comparison, the important dimensions of a packed column are not uniform and cannot be explicitly specified. It is postulated that the ease of specifying and measuring the dimensions of the fin-wall conduit will allow controlled design for desired characteristics.

Desorption of oxygen from water and absorption of ammonia into water were studied. Oxygen desorption is generally considered to be a case in which all of the resistance to transfer is contained in the liquid phase. Ammonia absorption into water was, at one time, assumed to be a case in which all of the resistance to transfer was contained in the gas phase; this is not now regarded as completely true. The oxygen-water equilibrium data of reference *4* and the ammonia-water equilibrium data of reference 7 were used.

The equipment utilized in this study consisted of four experimental conduits, designated as columns A, B, C, and D. The columns were rectangular conduits formed by two fin walls (aluminum) and two smooth walls (transparent plastic). The spacing between adjacent fins of the same fin wall is designated as S; the height of a fin as H; the minimum distance between fins of opposite fin walls as b; the width of the conduit along the fin wall as W. The minimum cross-sectional area for flow is A, or bW. The maximum cross-sectional area for flow is A + 2HW. Table 1 lists some dimensions of the conduits.

The conduit that was being studied was situated on top of the air-inlet box that was a 1-ft. cube. Air was introduced at the side of the box; it ascended through the fin-wall conduit, out the top, to the exhaust system. Water was introduced near the top of the conduit through small holes in a ⅜-in. copper tube designed to distribute the water evenly over the two fin walls (*10*). The water descended through the conduit into the air-inlet box from which it was withdrawn.

PRESSURE DROP

For flow in a circular pipe

$$\frac{\Delta P}{X} = \frac{2\rho f U^2}{g_c D} \tag{1}$$

In noncircular conduits, experience has led to the equivalent diameter concept. The equivalent diameter for use in Equation (1) is defined as

$$D_{eq} = \frac{4\ \text{(cross-sectional area of conduit)}}{\text{(wetted perimeter of conduit)}} \tag{2}$$

Thus in flow between infinite parallel plates the equivalent diameter is twice the plate spacing.

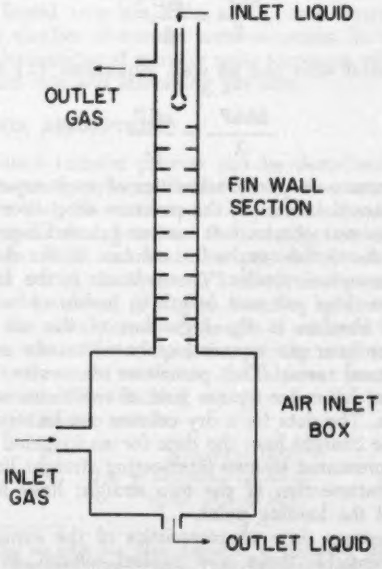

Fig. 1. Fin-wall conduit.

Thomas L. Sweeney is with Ohio State University, Columbus, Ohio. Seymour Calvert is with Pennsylvania State University, University Park, Pennsylvania.

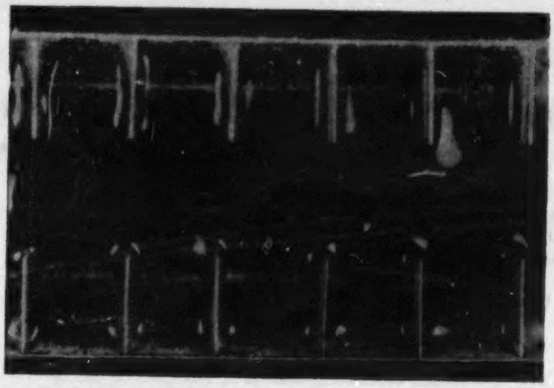

Fig. 2. Flow patterns between fins. Fin spacing = fin height.

In a fin-wall conduit with two fin walls, the equivalent diameter at the minimum cross-sectional area is

$$D_{eq} = \frac{4Wb}{2(W+b)} \tag{3}$$

The use of the equivalent diameter calculated at the minimum cross-sectional area is convenient in this work; it has been used in work on fin tubes (*2, 6*).

Equation (3) contains the term $(W + b)$, which is related to the sum of the drag on the fin walls and the drag on the smooth walls. If we neglect the drag due to the smooth walls, thereby replacing the term $(W + b)$ with the term (W), Equation (3) becomes

$$D_{eq} = 2b \tag{4}$$

There exist some pressure drop data for fin-wall conduits made of only one fin wall and three smooth walls (*1, 3*). If we neglect the drag of the smooth walls as compared to that of the fin wall, the equivalent diameter becomes

$$D_{eq} = 4h \tag{5}$$

The minimum distance between the fins and the opposite smooth wall is h.

For a conduit with two fin walls, Equations (1) and (4) yield

$$\frac{b\Delta P}{X} = \frac{\rho f U^2}{g_c} \tag{6}$$

For a conduit with one fin wall, Equations (1) and (5) yield

$$\frac{2h\Delta P}{X} = \frac{\rho f U^2}{g_c} \tag{7}$$

The pressure drop characteristics of each experimental column were determined; the pressure drop over the entire column was obtained at various gas and liquid rates. Figure 3 shows the results for column A; the data from other columns are similar. The ordinate is the logarithm of pressure drop per unit length in inches of water per foot. The abscissa is the logarithm of the air rate in pounds per hour per square foot based on the minimum cross-sectional area. The parameter is water rate in pounds per hour per square foot of minimum cross-sectional area. The data for a dry column can be represented by a single straight line; the data for an irrigated column can be represented by two intersecting straight lines. The point of intersection of the two straight lines herein is designated the loading point.

The pressure drop characteristics of the experimental columns resemble those of a packed column. In an irrigated packed column, however, three intersecting straight lines are usually required to represent the data. The slope of the line below the loading point is about the same in each case, that is 1.8 to 2.0. The pressure drop in wet drained packing is higher than the pressure drop in dry packing; this difference is not present in the fin-wall conduit.

TABLE 1. COLUMN DIMENSIONS

	Column A	Column B	Column C	Column D
Fin-wall length, ft.	3.22	3.22	3.25	3.25
b, ft.	0.0495	0.0938	0.0495	0.0495
S, ft.	0.0379	0.0379	0.0807	0.0807
H, ft.	0.0388	0.0388	0.0402	0.0812
S/H	0.976	0.976	2.01	0.994
A, sq. ft.	0.0251	0.0476	0.0251	0.0251
A', sq. ft.	0.0646	0.871	0.0660	0.108

Note: For each column the width, W, is 0.508 ft. The fin thickness is 0.00267 ft.

In Figure 4 the pressure drop per unit length in inches of water per foot in the experimental columns is compared with the pressure drop per unit length in columns packed with Raschig rings (*12*). The abscissa is the air rate based on the maximum cross-sectional area; the use of the maximum area is necessary for a direct comparison. The figure shows that the pressure drop for a fin-wall conduit is lower than that for Raschig rings.

The effect of liquid rate on pressure drop is shown for 1-in. and 1½-in. ceramic Raschig rings (*9*) in Figure 5. The data for fin-wall conduits, based on the maximum cross-sectional area for flow, are also shown. The ordinate A_L is the ratio of the pressure drop of an irrigated column to the pressure drop of a dry column, both at the same gas rate. The abscissa is liquid rate based on maximum cross-sectional area. The use of the maximum cross-sectional area is necessary for direct comparison; if the data for columns A, B, C, and D are plotted on a graph using the minimum cross-sectional area, three distinct curves are obtained; the data of columns A and B fall on the same curve. Figure 5 is valid for any gas rate below loading.

Calvert and Hodous (*3*) report pressure drop data for rectangular conduits with one fin wall. If we assume that all the momentum transfer is to the fin wall, we may use Equation (7). Figure 6 is a plot of $\frac{b\Delta P}{X}$ vs. air rate on

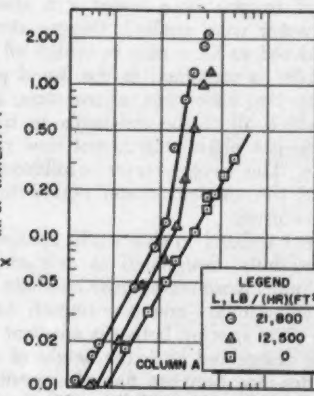

Fig. 3. Pressure drop vs. gas rate. Column A: air-water.

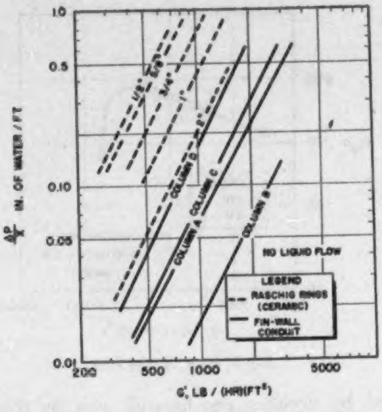

Fig. 4. Pressure drop vs. gas rate.

logarithmic coordinates for columns A, B, and D; it is also a plot of $\frac{2h\Delta P}{X}$ vs. air rate for the data of Calvert and Hodous. The data points are not shown. The fin height is approximately equal to the fin spacing. The lines for columns A, B, and D almost coincide; the lines for Calvert and Hodous's columns are definitely separate, with the line for the smallest minimum distance between the fin wall and the opposite smooth wall being the highest. The line for the largest spacing is lowest and is in the range of those for columns A, B, and D. In column C, the fin spacing is approximately twice the fin height; the line for column C, which is not shown in Figure 6, would be higher than the lines of columns A, B, and D.

The comparison shown in Figure 6 is not completely valid. A correction should be made to the data of single fin-wall conduits to account for the drag of the smooth walls. The correction would lower the three curves for the data of Calvert and Hodous by approximately 15%, which would enhance the correlation. The purpose of the graph, however, is to show that a close approximation of the pressure drop in a single fin-wall conduit can be obtained by merely neglecting the effect of the smooth wall.

The friction factor defined by Equation (6) for columns A, B, and D is approximately 0.07 at a Reynolds number, based on equivalent diameter, of 10,000; that of column C is approximately 0.09. Braun and Knudsen (2) presented plots of friction factor vs. the ratio of fin spacing to fin height for fin tubes. These plots show single maxima at ratios of from 4 to 5½. Column C has a ratio of 2, whereas the other columns have ratios of 1. Thus the higher friction factor for column C is in qualitative agreement with the results of Braun and Knudsen.

The friction factors, from Equation (7), calculated from the data of Calvert and Hodous (3) and those calculated from the data of Boelter et al. (1) also lie in the range 0.05 to 0.10. Friction factor plots are given in reference *10*. Additional work is necessary before a complete friction factor chart for fin-wall conduits can be prepared.

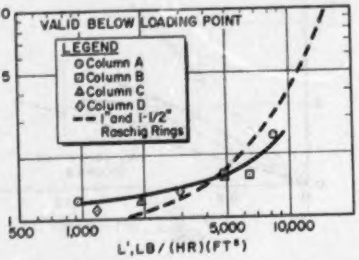

Fig. 5. Effect of liquid rate on pressure drop. A_L vs. liquid rate.

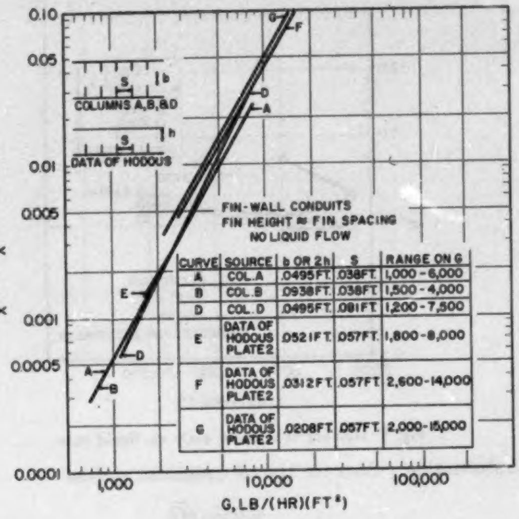

CURVE	SOURCE	b OR 2h	S	RANGE ON G
A	COL. A	.0495FT.	.038FT.	1,000 - 6,000
B	COL. B	.0938FT.	.038FT.	1,500 - 4,000
D	COL. D	.0495FT.	.081FT.	1,200 - 7,500
E	DATA OF HODOUS PLATE 2	.0521FT.	.057FT.	1,800 - 8,000
F	DATA OF HODOUS PLATE 2	.0312FT.	.057FT.	2,600 - 14,000
G	DATA OF HODOUS PLATE 2	.0208FT.	.057FT.	2,000 - 15,000

Fig. 6. $\frac{b\Delta P}{X}$ or $\frac{2h\Delta P}{X}$ vs. gas rate.

The gas and liquid rates at loading were determined from the pressure drop curves for each column; the data are well represented by

$$G = 4590 \left[\frac{L}{G}\right]^{-0.500} \tag{8}$$

OXYGEN DESORPTION

Figure 7 is a plot of the total number of liquid-phase transfer units for column A vs. the liquid rate in pounds per hour per square foot based on the minimum cross section for flow. The data have been corrected to 25°C. and have also been corrected for end effects; the end-effect correction is approximately 25% of the observed number of transfer units. The data for columns B, C, and D are similar and are given in Table 2.* Below the loaded region, liquid rate has little effect; with increasing gas rate the number of transfer units increases. In the loaded region the number of transfer units increases with increasing liquid rate and increasing gas rate.

AMMONIA ABSORPTION

The mass transfer process can be described in terms of a penetration theory model (*10*). Necessary assumptions are that the dominant transport mechanism in the gas phase is that between the rotating vortex and the wetted fin wall, and that the peripheral velocity of a captured vortex is about 1/3 the velocity of the gas through the column (*8*). Also, transfer between the vortex and the main stream of the gas is assumed to be very rapid, so that the composition of the captured vortex would be the same as that in the adjacent portion of the main stream. The resulting equation for the height of a gas-phase transfer unit is

$$H_a = \frac{0.767 S b \sqrt{G}}{\sqrt{D'} \, \rho (S + 2H)} \tag{9}$$

---

* Tabular material has been deposited as document 8404 with the American Documentation Institute, Photoduplication Service, Library of Congress, Washington 25, D. C., and may be obtained for $1.25 for photoprints or 35-mm. microfilm.

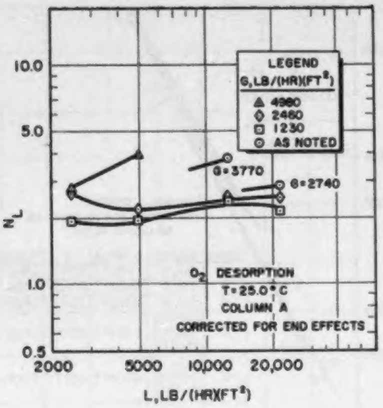

Fig. 7. Number of transfer units vs. liquid rate.

Substituting values for the air-ammonia system

$$H_a = \frac{3.0Sb\sqrt{G}}{\sqrt{S + 2H}} \tag{10}$$

If H_a is plotted against $Sb\sqrt{\frac{G}{S + 2H}}$, a straight line through the origin of slope 3.0 should be obtained.

The results for column A are shown in Figure 8; the results for all columns are given in Table 3.* Below the loaded region, the number of overall gas-phase transfer units decreases with increasing gas rate and increases with increasing liquid rate. Above the loading point, the number of transfer units increases with increasing gas rate and with increasing liquid rate. The data have been corrected for end effects; the end-effort correction is approximately 20% of the observed number of transfer units.

Figure 9 shows the results for columns A and B as a plot of $H_G a$ vs. gas rate. In this plot, the data have been corrected for end effects and for the expected liquid-phase resistance by use of the oxygen desorption data. The data for columns A and B, below the loaded region, are brought together by this plot. The agreement is very good; where the only variable is the spacing between fin walls, interpolation by this type of correlation is recommended. The surface of interface per unit volume, *a*, is calculated by dividing the fin-wall area by the free volume.

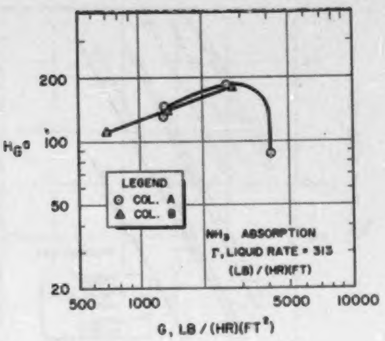

Fig. 9. $H_G a$ vs. gas rate.

$$a = \frac{2\,(S + 2H)}{Sb} \tag{11}$$

The prediction of Equation (10) is tested in Figure 10. Equation (10) predicts a straight line relationship between H_a and $Sb\sqrt{\frac{G}{S + 2H}}$ for columns where the fin spacing is approximately equal to the fin height. In similar graphs for columns A and D, the data can be represented by straight lines through the origin below the loading point. In a graph for column C, in which the fin spacing does not equal the fin height, the straight line relationship does not apply as well as in the graphs for columns A, B, and D.

Equation (10) predicts a slope of 3.0; the lines through the data points have slopes that are different from 3.0. The actual curves approach Equation (10) as the liquid rate increases. This disagreement of the data with Equation (10) arises, at least in part, from the assumption that the liquid-phase resistance in the ammonia-water system may be estimated using data obtained with the oxygen-water system.

From available data (9), one would expect that the height of a transfer unit obtained from corrected ammonia-water data would be three to four times larger than that obtained from other gas-phase controlling data. The agreement between ammonia-water data and gas-

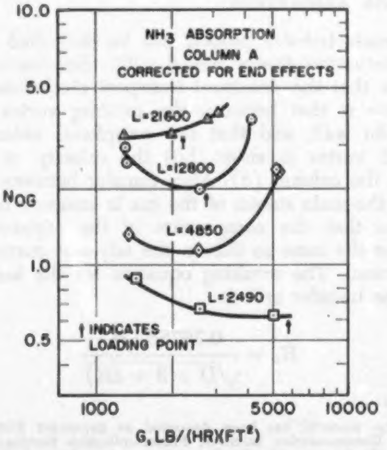

Fig. 8. Number of transfer units vs. gas rate.

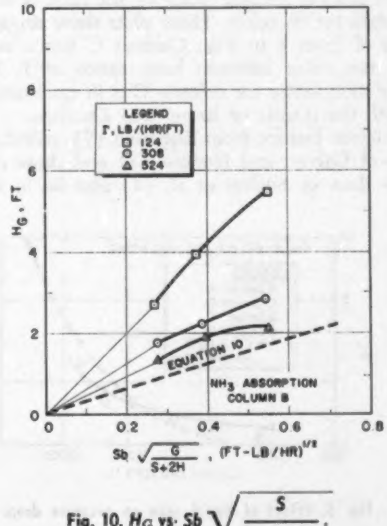

Fig. 10. H_G vs. $Sb\sqrt{\frac{S}{(S+2H)}}$.

---

* See footnote on page 787.

TABLE 5. AMMONIA-WATER DATA

$$H_{OG} = \frac{\alpha G^{\beta}}{\Gamma^{\gamma}}$$

Column	α	β	γ	Range on G	Range on
A	6.49	0.291	0.644	1,280 lb./(hr.)(sq. ft.) to loading point	61.5 to 536 lb./(hr.)(ft.)
B	2.66	0.442	0.573	680 lb./(hr.)(sq. ft.) to loading point	123 to 530 lb./(hr.)(ft.)
C	3.05	0.200	0.817	1,330 lb./(hr.)(sq. ft.) to loading point	129 to 540 lb./(hr.)(ft.)
D	2.88	0.523	0.836	1,280 lb./(hr.)(sq. ft.) to loading point	122 to 511 lb./(hr.)(ft.)

phase controlling data should improve as liquid rate is increased. In Figure 10, the height of a transfer unit observed for the ammonia-water system is several times larger than the predicted values for a gas-phase system; the agreement improves as the liquid rate is increased.

Ammonia absorption in column A is compared with ammonia absorption in 2-in. Raschig rings (*11*) in Table 4.* The pressure drop per transfer unit is 0.09 to 0.15 in. of water for 2-in. Raschig rings and 0.03 to 0.05 in. of water for column A. The height of a transfer unit is greater in the fin-wall conduit but the pressure drop per transfer unit is lower. Similar tables could be presented for other packings and other columns; the conclusions would be the same.

The ammonia-water data are summarized in Table 5 where empirical equations are presented.

CONCLUSIONS

An investigation of pressure drop and gas absorption in a fin-wall conduit has been described.

The pressure drop data, obtained with the air-water system, are presented as head loss per unit length. The pressure drop characteristics are similar to those of a packed column; the fin-wall conduit, however, has a much lower pressure drop per unit length than does the usual packed column. An accurate estimate of pressure drop and loading point in a fin-wall conduit can be made with the obtained data.

A postulated model for gas-phase controlled gas absorption indicates that the height of a transfer unit will increase with the square root of gas rate. The model will predict heights of gas-phase transfer units that are in reasonable agreement with the data if the fact that the ammonia-water system is not completely gas-phase controlled is recognized.

In the absence of the additional data required to present generalized results for design purposes, the equations of Table 5 are recommended.

ACKNOWLEDGMENT

The support by the U. S. Public Health Service through Research Grant S-84 and by the National Science Foundation through a fellowship is gratefully acknowledged.

NOTATION

a = surface of interface per unit volume, sq.ft./cu.ft.
A = minimum cross-sectional area for flow, sq.ft.
A' = maximum cross-sectional area for flow, sq.ft.
A_L = ratio of pressure drop in an irrigated column to pressure drop in a dry column, both at the same gas rate
b = minimum spacing between opposite fin walls in conduit containing two fin walls, ft.
D = diameter, ft.
D_{eq} = equivalent diameter, ft.
D' = diffusivity, sq.ft./hr.
f = friction factor
g_c = a conversion factor, 32.17 (lb.$_m$)(ft.)/(lb.$_f$)(sec.^{2})
G = gas rate based on minimum cross-sectional area, lb./(hr.)(sq.ft.)
G' = gas rate based on maximum cross-sectional area, lb./(hr.)(sq.ft.)
h = minimum spacing between fin wall and opposite plate in conduit with one fin wall, ft.
H = fin height, ft.
H_G = height of a gas-phase transfer unit, ft. (corrected for end effects)
H_{OG} = height of an overall gas-phase transfer unit, ft. (corrected for end effects)
L = liquid rate based on minimum cross-sectional area, lb./(hr.)(sq. ft.)
N_{OG} = number of overall gas-phase transfer units (corrected for end effects)
N_L = number of liquid-phase transfer units at 25°C. (corrected for end effects)
P = pressure, in. of water
S = fin spacing, ft.
U = average velocity through minimum cross-sectional area for flow, ft./sec.
W = width of conduit, ft.
X = length of column, ft.

Greek Letters

α see Table 5
β see Table 5
γ see Table 5
Γ = liquid flow rate, lb./(hr.)(ft.)
ρ = density

LITERATURE CITED

1. Boelter, L. M. K., G. Young, M. L. Greenfield, V. D. Sanders, and M. Morgan, *Natl. Advisory Committee Aeronaut. Tech. Note 2517* (1951).
2. Braun, F. W., Jr., and James G. Knudsen, *Chem. Eng. Progr.*, **48**, 517 (1952).
3. Calvert, Seymour, and Ralph Hodous, *Air Pollution Control Assoc. J.*, **12**, 326 (1962).
4. Gerster, J. A., Arthur B. Hill, Norman N. Hochgraf, and Donald G. Robinson, "Tray Efficiencies in Distillation Columns," Final Rept. Univ. Delaware, A.I.Ch.E., New York (1958).
5. Higbie, Ralph, *Trans. Am. Inst. Chem. Engrs.*, **31**, 365 (1935).
6. Knudsen, James George, Ph.D. thesis, Univ. Michigan, Ann Arbor, Michigan (1949).
7. Kowalke, O. L., O. A. Hougen, and K. M. Watson, *Bull. Univ. Wisconsin Engr. Expt. Stat. Ser.*, No. 68 (1925).
8. Roshko, Anatol, *Natl. Advisory Committee Aeronaut. Tech. Note 3488* (1955).
9. Sherwood, Thomas K., and Robert L. Pigford, "Absorption and Extraction," 2 ed., McGraw-Hill, New York (1952).
10. Sweeney, Thomas L., Ph.D. thesis, Case Inst. Technol., Cleveland, Ohio (1962).
11. Treybal, Robert E., "Mass Transfer Operations," McGraw-Hill, New York (1955).
12. "Technical Data Relating to Tower Packing," United States Stoneware Company, Akron, Ohio.

Manuscript received May 8, 1964; revision received March 22, 1965; paper accepted March 24, 1965.

---

* See footnote on page 787.

APPENDIX 12D

Reprinted from CHEMICAL ENGINEERING PROGRESS SYMPOSIUM SERIES, Volume 59, Number 46, 1963

EXPERIMENTAL AND ANALYTICAL STUDY OF PLATE-TYPE GAS ABSORBER DYNAMICS

Seymour Calvert
and
George A. Coulman

This research was directed at establishing a detailed dynamic mathematical model and computer simulation of a plate-type absorption column involving mass and heat transfer and significant thermal generation. An experimental system, air-sulfur dioxide-dimethylaniline, was selected to demonstrate these characteristics.

The transient response of the exhaust gas to step changes (of different sizes and direction) in the feed gas concentration showed agreement within 5% between the simulation and the laboratory equipment.

The effects of several parameters on the transient response were examined by use of the simulation. The most significant effect was on delay time, which was caused by changes in efficiency. A general analytic proof of the source and character of this effect was established.

A method of correlation was developed using the newly recognized time constant $B/(L + E\alpha G)$. It was proved that the normalized responses of the liquid and gas on a stage were not the same even at an efficiency of 1.00.

Automatic control has been an important part of the chemical process industries for many years so that a certain amount of knowledge about the unsteady-state behavior of these processes has been established. This limited knowledge has resulted from trial-and-error studies of the installed process to establish control settings. Recently, however, more interest has developed in the unsteady-state behavior of processes. Although still predominantly occupied with control, this interest has assumed a broader character than merely steady state control.

Knowledge of the unsteady-state behavior of a system is needed to establish optimum start-up procedures, or to establish optimum procedures for changing the level of operation, as well as to design more sophisticated control systems than have been used previously (such as dynamic optimizing feed forward control). In addition, it is conceivable that more knowledge of the basic properties of the process can be gained from studying the unsteady state, since the steady state is only a limited case thereof.

Chemical engineering has been based on the unit operations, and this subdivision appears suitable as a basis for the extension of study to the unsteady state. Two basically similar unit operations which are used widely in the process industries are absorption and extraction. The present study was concerned specifically with absorption, but it is immediately evident that this could be easily adapted to extraction. The specific system studied in this work was the absorption of sulfur dioxide from air by dimethylaniline in a perforated plate column.

During the past ten years considerable work has been done on the unsteady state of distillation columns for standard control applications. Early interest centered on batch systems which are most obviously unsteady state, but later work was concerned with continuous processes. During this same period a limited quantity of work was presented on unsteady-state absorption over a range extending from small perturbations to start-up transients of columns. Major emphasis was on demonstrating new tools for this type of work and not with engineering studies of the unsteady state per se.

It was assumed in the literature that each stage was a homogeneous unit. For steady-state studies this is acceptable, but unsteady-state studies should take into consideration the segmented nature of a stage. The literature solutions were not utilized to examine the effect of such process parameters as efficiency and in most cases were not capable of this. No examinations of results were made to yield useful generalizations or correlations of results. No experimental studies were involved.

The present work was intended as a basis for future studies of the effects of various parameters on unsteady-state behavior. The parameters may be process characteristics (efficiency, equilibrium relations, and so on), or design characteristics. In order to obtain accurate numerical data, a realistic and detailed mathematical model was developed and incorporated in a digital computer simulation of a

---

Case Institute of Technology, Cleveland, Ohio. G. A. Coulman is at the University of Waterloo, Waterloo, Ontario.

plate-type absorption column. The simulation was compared with an experimental installation to establish the accuracy of the mathematical model. Selected process parameters, such as efficiency and equilibrium relations, were examined with the simulation to determine if it would be possible to establish generalizations or correlation techniques more easily utilized than specific simulation of each case. Preliminary generalizations were obtained which indicated that detailed examination of specific parameters would result in useful correlation techniques of general applicability.

EXPERIMENTAL STUDY

PROCESS AND EQUIPMENT

The process used in this study was the absorption of SO_2 from air by dimethylaniline. This system was selected because:

1. it is industrially used for air pollution control and SO_2 recovery,
2. the heat of solution is quite high,
3. the equilibrium relationship is nonlinear.

This type of column was selected because it could be built in laboratory size and maintain most commercial column characteristics. The vapor distribution ruled out a bubble-cap column, and cooling caused problems with a packed column. A perforated-plate column was thus selected.

The major unit of equipment was the absorption column. It consisted of 4-in. Corning glass tees with 1-in. side ports for sampling. The column had five aluminum perforated trays with cooling coils. The feed rates to the column were controlled by rotameters and manual needle valves. In order to allow effective analysis, liquid and gas sample ports were provided on each tray of the equipment. A thermocouple well was located in the liquid layer on each tray. A schematic flow diagram of the experimental equipment is given in Figure 1.

ANALYSIS

The gas sampling system consisted of a 1/8-in. tubing manifold connected to each tray of the column and leading to a continuous analytical device. Valves were located to allow sampling one tray at a time. The analytical devices consisted of a miniature absorber with a small conductivity flow cell in the liquid holdup at the bottom. The cell was calibrated for a fixed gas and liquid rate using distilled water with a resistance of approximately 600,000 ohms. A Leeds and Northrup recording ohmmeter was attached to the cell for data recording. The dynamic response of the analytical system was examined and compensated for in the experimental data.

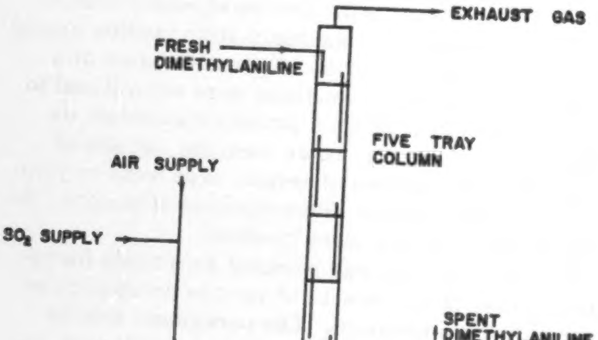

Fig. 1. Flow diagram of experimental equipment.

PROCEDURE

Because only manual control was available, only step changes in the feed streams could be studied. The two changes examined were step changes in the SO_2 feed rate and dimethylaniline feed rate. Changes were not made in the air-flow rate since this would have caused a simultaneous change in feed-gas composition, which would have been difficult to eliminate with manual control.

The start-up was initiated by turning on the air feed to the column at the operating level. The dimethylaniline feed pump was then started and the feed rate adjusted. While the column was loading, the cooling water to the column and the feed stream were turned on. The water to the analyzers was started and the sample gas rate adjusted. The bottom pump on the column was started and adjusted when the column was full. When the temperature in the column appeared steady and all the flow rates were steady, the recorder and a timer were started simultaneously. The SO_2 cylinder heater was turned on, and at a recorded time the SO_2 feed was turned on to a selected level. By continual observation and adjustment the several streams were maintained essentially constant. This was continued until a steady state was reached. Intermittently, the temperature on the lower tray was recorded. When steady state was established, the next step change was introduced. The minimum period between the introduction of transients was twenty minutes.

DATA REDUCTION

The resistance data, corrected for the analytical system response, were converted to concentration values, and these points were plotted vs. time. The smoothed data were then used to compute the normalized curve. The normalized concentration is the ratio of the change in concentration of a stream to the total change between initial and final steady state of that stream.

COMPUTER SIMULATION

MATHEMATICAL MODEL

Examination of the structural configuration of one stage indicated that at least three discrete segments were justified: a gas segment, an active liquid segment, and the downcomer liquid. This selected configuration is depicted in Figure 2. In a study dealing only with order of magnitude results, neglecting gas holdup is normally justified. In an absorption column the average molal holdups on a stage are active liquid 10/downcomer liquid 1.5/gas phase 1. Extraction will usually involve these factors in a ratio 10/1.5/10 respectively. It is apparent then

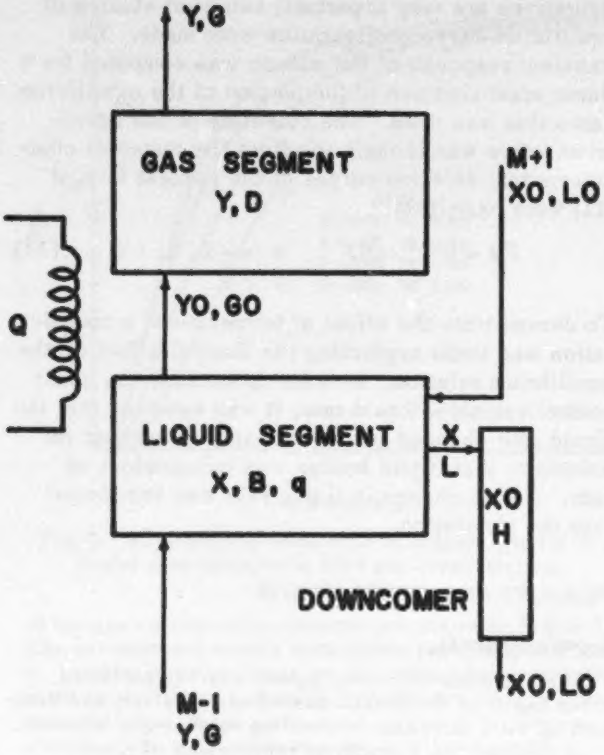

Fig. 2. Model of Mth stage.

that for studies with an accuracy better than 10%, the downcomer character must be considered and, depending on the ratio of the liquid rate to gas rate in the column, the gas must be included in the dynamics.

It has been recognized in the study of efficiency that a distribution exists in the concentration in the liquid and gas within a column. As more accurate models are required for process studies in the unsteady state, this also will have to be considered. Thermal and pressure effects can conceivably be important variables in many absorption or extraction systems.

The system mass equations were established based on the selected physical model. The assumptions intrinsic in each equation are tabulated after it.

$$(YO \cdot GO)_m - (YG)_m = \frac{d}{dt}(YD)_m \qquad (1)$$

1. Bulk flow is the only mass transfer mechanism.
2. Concentration is homogeneous throughout the element.

$$(XL)_m - (XO \cdot LO)_m = \frac{d}{dt}(XO \cdot H)_m \qquad (2)$$

(the same assumptions as (1))

$$(XO \cdot LO)_{m+1} + (Y \cdot G)_{m-1} - (X \cdot L)_m - (YO \cdot GO)_m = \frac{d}{dt}(X \cdot B)_m \qquad (3)$$

1. Concentration is homogeneous throughout the liquid.
2. Gas holdup is negligible.
3. All interphase mass transfer occurs in this element.
4. Entrainment is negligible.

A simplification was made at this point in the physical model. The active liquid and the gas phase were assumed to be in thermal equilibrium. The only energy effects considered were thermal, thus kinetic energy, pressure, and so on, were neglected.

$$q_m - Q_m + (A_g\,(G + GY))_{m-1} - (A_g\,(G + GY))_m + (A_1(LO + LO \cdot XO))_{m+1} - (A_1(L + L \cdot X))_m = \frac{d}{dt}(A_g(D + DY) + A_1\,(B + BX) + A_c M)_m \qquad (4)$$

$$(A_1(L + LX))_m - (A_1\,(LO + LO \cdot XO))_m = \frac{d}{dt}(A_1(H + H \cdot XO))_m \qquad (5)$$

In order to simplify these equations, the following assumptions were made:

1. L and G are constant throughout the column.
2. The holdup of nontransferring material in each segment of the column is constant and the same on each tray.
3. The enthalpy of a stream is equal to the sum of the enthalpies of the pure components.
4. The thermal generation is a linear function of the material transferred.
5. The heat transfer on the tray is a linear function of the temperature difference.
6. The cooling-water temperature changes negligibly on a stage.
7. The thermal capacitance of the column is negligible.
8. Pressure disturbances are negligible.

These assumptions resulted in the following simplified equations:

$$YO_m - Y_m = (D/G)\,\frac{d}{dt}(Y_m) \qquad (1a)$$

$$X_m - XO_m = (H/L)\,\frac{d}{dt}(XO_m) \qquad (2a)$$

$$XO_{m+1} - X_m + (G/L)(Y_{m-1} - YO_m) = (B/L)\frac{d}{dt}(X_m) \quad (3a)$$

$$G(K1 + K2 \cdot Y_{m-1})(T_{m-1} - T_m) + L(K3 + K2 \cdot XO_{m+1})(TO_{m+1} - T_m) + q_m - Q_m = (D(K1 + K2 \cdot Y_m) + B(K3 + K2 \cdot X_m))\frac{d}{dt}T_m \quad (4a)$$

$$(K3 + K2 \cdot X_m)(T_m - TO_m) = (H/L)(K3 + K2 \cdot XO_m)\frac{d}{dt}(TO_m) \quad (5a)$$

Other auxiliary equations needed to describe the entire column and the thermal and mass transfer are as follows:

$$E = (Y_{m-1} - YO_m)/(Y_{m-1} - YE_m) \quad (6)$$

$$P2_m = (\alpha \cdot X_m^2 + \beta \cdot X_m)\,\mathrm{EXP}(\mathrm{REF\text{-}HEAT}/(T_m + 459.6)) \quad (7)$$

$$q_m = FG(Y_{m-1} - YO_m) \quad (8)$$

$$Q_m = U(T_m - TW_m) \quad (9)$$

$$Y_f - Y_o = (S/G)\frac{d}{dt}(Y_o) \quad (10)$$

The SO_2 partial-pressure equation was established from the 77°F. partial-pressure isotherm and the Clausius-Clapeyron equation.

In addition to the equation defining efficiency, it is necessary to predict efficiency on a theoretical basis, independent of equipment operation. A technique adaptable to our equipment was presented by Calvert and Workman (*4*).

SIMULATION STUDY

The equations in differential equation form must be rewritten in finite difference form to be programmed on the digital computer. A forward or backward first-difference approximation was used to eliminate all requirements for future information. This material was programmed for computation on a Burroughs 220 Data Processor using an Algol compiler.

The computer-program results were compared to the experimental results. With these same data it was possible to demonstrate the effect of the size and direction of the step change. A step change was introduced in the gas-phase feed composition. These step changes demonstrated the transients of the temperature on each tray.

The response of the column was computed for a selected step change with several different efficiencies. Since equilibrium curves and their configurations are very important, two brief studies of equilibrium-curve configuration were made. The transient response of the column was computed for a linear approximation of the portion of the equilibrium curve that was used. The curvature of the equilibrium curve was thought to affect the response characteristics; so three curves of the general form of (11) were examined.

$$P2 = \alpha X^2 + \beta X \qquad \alpha = -\alpha,\ 0,\ +\alpha \quad \beta > 0 \quad (11)$$

To demonstrate the effect of temperature, a computation was made neglecting the thermal effect on the equilibrium relation. In order to examine the usual control variable, liquid rate, it was assumed that the liquid rate changed instantaneously throughout the column or that liquid holdup was independent of rate. A step change in liquid rate was introduced into the simulation.

RESULTS AND CONCLUSIONS

EXPERIMENTAL

The operating efficiency agreed with the predicted value based on the method described by Calvert and Workman (*4*) for a gas-phase controlling bubbler-type absorber. This method used a graphical relationship of f_g and $\sqrt{Dt_g/a^2}$.

f_g = fractional approach to equilibrium = 1.00 (calculated)
D = diffusivity coefficient for SO_2 – air = 0.122 cm^2/sec. (*13*)
t_g = residence time of a gas bubble = 0.0667 sec.
a = bubble radius = 0.238 cm.

It should be noted that in adapting this method to the present column, a superficial gas velocity was required to establish t_g. This velocity was based on the active area of the plate and not the total column cross section.

Normalized concentration transients determined from the operation of the column are shown in Figure 3. The concentration of the effluent gas responded more or less rapidly depending on the direction of the step change in the gas feed and its magnitude. It appeared that as the disturbance lessened, the response curves for a rise or fall in the feed gas would essentially merge. It is apparent that a computation predicting the optimum mode of changing operating level must consider the magnitude and direction of change. The temperature response of the lower tray was measured and is very roughly approximated in Figure 4. The crude measurements were the result of inadequate indicating equipment which was marked in 5°C. intervals. The general configuration and magnitude are apparent.

SIMULATION

Experimental Relationship. Five transients were studied on the experimental equipment. Four step changes in feed gas concentration and a step change in liquid feed rate were studied. The normalized responses

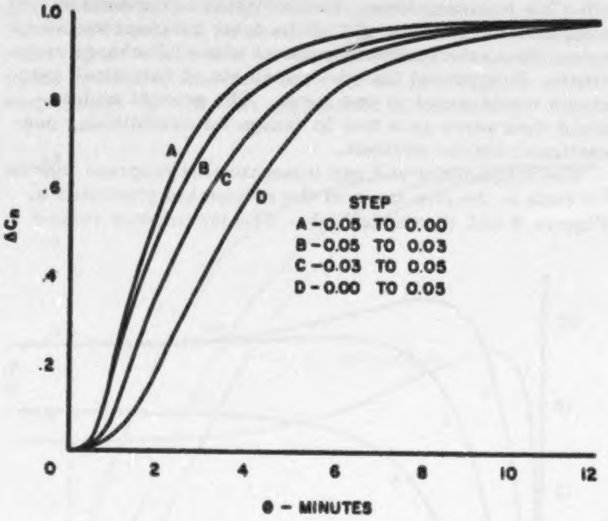

Fig. 3. Experimental transients of exhaust gas for selected step changes in feed gas concentration.

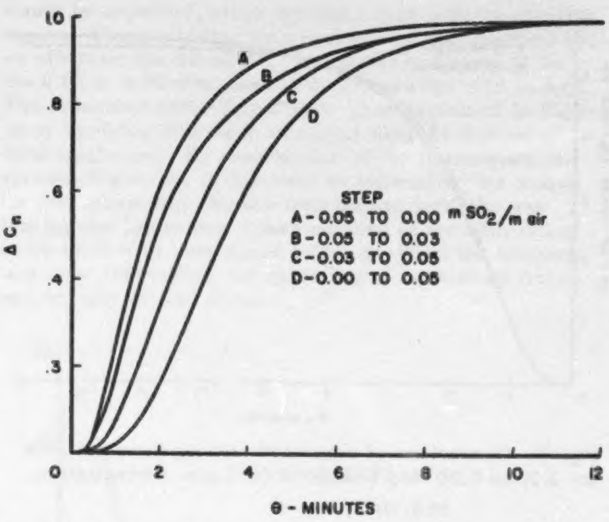

Fig. 5. Simulated transients of exhaust gas for selected step changes in feed gas concentration.

of the gas concentration changes are shown in Figure 5. The experimental values were shown previously in Figure 3. In order to demonstrate the deviation of these studies, the 0.00 to 0.05 step changes from the two studies have been replotted on the same graph in Figure 6. The deviation of the two curves was not very great, being a maximum of 5% of the total transient at any point in time. It was necessary to examine the actual concentration curves (Figure 7) to ascertain the source of this deviation. This examination demonstrated that the major source of error was not in the transient, but in the experimental determination of the steady-state values. This is understandable in a system which might be said to be in a dynamic steady state.

The system necessarily had noise or small deviations because of the mode of control, as did the analytical system. During the large transient this noise was negligible compared to the experimental disturbance, but at the two ends it again became important. Normalizing the data distributed this error over the transient and concealed its source.

Other sources of error which should be mentioned contributed to an error range in the experimental data of ±5% at best. The recorder had an accuracy of about ±1% depending on the portion of the scale being used. The gas-sampling device depended on column pressure which contributed to gas-sample rate disturbances. In addition, liquid rate, temperature, and random errors such as gas entrainment in the liquid and collection on the electrodes, contributed to error in the analytical device.

The evaluation of the liquid transient is presented in Figure 8 for both experimental and simulation studies.

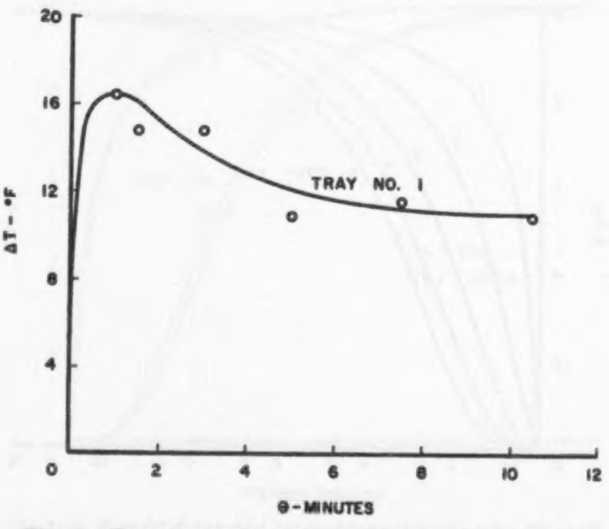

Fig. 4. Experimental transient of temperature for 0.00 to 0.05 step change in feed gas.

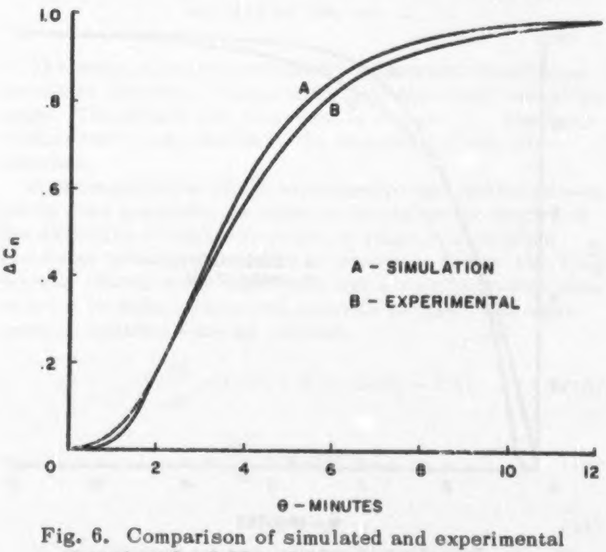

Fig. 6. Comparison of simulated and experimental transient for 0.00 to 0.05 step change in gas concentration.

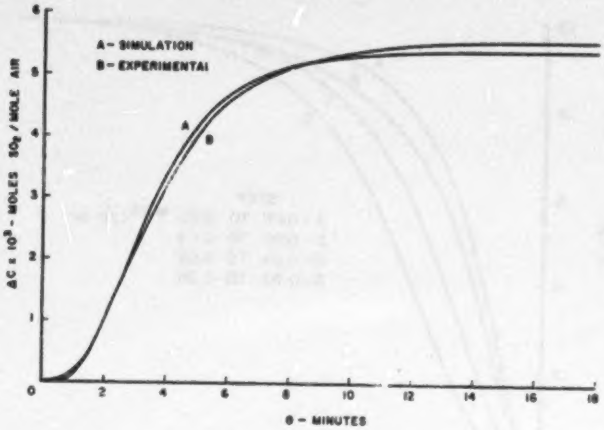

Fig. 7. Comparison of simulated and experimental data for 0.00 to 0.05 step change in feed gas concentration.

The deviation demonstrated here may be more influenced by the assumption of instantaneous response to a liquid rate change in the column than anything else. The experimental data indicated some higher order effects causing an effective time delay in the response. This could very well have been caused by a first or higher order response to the change in liquid flow rate which was neglected in the simulation.

Parameter Studies. A variety of process parameters were selected for study of their effect on the normal transient response of the column to step changes in feed-gas composition.

The four step changes were selected to demonstrate the difference in response because of the direction and magnitude of the change. The normalized data for these steps are shown in Figure 5. The complexity of the dynamic characteristics of this system became obvious by comparing the response curves in pairs of identical step changes of opposite direction. The deviation in time between the two large steps reached as much as 20% of the effective transient time. The deviation in normalized concentration reached 45% of the total transient magnitude. These deviations decreased with step-change magnitude. It appeared that the transients of very small magnitude would merge to one curve. The present model could then serve as a tool in design for establishing conventional control systems.

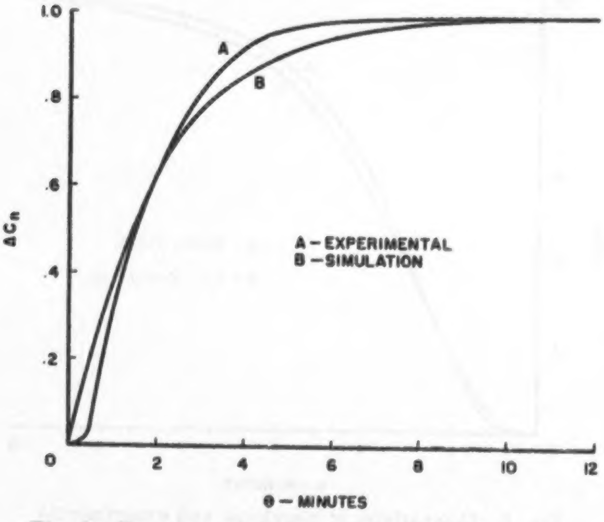

Fig. 8. Transient of exhaust gas for step change in liquid rate.

The temperature and gas concentration response curves for each of the five trays of the column are presented in Figures 9 and 10 respectively. The temperature curves demonstrated the well-damped higher order response of the thermal portion of this system.

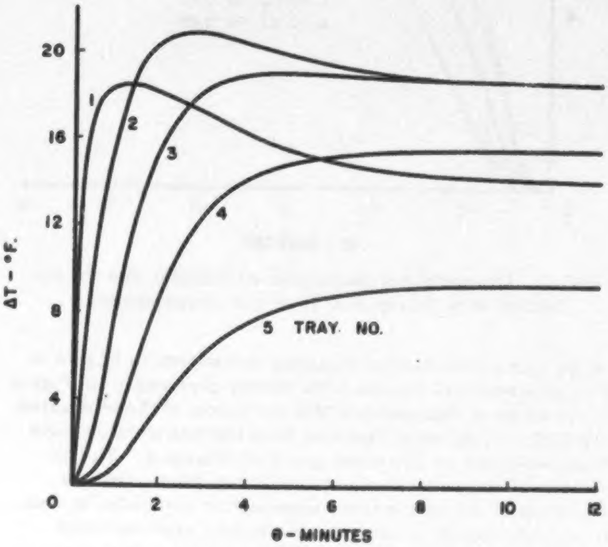

Fig. 9. Simulated temperature transients for 0.00 to 0.05 step change in feed gas concentration.

The efficiency appeared to have a very significant effect on the response of the column. The transient re-

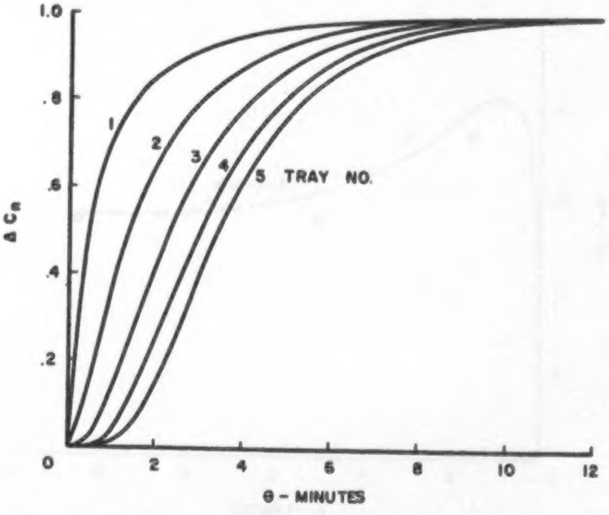

Fig. 10. Simulated transient of gas for 0.00 to 0.05 step change in feed gas concentration.

sponse for a step change in feed-gas composition is shown in Figure 11 for selected efficiencies. The major effect of the efficiency was on the effective time delay of the system or that time between the introduction of the step change and its first appearance at the output. The break in the response curve was much sharper for lower efficiency near the end of the transient.

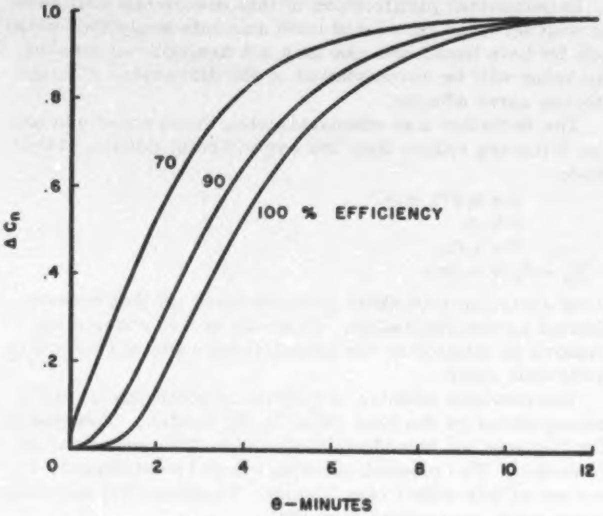

Fig. 11. Simulated transient of exhaust gas concentration for feed gas step change from 0.00 to 0.05 moles/sulfur dioxide/mole air.

An interesting result which was quite unexpected is illustrated in Figure 12. This plot shows the deviation of the normalized concentration transient of the liquid and gas on a tray. An examination of this same transient for a step in the other direction is shown in Figure 13. The magnitude of the deviation differed with direction as would be expected, since the transients differed significantly. Unexpectedly, the magnitude of the transient had no effect on the deviation. The curve in Figure 13 for the 0.05 to 0.00 step exactly duplicates the 0.05 to 0.03. The crossover noticed in Figure 12 is explained in Figure 13 by studying this same transient with the thermal effects neglected. By examination of the temperature response (Figure 9), it was easy to rationalize the reason for this crossover. As the temperature rose, the gas leaving the liquid was richer because of the equilibrium curve shift with less liquid build-up. When the temperature then descended, the liquid began to build up faster and the gas slowed down.

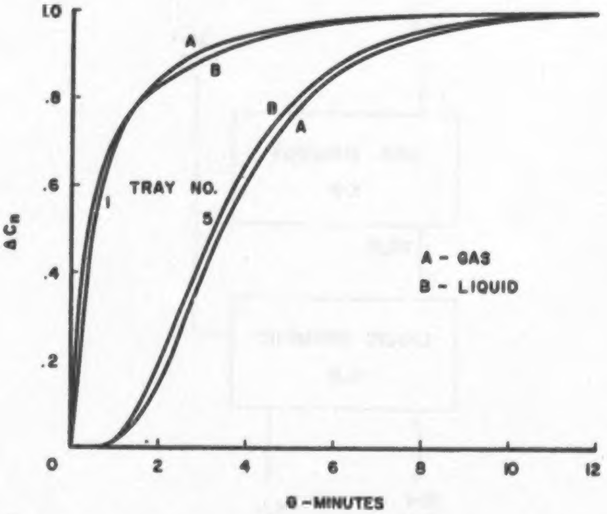

Fig. 12. Simulated transient for 0.00 to 0.05 step change in gas feed concentration.

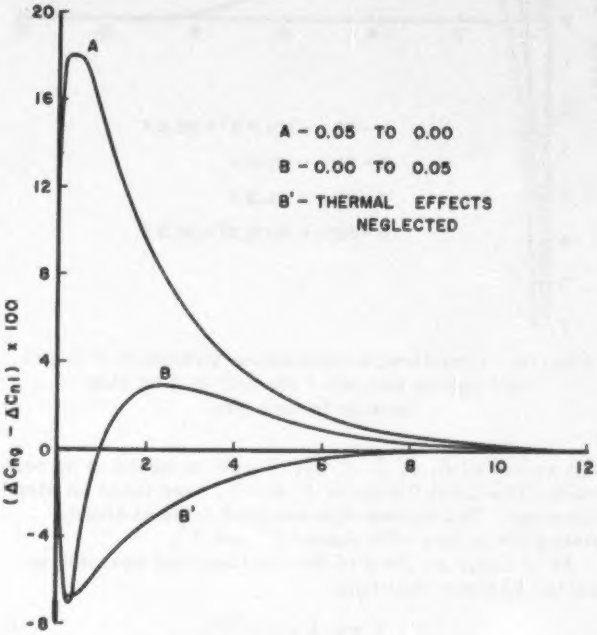

Fig. 13. Normalized concentration difference of liquid and gas on tray no. 1.

The same effect was examined for several equilibrium curves to determine what contribution the shape and slope made. These data are presented in Figure 14. The equilibrium curve contributed to the character of this phenomenon.

A rationalization of the existence of this deviation was not at first apparent. In order to determine the source of the deviation in response within a stage, a simplified one-stage model was studied as shown in Figure 15. The thermal effects were neglected, and a step input was used in order to make an analytic solution simple. The mass balance equations are as follows:

$$B\frac{dX}{dt} = L(X_1 - X) + G(Y_1 - YO) \tag{12}$$

$$D\frac{dY}{dt} = G(YO - Y) \tag{13}$$

$$YE = aX \tag{14}$$

$$E = (Y_1 - YO)/(Y_1 - YE) \tag{15}$$

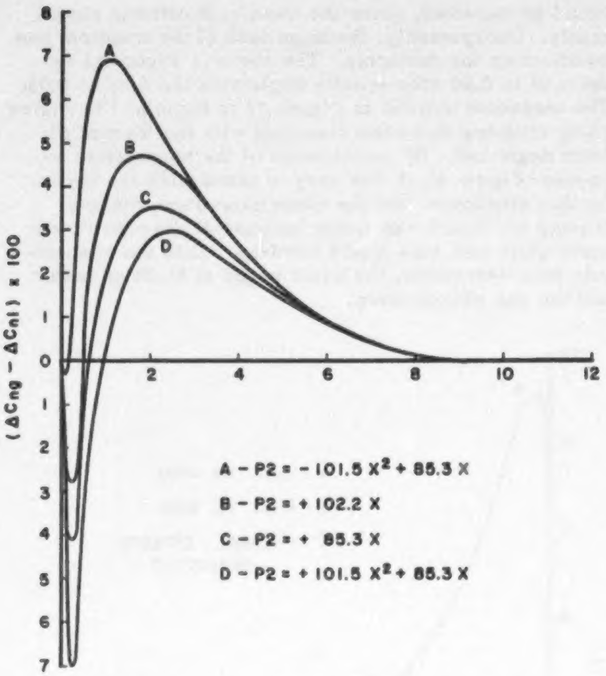

Fig. 14. Normalized concentration difference of liquid and gas on tray no. 1 for 0.00 to 0.05 step change in feed gas.

The values of L, G, B, E, and D were assumed to be constant. The input functions X_1 and Y_1 were taken as step functions. The system was assumed to be at steady state prior to this with values X^0 and Y^0.

An analytic solution to this problem was possible using the Laplace transform.

$$X = c/b + g\,e^{-bt} \tag{16}$$

$$Y = [Y^0 + Eagf/(b - f) - (1 - E)\,Y_1 - Eac/b]e^{-ft} - \\ -[Eagf/(b - f)]e^{-bt} + [(1 - E)\,Y + Eac/b] \tag{17}$$

Where: $b = (L + EaG)/B$
$c = (LX_1 + EGY_1)/B$
$f = G/D$
$g = (X^0 - c/b)$

Solving for the difference of the normalized concentrations and simplifying, resulted in the following equation:

$$Y_n - X_n = \left[\frac{Eag\,f}{(b - f)\,((1 - E)\,Y_1 + (Eac/b) - Y^0)} - 1\right] \times (e^{-ft} - e^{-bt}) \tag{18}$$

In previous work it was assumed that a stage was a completely uniform unit, and the gas holdup was negligible. On this basis the following equations result·

$$Y = YO = aX \qquad \text{for } E = 1.00 \tag{19}$$

$$Y_n - X_n = 0 \tag{20}$$

This established that the deviation between the response of the gas and the liquid on a stage was not recognized before because of the simplification in the stage model. This deviation was a result of the modeling which was much more accurate and realistic than that of prior studies.

An additional result of general value appeared in equation (16). It has been accepted practice to use D/L as the liquid-phase time constant for linear studies, but it is evident that a more accurate generalization is $1/b$.

Experimental justification of this occurrence will have to wait for much faster and more accurate analytical methods for both liquid and gas than are available at present. Its value will be demonstrated in the discussion of equilibrium curve effects.

The deviation was computed using these equations and the following values from the experimental portion of this work:

$t = 0.277$ min.
$a = .2$
$E = 1.00$
$Y_n - X_n = -.358$

This deviation was about twice as large as that demonstrated by the simulation. This was not considered excessive in relation to the assumptions made to attain this numerical value.

The previous mention of efficiency noted that it had a strong effect on the time delay in the system. The reason for this was not immediately available from numerical information. The present one-stage model demonstrates the source of this effect very clearly. Equation (17) has been rewritten in normalized form (21).

$$Y_n = \frac{Eagf/(b - f)}{(1 - EY_1 + (Eac/b) - Y^0}(e^{-ft} - e^{-bt}) + 1 - e^{-ft} \tag{21}$$

This equation may be considered in two portions. One portion is a pure first-order flow system or exponential rise. The other portion is the mass-transfer effect which consists of a coefficient and the difference of two exponentials of different values. In absorption f will be considerably larger than b.

The essential character of this equation and the effect of efficiency on its configuration is schematically illus-

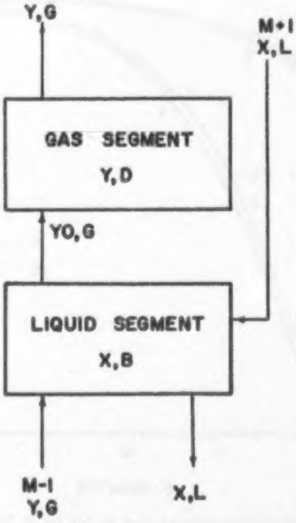

Fig. 15. Simplified model of M^{th} stage.

trated in Figure 16. The flow-system portion of the equation corresponds to the $E = 0.0$ curve. The mass-transfer portion of the equation is in the negative quadrant. The absolute magnitude of these curves is determined by the coefficient. The peak shifts and changes magnitude also because of the E in b. Addition of these curves yields the $E = 0.7$ and 1.0 curves. The relative magnitude was based on computation of the value of the coefficient for the process under study in this work. Its value was 1.04 for $E = 1.0$ and 0.51 for $E = 0.7$. This is a decrease of 50% of the coefficient range for a 30% change in efficiency. This corresponds with the delays demonstrated in Figure 11.

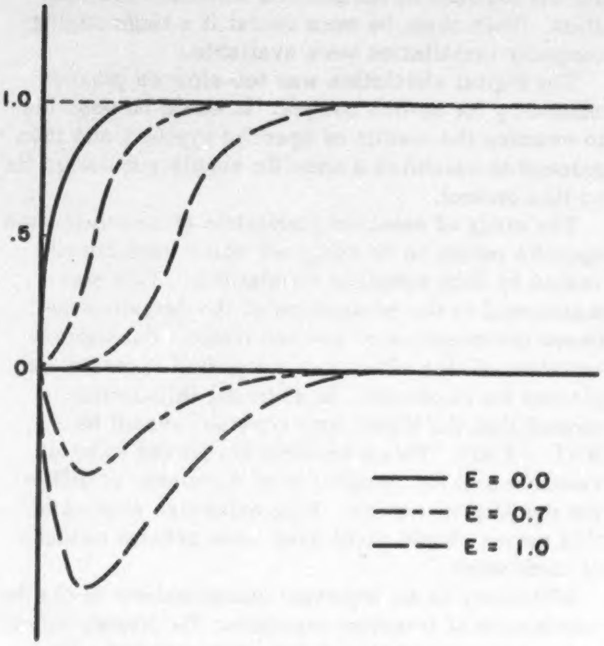

Fig. 16. Illustrative graph of equilibrium effect on transient response.

Further examination of this coefficient shows that the input magnitude as well as initial conditions are parameters. This demonstrates part of the cause of hysteresis and step-magnitude effects.

Of great importance in any equilibrium system is the choice of mathematical relationship selected to approximate the equilibrium data. In addition, it is important to know how various equilibrium configurations will affect a system.

In order to demonstrate the effect of the relation selected to describe the equilibrium, a linear approximation of the parabolic vapor-pressure curve used in this study was examined. The linear approximation was developed from the following relation. The range of X

$$\int_{0.0}^{0.25} (P2 - P2^0)\, dX = 0 \qquad (22)$$

$$P2 = 101.5X^2 + 85.3X \qquad (23)$$

$$P2^0 = 102.2X \qquad (24)$$

was selected on the basis of the operating range of the process. The transients resulting from identical disturbances using these equilibrium curves are presented in Figure 17.

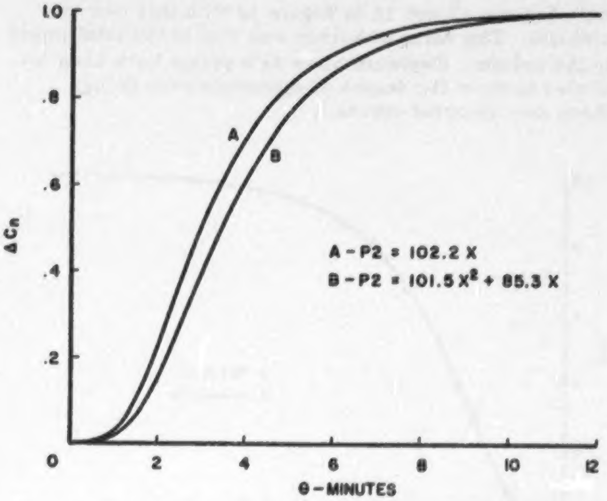

Fig. 17. Simulated transient of exhaust gas with linear approximation of equilibrium relation.

To examine briefly the effect of equilibrium-curve configuration, the following relations were selected:

$$P2 = 101.5X^2 + 85.3X \qquad (25)$$

$$P2 = 85.3X \qquad (26)$$

$$P2 = -101.5X^2 + 85.3X \qquad (27)$$

This resulted in three related curves with positive, zero, and negative second derivatives. The result of identical transients using these relations is shown in Figure 18.

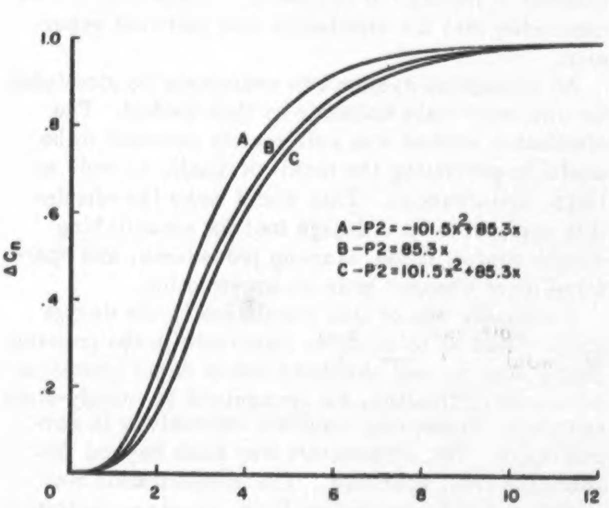

Fig. 18. Effect of equilibrium relationship in simulated exhaust gas transient.

A useful method of correlation was developed from the previous theoretical study of a one-stage model and the present linear equilibrium curves. The new time constant recognized earlier was used to give dimensionless time. The data of equations (24) and (26) were replotted from Figures 17 and 18 in Figure 19 with this new coordinate. The value of holdup was that of the total liquid in the column. Representative data points have been included to show the degree of agreement even though these are computed curves.

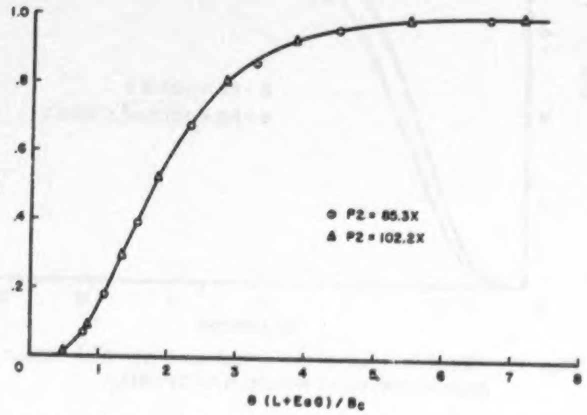

Fig. 19. Correlation of exhaust gas response for 0.00 to 0.05 step change in feed gas concentration.

CONCLUSIONS

The simulation reproduced the transients of the experimental system for large and small disturbances. Specifically, this justified the simulation which was established on the basis of the general concept of absorption equipment. Therefore, it was concluded that the simulation was justified generally.

An absorption system can accurately be simulated for unsteady-state behavior by this method. The simulation method was sufficiently accurate to be useful in predicting the result of small, as well as large, disturbances. This would make the simulation applicable as a design tool for establishing simple control loops, start-up procedures, and operating-level changes prior to construction.

A valuable use of this simulation in the design stage would be to examine transients in the process during start up and shutdown which could conceivably cause difficulties not recognized by steady-state analysis. These may manifest themselves in several ways. The temperature may peak beyond the operating limit specified. The concentration may peak beyond the saturation limit, causing precipitation and unit fouling. Evaluation of these possibilities and others may allow less overdesign where "engineering judgment" served before.

A complete simulation of this type would be valuable for staff training prior to construction and without the expense of the process materials and operation. This might be more useful if a large analog computer installation were available.

The digital simulation was too slow on present machinery for on-line control. It would be possible to examine the results of specific systems and then proceed to establish a specific simple simulation for on-line control.

The study of selected parametric effects indicated specific points to be analyzed which were not revealed by less complete simulations. This was manifested in the recognition of the deviation between the response of gas and liquid. Subsequent isolation of this effect in a simplified approach explained its existence. In addition, this demonstrated that the liquid time constant should be $B/(L + EaG)$. This time constant proved to be a valuable tool for correlation of transients of different equilibrium curves. More extensive studies of this nature should yield even more general methods of correlation.

Efficiency is an important characteristic in the determination of transient response. Its primary effect is on the apparent time delay of the system. The use of a simplified approach to obtain analytic solutions to the mass equations revealed the character of this effect. This could be a valuable tool for the determination of column efficiency. A theoretical prediction of time delay for an efficiency of 1.0 could be compared to the time delay of the process to establish its efficiency. This would require but one step change as contrasted to detailed column analyses needed for steady-state determinations.

Detailed simulation to determine process effects is very useful. Coupling this with analytic solutions of simplified models directed at specific characteristics proved to be a useful tool in developing a detailed understanding of the effect of individual process parameters. A continued effort of this type appears capable of establishing generalized correlations similar to the dimensionless time correlation. Inclusion of correlation techniques for efficiency and disturbance magnitude and direction appears possible from the present work. This type of correlation should prove to be a valuable design tool, avoiding costly simulation and experimental work.

FUTURE WORK

In this area of study a wide variety of work remains. The present work has indicated a few of these projects and exposed the nature of some effects of major interest.

The first important extension of this simulation work should be the establishment of detailed fluid dynamic characteristics of the column. The inclusion of these in the simulation would allow more accurate and realistic evaluation of important process parameters. The next important step beyond this is the determination of the fluid dynamic characteristics of columns during loading.

On completion of this work a realistic study of optimum start-up and operating level changes can be made. In addition, more precise control studies of advanced nature will be possible with a simulation which completely describes the process.

An important area for extension of the unsteady-state theory of processes is prediction of residence-time distributions and their use instead of the stirred-pot approach. This may be of significant importance in very large commercial installations of stagewise unit operations.

From a pure process theory and design point of view, it will be important to study the unsteady state to determine if knowledge of its characteristics can contribute to more effective process design. Detailed examination of the unsteady state should be made to determine if it can contribute to the advancement of process theory.

For purposes of standard control, generalized studies of process dynamics should be made which will yield design tools. These tools may be correlations which allow fast and simple prediction of transfer functions for standard control loops. This would eliminate costly simulation work or rule-of-thumb approximations. These tools may also serve to indicate control problems which could be corrected in the design stage.

NOTATION

A = energy
a = linear equilibrium coefficient—lb. moles DMA/lb. mole air
B = dimethylaniline holdup on tray—lb. moles
$b = (L + EaG)/B$
D = air holdup on tray—lb. moles
E = efficiency
F = heat of absorption—B.t.u./lb. mole SO_2
G = air rate—lb. moles/hr.
GO = air rate leaving liquid—lb. moles/hr.
H = dimethylaniline holdup in downcomer—lb. moles
$HEAT$ = coefficient in exponent for new temperature in Clausius-Clapeyron relation
K = specific heat—B.t.u./(lb. mole)(° F.) 1 — air 2 — SO_2 3 — dimethylaniline
L = dimethylaniline rate—lb. moles/hr.
LO = dimethylaniline rate leaving downcomer—lb. moles/hr.
$P2$ = SO_2 vapor pressure—mm. hg
Q = heat transfer rate—B.t.u./hr.
q = thermal generation—B.t.u./hr.
REF = reference exponent in Clausius-Clapeyron relation
S = air holdup below first tray—lb. moles
T = temperature on the stage—° F.
TE = temperature in the downcomer—° F.
TW = cooling-water temperature—° F.
U = heat transfer coefficient—B.t.u./(hr.)(° F.)
VF = cooling-water rate—lb./hr.
X = tray liquid concentration—lb. moles SO_2/lb. moles DMA
XO = downcomer liquid concentration—lb. moles SO_2/lb. moles DMA
Y = gas concentration—lb. moles SO_2/lb. moles air
YE = gas concentration in equilibrium with liquid
YO = gas concentration leaving liquid segment of tray
α = coefficient in vapor-pressure relation—(lb. moles DMA/lb. mole $SO_2)^2$ mm. Hg
β = coefficient in vapor-pressure relation—(lb. moles DMA/lb. mole SO_2) mm. Hg
Δ = change from initial value

SUBSCRIPTS

c = column
f = feed
g = gas
l = liquid
m = tray number from bottom of column
n = normalized value
o = below first stage
1 = input
2 = output

LITERATURE CITED

1. Acrivos, A., and N. R. Amundson, *Ind. Eng. Chem.*, **45**, No. 2, pp. 467-471 (February, 1953).
2. *Ibid.*, **47**, No. 8, pp. 1533-1541 (August, 1955).
3. Baber, M. F., L. L. Edwards, Jr., W. T. Harper, Jr., M. D. Witte and J. A. Gerster, Paper presented at Am. Inst. Chem. Engrs. meeting, Washington, D. C. (December, 1960).
4. Calvert, S., and W. Workman, *Talanta*, **4**, 89-100 (1960).
5. Coulman, G. A., Ph.D. thesis, Case Institute of Technology, Cleveland, Ohio (1962).
6. Hildebrand, F. B., "Methods of Applied Mathematics," Prentice-Hall, Englewood Cliffs, New Jersey (1952).
7. Jackson, R. F., and R. L. Pigford, *Ind. Eng. Chem.*, **48**, No. 6, pp. 1020-1026 (June, 1956).
8. Lapidus, L., and N. R. Amundson, *Ind. Eng. Chem.*, **42**, No. 6, pp. 1071-1078 (1950).

9. Lapidus, L., E. Shapiro, S. Shapiro and R. E. Stillman, *A.I.Ch.E. Journal*, **7**, No. 2, pp. 288–294 (June, 1961).

10. Mickley, H. S., T. K. Sherwood and C. E. Reed, "Applied Mathematics in Chemical Engineering," pp. 320–340, McGraw-Hill, New York (1957).

11. Rademaker, O., and J. E. Rijnsdorp, Paper presented at fifth World Petrol. Congr., New York, May 30–June 5, 1959.

12. *Ibid.*

13. Reid, R. C., and T. K. Sherwood, "Properties of Gases and Liquids," McGraw-Hill, New York (1958).

14. Rose, A., and R. C. Johnson, *Chem. Eng. Prog.*, **49**, No. 1, pp. 15–21 (January, 1953).

15. Rose, A., and T. J. Williams, *Ind. Eng. Chem.*, **47**, No. 11, pp. 2284–2289 (November, 1955).

16. Rose, A., C. L. Johnson and T. J. Williams, *Ind. Eng. Chem.*, **48**, No. 7, pp. 1173–1179 (July, 1956).

17. Williams, T. J., R. T. Harnett and A. Rose, *Ind. Eng. Chem.* **48**, No. 6, pp. 1008–1019 (June, 1956).

18. Williams, T. J., and R. T. Harnett, *Chem. Eng. Progr.* **53**, No. 5, pp. 220–225 (May 1957).

19. Williams, T. J., *Ind. Eng. Chem.*, **50**, No. 9, pp. 1214–1222 (September, 1958).

20. Yesberg, D., and A. F. Johnson, *Can. J. Chem. Eng.*, **38**, No. 2, pp. 49–54 (April, 1960).

268